OPTICAL METHODS FOR IDENTIFYING THAI JASMINE RICE

KAJPANYA SUWANSUKHO

King Mongkut's Institute of Technology Ladkrabang

A THESIS SUBMITTED IN FULFILLMENT

OF THE REQUIREMENT FOR THE DEGREE OF

DOCTOR OF PHILOSOPHY IN APPLIED PHYSICS

SCHOOL OF GRADUATE STUDIES

KING MONGKUT'S INSTITUTE OF TECHNOLOGY LADKRABANG

2014

KMITL-2014-SC-D-030-036

This material is reserved for educational use only, not allowed for commercial use.

Forbidden to modify the content, and cite the document when use.

COPYRIGHT 2014

FACULTY OF SCIENCE

KING MONGKUT'S INSTITUTE OF TECHNOLOGY LADKRABANG

This material is reserved for educational use only, not allowed for commercial use.

Forbidden to modify the content, and cite the document when use.

หัวข้อวิทยานิพนธ์	การระบุพันธุ์ข้าวขาวดอกมะลิด้วยวิธีการทางแสง
นักศึกษา	นายกาจปัญญา สุวรรณสุโข
รหัสนักศึกษา	51067001
ปริญญา	ปรัชญาดุษฎีบัณฑิต
สาขาวิชา	ฟิสิกส์ประยุกต์
อาจารย์ผู้ควบคุมวิทยานิพนธ์	ดร.ประธาน บุรณศิริ
อาจารย์ผู้ควบคุมวิทยานิพนธ์ร่วม	ดร.ศรัณย์ สัมฤทธิ์เดชขจร

บทคัดย่อ

ในงานวิจัยนี้ จะเป็นการศึกษาวิธีการทางแสงแบบทำลายและไม่ทำลายเพื่อบ่งชี้ข้าวสารพันธุ์ขาวดอกมะลิ 105 วิธีการตรวจสอบแบบทำลายจะประกอบด้วย วิธีสเปกโตรสโคปี (spectroscopy) และการวัดดัชนีหักเห (refractrometry) โดยร่วมกับวิธีการทางเคมี ในวิธีการสเปกโตรสโคปี แทนที่เราจะใช้วิธีการตรวจสอบแบบดั้งเดิม คือ การละลายข้าวสารในสารละลายอัลคาไลน์ (alkaline solution) งานวิจัยในส่วนนี้ เราจะนำเสนอการตรวจสอบอีกวิธีหนึ่งด้วยการละลายข้าวสารในสารละลายอัลคาไลน์ของเรา แล้ววิเคราะห์ด้วยวิธีสเปกโตรสโคปี ในการศึกษาจะใช้ข้าว 4 สายพันธุ์คือ ขาวดอกมะลิ 105 ปทุมธานี 1 ชัยนาท 1 และข้าวเหนียว กข 6 ข้าวทั้ง 4 พันธุ์นี้ จะถูกบดเป็นผง และละลายด้วยสารละลายโพแทสเซียมไฮดรอกไซด์ (KOH) ความเข้มข้น 10% เวลาที่ใช้ในการละลายจะเป็นตัวแปรหนึ่ง และที่เวลานั้นๆ จะทำการวัดสเปคตรัมการส่งผ่านแสงของสารละลายข้าวที่ความยาวคลื่น 500-800 นาโนเมตร และอนุพันธ์อันดับหนึ่งของช่วงสเปคตรัมนี้ จะถูกใช้ในการบ่งชี้ข้าวสารพันธุ์ขาวดอกมะลิ 105 จากการศึกษาพบว่า เงื่อนไขที่ดีที่สุด คือ ใช้ผงข้าว 0.10 g ละลายในโพแทสเซียมไฮดรอกไซด์ ความเข้มข้น 10% เป็นเวลา 10 นาที จะได้อัตราการคัดออกผิดพลาด (false rejection rate) 15.0% งานวิจัยต่อมาจะเป็นการวัดดัชนีหักเหของแสง ซึ่งในงานวิจัยนี้ จะนำเสนอการวัดดัชนีหักของแสงเพื่อนำไปใช้ในการวิเคราะห์ผงข้าวที่ละลายในโพแทสเซียมไฮดรอกไซด์ ความเข้มข้น 10% ซึ่งแนวความคิดมาจากความจริงที่ว่า ข้าวแต่ละสายพันธุ์จะมีปริมาณอะไมโลส (amylose) แตกต่างกัน ดังนั้นค่าดัชนีหักเหของสารละลายข้าวจึงสามารถที่จะใช้ในการบ่งชี้ข้าวสารพันธุ์ขาวดอกมะลิ 105 ออกจากพันธุ์อื่นๆ ได้ จากผลการศึกษาพบว่า เราสามารถแยกข้าวขาวดอกมะลิ 105 ออกจากอีก 3 พันธุ์ข้างต้น ได้ด้วยความผิดพลาดทั้งหมด 6.7% และใช้เวลาในการวัดน้อยกว่า 20 วินาที

ในกรณีการตรวจสอบทางแสงแบบไม่ทำลาย งานวิจัยจะแบ่งออกเป็น 5 หัวข้อ ในหัวข้อที่ 1 จะใช้ภาพหลายสเปคตรัม (multispectral image) ร่วมกับเทคนิคการประมวลผลภาพขั้นพื้นฐาน ซึ่งเราจะเลือก 2 ความยาวคลื่นในช่วงสเปคตรัมระหว่าง 500-580 nm และใช้การทำภาพ threshold การกรองและวิเคราะห์ด้วย เทคนิค

This material is reserved for educational use only, not allowed for commercial use.

Forbidden to modify the content, and cite the document when use.

blob เพื่อระบุพันธุ์ข้าว 8 สายพันธุ์ คือ 4 พันธุ์ที่กล่าวข้างต้น กับอีก 4 พันธุ์ คือ หอมพิษณุโลก 2 หอมสุพรรณบุรี กข 15 และ กข 23 ในการศึกษา เราจะใช้ แหล่งกำเนิดแสงในย่าน UVC ตัวกรองทางแสงที่ปรับเลือกค่าได้ชนิดผลึกคริสตัลเหลว (liquid crystal tunable optical filter) และกล้องดิจิตอลขนาด 644×488 พิกเซล เพื่อใช้เป็นแสงกระตุ้น และบันทึกภาพสเปคตรัมในย่านที่ต้องการ จากผลการทดลองแสดงให้เห็นว่า การเลือกค่า threshold การกรองและวิเคราะห์ด้วย เทคนิค blob ที่เหมาะสมในการวิเคราะห์ภาพเปล่งแสงของเมล็ดข้าว สามารถบ่งชี้ข้าวสารทั้ง 8 พันธุ์ได้อย่างมีนัยสำคัญ ในหัวข้อที่ 2 เราจะสาธิตให้เห็นว่า ภาพสเปคตรัมความยาวคลื่นเดียวสามารถใช้บ่งชี้ข้าวสารพันธุ์ ขาวดอกมะลิ 105 ได้ ในการศึกษานี้ เราจะใช้ภาพเปล่งแสงร่วมกับเทคนิคการประมวลผลภาพตามที่ระบุไว้ข้างต้น แล้วใช้วิธีการลบภาพที่ความยาวคลื่น 545 nm และ 575 nm ในการบ่งชี้ข้าวขาวดอกมะลิ 105 ผลการศึกษาพบว่า การระบุพันธุ์ข้าวขาวดอกมะลิ 105 มีอัตราการรับผิดพลาด (false acceptance rate) ในระดับปานกลางแต่ใช้เวลาในการตรวจสอบที่รวดเร็วคือ 25 ms ทำให้เห็นว่ามีความเป็นไปได้ที่จะนำไปใช้จริงในทางปฏิบัติ ในหัวข้อที่ 3 แทนที่จะพิจารณาความเข้มของการเปล่งแสงที่กระจายบนเมล็ดข้าวสาร หัวข้อนี้จะทำให้เห็นว่าการบ่งชี้ข้าวขาวดอกมะลิ 105 ด้วยภาพสเปคตรัมความยาวคลื่นเดียวสามารถปรับปรุงได้ด้วยการวิเคราะห์รูปร่างและขนาดของภาพเมล็ดข้าวแต่ละสายพันธุ์ของภาพ threshold ซึ่งรูปร่างและขนาดของภาพเมล็ดข้าวแต่ละสายพันธุ์จะถูกอธิบายด้วยการทำ chain code และ การอธิบายด้วยฟูเรียร์เชิงวงรี (elliptic Fourier descriptor, EFD) แล้วใช้โครงข่ายประสาทเทียมเป็นตัวบ่งชี้ ผลการศึกษาพบว่าค่าอัตราการรับผิดพลาด เท่ากับ 11.0% และค่าอัตราการคัดออกผิดพลาด เท่ากับ 19.0% ในการระบุข้าวขาวดอกมะลิ 105 ออกจากพันธุ์อื่น ๆ ในหัวข้อที่ 4 แทนที่จะใช้ EFD ที่ซับซ้อน เราจะทำให้เห็นว่าเพียงแค่การฟิตด้วยฟังก์โพลิโนเมียล (polynomial function fitting) บน chain code และการใช้โครงข่ายประสาทเทียม ทำให้ได้ค่าอัตราการรับผิดพลาดและค่าอัตราการคัดออกผิดพลาด ที่ต่ำมาก คือ น้อยกว่า 3.0% และ 0.3% ตามลำดับ ในการแยกพันธุ์ข้าวขาวดอกมะลิ 105 ออกจาก ชัยนาท 1 ปทุมธานี1 และ หอมพิษณุโลก 2 และด้วยวิธีการนี้เวลาที่ใช้ในการวิเคราะห์ลดลงจาก 4,250 s เป็น 2 s ชี้ให้เห็นว่ามีศักยภาพสูงมากที่จะพัฒนาในทางปฏิบัติ สุดท้าย เราจะเน้นย้ำให้เห็นว่า การใช้ฟังก์โพลิโนเมียล บน chain code การออกแบบและฝึกโครงข่ายประสาทเทียมที่ดี มีประสิทธิภาพที่สูงเพียงพอที่จะให้ค่าอัตราการรับผิดพลาดและค่าอัตราการคัดออกผิดพลาดที่ต่ำ ในการทดลองเชิงปฏิบัติพบว่าการบ่งชี้ข้าวขาวดอกมะลิออกจากพันธุ์อื่นๆ อีก 6 สายพันธุ์ได้ค่า ค่าอัตราการรับผิดพลาดและค่าอัตราการคัดออกผิดพลาด คือ 6.2% และ 7.1% ตามลำดับ

คำสำคัญ : สเปคโตรสโคปี การวัดดัชนีหักเหของแสง ภาพสเปคตรัม ภาพฟลูออเรสเซนต์ การประมวลผลภาพ การวิเคราะห์ด้วย Blob รหัสลูกโซ่ การอธิบายด้วยฟูเรียร์แบบวงรี โครงข่ายประสาทเทียม และ ข้าว

This material is reserved for educational use only, not allowed for commercial use.
Forbidden to modify the content, and cite the document when use.

Thesis Title	OPTICAL METHODS FOR IDENTIFYING THAI JASMINE RICE
Student	Mr. Kajpanya Suwansukho
Student ID	51067001
Degree	Doctor of Philosophy
Program	Applied Physics
Thesis Advisor	Dr. Prathan Buranasiri
Co – Thesis Advisor	Dr. Sarun Sumriddetchkajorn

ABSTRACT

In this dissertation, destructive and nondestructive optical investigation methods for identifying Thai jasmine milled rice have been presented by spectrometry and refractrometry in cooperation with chemical technique. In the spectrometry method, instead of using traditional time consuming methods based on the disintegration of the rice kernel in an alkali solution, we analyze the milled rice powder dissolved in the alkali solution via a spectroscopic method. In this study, four Thai rice varieties, Kaw Dawk Mali 105 (KDML105), Pathumthani1 (PTT1), Chainat1 (CNT1), and Thai sticky rice (RD6), have been chosen. Then each milled rice sample is grounded and then dissolved in 10% potassium hydroxide (KOH). At a certain time of dissolution, the relative optical transmission spectrum of the milled rice solution at wavelength of 500-800 is measured and only its first derivative is used for the identification of the KDML105 milled rice. We have founded that the best condition is 0.10 g milled rice powder dissolved in 10% KOH for 10 minutes, provides the lowest false rejection rate (FRR) of 15%. In the refractometry method, we analyze the ground milled rice grains dissolved in 10% KOH. The idea comes from the fact that due to differences in the amount of amylose content in each rice variety, the refractive index of the milled rice powder dissolved in the alkaline solution can be used to distinguish the desired KDML105 rice from others. The result shows that the milled KDML105 rice can be distinguished from the remaining three rice varieties with a total false error rate of 6.7% together with the required measurement time of < 20 seconds.

Nondestructive optical method is divided into four parts. First, this research combines multispectral imaging with simple imaging techniques. Especially, we exploit only two fluorescent wavelengths of 500-580 nm and utilize simple image thresholding, blob filtering, and blob analysis techniques in order to identify 8 different Thai rice breeds (i.e. KDML105, PTT1, CNT1, RD6, Hom Pitsanulok 2 (HPSL2), Hom Supanburi

This material is reserved for educational use only, not allowed for commercial use.
Forbidden to modify the content, and cite the document when use.

(HSPR), RD15, and RD23). In our experimental study, UVC light, a liquid crystal tunable optical filter, and a 644×488 active pixels digital camera have been used. The experimental result shows that by appropiately applying image thresholding, blob filtering, and blob analysis to fluorescent images, all Thai rice breeds have been effectively identified. Second, single-wavelength spectral-imaging-based Thai jasmine rice breed identification is demonstrated. Our nondestructive identification approach relies on a combination of fluorescent imaging and simple imaging technique as above mentioned. We apply image subtracting processes to either a 545 or a 575 nm image for identification. The result shown that the Thai jasmine rice breed has been identified with moderated false acceptance rates (FAR) and fast identification time of 25 ms, showing high potential for real-time applications. Third, instead of considering only the amount of fluorescent signals spatially distributed on the image of milled rice grains, this part shows how the single-wavelength spectral-imaging-based KDML105 milled rice identification system have been improved by analyzing the shape and size of the image of each milled rice variety especially during the image threshold operation. The image of each milled rice variety is expressed as chain codes and elliptic Fourier descriptor (EFD). After that, a feed-forward back-propagation neural network model is applied, resulting in an improved FAR of 11.0% and FRR of 19.0% for identifying KDML105 milled rice from the unwanted four milled rice varieties. Fourth, instead of use complex EFD, we highlighted that only a polynomial function fitting on the determined chain code and the neural network analysis are highly sufficient in obtaining a very low FAR of < 3.0% and a very low 0.3% FRR for the separation of Thai jasmine rice from CNT1, PTT1, and HPSL2 rice varieties. With this proposed approach, the analytical time is tremendously suppressed from 4,250 seconds down to 2 seconds, implying extremely high potential in practical deployment. Finally, we emphasized here that a combination of an appropriate polynomial fitting function on the determined chain code and a well-trained neural network configuration is highly sufficient in achieving a low FAR and FRR. Experimental demonstration shows promising results in identifying our desired KDML105 from six unwanted rice varieties with FAR and FRR values of 6.2% and 7.1%, respectively.

Keyword: Spectroscopy, Refractometry, Spectral imaging, Fluorescent imaging, Image processing, Blob analysis, Chain code, Elliptic Fourier descriptor, Polynomial function, and Artificial neural network, Rice

This material is reserved for educational use only, not allowed for commercial use.
Forbidden to modify the content, and cite the document when use.

ACKNOWLEDGEMENT

I would like to gratefully acknowledge the scholarship and support provided by Thailand Graduate Institute of Science and Technology (Grant No. TGIST 01–51-071) and Applied Physics Department, Science Faculty, King Mongkut's Institute Technology of Ladkrabang. Also, I would like to thank the Rice Research Institute at the Department of Rice, Ministry of Agriculture and Cooperatives for supplying rice samples.

I would like to take this opportunity to express my deep gratitude to my advisor and co-adviser, Dr. Prathan Buranasiri and Dr. Sarun Sumriddetchkajorn, for their constant help, support and guidance which has steered me toward my destination. Their enthusiasm and new ideas have motivated me to explore new areas in the field of optics.

I would like to thank Mr. Yutthana Intaravanne of Intelligent Devices and Systems Research Unit National Electronics and Computer Technology Center (NECTEC), Mr. Pornprasert Puttanarakul, Miss Kedsinee Katenuam, my colleagues, and my students at applied physics department which to be friend, brothers and sisters whose always supported and helped me.

I would like to express my sincere deeply thank to my parent for everything in my life.

Finally, I would like to really thank my share, lovely wife, which stand for me, always forgive for my mistake, and encourage me.

Kajpanya Suwansukho

May 29, 2014

This material is reserved for educational use only, not allowed for commercial use.

Forbidden to modify the content, and cite the document when use.

TABLE OF CONTENTS

		PAGE
ABSTRACT (THAI)		I
ABSTRACT (ENGLISH)		III
ACKNOWLEDGEMENT		V
TABLE OF CONTENTS		VI
LIST OF FIGURES		X
LIST OF TABLES		XVI
CHAPTER 1 INTRODUCTION		1
1.1	Motivation	1
1.2	Scope of Study	3
1.3	Expected Results	3
1.4	References	4
CHAPTER 2 THEORITICAL BACKGROUND		**5**
2.1	Ultraviolet, Visible, and Near-Infrared Spectrophotometer	5
	2.1.1 Absorption and Concentration	5
	2.1.1.1 Lambert's Law	5
	2.1.1.2 Beer's Law	6
2.2	Basic of Refractrometry	8
2.3	Binary Image Analysis	9
	2.3.1 Binary Large Object	10
	2.3.1.1 Image Thresholding	10
	2.3.1.2 Image Analysis	11
2.4	Chain Coding	12
2.5	Elliptic Fourier Descriptor	14
2.6	Polynomial Function	16
2.7	Shape Analysis	17
2.8.1	Neural Network Analysis	18

This material is reserved for educational use only, not allowed for commercial use.
Forbidden to modify the content, and cite the document when use.

2.8.1 Artificial Neural Network Structure 19
2.8.2 Artificial Neural Network Operation 19
2.8.3 Artificial Neural Network Learning 20
2.8.4 Backpropagation Neural Network Structure 21
2.9 Reference 23
CHAPTER 3 DESTRUCTIVE OPTICAL METHODS 26
3.1 Combination of Simple Chemical and Spectroscopic Methods for the Identification of Thai Hom Mali Rice 25
3.1.1 Materials and Method 26
3.1.1.1 Materials 26
3.1.1.2 Sample Preparation 26
3.1.1.3 Spectrum Measurement 27
3.1.1.4 Data Analysis 28
3.1.2 Results and Discussion 28
3.1.2.1 Visual Inspection 28
3.1.2.2 Spectral Measurement 29
3.2 Identification of Thai Hom Mali Rice using a Refractometer 36
3.2.1 Proposed Method 36
3.2.2 Experimental Prove of Concept 37
3.2.2.1 Refractive Index Measurement 37
3.2.2.2 KDML105 Identification 38
3.3 References 40
CHAPTER 4 NON-DESTRUCTIVE OPTICAL METHODS 41
4.1 Two-Wavelength Spectral Imaging-based Thai Rice Breed Identification 41
4.1.1 Proposed two-wavelength spectral imaging-based rice breeds identifier 41
4.1.1.1 Architecture of the system 41
4.1.1.2 Procedures of analysis 43
4.1.2 Experimental demonstration 44

This material is reserved for educational use only, not allowed for commercial use.
Forbidden to modify the content, and cite the document when use.

4.1.2.1 Experimental setup 44
4.1.2.2 Analysis 46
4.2 Demonstration of a single-wavelength spectral-imaging-based Thai jasmine rice identification 50
4.2.1 Single-Wavelength Spectral-Imaging-Based KDML105 Milled Rice Breed Identifier 50
4.2.1.1 Architecture of the System 50
4.2.1.2 Analytical Procedures 51
4.2.2 Experimental Demonstration 52
4.2.2.1 Experimental Setup 52
4.2.3 Results and Discussions 53
4.2.3.1 Fluorescent Signals 53
4.2.3.2 Analysis 55
4.3 Improvement of Single-Wavelength based Thai Jasmine Rice Identification with Elliptic Fourier Descriptor and Neural Network Analysis 59
4.3.1 Single-wavelength based Thai jasmine milled rice variety identifier 59
4.3.2 Image Analysis 60
4.3.3 Demonstration 61
4.3.3.1 Prototype Setup 61
4.3.3.2 Materials 63
4.3.4 Results and Discussion 64
4.4 Single-Wavelength based Thai Jasmine Rice Identification with Polynomial Fitting Function and Neural Network Analysis 67
4.4.1. Introduction 67
4.4.2 Image analysis 67
4.4.3 Materials 67
4.4.4. Results and Discussion 68
4.4.5 Experimental Demonstration 71
4.4.5.1 Materials 72

This material is reserved for educational use only, not allowed for commercial use.
Forbidden to modify the content, and cite the document when use.

4.4.5.2 Experimental Results 72

4.5 References 76

CHAPTER 5 SUMMARY 80

APPENDIX A 82

APPENDIX B 84

APPENDIX C 87

APPENDIX D 94

APPENDIX E 97

APPENDIX F 99

APPENDIX H 107

This material is reserved for educational use only, not allowed for commercial use.
Forbidden to modify the content, and cite the document when use.

LIST OF FIGURES

	PAGE
Figure 1.1 7 dissolved levels of alkaline spreading method.	1
Figure 1.2 completely dissolved KDML105 compare to RD23 and CNT1	2
Figure 1.3 Color lightly sticks on KDML105 compare to the other milled rice variety	2
Figure 1.4 completely and incompletely rice cooked by boiled rice method	3
Figure 2.1 Diagrammatic representation of relationship between transmission and absorption	6
Figure 2.2 Transmission plotted against concentration	7
Figure 2.3 Absorbance plotted against concentration	7
Figure 2.4 Light crossing from any transparent medium into another in which it has a different speed, is refracted, i.e., bent from its original path. In the case shown, the speed of light in medium A is greater than the speed of light in medium B	9
Figure 2.5 Ellipse shape of rice grain for defined area and perimeter	11
Figure 2.6 Ellipse shape of rice grain for defined ratio of equivalent ellipse axes and Elongation factor	12
Figure 2.7 (a) Binary pixels of a shape pattern with a differential chain code sequence of 00000000707766554544444444343432210101 starting from upper left hand corner and (b) eight connected grids	13
Figure 2.8 Illustration of the parameters used for computing the Fourier coefficients of an EFD on an outline	15
Figure 2.9 Diagram of common neural network procedure	18
Figure 2.10 Simple ANN structure	19
Figure 2.11 Neural weights adjustment	20
Figure 3.1 shows four Thai rice varieties (a) KDML105, (b) CNT1, (c) PTT1, and (d) RD6 used in our study	26
Figure 3.2 a) Laboratory grinder and b) grind ball	27
Figure 3.3 4-digits weighing machine	27
Figure 3.4 (a) The UV/VIS spectrometer and (b) Inside view of spectrometer box	28

This material is reserved for educational use only, not allowed for commercial use.
Forbidden to modify the content, and cite the document when use.

Figure 3.5 shows 2 ml of our milled rice solutions for 0.10 g of (a) KDML105, (b) CNT1, (c) PTT1, and (d) RD6 rice varieties. Images from left to right are for our 10% KOH solution followed by the 5th, 10th, 15th, and 20th minutes of observation, respectively. A black solid line is used to show turbidity of the solution 29

Figure 3.6 shows 2 ml of our milled rice solutions for 0.20 g of (a) KDML105, (b) CNT1, (c) PTT1 and (d) RD6 rice varieties. Images from left to right are for our 10% KOH solution followed by the 5th, 10th, 15th, and 20th minutes of observation, respectively. A black solid line is used to show turbidity of the solution 29

Figure 3.7 shows 2 ml of our milled rice solutions for 0.30 g of (a) KDML105, (b) CNT1, (c) PTT1 and (d) RD6 rice varieties. Images from left to right are for our 10% KOH solution followed by the 5th, 10th, 15th, and 20th minutes of observation, respectively. A black solid line is used to show turbidity of the solution 29

Figure 3.8 Example of measured relative transmission spectra for 0.10 g of the milled rice powder dissolved in our 10% KOH solution for 5 minutes. 30

Figure 3.9 Measured relative optical transmittance of 0.10 g of the milled rice powder dissolved in our 10% KOH solution for four rice varieties at the (a) 5th, (b) 10th, (c) 15th, and (d) 20th minutes of our measurements 30

Figure 3.10 Slope values calculated from the measured relative optical transmittance of 0.10 g of the milled rice powder dissolved in our 10% KOH solution for (a) 5 minutes, (b) 10 minutes, (c) 15 minutes, and (d) 20 minutes 31

Figure 3.11 Measured relative optical transmittance of 0.20 g of the milled rice powder dissolved in our 10% KOH solution for four rice varieties at the (a) 5th, (b) 10th, (c) 15th, and (d) 20th minutes of our measurements 32

Figure 3.12 Slope values calculated from the measured relative optical transmittance of 0.20 g of the milled rice powder dissolved in our 10% KOH solution for (a) 5 minutes, (b) 10 minutes, (c) 15 minutes, and (d) 20 minutes 33

Figure 3.13 Measured relative optical transmittance of 0.30 g of the milled rice powder dissolved in our 10% KOH solution for four rice varieties at the (a) 5th, (b) 10th, (c) 15th, and (d) 20th minutes of our measurements 34

This material is reserved for educational use only, not allowed for commercial use.
Forbidden to modify the content, and cite the document when use.

Figure 3.14 Slope values calculated from the measured relative optical transmittance of 0.30 g of the milled rice powder dissolved in our 10% KOH solution for (a) 5 minutes, (b) 10 minutes, (c) 15 minutes, and (d) 20 minutes 34

Figure 3.15 (a) Proposed method where we combine chemical and optical techniques for identifying the KDML105 milled rice and (b) The ATAGO refractrometry and perspective view of liquid droplet channel which black cover was opened 36

Figure 3.16 Measured refractive index differences of CNT1, PTT1 and RD6 milled rice solutions compared to the KDML105 milled rice solution for (a) 0.1 grams, (b) 0.2 grams, and (c) 0.3 grams of the milled rice powder 38

Figure 3.17 Measured refractive index values of 0.1 grams of KDML105, CNT1, PTT1 and RD6 milled rice powders each dissolved in 10 ml of our 10% KOH solution for 5 minutes 39

Figure 4.1 Structure of our proposed multispectral imaging-based rice breed identification system 42

Figure 4.2 Flowchart for analysis of spectral images in order to identify breeds of all milled rice Grains 43

Figure 4.3 Experimental setup for milled rice breed identification 44

Figure 4.4 Eight breeds of Thai milled rice grains 45

Figure 4.5 (a) Fluorescent image emitted from all milled rice grains under UVC illumination and (b) fluorescent signals 45

Figure 4.7 Fluorescent images of milled rice grains from eight rice breeds at 540 nm and 575 nm Wavelengths 46

Figure 4.7 Results of image manipulation through image thresholding and blob filtering processes for the fluorescent image at 540 nm. (a) Thresholding interval (T) of 30-150 and blob filtering (B) between 660 and 4000 pixels. (b) T = 29-150, B = 400-4000 pixels 46

Figure 4.8 Results of image manipulation through image thresholding and blob filtering for the fluorescent image at 575 nm with different thresholding (T) and blob filtering (B) levels. (a) T = 39-150, B = 30-4000 pixels, (b) T = 33-150, B = 455-4000 pixels, (c) T = 30-150, B = 900-4000 pixels, (d) T = 29-150,

This material is reserved for educational use only, not allowed for commercial use.
Forbidden to modify the content, and cite the document when use.

B = 1200-4000 pixels, (e) T = 28-150, B = 550-4000 pixels, and (f) T = 27-150, B = 400-4000 pixels 47

Figure 4.9 All milled rice breeds are identified from the two fluorescent images at 540 nm and 575 nm wavelengths. (a) RD6, (b) KDML105, (c) HSPR60, (d) PTT1, (e) RD15, (f) RD23, (g) CNT1, and (h) HPSL2 48

Figure 4.10 Structure of our single-wavelength spectral imaging-based KDML105 milled rice breed identification system 50

Figure 4.11 Flowchart for analysis of the selected spectral image in order to identify KDML105 milled rice grains 51

Figure 4.12 Experimental setup for KDML105 milled rice breed identification: (a) diagram and (b) perspective view 52

Figure 4.13 Close-up view of Thai milled rice grains (a) CNT1, (b) HPSL2, (c) HSPR60, (d) KDML105, (e) PTT1, (f) RD6, (g) RD15, and (h) RD23 53

Figure 4.14 Arrangement of milled rice grains for (a) Set A and Set B and (b) Set C 54

Figure 4.15 (a) Normalized fluorescent signal measured at the center of each milled rice grain under the UVC illumination. (b) Normalized fluorescent images at 545 nm (top) and 575 nm (bottom) wavelengths for three arrangements of milled rice grains 54

Figure 4.16 Example of the normalized spectral image at 545 nm wavelength after it goes through (a) image thresholding, (b) area filtering, (c) perimeter filtering, (d) RE filtering, and (e) EF filtering. Our first and second image filtering processes are applied to images on the left hand side and in the middle, respectively. Mark red signs correspond to locations of KDML milled rice grains 55

Figure 4.17 Example of the normalized spectral image at 575 nm wavelength after it goes through (a) image thresholding, (b) area filtering, (c) perimeter filtering, (d) RE filtering, and (e) EF filtering. Our first and second image filtering processes are applied to images on the left hand side and in the middle, respectively. Mark red signs correspond to locations of KDML105 milled rice grains 57

This material is reserved for educational use only, not allowed for commercial use.
Forbidden to modify the content, and cite the document when use.

Figure 4.18 Structure of single-wavelength spectral-imaging based KDML105 milled rice breed identification 60

Figure 4.19 Prototype of our spectral imaging system for KDML105 milled rice breed Identification 62

Figure 4.20 Light uniformity measurement (a) 50 mm-diameter of active area with line intensity measured on white balance material and (b) gray scale value of each line on white balance material which related to light intensity measured by LabVIEW programming. 62

Figure 4.21 Close-up view of Thai milled rice grains (a) CNT1, (b) HPSL2, (c) KDML105, and (d) PTT1 used in our demonstration 63

Figure 4.22 (a) Arrangement of milled rice grains on a black rice tray, (b) a spectral image of milled rice grains, and (c) a normalized spectral image of milled rice grains 63

Figure 4.23 Eleven threshold images under different levels of the lower threshold 64

Figure 4.24 Seventeen normalized EFD harmonics of the "threshold 30" in Fig. 3.24 64

Figure 4.25 PCA of milled rice grain geometry 65

Figure 4.26 Training results of each data pair (a) CNT1-KDML105, (b) HPSL2-KDML105, and (c) PTT1-KDML105 66

Figure 4.27 Testing results of each data pair (a) CNT1-KDML105, (b) HPSL2-KDML105, and (c) PTT1-KDML105 66

Figure 4.28 Zoomed image of Thai milled rice grains (a) CNT1, (b) HPSL, (c) KDML105, and (d) PTT1 used in our demonstration 68

Figure 4.29 (a) 235×305 image size of a spectral image of milled rice grains and (b) a threshold image of milled rice grains 68

Figure 4.30 (a) Boundary of the threshold image computed from the chain coding process. (b-c) Line segments of the image boundary projected on the x and y axes, respectively 69

Figure 4.31 Fitted line segments of the travelling distances along the (a) x axis and (b) y axis. (c) Reconstructed image contour from the fitted line segments in (a) and (b) 70

This material is reserved for educational use only, not allowed for commercial use.
Forbidden to modify the content, and cite the document when use.

Figure 4.32 Training results of each data pair (a) CNT1-KDML105, (b) HPSL-KDML105, and (c) PTT1-KDML105 71

Figure 4.33 Testing results of each data pair (a) CNT1-KDML105, (b) HPSL2-KDML105, and (c) PTT1-KDML105 71

Figure 4.34 Zoomed images of Thai milled rice grains from six varieties: (a) CNT1, (b) HPSL2, (c) HSPR60, (d) KDML105, (e) PTT1, (f) RD15, and (g) RD23 72

Figure 4.35 Plotted graphs of the extracted (a) perimeter, (b) area, and (c) eccentricity parameter 73

Figure 4.36 Principal component analysis of three shape parameters 74

Figure 4.37 FFNN results during (a) the training period and (b) test with the unknown data set 75

Figure 4.38 Examples of two spectral images used during field operation tests 75

Figure 4.39 Testing results of KDML105 identification in practice 75

King Mongkut's Institute of Technology Ladkrabang

This material is reserved for educational use only, not allowed for commercial use.
Forbidden to modify the content, and cite the document when use.

LIST OF TABLES

	PAGE
Table 3.1 KDML105 identification performance	35
Table 4.1 Parameters used during our image filtering processes for the selected 545-nm fluorescent image	56
Table 4.2 Parameters used during our image filtering processes for the selected 575-nm fluorescent image	58
Table 4.3 Average values of three shape parameters	73

King Mongkut's Institute of Technology Ladkrabang

This material is reserved for educational use only, not allowed for commercial use.
Forbidden to modify the content, and cite the document when use.

CHAPTER 1

INTRODUCTION

1.1 Motivation

It is known that Thai jasmine rice, also called Kaw Dawk Mali 105 (KDML105), is one of the best rice breed in the world. In October 2013, its economic value reached up to 4.70 billion Baht [1]. Recently, there have increasingly been intentional impurities of KDML105 milled rice products with other lower price foreign rice varieties as well as other lower price Thai rice varieties, such as Chainat 1 (CNT1), Hom Pitsanulok 2 (HPSL2), Hom Supanburi 60 (HSPR60), Pathumthani 1 (PTT1), Ko Kor 15 (RD15), and Ko Kor 23 (RD23). Although these rice varieties have similar physical characteristics, they are different in cooking qualities and nutrient contents, leading to unqualified KDML105 milled rice grain products for export and unwanted unmilled rice seeds for next plants. Chemical methods were used to inspection KDML105 milled rice by using different amylose content characteristic of each milled rice varieties. First, alkaline spreading values [2], 1.7% potassium hydroxide concentration was used to dissolving milled rice varieties which dissolution levels were divided into particularly seven levels as shown in Fig. 1.1 and KDML105 was completely dissolved in 23 hours compare to the other rice varieties (see Fig. 1.2).

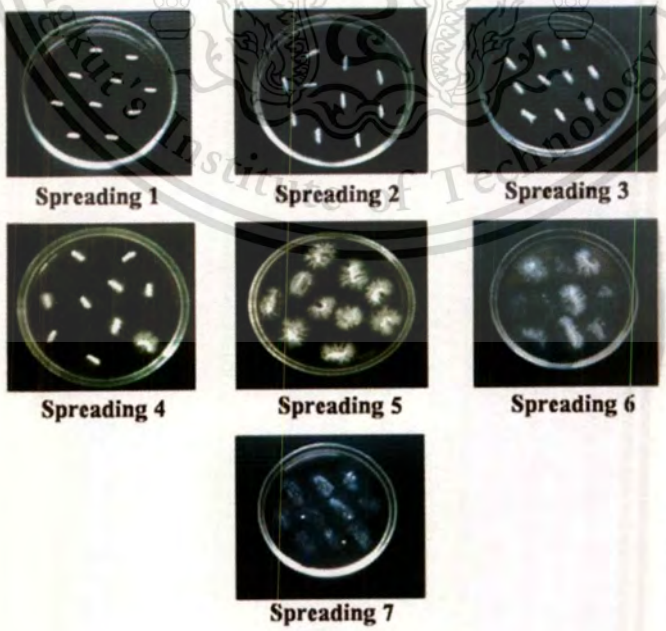

Figure 1.1 7 dissolved levels of alkaline spreading method [3].

This material is reserved for educational use only, not allowed for commercial use.
Forbidden to modify the content, and cite the document when use.

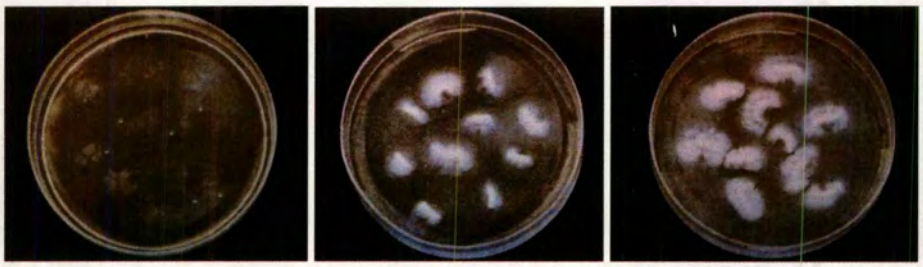

Figure 1.2 Completely dissolved KDML105 compare to RD23 and CNT1 [2].

Second, dyeing method [2], this method used several chemical solutions and procedures to dyeing milled rice which the result shown that dye color has little struck on KDML105 compare to the other rice varieties with have high amylose content as shown in Fig.1.3

Figure 1.3 Color lightly sticks on KDML105 compare to the other milled rice variety [2].

Finally, boiled rice method, this technique used a characteristic of cooked rice with different time to identify KDML105 milled rice. At specific boiling time and pressed by mirror plate, KDML105 has been shown completely cooked while the other has been incompletely cooked as shown in Fig. 1.4. Another method, DNA technology [4] was used to identify KDML105 with high accuracy testing as known. However, chemical and biological methods are time consuming, complex procedure, and expensive. In addition, these unwanted added rice varieties have similar shape and color to the KDML105 rice. Y. Liu et al [5] had been proposed a technique using machine vision and neural network to identify 5 Chinese rice seeds. The result shown that

This material is reserved for educational use only, not allowed for commercial use.
Forbidden to modify the content, and cite the document when use.

differently seed shapes had accuracy identification more than 90%. However, similarly seed shapes had accuracy identification about 70%. In addition, T. Kaveemongkolrat et al [6] had been reported to identification KDML105 from CNT1, PTT1 and HSPR by using simple image processing and principle component analysis. The results shown that percentage error to classification KDML105 from the others rice varieties had values between 43.0% - 86.5%. This implies that a simple image processing and machine vision technique [7-10] cannot be used to separate these rice varieties from each other.

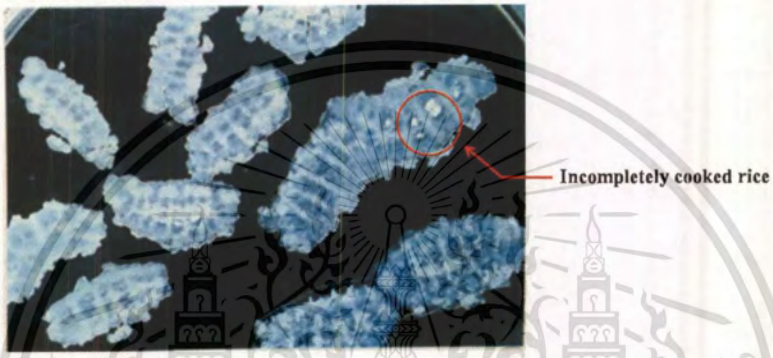

Figure 1.4 Completely and incompletely rice cooked by boiled rice method [2].

Therefore, the dissertation is focused on the study and the development of destructive and nondestructive techniques using optical techniques to identification the KDML105 milled rice variety from the other milled rice varieties.

1.2 Scope of Study

The scope of this study is as follow,

1.2.1 To study the spectroscopy method for identify the KDML105 milled rice variety.

1.2.2 To study the refractrometry method for identify the KDML105 milled rice variety.

1.2.3 To study the multispectral imaging techniques of the milled rice varieties.

1.2.4 To study the image processing methods for identify the milled rice varieties.

1.2.5 To identification KDML105 with accuracy more than 85%.

1.2.6 To develop a prototype use in the research laboratory.

This material is reserved for educational use only, not allowed for commercial use.
Forbidden to modify the content, and cite the document when use.

1.3 Expected Results

The destructive and nondestructive optical methods to identify the KDML105 milled rice variety were studied with the key features of simplicity technique, less or no waste product, fast identification time, moderate or high accuracy, and reliability technique. A prototype of KDML105 milled rice identification was developed.

1.4 References

[1] Office of Agriculture Economics, Ministry of Agriculture and Cooperatives, Thai Government, http://www.oae.go.th/oae_report/export_import/export.php, accessed on Dec. 15, (2013).

[2] N. Kongseri, J. Bangvarg, K. Cheapun, S. Wongpiyachon, V. Sukvivat, P. Sawangjit, and S. Tangvisuttijit, **Quality and investigation of Thai jasmine rice**, academic agriculture department, ministry of agriculture and cooperatives, ISBN 974-436-343-6 (2004).

[3] อรอนงค์ นัยวิกุล, **ข้าว : วิทยาศาสตร์และเทคโนโลยี** , กรุงเทพฯ : สำนักพิมพ์มหาวิทยาลัยเกษตรศาสตร์ , บทที่ 6 (2556)

[4] A. Vanavichit, S. Tragoonrung, and T. Toojinda, "Biotechnology and rice varieties improvement," Chap.4 in Science and Technology with Thai Rice, Thailand's National Science and Technology Development Agency, June (2003).

[7] A. J. Cullen, R. C. Hoseney, and J. M. Faubion, "Identification of wheat cultivars by visual imaging," *US Patent*, 5321764, Jun. 14, (1994).

[8] Y.- N. Wan, "Grain sorting method and a device thereof," *US Patent*, 5973286, Oct. 26, (1999).

[9] E. G. Kokko and B. D. Hill, "Method and apparatus for identifying and quantifying characteristics of seeds and other small objects," *US Patent*, 7218775, May 15, (2007).

[10] Y. Liu, A. Ouyang, J. Wu, and Y. Ying, "An automatic method for identifying different variety of rice seeds using machine vision technology," *Proc. SPIE* **5996**, pp. 59961H (2005).

[5] L. Z. Yan, C. Fang, Y. Y. Bin, and R. X. Qin, "Identification of rice seed varieties using neural network," J. Zhejiang Univ: SCI. 6B, **11**, pp.1095-1100 (2005).

[6] ทิศากร กวีมงคลรัตน์, พลนน อ่อนไสว, วุฒินันท์ สาทสุทธิ และ ปานมนัส ศิริสมบูรณ์, "**การจำแนกพันธุ์ข้าวในประเทศไทยเฉพาะพันธุ์ที่มีการปลอมปนโดยวิธี** Image processing," ปริญญานิพนธ์ (วศ.บ. (วิศวกรรมเกษตร)), ปพ.519ก, สถาบันเทคโนโลยีพระจอมเกล้าเจ้าคุณทหารลาดกระบัง, (2551)

This material is reserved for educational use only, not allowed for commercial use.
Forbidden to modify the content, and cite the document when use.

CHAPTER 2

THEORITICAL BACKGROUD

2.1 Ultraviolet, Visible, and Near-Infrared Spectrophotometer

Spectrophotometers for the ultraviolet (UV), visible (Vis), and near-infrared (NIR) regions will be discuss in this chapter. Typically, the UV region is considered to extend from 190 to 350 nm, the visible region from 350 to 800 nm, and the NIR from 800 to 2500 nm. However, considerable latitude can be found in the definitions of these regions; the UV might be extended up to 400 nm and the short wavelength NIR from 600 to 1100 nm. The total wavelength range from 190 to 2500 nm is equivalent to a frequency range of 50, 500-4000 cm^{-1}. Absorptions in the UV-Vis regions are due to electronic transitions. Most UV-Vis absorptions by organic molecules are attributed to transition involving nonbonding (n) electrons or electrons in molecular orbitals found in unsaturated molecules. Generally, the absorptions are due to $n \rightarrow \pi^*$ and $\pi \rightarrow \pi^*$ transitions; thus, molecules with double bonds and especially conjugated double bonds such as aromatic compounds are stronger absorbers.

2.1.1 Absorption and Concentration

2.1.1.1 Lambert's Law

The proportion of incident light absorbed by a transparent medium is independent of the intensity of the light (provided that there is no other physical or chemical change to the medium). Therefore successive layers of equal thickness will transmit an equal proportion of the incident energy as shown in Fig. 2.1. Lambert's law is expressed by

$$T = \frac{I}{I_0}. \tag{2.1}$$

where I is the intensity of the transmitted light, I_O is the intensity of the incident light, and T is the transmittance. It is customary to express transmittance as a percentage

$$T = \frac{I}{I_0} \times 100. \tag{2.2}$$

This material is reserved for educational use only, not allowed for commercial use.
Forbidden to modify the content, and cite the document when use.

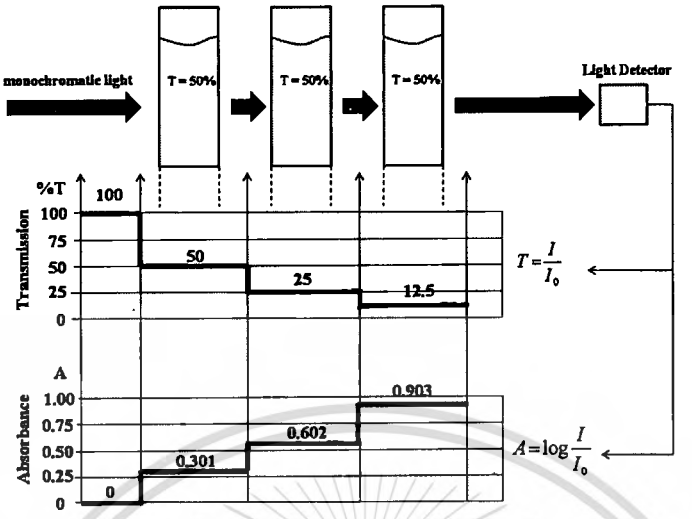

Figure 2.1 Diagrammatic representation of relationship between transmission and absorption.

2.1.1.2 Beer's Law

The absorption of light is directly proportional to both the concentration of the absorbing medium and the thickness of the medium in the light path (see Fig. 2.1). A combination of the two laws (known jointly as the Beer-Lambert Law) defines the relationship between absorbance (A) and transmittance (T)

$$A=\log\frac{I}{I_0}=\log\frac{100}{T}=\varepsilon cb \cdot \qquad (2.3)$$

where A is absorbance (no unit of measurement), ε is molar absorptivity (dm^3 mol^{-1} cm^{-1}), c is molar concentration (mol dm^{-3}), and b is path length (cm). It is important to note that ε is a function of wavelength and so the Beer-Lambert law is true only for light of a single wavelength, or monochromatic light. Fig. 2.1 illustrates the conditions when three samples (e.g. standard solutions) having identical absorption are introduced into a beam of monochromatic light. Each of the samples is chosen so that precisely one half of the intensity of the incident radiation is transmitted (T = 50%). If the intensity of the incident radiation is 100%T, then the intensity after passed through each sample will be 100% x 0.5 = 50%T, 50% x 0.5 = 25%T, and 25% x 0.5 = 12.5%T, respectively. The three samples may be considered as known concentrations of an absorbing medium and it therefore becomes possible to plot concentration against transmission. It will be found that the resultant graph is exponential, and so of limited value (Fig. 2.2).

This material is reserved for educational use only, not allowed for commercial use.
Forbidden to modify the content, and cite the document when use.

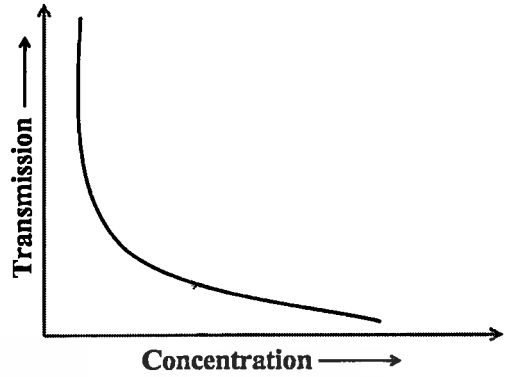

Figure 2.2 Transmission plotted against concentration.

However, providing the light is monochromatic and the Beer-Lambert law is obeyed, it becomes possible to define the process in terms of absorbance (A). In the example above, the expression relating A to T (A = log 100 / T) shows that the absorbance after each sample will be 0.301, 0.602, and 0.903, respectively. It can at once be seen that a plot of absorbance against concentration will be linear as shown in Fig. 2.3. It is therefore more convenient to express results in absorbance rather than transmission when measuring unknown concentrations, since linear calibration plots will be available.

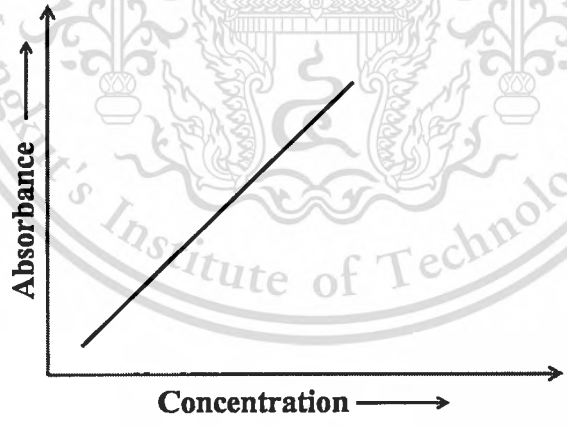

Figure 2.3 Absorbance plotted against concentration.

An alternative to plotting calibration curves is to make use of the relationship of

$$C = k A \tag{2.4}$$

This material is reserved for educational use only, not allowed for commercial use.
Forbidden to modify the content, and cite the document when use.

where C is the concentration of the unknown, A is the measured absorbance of the unknown, and k is a factor derived from the reference or standard solution. To determine the factor, measure the absorbance of a standard solution of known concentration and divide the concentration by the absorbance.

$$k = \frac{Concentration}{Absorbance}. \tag{2.5}$$

The factor k may be applied to a series of absorbance measurements on similar solutions measured in the same conditions to give results directly in concentration. In many of today's spectrophotometers, the output electronics provide the means of entering the concentration value of the standard or the factor to the calculation so that instrument readings are directly in concentration units.

2.2 Basic of Refractrometry

The speed of light in a vacuum is always the same, but when light moves through any other medium it travels more slowly since it is constantly being absorbed and reemitted by the atoms in the material. The ratio of the speed of light in a vacuum to the speed of light in another substance is defined as the index of refraction (n) for the substance.

$$n = \frac{Speed\ of\ Light\ in\ Vaccum}{Speed\ of\ Light\ in\ Substance}. \tag{2.6}$$

Whenever light changes speed as it crosses a boundary from one medium into another its direction of travel also changes, i.e., it is refracted (Fig. 2.4). (In the special case of the light traveling perpendicular to the boundary there is no change in direction upon entering the new medium.) The relationship between light's speed in the two mediums (v_A and v_B), the angles of incidence (θ_A) and refraction (θ_B) and the refractive indexes of the two mediums (n_A and n_B) is shown below:

This material is reserved for educational use only, not allowed for commercial use.
Forbidden to modify the content, and cite the document when use.

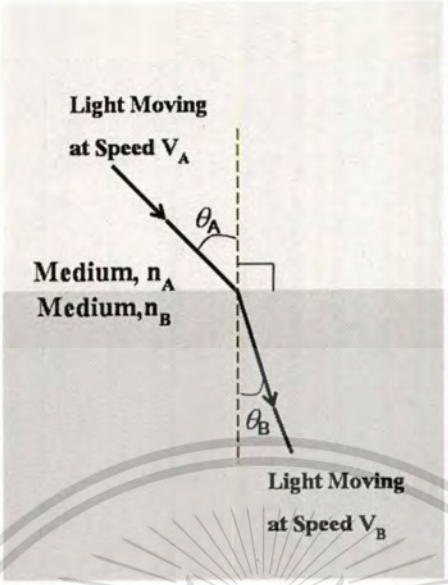

Figure 2.4 Light crossing from any transparent medium into another in which it has a different speed, is refracted, i.e., bent from its original path. In the case shown, the speed of light in medium A is greater than the speed of light in medium B.

$$\frac{V_A}{V_B} = \frac{\sin\theta_A}{\sin\theta_B} = \frac{n_B}{n_A}. \tag{2.7}$$

Thus, it is not necessary to measure the speed of light in a sample in order to determine its index of refraction. Instead, by measuring the angle of refraction, and knowing the index of refraction of the layer that is in contact with the sample, it is possible to determine the refractive index of the sample quite accurately. Nearly all refractometers utilize this principle, but may differ in their optical design.

2.3 Binary Image Analysis

Binary images are images whose pixels have only two possible intensity values. They are normally displayed as black and white. Numerically, the two values are often 0 for black, and either 1 or 255 for white. Binary images are often produced by thresholding a grayscale or color image, in order to separate an object in the image from the background. The color of the object (usually white) is referred to as the foreground color. The rest (usually black) is referred to as the background color. However, depending on the image which is to be thresholded, this polarity might be inverted, in which case the object is displayed with 0 and the background is with a non-zero value. The division of an image into meaningful structures, image

This material is reserved for educational use only, not allowed for commercial use.
Forbidden to modify the content, and cite the document when use.

segmentation, is often an essential step in image analysis, object representation, visualization, and many other image processing tasks.

2.3.1 Binary Large Object

The former process is known as Blobextraction and the latter as Blob classification. Blob stands for binary large object and refers to a group of connected pixels in a binary image. The term large indicates that only objects of a certain size are of interest and that small binary objects are usually noise. The title of the topic refers to analysis binary images by first extracting the Blobs, then representing them compactly, and finally classifying the type of each Blob. The basic of the Blob analysis are described below.

2.3.1.1 Image Thresholding

Segmentation involves separating an image into regions (or their contours) corresponding to objects. We usually try to segment regions by identifying common properties. Or, similarly, we identify contours by identifying differences between regions (edges). The simplest property that pixels in a region can share is intensity. So, a natural way to segment such regions is through thresholding, the separation of light and dark regions. Thresholding creates binary images from grey-level ones by turning all pixels below some threshold to zero and all pixels about that threshold to one.

$$I'(x,y)=\begin{cases} 255, Th_{min} \le I(x,y) \le Th_{max} \\ 0, Otherwise \end{cases} \quad (2.8)$$

From Eq(2.8), if the gray scale value I(x, y) of each image pixel remains within the desired Th_{min} and Th_{max}, its new gray scale value $I'(x, y)$ will be changed to a maximum gray scale value (e.g., 255 for an 8-bit image). On the other hand, the new gray scale value $I'(x, y)$ of 0 will be assigned if the gray scale value I(x, y) is out of the desired range.

This material is reserved for educational use only, not allowed for commercial use.
Forbidden to modify the content, and cite the document when use.

2.3.1.2 Image Analysis

After thresholding, Blob filtering processes via area and perimeter analysis are applied in order to roughly eliminate unwanted pixels. Because milled rice grains have elliptical shape, the area and perimeter of each milled rice grain can be computed as

$$\text{Area} = \pi ab, \tag{2.9}$$

and

$$\text{Perimeter} = \pi\sqrt{2\left(a^2 + b^2\right)}, \tag{2.10}$$

respectively. Here, a and b are a semi-major axis and a semi-minor axis of the ellipse, respectively as shown in Fig.2.5. In this case, the interesting areas, whose shape falls within the desired range, will be kept. Similarly, we focus our interest in the image area inside the normalized image whose perimeter stays within the appropriate range.

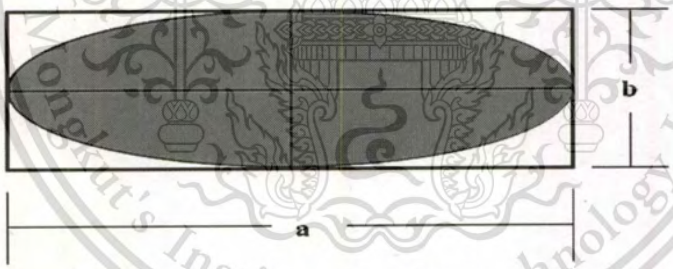

Figure 2.5 Ellipse shape of rice grain for defined area and perimeter.

Then, the other blob filtering processes via analysis of the ratio of equivalent ellipse axes (RA) and the elongation factor (EF) are applied in order to delicately eliminate the remaining unwanted pixels. RA can be simply written as

$$\text{RA} = \frac{a}{b}. \tag{2.11}$$

The EF of each milled rice grain can be calculated as follows.

This material is reserved for educational use only, not allowed for commercial use.
Forbidden to modify the content, and cite the document when use.

$$EF = \frac{FD_{max}}{\overline{PI}}, \tag{2.12}$$

where FD_{max}, the maximum Feret diameter, is the maximum distance between two tangents on opposite side of the interesting image area (Eqn. 2.12) and $\overline{PI}$ is the mean perpendicular intercept to the FD_{max} as shown in Fig.2.6. For each milled rice grain inside the normalized spectral image, it will be kept in the image if its RE and EF values are in the desired ranges.

$$FD_{max} = \sqrt{(F_{y2} - F_{y1})^2 + (F_{x2} - F_{x1})^2}. \tag{2.12}$$

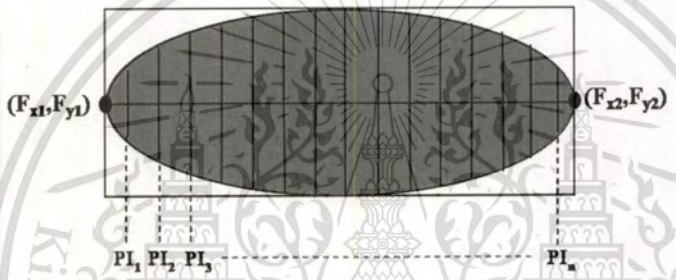

Figure 2.6 Ellipse like shape for rice grain for defined ratio of equivalent ellipse axes and elongation factor.

2.4 Chain Coding

The closed-contour is defined with Freeman chain codes [6-7], represented by a sequence of unit vectors and directional coding as shown in Fig. 2.7. Individual grain boundary pixels are used to describe the chain code, starting with the upper left pixel of the contour and tracing the boundary clockwise. The chain code enumeration is completed when the original starting point is reached. From Fig. 2.7(a), a chain code of 00000000707766554544444444343432210101 is obtained by following code directions in Fig. 2.7(b). It can be assumed that a point at the starting position is travelling along the image boundary with a constant speed. The time used to travel between links depending on the code of the chain which is mathematically written as in Eqn.(2.13).

This material is reserved for educational use only, not allowed for commercial use.
Forbidden to modify the content, and cite the document when use.

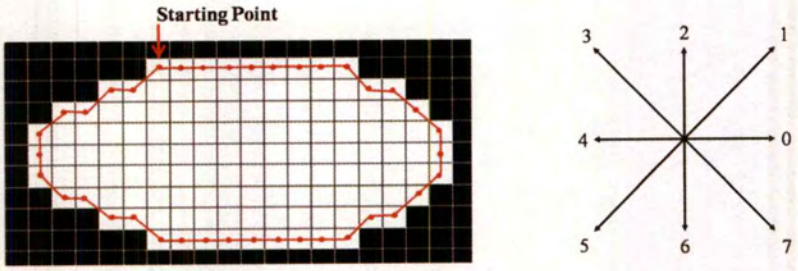

(a) (b)

Figure 2.7 (a) Binary pixels of a shape pattern with a differential chain code sequence of 000000007077665545444444443434322101 01 starting from upper left hand corner and (b) eight connected grids [9].

$$\Delta t_i = 1 + \left(\frac{\sqrt{2}-1}{2}\right)\left(1-(-1)^{a_i}\right), \tag{2.13}$$

where a_i is the i^{th} code of the chain code. Eqn. (2.13) is equal to 1 if a code is an even and $\sqrt{2}$ if a code is an odd. For a close contour pattern, the roundtrip time (t_p) can be written as.

$$t_p = \sum_{i=1}^{p} \Delta t_i . \tag{2.14}$$

Once the Δt_i is known, its corresponding travelling distances along the x and y axes can be found as follows.

$$\Delta x_i = signum(6-a_i)\,signum(2-a_i), \tag{2.15}$$

$$\Delta y_i = signum(4-a_i)\,signum(a_i), \tag{2.16}$$

where

$$signum(z) = \begin{cases} 1, & z>0 \\ 0, & z=0 \\ -1, & z<0 \end{cases} . \tag{2.17}$$

Similarly, close-loop travelling distances along x and y axes can be written as.

This material is reserved for educational use only, not allowed for commercial use.
Forbidden to modify the content, and cite the document when use.

$$x_p = \sum_{i=1}^{p} \Delta x_i, \tag{2.18}$$

$$y_p = \sum_{i=1}^{p} \Delta y_i \,. \tag{2.19}$$

2.5 Elliptic Fourier Descriptor

As the chain code is a function of time and line segments along the boundary, we can consider it as a discrete periodic pattern whereby it can be mathematically analyzed by Fourier series. In this case, the Fourier series expansion of the closed-contour which is a projection of the contour on the x and y axes can be obtained as follows.

$$x_n = A_0 + \sum_{n=1}^{N} a_n \cos\frac{2n\pi t}{T} + b_n \sin\frac{2n\pi t}{T}, \tag{2.20}$$

$$y_n = C_0 + \sum_{n=1}^{N} c_n \cos\frac{2n\pi t}{T} + d_n \sin\frac{2n\pi t}{T}, \tag{2.21}$$

where n is the order of the harmonic being considered and N is a maximum number of harmonics. T is the perimeter of the closed contour. From Eqns(2.20-2.21), a_n, b_n, c_n and d_n are the Fourier coefficients of the n^{th} harmonic and they can be found by using the following expressions.

$$a_n = \frac{T}{2n^2\pi^2} \sum_{p=1}^{K} \frac{\Delta x_p}{\Delta t_p} \left[\cos\frac{2n\pi t_p}{T} - \cos\frac{2n\pi t_{p-1}}{T} \right], \tag{2.22}$$

$$b_n = \frac{T}{2n^2\pi^2} \sum_{p=1}^{K} \frac{\Delta x_p}{\Delta t_p} \left[\sin\frac{2n\pi t_p}{T} - \sin\frac{2n\pi t_{p-1}}{T} \right], \tag{2.23}$$

$$c_n = \frac{T}{2n^2\pi^2} \sum_{p=1}^{K} \frac{\Delta y_p}{\Delta t_p} \left[\cos\frac{2n\pi t_p}{T} - \cos\frac{2n\pi t_{p-1}}{T} \right], \tag{2.24}$$

$$d_n = \frac{T}{2n^2\pi^2} \sum_{p=1}^{K} \frac{\Delta y_p}{\Delta t_p} \left[\sin\frac{2n\pi t_p}{T} - \sin\frac{2n\pi t_{p-1}}{T} \right]. \tag{2.25}$$

This material is reserved for educational use only, not allowed for commercial use.
Forbidden to modify the content, and cite the document when use.

The two constant terms A_0 and C_0 are calculated as

$$A_0 = \frac{1}{T}\sum_{p=1}^{K}\frac{1}{2}\frac{\Delta x_p}{\Delta t_p}\left(t_p^2 - t_{p-1}^2\right) - \frac{\Delta x_p}{\Delta t_p}t_p, \tag{2.26}$$

$$C_0 = \frac{1}{T}\sum_{p=1}^{K}\frac{1}{2}\frac{\Delta y_p}{\Delta t_p}\left(t_p^2 - t_{p-1}^2\right) - \frac{\Delta y_p}{\Delta t_p}t_p. \tag{2.27}$$

Here, as shown in Fig. 2.8, Δx_p and Δy_p are the segments between p and p + 1 of the closed-contour projected onto the x and y axes, respectively. Δt_p is the step between p and p + 1 of the closed-contour. t_p is the curvilinear coordinate of the point p and K is the number of sampling points on the closed-contour. The shape descriptor determined using Eqns(2.22–2.27) clearly depends upon the size of grains, the orientation of grains, and the starting point of the chain-code. As a result, they cannot directly be used to indicate the variability for comparison of the grain kernels. To alleviate these problems, the normalized Fourier coefficients (a_n^{**},b_n^{**},c_n^{**} and d_n^{**}) are considered based upon the ellipse of the first harmonic as follows.

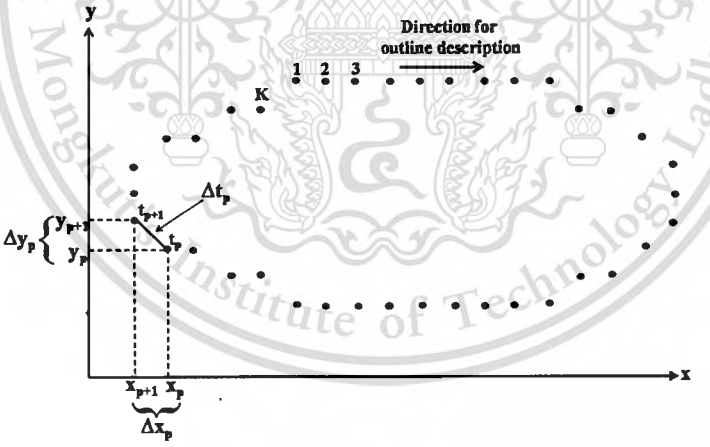

Figure 2.8 Illustration of the parameters used for computing the Fourier coefficients of an EFD on an outline [10].

$$\begin{bmatrix} a_n^{**} & b_n^{**} \\ c_n^{**} & d_n^{**} \end{bmatrix} = \frac{1}{E^*}\begin{bmatrix} \cos\psi & \sin\psi \\ -\sin\psi & \cos\psi \end{bmatrix}\begin{bmatrix} a_n & b_n \\ c_n & d_n \end{bmatrix}\begin{bmatrix} \cos n\theta & -\sin n\theta \\ \sin n\theta & \cos n\theta \end{bmatrix}, \tag{2.28}$$

where

This material is reserved for educational use only, not allowed for commercial use.
Forbidden to modify the content, and cite the document when use.

$$E^* = \left(a_1^{*2} + c_1^{*2}\right)^{1/2}, \begin{bmatrix} a_1^* \\ c_1^* \end{bmatrix} = \begin{bmatrix} a_1 & b_1 \\ c_1 & d_1 \end{bmatrix} \begin{bmatrix} \cos\theta \\ \sin\theta \end{bmatrix}, \tag{2.29}$$

$$\theta = \frac{1}{2}\arctan\left[\frac{2(a_1 b_1 + c_1 d_1)}{a_1^2 + c_1^2 - b_1^2 - d_1^2}\right], \; 0 \le \theta \le \pi, \tag{2.30}$$

$$\psi = \arctan\left[\frac{c_1^*}{a_1^*}\right], \; 0 \le \psi \le 2\pi. \tag{2.31}$$

The number of sets of elliptic Fourier coefficients increases as the number of harmonics increases. For each harmonic set, four coefficients are always generated. The Fourier amplitude (FA) is related to the number of harmonics by the following expression [15].

$$FA = 2n\pi\sqrt{\frac{\left(a_n^{**}\cos\psi + c_n^{**}\sin\psi\right)^2 + \left(-b_n^{**}\sin\psi + d_n^{**}\cos\psi\right)^2}{2}}. \tag{2.32}$$

2.6 Polynomial Function

A polynomial function is a function such as a quadratic, a cubic, a quartic, and so on, involving only non-negative integer powers of x. We can give a general definition of a polynomial, and define its degree. A polynomial of degree n is a function of the form

$$f(x) = a_n x^n + a_{n-1}x^{n-1} + \cdots + a_2 x^2 + a_1 x + a_0. \tag{2.33}$$

The degree of a polynomial is the highest power of x in its expression. Constant (non-zero) polynomials, linear polynomials, quadratics, cubic and quartic are polynomials of degree 0, 1, 2 , 3 and 4 respectively. The function f(x) = 0 is also a polynomial, but we say that its degree is undefined.

This material is reserved for educational use only, not allowed for commercial use.
Forbidden to modify the content, and cite the document when use.

2.7 Shape Analysis

Using these normalized harmonic coefficients, each harmonic can be graphically represented as an ellipse and can be analyzed in terms of semi-major axis (SMJA), semi-minor axis (SMNA), area, and perimeter by using the following equations.

$$SMJA = abs(a_n^{**}\cos\psi + c_n^{**}\sin\psi), \tag{2.34}$$

$$SMNA = abs(-b_n^{**}\sin\psi + d_n^{**}\cos\psi), \tag{2.35}$$

$$Area = \pi \cdot SMJA \cdot SMNA, \tag{2.36}$$

$$Perimeter = 2\pi\sqrt{\frac{SMJA^2 + SMNA^2}{2}}. \tag{2.37}$$

Using the chain coding and the fitted boundary, a geometry feature can be analyzed in terms of perimeter [16], area, and eccentricity [17] by the following equations.

$$Perimeter = 0.95 \cdot \sum_{i=0}^{p-1} length(c_i). \tag{2.38}$$

and

$$Area = \frac{1}{2}\left|\sum_{i=0}^{p-1}(x_i y_{i+1} - x_{i+1} y_i)\right|. \tag{2.39}$$

where,

$$length(c) = \begin{cases} 1 & for\ c=0,2,4,6, \\ \sqrt{2} & for\ c=1,3,5,7. \end{cases}. \tag{2.40}$$

The lengths of the two principal axes, known as major and minor axes, are equal to the eigenvalues λ_1 and λ_2 of the covariance matrix C of a closed contour, respectively. The matrix C contains a sequence of the ordered

This material is reserved for educational use only, not allowed for commercial use.
Forbidden to modify the content, and cite the document when use.

pair (x, y) of an image boundary which is projected on x and y axes. The eigenvalues λ_1, λ_2, and the eccentricity can be computed as

$$\det(C - \lambda_{1,2} I) = 0 . \tag{2.41}$$

$$Eccentricity = \frac{\lambda_2}{\lambda_1} . \tag{2.42}$$

2.8 Neural Network Analysis

In many real-world applications, we want our computers to perform complex pattern recognition problems. Since our conventional computers are obviously not suited to this type of problem, we therefore borrow features from the physiology of the brain as the basis for our new processing models. Hence, the technology has come to be known as artificial neural network technology, or simply neural networks (NN). Neural networks are composed of simple elements operating in parallel. These elements are inspired by biological nervous systems. As in nature, the network function is determined largely by the connections between elements. We can train a neural network to perform a particular function by adjusting the values of the connections (weights) between elements. Commonly neural networks are adjusted, or trained, so that a particular input leads to a specific target output. Such a situation is shown in Fig. 2.9. There, the network is adjusted, based on a comparison of the output and the target, until the network output matches the target. Typically many such input/target pairs are needed to train a network.

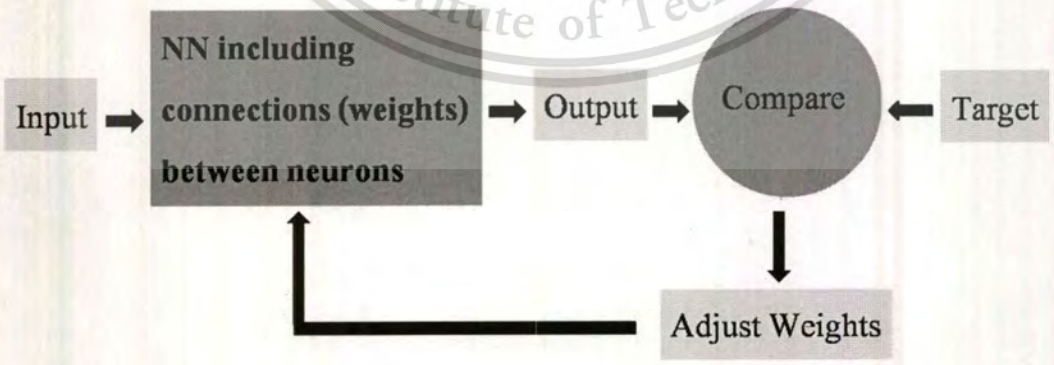

Figure 2.9 Diagram of common neural network procedure.

This material is reserved for educational use only, not allowed for commercial use.
Forbidden to modify the content, and cite the document when use.

2.8.1 Artificial Neural Network Structure

A simple ANN structure is models of a single neural network. The starting point for most neural networks is a model neuron, as shown in Fig. 2.10.

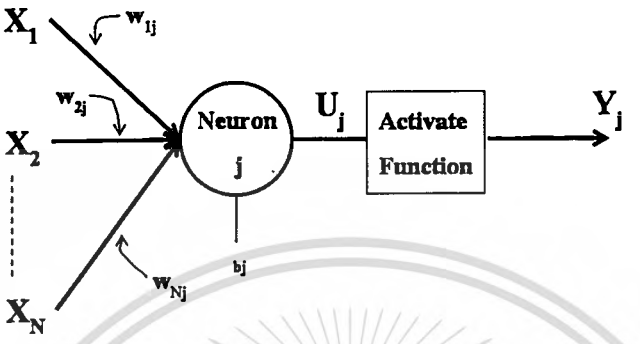

Figure 2.10 Simple ANN structure.

This neuron consists of multiple inputs and a single output. Each input is modified by a weight, which multiplies with the input value. The neuron will combine these weighted inputs and, with reference to a threshold value and activation function, use these to determine its output. This behavior follows closely our understanding of how real neurons work.

2.8.2 Artificial Neural Network Operation

From fig.2.10, the output of each neuron is a function of its inputs. In particular, the output of the j^{th} neuron in any layer is described by two sets of equations

$$U_j = \sum_{i=1}^{N} \left(X_i \cdot w_{Nj} \right) \tag{2.43}$$

$$Y_j = F_{th}\left(U_j + b_j \right) \tag{2.44}$$

For every neuron, j, in a layer, each of the i inputs, X_i, to that layer is multiplied by a weight, w_{ij}. These are all summed together, resulting in the internal value of this operation, U_j. This value is then biased by a threshold value or bias value, b_j, and sent through an activation function, F_{th}. This activation function is usually the sigmoid function, logsigmoid function, and linear function etc. which has an input to output mapping. The

This material is reserved for educational use only, not allowed for commercial use.
Forbidden to modify the content, and cite the document when use.

resulting output, Y_j, is an input to the next layer or it is a response of the neural network if it is the last layer. In essence, Eqn.(2.43) implements the combination operation of the neuron and Eqn.(2.44) implements the firing of the neuron. From these equations, a predetermined set of weights, a predetermined set of threshold values and a description of the network structure (that is the number of layers and the number of neurons in each layer), it is possible to compute the response of the neural network to any set of inputs.

2.8.3 Artificial Neural Network Learning

Learning in a neural network is called training. Like training in athletics, training in a neural network requires a coach, someone that describes to the neural network what it should have produced as a response. From the difference between the desired response and the actual response, the error is determined and a portion of it is propagated backward through the network. At each neuron in the network the error is used to adjust the weights and bias values of the neuron, so that the next time, the error in the network response will be less for the same inputs.

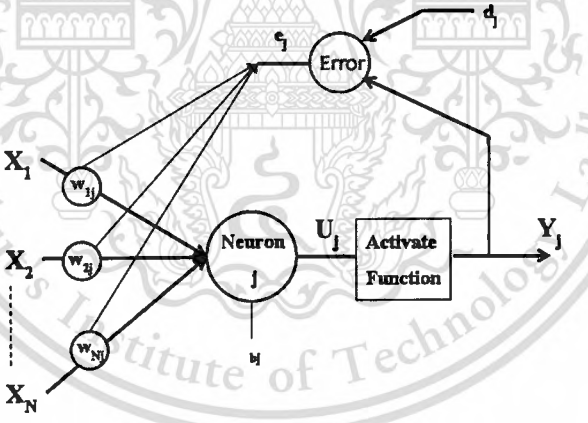

Figure 2.11 Neural weights adjustment.

This corrective procedure is called backpropagation and it is applied continuously and repetitively for each set of inputs and corresponding set of outputs produced in response to the inputs. This procedure continues so long as the individual or total errors in the responses exceed a specified level or until there are no measurable errors. At this point, the neural network has learned the training material and you can stop the training process and use the neural network to produce responses to new input data.

This material is reserved for educational use only, not allowed for commercial use.
Forbidden to modify the content, and cite the document when use.

2.8.4 Backpropagation Neural Network Structure

Although there are many different kinds of learning rules used by neural networks, this thesis is concerned only with one; the delta rule. The delta rule is often utilized by the most common class of ANNs called backpropagational neural networks (BPNNs). Backpropagation is an abbreviation for the backwards propagation of error. From Fig. 2.10, backpropagation starts at the output layer with the following equations

$$w_{Nj} = w'_{Nj} + LR \cdot e_j \cdot X_i, \tag{2.45}$$

$$e_j = Y_j \cdot (1 - Y_j) \cdot (d_j - Y_j). \tag{2.46}$$

For the i^{th} input of the j^{th} neuron in the output layer, the weight w_{Nj} is adjusted by adding to the previous weight value, w'_{Nj}, a term determined by the product of a learning rate, LR, an error term, e_j, and the value of the i^{th} input, X_i. The error term, e_j, for the j^{th} neuron is determined by the product of the actual output, Y_j, its complement, $1 - Y_j$, and the difference between the desired output, d_j, and the actual output. Once the error terms are computed and weights are adjusted for the output layer, the values are recorded and the next layer back is adjusted. The same weight adjustment process, determined by Eqn.(2.45), is followed, but the error term is generated by a slightly modified version of Eqn.(2.46). This modification is

$$e_j = Y_i \cdot (1 - Y_j) \cdot \sum (e_k \cdot w'_{jk}) \tag{2.47}$$

In this version, the difference between the desired output and the actual output is replaced by the sum of the error terms for each neuron, k, in the layer immediately succeeding the layer being processed (remember, we are going backwards through the layers so these terms have already been computed) times the respective pre-adjustment weights.

The LR applies a greater or lesser portion of the respective adjustment to the old weight. If the factor is set to a large value, then the neural network may learn more quickly, but if there is a large variability in the input set then the network may not learn very well or at all. In real terms, setting the learning rate to a large value is analogous to giving a child a spanking, but that is inappropriate and counter-productive to learning if the offense is so simple as forgetting to tie their shoelaces. Usually, it is better to set the factor to a small value

This material is reserved for educational use only, not allowed for commercial use.
Forbidden to modify the content, and cite the document when use.

and edge it upward if the learning rate seems slow. In many cases, it is useful to use a revised weight adjustment process. This is described by the equation

$$w_{Nj} = w'_{Nj} + (1-M) \cdot LR \cdot e_j \cdot X_i + M \cdot (w'_{Nj} - w''_{Nj}) \quad (2.48)$$

This is similar to Eqn.(2.45), with a momentum factor, M, the previous weight, w'_{Nj}, and the next to previous weight, w''_{Nj}, included in the last term. This extra term allows for momentum in weight adjustment. Momentum basically allows a change to the weights to persist for a number of adjustment cycles. The magnitude of the persistence is controlled by the momentum factor. If the momentum factor is set to 0, then the equation reduces to that of Eqn.(2.45). If the momentum factor is increased from 0, then increasingly greater persistence of previous adjustments is allowed in modifying the current adjustment. This can improve the learning rate in some situations, by helping to smooth out unusual conditions in the training set.

In a BPNN, there are two steps during training that are used alternately. The backpropagation step calculates the error in the gradient descent and propagates it backwards to each neuron in the output layer, then hidden layer. In the second step, the weights and biases are then recomputed, and the output from the activated neurons is then propagated forward from the hidden layer to the output layer. The network is initialized with random weights and biases, and was then trained using the Levenberg-Marquardt algorithm. The weights and biases are updated according to

$$D_{n+1} = D_n - [J^T J + \mu I]^{-1} J^T e, \quad (2.44)$$

where D_n is a matrix containing the current weights and biases, D_{n+1} is a matrix containing the new weights and biases, e is the network error, J is a Jacobean matrix containing the 1st derivative of e with respect to the current weights and biases, I is the identity matrix and μ is a variable that increases or decreases based on the performance function. The gradient of the error surface is equal to $J^T e$.

This material is reserved for educational use only, not allowed for commercial use.
Forbidden to modify the content, and cite the document when use.

2.9 Reference

[1] J. Cazes, **Analytical instrumentation handbook,** 3rd, Marcel Dekker, New York, pp. 127-139 (2005).

[2] G. Ganglitz and T. Vo-Dinh, **Handbook of spectroscopy vol. 1,** WILEY-VCH verlag, Weinhein, pp. 39-44 (2003).

[3] W. Burger, and M. J. Burge, **Digital image processing: an algorithmic introduction using Java,** Springer, (2008).

[4] L. G. Shapiro and G. C. Stockman, **Computer vision,** Upper Saddle River : Prentice Hall, pp. 51-85 (2001).

[5] L. F. Costa and R. M. Cesar, **Shape classification and analysis: theory and practice,** in Image Processing Series, P. A. Laplants, ed., pp. 411–414 (2009).

[6] Freeman, H., "On the encoding of arbitrary geometric configuration," IRE Trans. Elec. Comp. 260-268 (1961).

[7] Freeman, H., "Computer processing of line drawing images," Comp. Surv. 6 pp. 57-97 (1974).

[8] Kuhl, F. P. and Giardina, C. R., "Elliptic Fourier features of a closed contour," Compo. Graph. Ima. Proc. 18, 236-258 (1982).

[9] Neto, J. C., Meyer, G. E., Jones, D. D. and Samal, A. K., "Plant species identification using elliptic Fourier leaf shape analysis," Comp. Elect. Argric. 50, 121-134 (2006).

[10] Tort, A., "Elliptical Fourier functions as a morphological descriptor of the genus Stenosarina Brachiopoda, Terebratulida, new caledonia," Mathematical Geology. 35, 873-885 (2003).

[11] Ninomiya, S., Ohsawa, R. and Yoshida, M., "Evaluation of buckwheat and tartary buckwheat kernel shape by elliptic Fourier method," Curr. Adv. Buck. Res. 389-396 (1995).

[12] Iwata, H., Niikura, S., Matsuura, S., Takano, Y. and Ukai, Y., "Evaluation of variation of root shape of Japanese radish (Raphanus sativus L.) based on image analysis using elliptic Fourier descriptors," Euphytica 102, 143-149 (1998).

[13] Y. Hiraoka and N. Kuramoto, "Identification of *Rhus succedanea* L. Cultivars Using Elliptic Fourier Descriptors Based on Fruit Shape," Silv. Gene. **53** pp. 221–226 (2004).

This material is reserved for educational use only, not allowed for commercial use.
Forbidden to modify the content, and cite the document when use.

[14] Mebatsion, H. K., Paliwal, J., and Jayas, D.S., "Evaluation of variations in the shape of grain types using principal components analysis of the elliptic Fourier descriptor," Comp. Elec. Agri. **80** pp.63-70 (2012).

[15] Nafe, R. and Schlote, W., "Methods for shape analysis of two-dimensional closed cotours – a biologically importance, but widely neglected field in histopathology," Elec. J. Pathol. Histol. 8.2, 022-02 (2002).

[16] Burger, W., and Burge, M. J., [Digital image processing: an algorithmic introduction using Java], Springer Publisher, New York, 223 (2008).

[17] Mingqiang, Y., Kidiyo, K., and Joseph, R., "A survey of shape feature extraction techniques," *Patt. Rec.* 43-90 (2008).

[18] H. Honda, N. Takikawa, H. Nogushi, T. Hanai, and T. Kobayashi, "Image Analysis Associated with a Fuzzy Neural Network and Estimation of Shoot Length of Regenerated Rice Callus," J. Ferm. Bioen. **84** (4) pp. 342-347 (1997).

[19] Z. Y. Liua, H. F. Wuc, and J.F. Huang, "Application of neural networks to discriminate fungal infection levels in rice panicles using hyperspectral reflectance and principal components analysis," Comp. Elec. Agri. **72** pp.99-106 (2010).

[20] National Instruments Corporation, **NI Vision Concepts Manual**, National instruments corporate headquarters, Texas, USA, pp.8-15 (2005).

[21] Neural Networks Toolbox (4.0) User's Guide, The MathWorks, Natick, MA, 2000, pp. 2-2–2-22, 5-2–2-56.

This material is reserved for educational use only, not allowed for commercial use.
Forbidden to modify the content, and cite the document when use.

CHAPTER 3

DESTRUCTIVE OPTICAL METHODS

In this chapter, the destructive optical methods for milled rice identification were proposed. The methods are based on a traditional alkaline spreading method. The basic of these methods were based on the difference of amylose content in each milled rice variety that the amylose molecules are dissolved in alkaline solution. In practice, 1.7% concentration of KOH solution was used and KDML105 milled rice variety was completely dissolved in 23 hours. By this result, the alkaline spreading method was used in present field testing. However, time consumption is an issue. Therefore, the research relies on this traditional method by speeds up time testing with increases KOH solution concentration and uses spectrometer and refrectrometry methods for identifying KDML105 milled rice variety.

3.1 Combination of Simple Chemical and Spectroscopic Methods for the identification of Thai Hom Mali rice

Spectroscopy is one of the interesting techniques that can be used to study rice characteristics. Previously, transmission spectra in a near infrared of 850-1050 nm wavelength band of milled rice grains were performed to discriminate Basmati rice grains from undesired rice grains with a 20% error rate [1]. Reflectance spectrum of one zone in visible region and two zones in the infrared region was also studied to classify 139 Korean domestic rice grains from 141 unwanted rice grains [2]. A simpler and possibly cheaper approach via the use of only a visible spectrum in 400-1000 nm wavelength was investigated, showing a classification rate of 89% in identifying two different rice varieties [3]. With these concepts in mind, it would be desirable to follow standards inspection but with a faster analytical technique. This topic studies the combination of chemical and spectroscopic methods to identify the milled KDML105 rice [4]. In approach, powder of the milled rice is dissolved in an alkali solution and its transmission spectrum only in a 500-800 nm wavelength region is investigated.

This material is reserved for educational use only, not allowed for commercial use.
Forbidden to modify the content, and cite the document when use.

3.1.1 Materials and Methods

3.1.1.1 Materials

Four varieties of Thai rice, KDML105, CNT1, PTT1 and RD6, were obtained from the Rice Research Institute, at the Department of Rice, Ministry of Agriculture and Cooperatives of Thailand. All of them were harvested in 2007 with ≈ 12%-14% moisture content. The KDML105 has amylose content in the range of 13%-18%. The PTT1 rice has equivalent amount of amylose content to that of the KDML105 rice but its weight per seed is 80.5% less (i.e., 0.0174 grams). These two rice varieties are classified as low amylose content rice. The CNT1 rice has its amylose content in 27%-30% and it is classified as one of the high-amylose content rice varieties. Its weight is 98.6% (i.e., 0.0213 grams) compared to the KDML105 rice. For the RD6, it is classified as very low amylose content rice (0%-2%) and its weight is 88.3% (i.e., 0.0191 grams) than the KDML105 milled rice. Fig.3.1 shows images of four Thai rice varieties taken under white light illumination.

Figure 3.1 shows four Thai rice varieties (a) KDML105, (b) CNT1, (c) PTT1, and (d) RD6 used in our study.

3.1.1.2 Sample Preparation

Because these four rice varieties have different weight per grain and they can be dissolved in an alkali solution, we prepare our alkali solution as follows. Our 10% solution of potassium hydroxide (KOH) was prepared by dissolving 10.0 g of KOH pallets in 100 ml of deionized water. Note that we choose a higher concentration of the KOH solution compared to a 1.7% concentration previously used in the alkali spreading

This material is reserved for educational use only, not allowed for commercial use.
Forbidden to modify the content, and cite the document when use.

method because we would like to speed up the dissolution process. Each rice variety was separately ground by using a laboratory grinder as shown in Fig. 3.2 and kept in a zip pack. They were stored in a room where the temperature and the relative humidity varied between 24°C-28 °C and 50%-70%, respectively. In the study, we divide rice powder into different weights of 0.10 g, 0.20 g, and 0.30 g by using 4 digits weighing (see Fig.3.3). The prepared milled rice powder was dissolved in 10 ml of our KOH solution under a magnetic stirrer for 5 minutes without heating. Then, a 2-ml milled rice solution was poured into a 10-mm wide quartz cuvette. The remaining milled rice solution was left to allow the milled rice powder dissolve more for 10, 15, and 20 minutes prior to the next measurements. In each measurement (i.e., 4 measurements for 5^{th}, 10^{th}, 15^{th}, and 20^{th} minutes), there are 15 samples per rice variety.

(a) (b)

Figure 3.2 a) Laboratory grinder and b) grind ball.

Figure 3.3 4-digits weighing machine.

3.1.1.3 Spectrum Measurement

A commercial UV/VIS spectrometer model Heλios α from Thermo Electron Corporation was used to measure the transmission spectrum of our milled rice solution as shown in Fig 3.4. Only a spectral range in 500-800 nm was analyzed. Scanning speed was set at 4 nm/s with the wavelength interval of 1 nm, indicating

This material is reserved for educational use only, not allowed for commercial use.
Forbidden to modify the content, and cite the document when use.

a complete 75 second per measurement cycle with 301 data points. Our experiment was performed in an air conditioned room having 24°C-26°C and 50%-60% relative humidity.

(a) (b)

Figure 3.4 (a) The UV/VIS spectrometer and (b) Inside view of spectrometer box.

3.1.1.4 Data Analysis

To reduce the data fluctuation during our transmission measurement, we investigated the transmission spectrum of the milled rice solution with respect to the transmission spectrum of our 10% KOH solution. After that, the first derivative of the measured relative optical transmission spectrum was analyzed. By appropriately assigning the slope interval for our classification, the KDML105 milled rice can be distinguishable.

3.1.2 Results and Discussion

3.1.2.1 Visual Inspection

Fig.3.5 shows our 10% KOH solution having 0.10 g of the milled rice powder dissolved in it for 5, 10, 15, and 20 minutes. Visually, these milled rice solutions have similar turbidity. At the 5th minute of dissolution, the KDML105 milled rice powder seems to show higher capability to dissolve in our 10% KOH solution than the remaining three rice varieties. In this case, a measured relative optical transmissivity at a 635-nm wavelength for the KDML105 milled solution is ~4% higher than the others. When these milled rice powders spend more time in our 10% KOH solution up to 20 minutes, there is an increase in the measured relative optical transmissivity of 2%-7%. By adding the milled rice powder more in our 10% KOH solution, the turbidity gets increased as shown in Figs.3.6-3.7 with a maximum drop of measured relative optical transmissivity of 9%. These variations in measured relative optical transmissivities also confirm that the optical density measurement cannot be used to identify our desired KDML105 milled rice.

This material is reserved for educational use only, not allowed for commercial use.
Forbidden to modify the content, and cite the document when use.

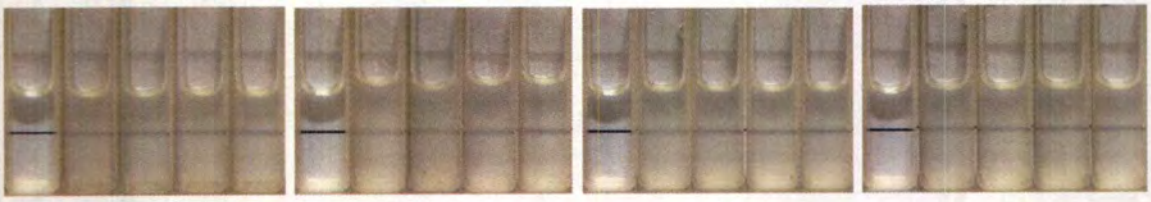

(a) (b) (c) (d)

Figure 3.5 shows 2 ml of our milled rice solutions for 0.10 g of (a) KDML105, (b) CNT1, (c) PTT1, and (d) RD6 rice varieties. Images from left to right are for our 10% KOH solution followed by the 5th, 10th, 15th, and 20th minutes of observation, respectively. A black solid line is used to show turbidity of the solution.

(a) (b) (c) (d)

Figure 3.6 shows 2 ml of our milled rice solutions for 0.20 g of (a) KDML105, (b) CNT1, (c) PTT1 and (d) RD6 rice varieties. Images from left to right are for our 10% KOH solution followed by the 5th, 10th, 15th, and 20th minutes of observation, respectively. A black solid line is used to show turbidity of the solution.

(a) (b) (c) (d)

Figure 3.7 shows 2 ml of our milled rice solutions for 0.30 g of (a) KDML105, (b) CNT1, (c) PTT1 and (d) RD6 rice varieties. Images from left to right are for our 10% KOH solution followed by the 5th, 10th, 15th, and 20th minutes of observation, respectively. A black solid line is used to show turbidity of the solution.

3.1.2.2 Spectral Measurement

Instead of measuring the optical density of the milled rice solution, we investigate the optical transmittance of the milled rice solution with respect to the optical transmittance of our 10% KOH solution in the visible wavelength. Fig.3.8 shows measured relative optical transmittance of four milled rice solutions in a 325-1100 nm wavelength. Specifically, we analyze these spectra only in a 500-800 nm wavelength as it gives the most linear behavior. In this case, a slope of the spectrum in this zone is simply used for the identification

This material is reserved for educational use only, not allowed for commercial use.
Forbidden to modify the content, and cite the document when use.

of our KDML105 milled rice. For the 0.10 g of the milled rice powder, measured relative optical transmittance spectra of the four rice varieties are shown in Fig.3.19. At the beginning of our analysis (e.g., at the 5th minute), the KDML105 milled rice solution shows a higher optical transmittance than the remaining three rice varieties over a 300-nm wavelength (see Fig.3.9 (a)).

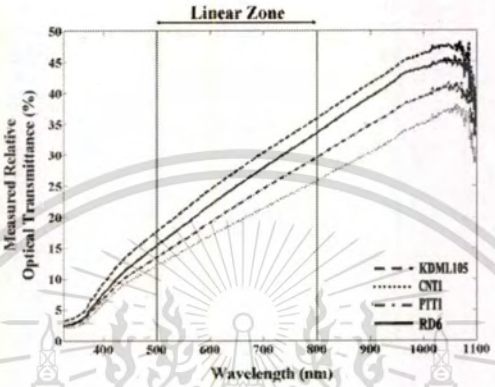

Figure 3.8 Example of measured relative transmission spectra for 0.10 g of the milled rice powder dissolved in our 10% KOH solution for 5 minutes.

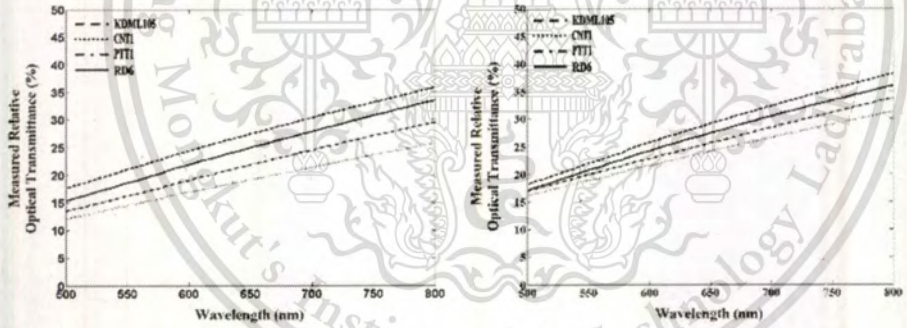

Figure 3.9 Measured relative optical transmittance of 0.10 g of the milled rice powder dissolved in our 10% KOH solution for four rice varieties at the (a) 5th, (b) 10th, (c) 15th, and (d) 20th minutes of our measurements.

As these milled rice powders spend more time in our 10% KOH solution for 10, 15, and 20 minutes as shown in Figs.3.9(b)-(d), the KDML105, CNT1, and PTT1 seem to have an equal capability to be dissolved in our 10% KOH solution. Only the RD6 rice variety has a higher efficiency in dissolving in our 10% KOH solution due to its low amylose content.

This material is reserved for educational use only, not allowed for commercial use.
Forbidden to modify the content, and cite the document when use.

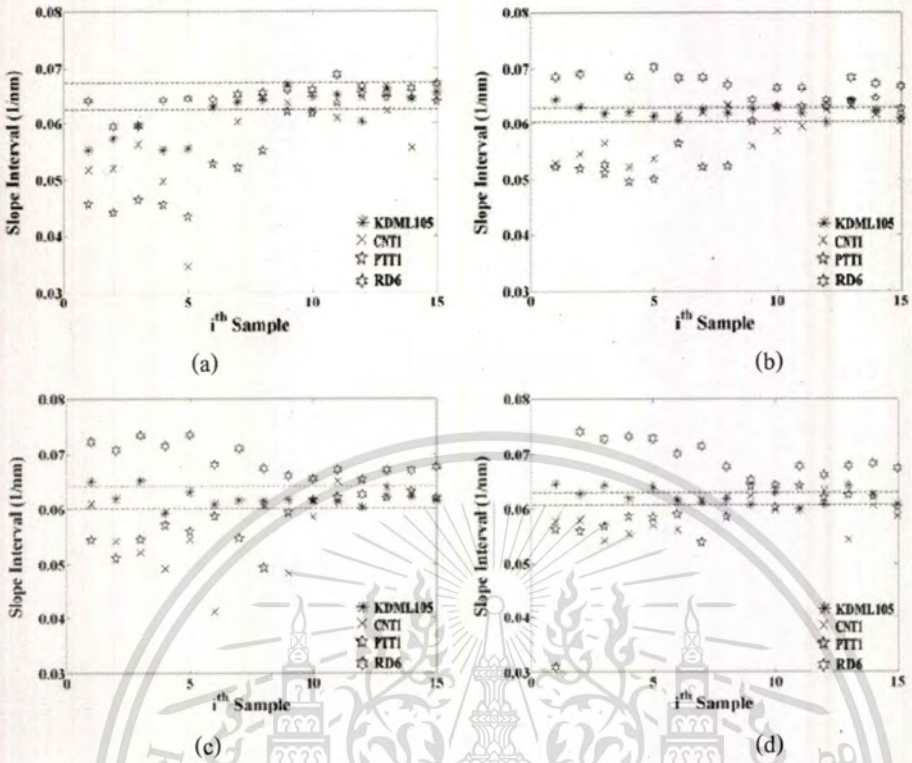

Figure 3.10 Slope values calculated from the measured relative optical transmittance of 0.10 g of the milled rice powder dissolved in our 10% KOH solution for (a) 5 minutes, (b) 10 minutes, (c) 15 minutes, and (d) 20 minutes.

From the linear zone shown in Fig.3.9, calculated slope values for all rice samples are shown in Fig.3.10. By appropriately assigning the slope interval, a false error rate for identifying the desired KDML105 milled rice can be simply determined. In this case, we choose slope intervals of 0.06250-0.06750 nm^{-1}, 0.06017-0.06280 nm^{-1}, 0.06015-0.06400 nm^{-1}, and 0.06065-0.06300 nm^{-1} for our 5^{th}, 10^{th}, 15^{th}, and 20^{th} minutes of measurements, respectively. As a result, we obtain corresponding false error rates of 46.7%, 15.0%, 26.7%, and 18.3%. If only 15 samples of the KDML105 milled rice are taken into account, calculated false error rates for the identification of this rice variety are 40.0%, 13.3%, 20.0%, and 33.3% at the 5^{th}, 10^{th}, 15^{th}, and 20^{th} minutes of our measurements, respectively. A narrower slope interval also gives a lower false error rate.

This material is reserved for educational use only, not allowed for commercial use.
Forbidden to modify the content, and cite the document when use.

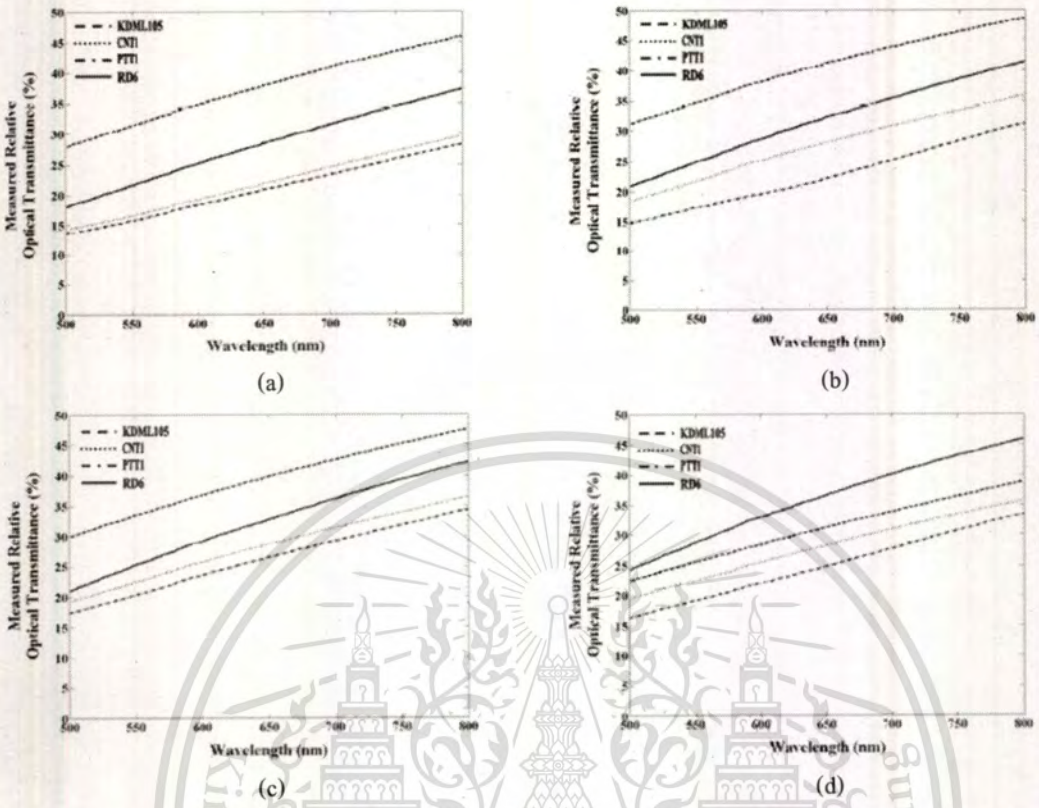

Figure 3.11 Measured relative optical transmittance of 0.20 g of the milled rice powder dissolved in our 10% KOH solution for four rice varieties at the (a) 5th, (b) 10th, (c) 15th, and (d) 20th minutes of our measurements.

When the 0.20 g of the milled rice powder is used, the measured relative optical transmission spectrum of the KDML105 milled rice powder slightly increases as the time passes from 5 minutes to 15 minutes and then drops below those of the CNT1, PTT1, and RD6 at the 20th minute of our measurement as shown in Fig.3.11(a). On the other hand, there is 5% increase in the measured relative optical transmission spectra for the remaining three rice varieties as the time goes by from 5 minutes to 20 minute (see Figs. 3.11(b)-(c)). Calculated slope values for 4 different dissolution times are shown in Fig.3.12. By choosing slope intervals of 0.0550-0.0607 nm^{-1}, 0.0540-0.0633 nm^{-1}, 0.0578-0.0630 nm^{-1}, and 0.0579-0.0630 nm^{-1}, we obtain false error rates of 18.3%, 46.7%, 21.7%, and 23.3% at the 5th, 10th, 15th, and 20th minutes of our measurements, respectively. In the case, if only 15 samples of the KDML105 milled rice are taken into account, calculated false error rates for the identification of this rice variety are 26.7%, 20.0%, 33.3%, and 46.7%, respectively. As expected, slope values for the 0.20 g case are also less than those from the previous case.

This material is reserved for educational use only, not allowed for commercial use.
Forbidden to modify the content, and cite the document when use.

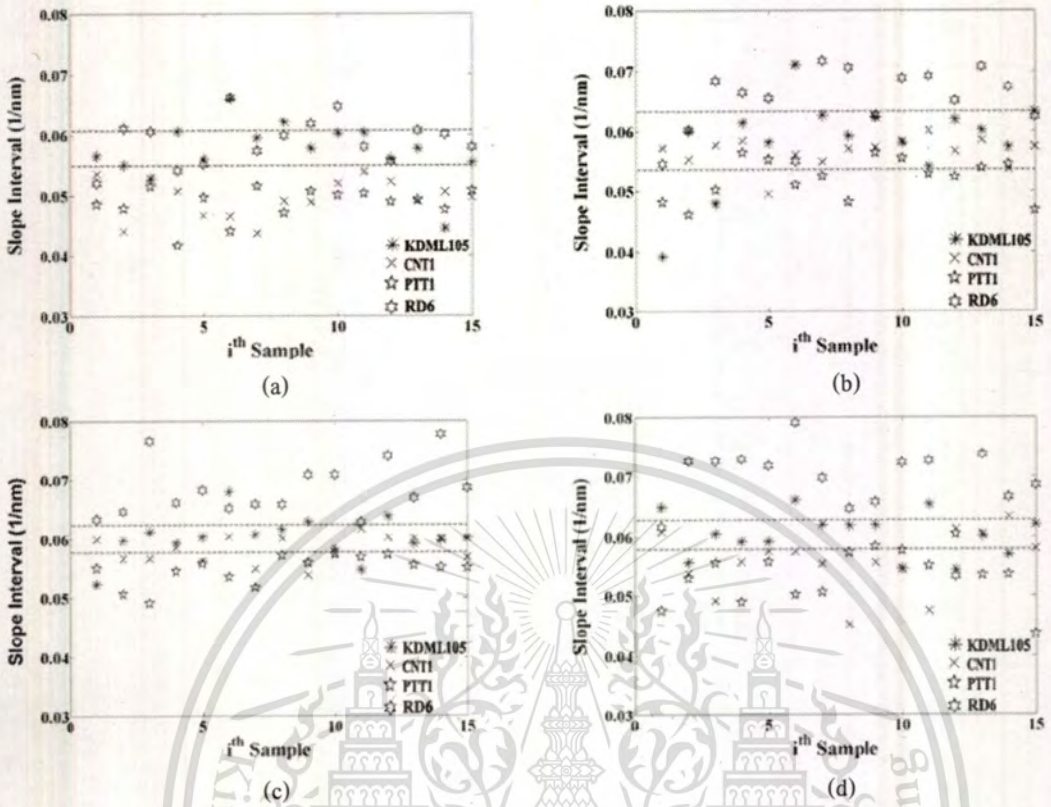

Figure 3.12 Slope values calculated from the measured relative optical transmittance of 0.20 g of the milled rice powder dissolved in our 10% KOH solution for (a) 5 minutes, (b) 10 minutes, (c) 15 minutes, and (d) 20 minutes.

With the use of a 0.30-g milled rice powder, the RD6 milled rice shows highest capability in dissolving in our 10% KOH solution. Measured relative optical transmission values for all rice varieties are also less than those in the two previous cases (see Fig. 3.13). In addition, as expected, calculated slope values shown in Fig. 3.14 are smaller. By assigning slope intervals of 0.041400-0.051500 nm^{-1}, 0.049300-0.059700 nm^{-1}, 0.049870-0.058600 nm^{-1}, and 0.050010-0.060240 nm^{-1}, high false error rates of 23.3%, 36.7%, 23.3%, and 30.0% are achieved in identifying the KDML105 milled rice at the 5^{th}, 10^{th}, 15^{th}, and 20^{th} minutes of our measurements, respectively. With only the KDML105 milled rice, higher false rejection rates of 60.0%, 53.3%, 33.3%, and 40.0% are determined.

This material is reserved for educational use only, not allowed for commercial use.
Forbidden to modify the content, and cite the document when use.

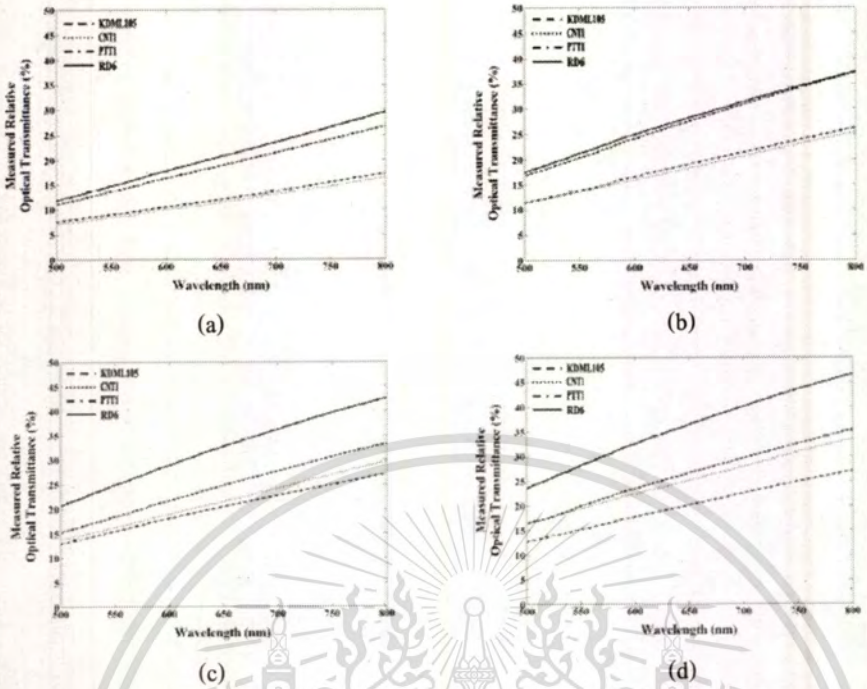

Figure 3.13 Measured relative optical transmittance of 0.30 g of the milled rice powder dissolved in our 10% KOH solution for four rice varieties at the (a) 5th, (b) 10th, (c) 15th, and (d) 20th minutes of our measurements.

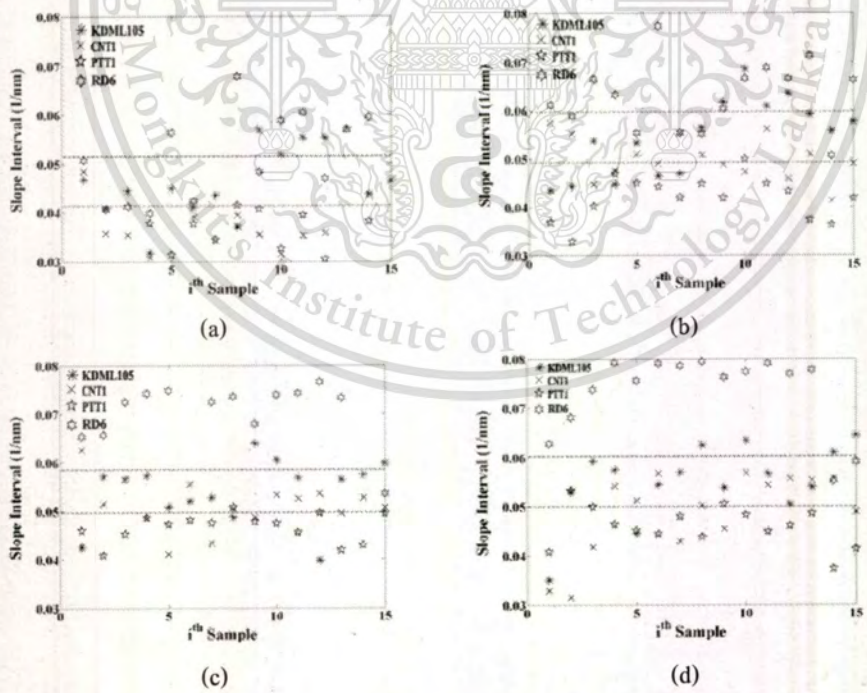

Figure 3.14 Slope values calculated from the measured relative optical transmittance of 0.30 g of the milled rice powder dissolved in our 10%KOH solution for (a) 5 minutes, (b) 10 minutes, (c) 15 minutes, and (d) 20 minutes.

This material is reserved for educational use only; not allowed for commercial use.
Forbidden to modify the content, and cite the document when use.

Table 3.1 KDML105 identification performance

Dissolution Time (minutes)	Measured false rejection rate for three different weights of the milled rice powder (%)					
	0.10 g		0.20 g		0.30 g	
	All rice Varieties (60 samples)	Only KDML105 (15 samples)	All rice Varieties (60 samples)	Only KDML105 (15 samples)	All rice Varieties (60 samples)	Only KDML105 (15 samples)
5	46.7	40.0	18.3	26.7	23.3	60.0
10	15.0	13.3	46.7	20.0	36.7	53.3
15	26.7	20.0	21.7	33.3	23.3	33.3
20	18.3	33.3	23.3	46.7	30.0	40.0

Table 3.1 summarizes our study in distinguishing the KDML105 milled rice from the remaining three rice varieties. It can be seen that the measured false rejection rate depends on the weight of the milled rice powder, its ability to be dissolved in our 10% KOH solution, and the dissolution time. Based on our study, the best procedure is to use 0.10 g of the milled rice powder and dissolve it in our 10% KOH solution for 10 minutes, offering a fast analysis with less amount of waste and a low 15% overall false rejection rate. In addition, a faster identification time with a slightly higher 18.3% false rejection rate can be obtained by using a 0.2-g milled rice powder and dissolving it in our 10% KOH solution for 5 minutes. Optimizing the weight of the milled rice powder, the dissolution time, and the concentration of our KOH solution can help improve the efficiency in identifying the KDML105 milled rice.

This material is reserved for educational use only, not allowed for commercial use.
Forbidden to modify the content, and cite the document when use.

3.2 Identification of Thai Hom Mali Rice using a Refractometer

Another promising technique is based on optical refractometry. Previously, it was used for process control [5] and the study of rice starch characteristics [6]. This topic proposel to analyze milled rice grains dissolved in the KOH solution via an optical refractometer. Our idea comes from the fact that due to differences in the amount of amylose content in the two rice varieties typically mixed with the KDML105 rice, the refractive index of the milled rice grain dissolved in the KOH solution can be used to identify the KDML105 milled rice.

3.2.1 Proposed Method

As mentioned earlier section, it is impossible to visually separate the two rice varieties PTT1 and CNT1 from the desired KDML105 rice. This is the reason that people have to investigate them chemically and biologically. Our simpler proposed procedure is to grind the desired amount of milled rice, dissolve it in the KOH solution, and then measured its refractive index by using an optical refractometer as shown in Fig. 3.15.

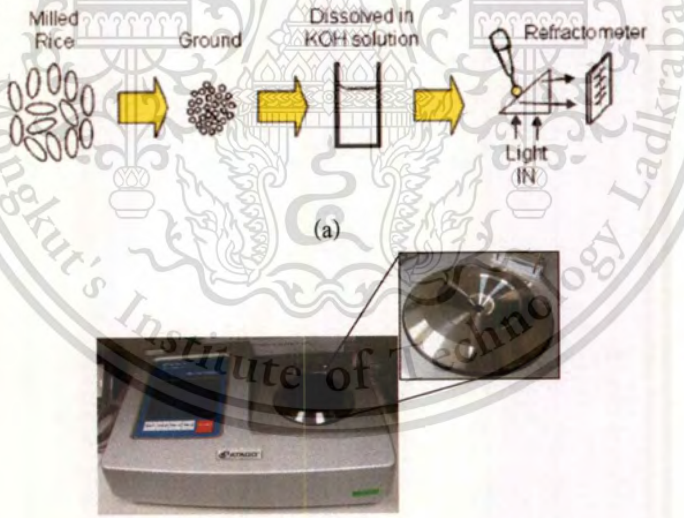

Figure 3.15 (a) Proposed method where we combine chemical and optical techniques for identifying the KDML105 milled rice and (b) The ATAGO refractrometry and perspective view of liquid droplet channel which black cover was opened.

In our proposed method, we prepare a 10% KOH solution as described. Our KOH solution can be prepared in advance if we plan to verify the KDML105 rice in the field. After that, the desired amount of ground milled rice grains is gradually poured into a 10-ml KOH solution under a magnetic bar stirrer at about 2400 rpm

This material is reserved for educational use only, not allowed for commercial use.
Forbidden to modify the content, and cite the document when use.

without heating. This process is finished within 2 minutes. At the 4.5th minute, the stirrer speed is adjusted to zero but the magnetic bar is still moving with the remaining inertia force. At the specified minute of measurement (e.g., 5th and 10th minutes), a dropper is used to suck a 0.5-ml milled rice solution and drop it in a light emitting diode (LED)-based optical refractometer where a refractive index is measured with a > + 0.0003 accuracy at 25°C. The optical refractometer can be an off-the-shelf portable digital version which is suitable for field operation.

3.2.2 Experimental Prove of Concept

3.2.2.1 Refractive Index Measurement

At the 5th and 10th minutes of our measurements, we use a plastic dropper to suck and then drop a 0.5-ml milled rice solution on the LED-based optical refractometer from Atago model RX-7000-α. The measurement temperature is fixed at 25°C and the measurement time at this state is less than 20 seconds. Note that the sensing element of the LED-based optical refractometer is a Sapphire prism and it can determine the refractive index from 1.3250 to 1.7000 with the measurement accuracy and repeatability of +0.0001 and +0.00005, respectively. Refractive index values of the solutions from three Thai milled rice varieties compared with one from the KDML105 milled rice measured at the 5th and 10th minute measurements for three different weights of milled rice powder are first studied as shown in Fig. 3.16. As expected, the refractive index of the CNT1 milled rice solution is lower than that of the KDML105 milled rice solution while the refractive index of the PTT1 milled rice solution is higher than that of the KDML105 milled rice solution. By increasing the amount of the milled rice powder dissolved in our 10% KOH solution from 0.1 grams to 0.2 grams and 0.3 grams, the difference in refractive index between CNT1 and KDML105 milled rice solutions is larger. For the PTT1 milled rice solution, its difference with the KDML105 milled rice solution gets increased with the 0.2 grams and it is drop for the 0.3 grams. For the RD6 milled rice solution, increasing the amount of milled rice grains in our 10% KOH solution makes the refractive index difference drop. In addition, spending more time for 0.1 grams and 0.2 grams of milled rice powder to be dissolved more in our 10% KOH solution cannot enhance the refractive index differences. In this approach, using the 0.3 grams of the milled rice powder shows some enhancement only for the CNT1 and PTT1.

This material is reserved for educational use only, not allowed for commercial use.
Forbidden to modify the content, and cite the document when use.

3.2.2.2 KDML105 Identification

Based on the comparison of the refractive indices of four milled rice solutions, KDML105 is base line, in Fig. 3.16 and with requirements to use less amount of sample and reduce operating time, we select 0.1 grams of the milled rice powder dissolved in our 10% KOH solution for 5 minutes for our study in identifying the KDML105 rice. Fig. 3.17 shows measured refractive index of 0.1 grams of KDML105, CNT1, PTT1, and RD6 milled rice powders dissolved in our 10% KOH solution. The number of samples is 15 for each rice variety. Fluctuation of measured refractive indices is due to the way we dissolve the milled rice powder.

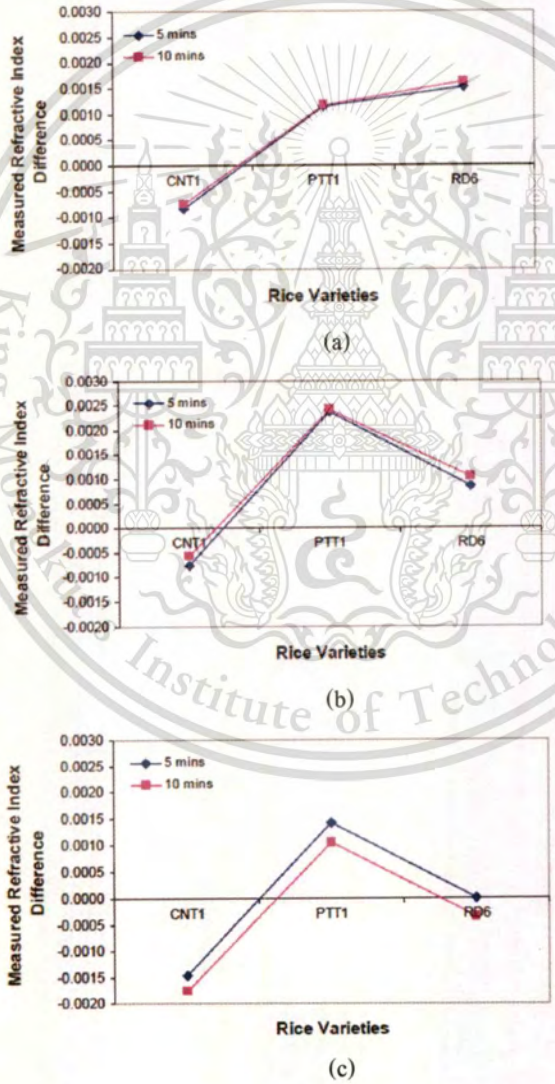

Figure 3.16 Measured refractive index differences of CNT1, PTT1 and RD6 milled rice solutions compared to the KDML105 milled rice solution (base line) for (a) 0.1 grams, (b) 0.2 grams, and (c) 0.3 grams of the milled rice powder.

This material is reserved for educational use only, not allowed for commercial use.
Forbidden to modify the content, and cite the document when use.

By appropriately choosing the upper and lower refractive indices of 1.3494 and 1.3474 as our threshold interval, we find that we can 100% identify all milled rice grains that are not KDML105, i.e., their refractive index values stay inside our threshold interval. For the identification of the KDML105 milled rice, we achieve a false error rate of 100×4/15 = 26.7%. These results imply that we can identify 15 KDML105 milled rice samples from 60 milled rice samples with a false error rate of 100×4/60 = 6.7%. With better sample preparation processes, false error rates can significantly be reduced.

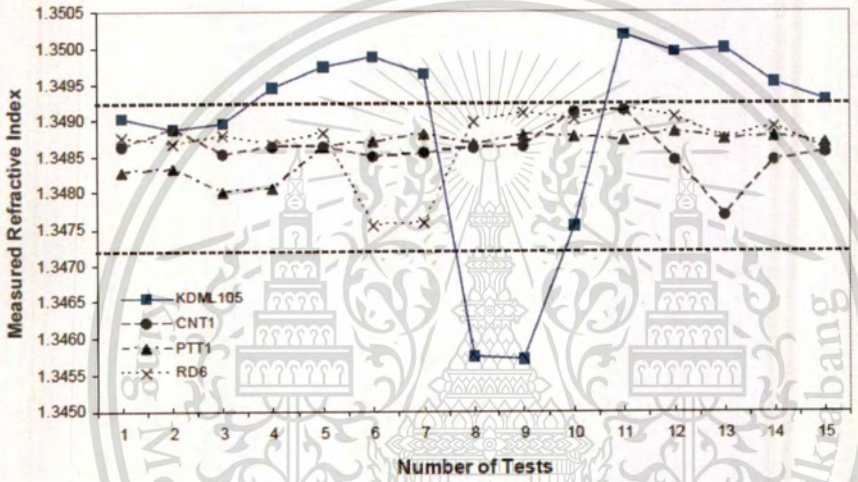

Figure 3.17 Measured refractive index values of 0.1 grams of KDML105, CNT1, PTT1 and RD6 milled rice powders each dissolved in 10 ml of our 10% KOH solution for 5 minutes.

This material is reserved for educational use only, not allowed for commercial use.
Forbidden to modify the content, and cite the document when use.

3.3 References

[1] B. G. Osborne, B. Mertens, M. Thompson, and T. Fearn, "Authentication of Basmati rice using near infrared spectroscopy," *J. of Near Infrared Spectro.* 1, pp.77-83 (1993).

[2] S. S. Kim, M. R. Rhyu, J. M. Kim, and S. H. Lee, "Authentication of rice using near-infrared reflectance spectroscopy", *Cereal Chem.* 80, pp. 346-349 (2003).

[3] Y. Shao, Y. He, and F. Cao, "Identification of rough rice species and years by visible/near-infrared reflectance spectroscopy," *Comp. Intel. and Security* 2, 3-6 Nov. 988-991 (2006)

[4] K. Suwansukho, S. Sumriddetchkajorn, and P. Buranasiri, "Combination of simple chemical and spectroscopic methods for the identification of Thai Hom Mali rice," Proc. SPIE 7315, 73150W (2009).

[5] A. Cusano, A. Cutolo, M. Giordano, and L. Nicolais, "Optoelectronic refractive index measurements: application to smart processing," *IEEE Sensors J.* 3, pp. 781-787 (2003).

[6] M.- H. Chen and C. J. Bergman, "Method for determining the amylose content, molecular weights, and weight- and molar-based distributions of degree of polymerization of amylose and fine-structure of amylopectin," *Carbohydrate Pol.* 69, pp. 562-578 (2007).

This material is reserved for educational use only, not allowed for commercial use.
Forbidden to modify the content, and cite the document when use.

CHAPTER 4

NON-DESTRUCTIVE OPTICAL METHODS

In this chapter, non-destructive optical methods for identifying Thai jasmine milled rice were presented. A hypothesis was laid down on the difference of morphology of each milled rice variety. The difference of plant physiology in nature of each milled rice variety such as rice stem size, width and length of rice leaf, panicle features, embryo size, etc. affect grain features of each rice variety. By this basic, shape analysis was developed base on image processing with simple and complex mathematical model for exploring the features of each milled rice variety. Moreover, simple and advance methods such as image subtraction and artificial neural network were used to identify Thai jasmine milled rice variety.

4.1 Two-Wavelength Spectral Imaging-based Thai Rice Breed Identification

Instead of used destructive investigation [1-2] as in chapter 2, the promisingly nondestructive approach is the fluorescent imaging. Previously, all milled rice grains were illuminated with 365 nm wavelength light and its fluorescent radiation at 460 nm was investigated through histogram analysis [3-4]. However, this single wavelength concept is suitable only for the identification of rice varieties that have different amount of amylose content. Instead of investigating at only one wavelength, several wavelength bands of fluorescent radiation under the UVA light have been studied for contamination detection in fruits, meats, and plant leaves [5-7]. With this concept, this topic proposes a non-destructive multispectral-imaging based method for identifying rice breeds. Especially, we utilize only two wavelengths of the fluorescent radiation under a higher energy UVC light source that can induce more fluorescent wavelength bands.

4.1.1 Proposed Two-Wavelength Spectral Imaging-Based Rice Breeds Identifier

4.1.1.1 Architecture of the System

Our proposed two-wavelength spectral imaging-based rice breed identification system is shown in Fig. 4.1. The main components are an exciting high energy light source (e.g., UVC at 253.7 nm wavelength), a tunable optical filter, an imaging lens system, a two-dimensional (2-D) digital camera, and an electronic controlling and processing unit. There is a region in which we can scatter unknown breeds of milled rice grains for analysis. This region is also in the field of view of the imaging lens system. The tunable optical

This material is reserved for educational use only, not allowed for commercial use.
Forbidden to modify the content, and cite the document when use.

filter is working in the visible spectrum and it can be based on several off-the-shelf technologies with and without moving part such as optical interference filters, acousto-optic tunable filters, a combination of two prisms and a grating, tunable Bragg grating, and liquid crystal retarders [8].

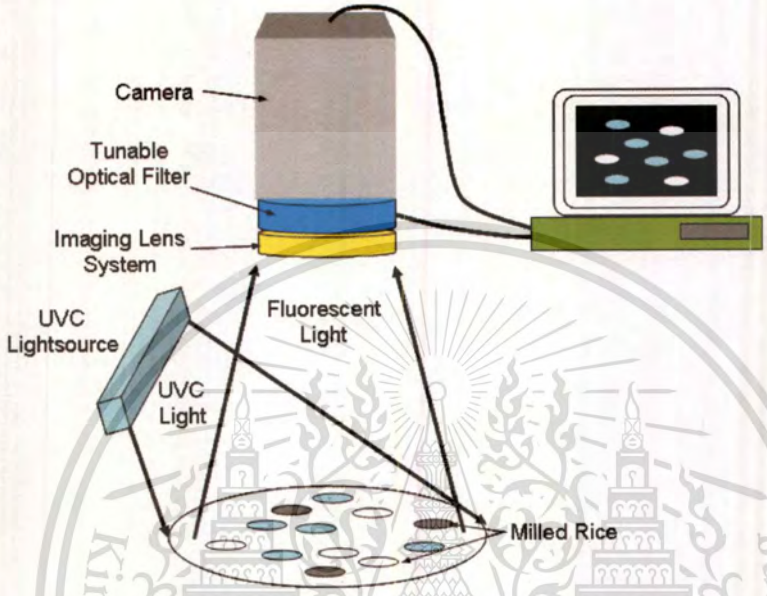

Figure 4.1 Structure of our proposed multispectral imaging-based rice breed identification system.

When the UVC light is shining on all milled rice grains, the corresponding fluorescent radiation is emitted from all milled rice grains and passes through the imaging lens system. The tunable optical filter is electrically controlled in such a way that only the desired wavelength spectrum bands can get through to the 2-D digital camera. Based on our current study [9], we found two very strong fluorescent spectra at 540 nm and 575 nm. In addition, each rice breed gives out different amount of fluorescent radiation. This is probably due to the difference in the amount of amylose content and the level of glutinousness. Therefore, we focus on these two fluorescent wavelengths and two corresponding spectral images are transmitted to our processing unit. Note that unlike the single wavelength analysis used in refs. [3-4], our analysis of two-wavelength spectral offers more information that is needed for identifying rice breeds having the same amount of amylose content. In addition, because UVC light is known as the germicidal light and therefore the use of UVC light during our rice breed identification provides one more advantage in that it can kill unwanted germs attached to milled rice grains.

This material is reserved for educational use only, not allowed for commercial use.
Forbidden to modify the content, and cite the document when use.

4.1.1.2 Procedures of Analysis

Once we have two spectral images associated with 540 nm and 575 nm fluorescent spectral from the milled rice grains, we follow the procedures shown in Fig. 4.2. In this case, the maximum number of wavelengths (N) is equal to 2. Because each rice breed emits different amount of fluorescent radiation, each spectral image goes through two-level image thresholding several times. In each time, the blob filtering is also applied in order to eliminate unwanted image areas. The total number of the resulting images is equal to M and these M images are binary. After we have M binary images, we do image subtraction for two selected binary images. In this way, the remaining image areas correspond to the rice breeds that we are looking for. The coordinate of the remaining image areas tells us the location of the rice breed that we are looking for. Knowing the size of the desired image area, the number of milled rice grains associated can be estimated as well.

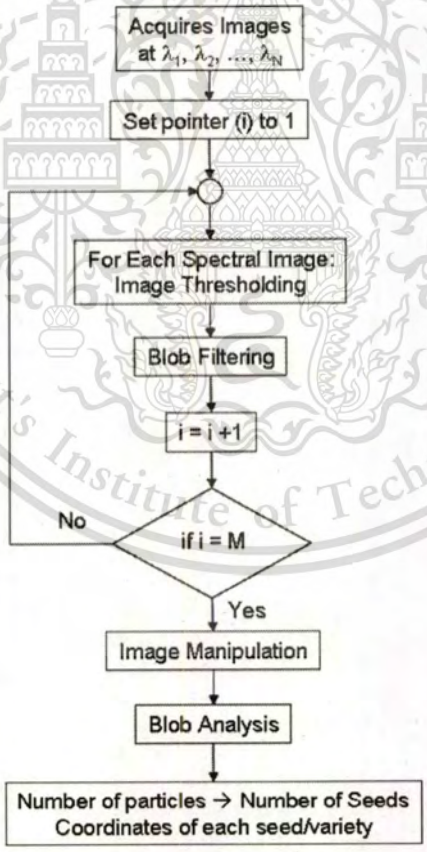

Figure 4.2 Flowchart for analysis of spectral images in order to identify breeds of all milled rice grains.

This material is reserved for educational use only, not allowed for commercial use.
Forbidden to modify the content, and cite the document when use.

4.1.2 Experimental Demonstration

4.1.2.1 Experimental Setup

Our imaging spectrometer is shown in Fig. 4.3 and its wavelength selection scheme is based on the use of a liquid crystal tunable filter (LCTF) [8]. The LCTF is from VariSpec and its model is VIS-7-HC-20. It can be electrically controlled to let the visible light from 400 to 720 nm pass through with an FWHM of 7 nm at a speed of 6 nm/s. The optical transmission depends on the wavelength which the lowest transmission is on the left wing of the spectrum and the highest transmission is on the right edge of the spectrum. The active area is 20 mm in diameter. It is interfaced to the computer via a universal serial bus (USB). For our 2-D image device, we choose a complementary metal oxide semiconductor-based digital camera that provides an 8-bit digital image. It sensing area has 644 (H) × 488 (V) pixels with a pixel dimensions of 8.4 μm × 8.4 μm. This digital camera communicates with a computer through a USB-based frame grabber. The imaging lens system has a specified focal distance of 3.7 mm. UVC light source is an 18-W mercury lamp in a TUV style package from Philips. It emits only one peak wavelength radiation at 253.7 nm. It is settled at the left hand side of the milled rice grains at a distance of 116 mm and it is above milled rice grains at a distance of 65 mm. In this way, UVC light shines uniformly in the area of 40 mm in diameter. We also place a UV block filter that allows only the measured visible wavelength spectrum starting from 410 nm pass through the imaging lens system and fall on the 2-D digital camera.

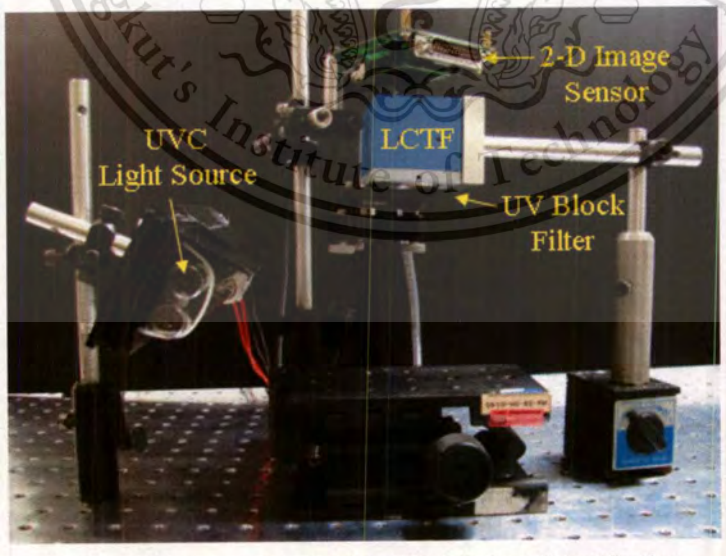

Figure 4.3 Experimental setup for milled rice breed identification.

This material is reserved for educational use only, not allowed for commercial use.
Forbidden to modify the content, and cite the document when use.

Our milled rice grains are from 8 different Thai rice breeds as shown in Fig. 4.4. Four milled rice varieties were mentioned. Other milled rice varieties with specified as low amylose content such as Ko Kor 15 (RD15) and with specified as high amylose content such as Hom Supanburi (HPSR), Hom Pitsanulok (HPSL2), and Ko Kor 23 (RD23) are included. For each milled rice breed, we randomly select 4 milled rice grains and place them on a specific location shown in Fig. 4.5.(a) There are 3 main fluorescent spectral regions in 432-438 nm, 539-553 nm, and 570-585 nm. (see Fig.4.5(b)) All milled rice grains emit fluorescent radiation for which the RD6 shows the strongest fluorescent signal followed with KDML105 milled rice. As the last two fluorescent wavelength bands have the strongest spectral signals for KDML105 milled rice, this topic analyzes spectral images from these two wavelengths. Especially, we choose strong fluorescent spectral signals at 545 nm and 575 nm (see Fig. 4.6). In this case, a measured LCTF switching time between these two selected wavelengths is 45.10 ms.

Figure 4.4 Eight breeds of Thai milled rice grains.

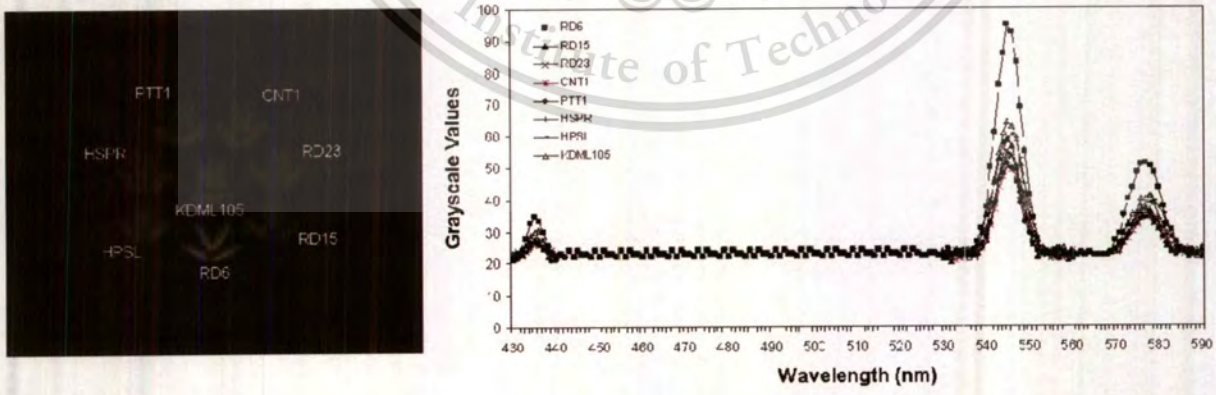

(a) (b)

Figure 4.5 (a) Fluorescent image emitted from all milled rice grains under UVC illumination and (b) fluorescent signals.

This material is reserved for educational use only, not allowed for commercial use.
Forbidden to modify the content, and cite the document when use.

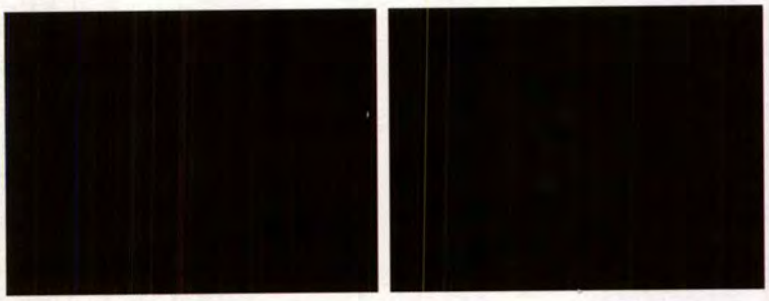

540 nm 575 nm

Figure 4.6 Fluorescent images of milled rice grains from eight rice breeds at 540 nm and 575 nm wavelengths.

4.1.2.2 Analysis

For the fluorescent image at 540 nm wavelength, we first set the image threshold interval at 30-150. In this way, pixels that have their grayscale value less than 30 or more than 150 are highlighted as black while the remaining pixels are set to red. By selecting image areas that have pixels between 660 and 4000 pixels, we obtain the image areas where milled rice grains for RD6 and RD15 appear as shown in Fig. 4.7(a). Lowering the lower limits of the image thresholding interval to 29 and of the blob filtering to 400 makes the two image areas associated with KDML105 and RD23 milled rice grains appear as shown in Fig. 4.7(b).

(a) (b)

Figure 4.7 Results of image manipulation through image thresholding and blob filtering processes for the fluorescent image at 540 nm. (a) Thresholding interval (T) of 30-150 and blob filtering (B) between 660 and 4000 pixels. (b) T = 29-150, B = 400-4000 pixels.

Similarly, for the fluorescent image at 575 nm wavelength, we first set the image threshold interval at 39-150. In addition, by keeping images that contain 30-4000 pixels, we can immediately locate the areas that have only the RD6 milled rice grains as shown in Fig. 4.8(a). Lowering the lower limit of the threshold level to 33 and increasing the lower limit of the blob filtering to 455 pixels let the KDML105 milled rice grains appear along side with the RD6 milled rice grains as shown in Fig. 4.8(b). Three additional image areas that

This material is reserved for educational use only, not allowed for commercial use.
Forbidden to modify the content, and cite the document when use.

contain RD23, RD15, and HSPR60 milled rice grains are highlighted by setting the image threshold level at 30-150 and the blob filtering between 900 and 4000 pixels as shown in Fig. 4.8(c).

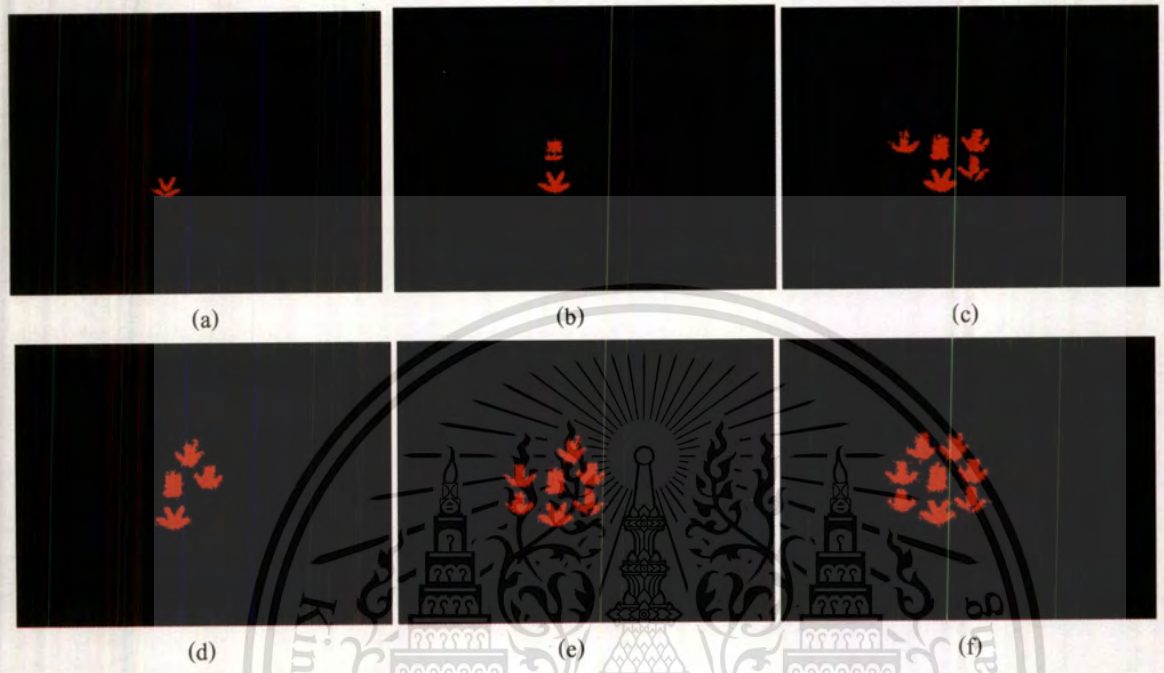

Figure 4.8 Results of image manipulation through image thresholding and blob filtering for the fluorescent image at 575 nm with different thresholding (T) and blob filtering (B) levels. (a) T = 39-150, B = 30-4000 pixels, (b) T = 33-150, B = 455-4000 pixels, (c) T = 30-150, B = 900-4000 pixels, (d) T = 29-150, B = 1200-4000 pixels, (e) T = 28-150, B = 550-4000 pixels, and (f) T = 27-150, B = 400-4000 pixels.

With the image threshold level of 29-150 and the blob filtering set at 1200-4000 pixels, HSPR60 and RD15 milled rice grains disappear while CNT1 milled rice grains show up (see Fig. 4.8(d)). Now, all except PTT1 milled rice grains are shown up when we set the image threshold level to 28-150 and the blob filtering to 550-4000 pixels. In addition, all images of eight rice breeds appear when the image thresholding level and the blob filtering are set to 27-150 and 400-4000 pixels, respectively.

This material is reserved for educational use only, not allowed for commercial use.
Forbidden to modify the content, and cite the document when use.

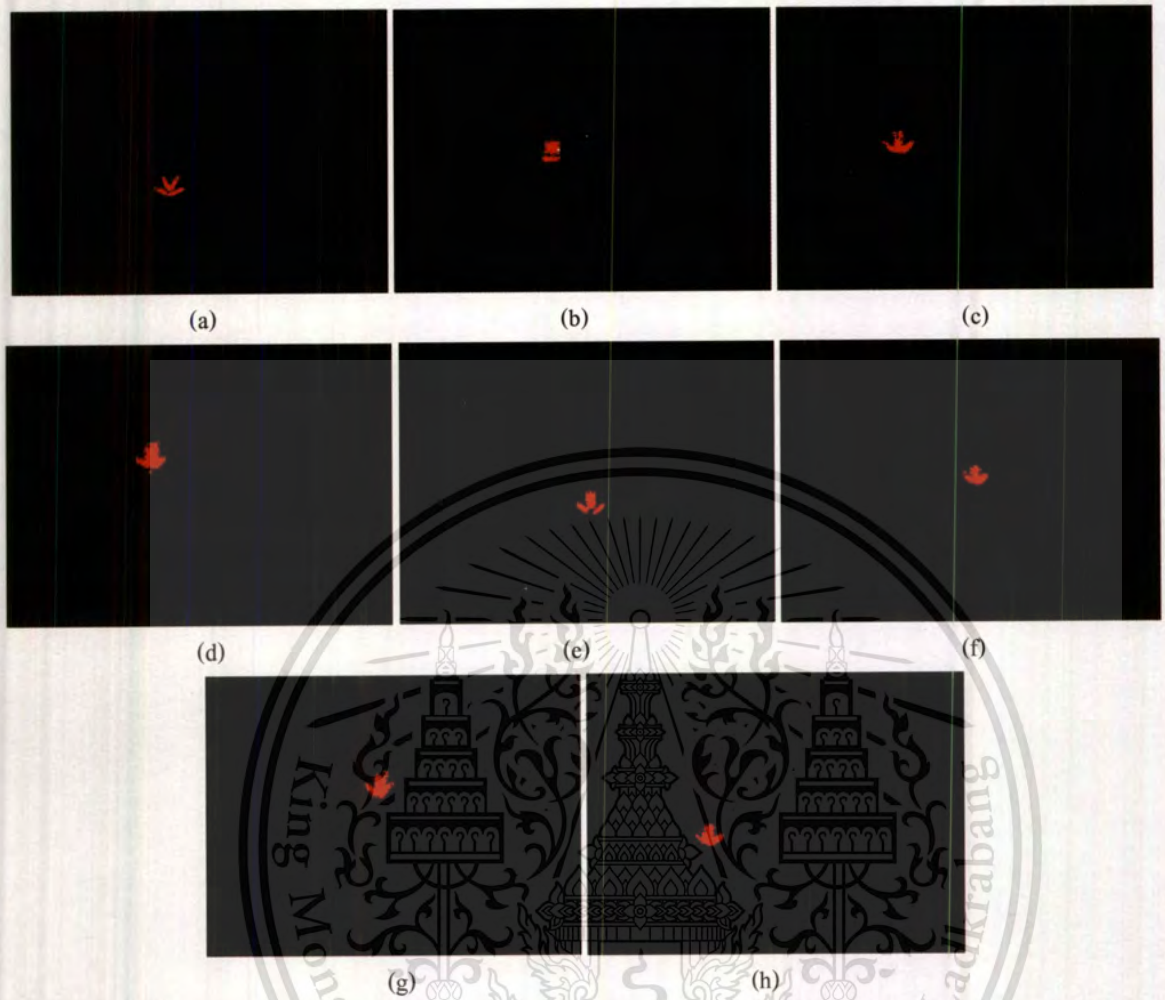

Figure 4.9 All milled rice breeds are identified from the two fluorescent images at 540 nm and 575 nm wavelengths. (a) RD6, (b) KDML105, (c) HSPR60, (d) PTT1, (e) RD15, (f) RD23, (g) CNT1, and (h) HPSL2.

To identify locations of all eight rice breeds, simple image subtraction and blob filtering are employed as follows. Note that from Fig. 4.8(a), RD6 milled rice grains are already identified. By subtracting Fig. 4.8(b) with Fig. 4.8(a) and keeping images that contain pixels between 50 and 4000 pixels, the location of the KDML105 milled rice can be determined as shown in Fig. 4.9(b). Similarly, subtracting images in Fig. 4.8(c) with Fig. 4.7(b) and applying 150-4000 pixels of blob filtering indicates the location of the HSPR60 milled rice grains (see Fig. 4.9(c)). The position of PTT1 milled rice grains (Fig. 4.9(d)) can be found from Figs. 4.8(e)-(f) with blob filtering set at 50-4000 pixels. Image manipulation of Fig. 4.7(a) and Fig. 4.8(a) under blob filtering set at 50-4000 pixels highlights the position of RD15 milled rice grains as manifested in Fig. 4.9(e). With the two images shown in Fig.7 and the image of KDML105 milled rice grains

This material is reserved for educational use only, not allowed for commercial use.
Forbidden to modify the content, and cite the document when use.

in Fig. 4.9(b), RD23 milled rice grains can be identified under the same level of blob filtering. Subtraction of two images in Fig. 4.8(d) and Fig. 4.7(b) together will highlight two positions corresponding to CNT1 and RD15 milled rice grains, respectively. Because RD15 milled rice grains are already determined in Fig. 4.9(e), it can immediately identify the CNT1 milled rice grains. In this case, blob filtering between 200-4000 pixels is also needed. Knowing the location of the CNT1 milled rice grains, the HPSL2 milled rice grains can be identified by subtracting the image in Fig. 4.8(e) with Fig. 4.8(c) and applying blob filtering of 50-4000 pixels. At this stage, all eight breeds of milled rice are identified. As images capturing from these two wavelength spectral can be achieved at a fast 45 ms and the image processing above can be done within 100 ms, real time rice breed identification can easily be accomplished.

King Mongkut's Institute of Technology Ladkrabang

This material is reserved for educational use only, not allowed for commercial use.
Forbidden to modify the content, and cite the document when use.

4.2 Demonstration of a Single-Wavelength Spectral Imaging-based Thai Jasmine Rice Identification

By using higher energy light sources in the UVC spectrum, simultaneous analysis of two-wavelength spectral images near 545 and 575nm wavelengths was preliminarily demonstrated by us for identifying a variety of Thai rice breeds [10]. The use of high-energy UVC light also provides an inherent advantage by reducing contamination levels without generating waste effluents [11]. Based on previous topic, we show here how efficient a single-wavelength spectral image under high-energy UVC light can be used to distinguish our high-quality KDML105 milled rice grains from other rice varieties. In particular, the selected spectral image just goes through a set of blob filtering processes twice, leading to fast identification.

4.2.1 Single-Wavelength Spectral-Imaging-Based KDML105 Milled Rice Breed Identifier

4.2.1.1 Architecture of the System

The arrangement of our single-wavelength spectral imaging-based KDML105 milled rice breed identification system is shown in Fig. 4.10. The main components are still similarly to the previous section. However, the UVC light source was added by one. There is a region in which we can scatter unknown breeds of milled rice grains for analysis. This region is also in the field of view of the imaging lens system. Under the UVC illumination, all milled rice grains are induced to give up their fluorescent radiation. A series of UV block filter and a narrow bandpass optical filter are mounted in front of the 2-D digital camera. The desired fluorescent spectral image is then obtained from the camera.

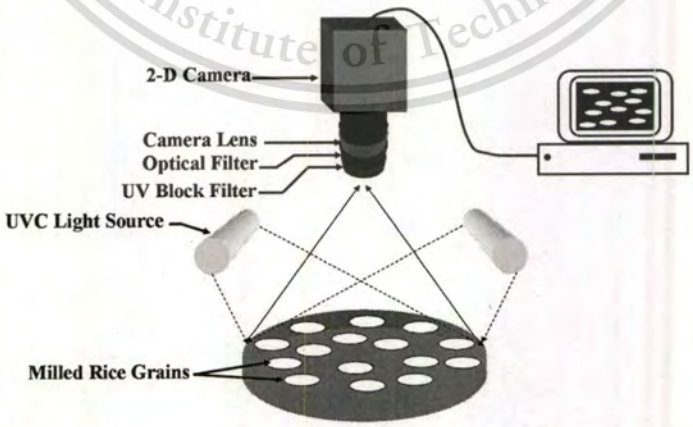

Figure 4.10 Structure of our single-wavelength spectral imaging-based KDML105 milled rice breed identification system.

This material is reserved for educational use only, not allowed for commercial use.
Forbidden to modify the content, and cite the document when use.

4.2.1.2 Analytical Procedures

Once we have the desired spectral image associated with the 545 or 575nm fluorescent wavelength emerging from the milled rice grains, we follow the procedures shown in Fig. 4.11. Each spectral image is normalized by a reference white image. Realizing that each rice breed spatially emits a different amount of fluorescent radiation due to the amount of amylose, amylopectin, and glutin [12–14], the normalized spectral image goes through an image thresholding process in order to filter out unwanted image areas. Our image thresholding can be simply expressed as Eqn. (2.8).

From Eq(2.8), if the gray scale value I(x, y) of each image pixel remains within the desired Th_{min} and Th_{max}, its new gray scale value $I'(x, y)$ will be changed to a maximum gray scale value (e.g., 255 for an 8-bit image). On the other hand, the new gray scale value $I'(x, y)$ of 0 will be assigned if the gray scale value I(x, y) is out of the desired range.

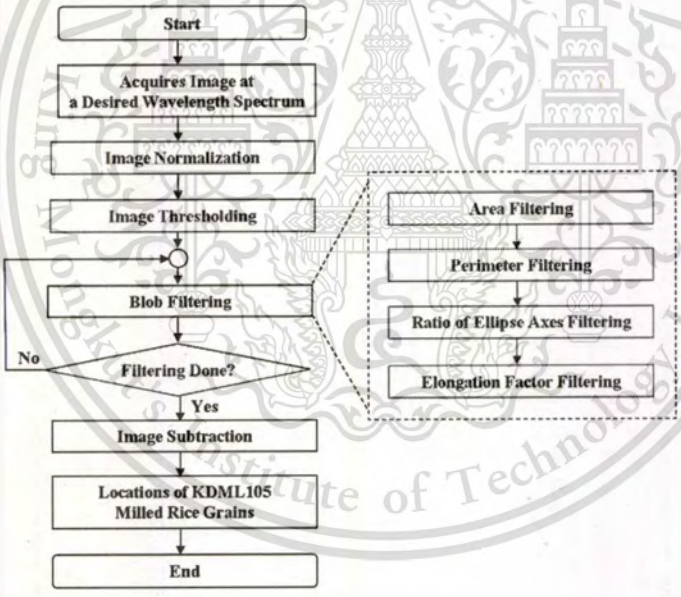

Figure 4.11 Flowchart for analysis of the selected spectral image in order to identify KDML105 milled rice grains.

After that, two blob filtering processes via area and perimeter analysis are applied in order to roughly eliminate unwanted pixels. Because milled rice grains have elliptical shape, the area and perimeter of each milled rice grain can be computed as Eqn. (2.9-2.10). In this case, the interesting areas, whose shape falls within the desired range, will be kept. Similarly, we focus our interest in the image area inside the

This material is reserved for educational use only, not allowed for commercial use.
Forbidden to modify the content, and cite the document when use.

normalized image whose perimeter stays within the appropriate range. Then, the other blob filtering processes via analysis of the ratio of equivalent ellipse axes (RE) and the elongation factor (EF) are applied in order to delicately eliminate the remaining unwanted pixels which can be expressed as Eqn. (2.11-2.12). For each milled rice grain inside the normalized spectral image, it will be kept in the image if its RE and EF values are in the desired ranges. To identify the location of KDML105 milled rice grains, the thresholded spectral image is fed through the above set of blob filtering processes twice. Under the first set of our image filtering process, all KDML105 milled rice grains are kept in the image while milled rice grains from the remaining rice breeds are filtered out as many as possible. On the contrary, our second image filtering process considers the thresholded spectral image and tries to eliminate all KDML105 milled rice grains without affecting milled rice grains from other rice breeds. After that, one filtered image is subtracted by another and the remaining image areas correspond to the locations of KDML105 milled rice grains.

4.2.2 Experimental Demonstration

4.2.2.1 Experimental Setup

Our fluorescent imaging spectrometer is shown in Fig. 4.12. Instead of mechanically changing the optical filter from 545 nm to 575 nm, wavelength during our demonstration, our wavelength selection scheme is based on the use of LCTF. The measured distance between the object plane and the UV block filter is 195 mm. Our imaging device is an 8-bit complementary metal oxide semiconductor-based digital camera modelled Basler scA750-60gc. Its resolution is 752 (H) × 480 (V) pixels with pixel dimensions of 6.0 μm × 6.0 μm and its specified image capturing speed is 60 frames/s.

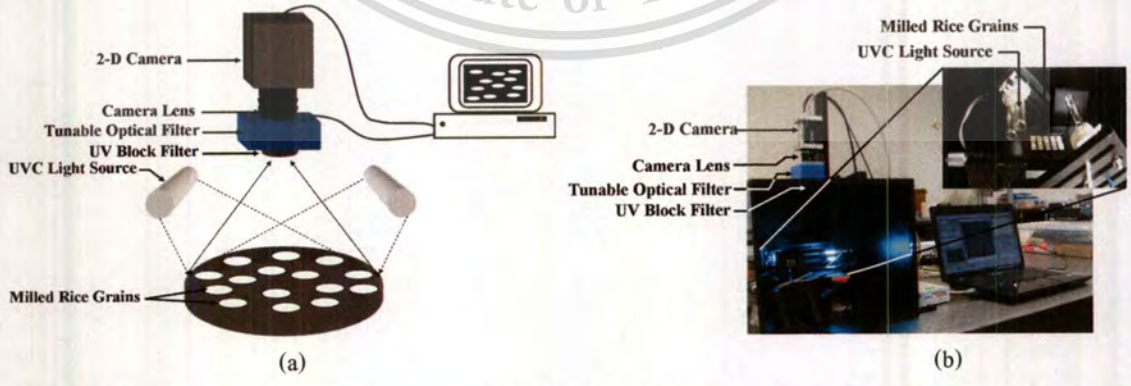

Figure 4.12 Experimental setup for KDML105 milled rice breed identification: (a) diagram and (b) perspective view.

This material is reserved for educational use only, not allowed for commercial use.
Forbidden to modify the content, and cite the document when use.

UVC light source is a 5-W mercury lamp in a TUV style package from Philips. On each side of the whole milled rice grains, two UVC lamps are positioned in such a way that UVC light shines uniformly in the area of 50 mm in diameter. With the use of a 50x50 mm^2 white target from Labsphere, measured variation coefficients of the fluorescent intensity at 545 nm and 575 nm wavelengths are 7.3% and 6.9%, respectively.

4.2.3 Results and Discussions

4.2.3.1 Fluorescent Signals

Our milled rice grains are from 8 different Thai rice breeds as shown in Fig. 4.13. For each milled rice breed, we randomly select 5 milled rice grains. Forty milled rice grains are placed on a specific location in a black sticky plate to prevent grains from touching one another. We prepare three black sticky plates.

Figure 4.13 Close-up view of Thai milled rice grains (a) CNT1, (b) HPSL2, (c) HSPR60, (d) KDML105, (e) PTT1, (f) RD6, (g) RD15, and (h) RD23.

The first two plates (i.e., Set A and Set B) contain 40 milled rice grains arranged according to Fig. 4.14(a) while milled rice grains on the last plate (i.e., Set C) are positioned corresponding to their breeds as shown in Fig. 4.14 (b). Each set is loaded and unloaded to our experimental setup in Fig.4.12 one at a time. Each milled rice grain extends approximately 10×32 pixels in the spectral image. Under the UVC illumination, we observe three main fluorescent spectral bands including 430-448 nm, 540-555 nm, and 570-585 nm wavelengths (see Fig.4.15 (a)).

This material is reserved for educational use only, not allowed for commercial use.
Forbidden to modify the content, and cite the document when use.

CNT1	HPSL	HSPR	KDML105	PTT1
HPSL	HSPR	KDML105	PTT1	RD6
HSPR	KDML105	PTT1	RD6	RD15
KDML105	PTT1	RD6	RD15	RD23
PTT1	RD6	RD15	RD23	CNT1
RD6	RD15	RD23	CNT1	HPSL
RD15	RD23	CNT1	HPSL	HSPR
RD23	CNT1	HPSL	HSPR	KDML105

(a)

KDML105	PTT1	RD6	RD15	RD23
PTT1	RD6	RD15	RD23	CNT1
RD6	RD15	RD23	CNT1	HPSL
RD15	RD23	CNT1	HPSL	HSPR
RD23	CNT1	HPSL	HSPR	KDML105
CNT1	HPSL	HSPR	KDML105	PTT1
HPSL	HSPR	KDML105	PTT1	RD6
HSPR	KDML105	PTT1	RD6	RD15

(b)

Figure 4.14 Arrangement of milled rice grains for (a) Set A and Set B and (b) Set C.

As the last two fluorescent wavelength bands have the strongest spectral signals, we focus on these two fluorescent bands and show how effective a strong fluorescent signal at 545 nm and 575 nm wavelengths can be used for distinguishing our desired KDML105 milled rice grains from ones from other remaining seven rice breeds. It can also be seen from Figs. 4.15 (b)-(c) that RD6 provides the strongest fluorescent signal as it has the lowest amylose content level. In addition, measured variation coefficients in optical intensity of the normalized spectral image at the center of each rice grain vary between 4.9% and 8.7% and between 3.1% and 7.1% for the 545-nm and 575-nm fluorescent radiations, respectively. RD6 also has the lowest intensity fluctuation levels of 4.9% and 3.1% at 545-nm and 575-nm fluorescent radiations, respectively. As a result, locations of all RD6 milled rice grains can be immediately distinguished from the remaining milled rice varieties.

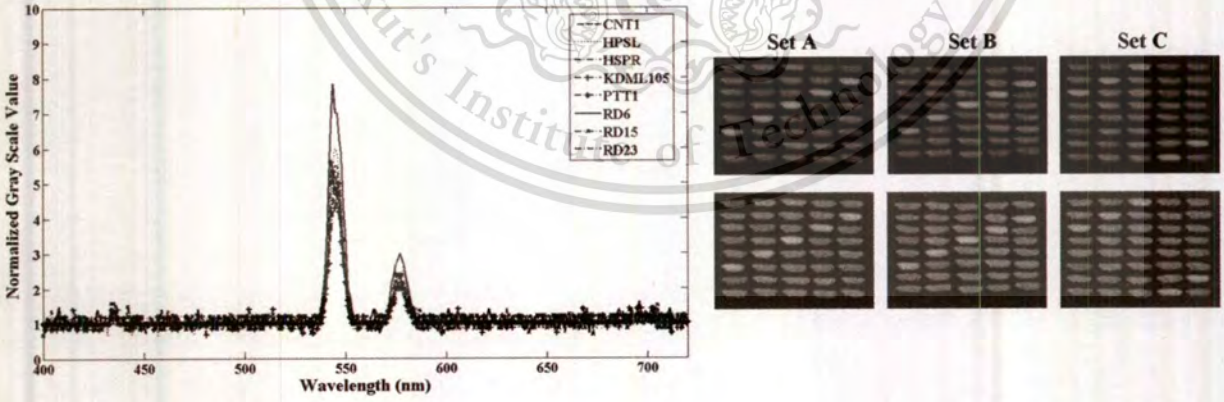

(a) (b)

Figure 4.15 (a) Normalized fluorescent signal measured at the center of each milled rice grain under the UVC illumination. (b) Normalized fluorescent images at 545 nm (top) and 575 nm (bottom) wavelengths for three arrangements of milled rice grains.

This material is reserved for educational use only, not allowed for commercial use.
Forbidden to modify the content, and cite the document when use.

4.2.3.2 Analysis

In this section, the selected normalized fluorescent image goes through our image thresholding process. The range of image thresholding is set to 57-91 for the normalized spectral images at 545-nm wavelength. At this step, image pixels whose grayscale values stay within the desired ranges are highlighted as white while the remaining pixels are set to black (see Fig. 4.16(a)). As a result, 57.1%, 28.6%, and 40.0% of the unwanted milled rice grains in Sets A, B, and C are eliminated, respectively. After that, the normalized spectral image passes through our first blob filtering process with all needed parameters set according to Table 1 in order to let all KDML105 milled rice grains stay in the image while simultaneously eliminate as many other milled rice breeds as possible. In this way, numbers of unwanted milled rice grains in Set A remain at 31.4%, 25.7%, 17.1% and 11.4% inside the image, respectively, as shown in Figs. 4.16(b)-(e) on the left hand side. Similarly, unwanted milled rice grains in Sets B and C are 14.3% and 37.1% left at the end of our first blob filtering process, respectively.

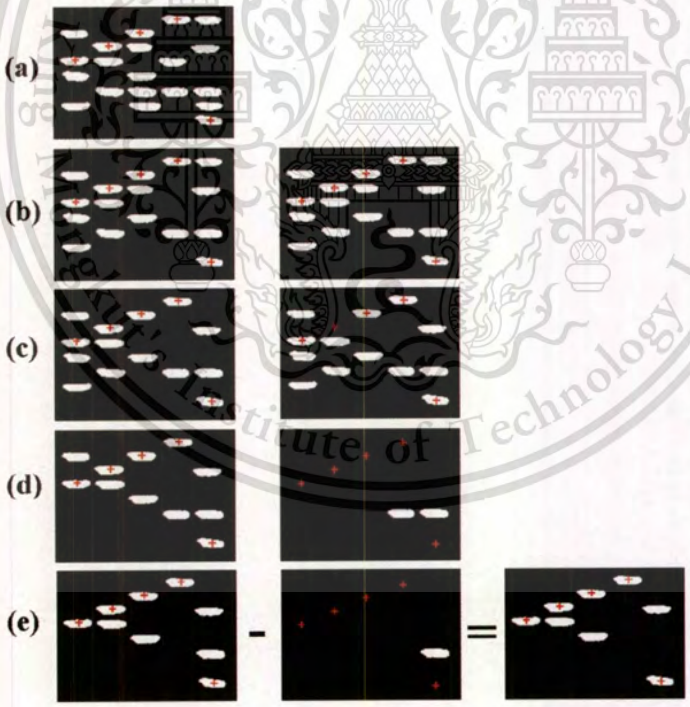

Figure 4.16 Example of the normalized spectral image at 545 nm wavelength after it goes through (a) image thresholding, (b) area filtering, (c) perimeter filtering, (d) RE filtering, and (e) EF filtering. Our first and second image filtering processes are applied to images on the left hand side and in the middle, respectively. Mark red signs correspond to locations of KDML milled rice grains.

This material is reserved for educational use only, not allowed for commercial use.
Forbidden to modify the content, and cite the document when use.

The same binary image shown in Fig. 4.16(a) also passes through our second blob filtering process tabulated in the last column of Table 4.1 in order to eliminate all KDML105 milled rice grains while keeping as many other rice breeds as possible. In this case, ranges of perimeter, RA, and EF parameters are 14%, 71%, and 79% lower compared to those used in our first blob filtering process, respectively. All KDML105 milled rice grains are gradually removed from the image when the selected binary image enters to the area filtering process and emerges at the EF filtering process. At this last step of our blob filtering process, 1, 2, and 4 grains of unwanted milled rice breeds remain in the images of Sets A (see Fig.4.16(e) in the middle), B, and C, respectively. To identify locations of all KDML105 milled rice grains, we subtract Fig.4.16(e) on the left hand side with Fig.4.16(e) in the middle and the resulting image is shown in Fig.4.16(e) on the right hand side. It can be observed that all KDML105 milled rice grains still appear in the image, implying that we obtain a false rejection rate (FRR) of 0%. In addition, some of unwanted milled rice grains remain inside the image, indicating a false acceptance rate (FAR) of $100\times3/35 = 8.6\%$. For Sets B and C, we achieve 0% FRR for both cases while FARs of $100\times3/35 = 8.6\%$ and $100\times8/35 = 22.9\%$ are accomplished, respectively. These results indicate an average FAR of 13.4%. Our analytical process takes only 25 ms.

Table 4.1 Parameters used during our image filtering processes for the selected 545-nm fluorescent image

	1st Image Filtering Process		2nd Image Filtering Process	
Parameters	Lower Value	Upper Value	Lower Value	Upper Value
Area (pixel^2)	240.00	284.00	240.00	284.00
Perimeter (pixels)	69.30	75.90	69.60	75.30
Ratio of Ellipse Axes	2.62	2.99	2.65	2.76
Elongation Factor	3.64	4.11	3.72	3.82

Similarly for the 575 nm spectral image, because its normalized spectral values are higher compared to those of the 545-nm spectral image (see also Fig. 4.15(b)), we assign a higher expected range of image thresholding to 90-144 which in turn leads to a binary image shown in Fig.4.17(a). In this case, 8.6%, 8.6%, and 5.7% of the unwanted milled rice grains for Sets A, B, and C are eliminated, respectively. After that, the normalized spectral image passes through our first blob filtering process with all needed parameters set according to Table 4.2 in order to let all KDML105 milled rice grains stay in the image while eliminating as many other milled rice breeds as possible. In this way, numbers of unwanted milled rice grains for Set A are

This material is reserved for educational use only, not allowed for commercial use.
Forbidden to modify the content, and cite the document when use.

much reduced to 34.3%, 57.1%, 65.7%, and 68.6%, respectively, as shown in Figs.4.17(b)-(e) on the left hand side. Similarly, unwanted milled rice grains in Sets B and C remain at 65.7% and 65.7% at the end of our first blob filtering process.

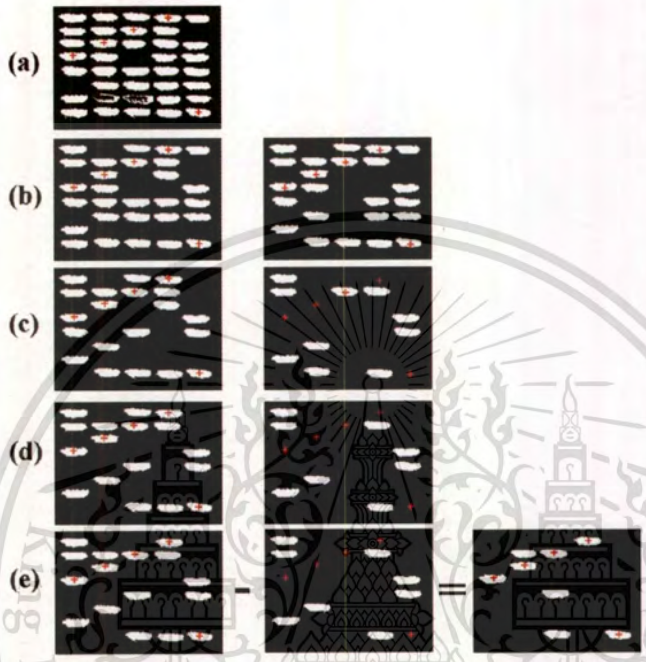

Figure 4.17 Example of the normalized spectral image at 575 nm wavelength after it goes through (a) image thresholding, (b) area filtering, (c) perimeter filtering, (d) RE filtering, and (e) EF filtering. Our first and second image filtering processes are applied to images on the left hand side and in the middle, respectively. Mark red signs correspond to locations of KDML105 milled rice grains.

The same binary image shown in Fig.4.17(a) also passes through our second blob filtering process tabulated in the last column of Table 4.2 in order to eliminate all KDML105 milled rice grains and simultaneously keep as many milled rice grains of the remaining rice breeds as possible. In this case, ranges of area, perimeter, RA, and EF parameters are 35%, 43%, 32%, and 33% lower compared to those used in our first blob filtering process, respectively. All KDML105 milled rice grains are gradually removed from the image when it is entered to the area filtering process and emerges at the EF filtering process. At this last step of our blob filtering process, 8, 3, and 8 grains of unwanted milled rice breeds remain in the images of Sets A (see Fig. 4.17(e) in the middle), B, and C, respectively. To identify locations of all KDML105 milled rice grains, we subtract an image on the left hand side of Fig. 4.17(e) by the image in the middle and the resulting image is shown on the right hand side. It can be observed that all KDML105 milled rice grains still appear in

This material is reserved for educational use only, not allowed for commercial use.
Forbidden to modify the content, and cite the document when use.

the image, pointing out an FRR of 0%. Nevertheless, some of unwanted milled rice grains remain inside the image, indicating an FAR of 100×3/35 = 8.6%. For Sets B and C, we also achieve 0% FRR for both cases while FARs of 100×9/35 = 25.7% and 100×4/35 = 11.4% are accomplished, respectively. This result indicates an average FAR of 15.2%.

Table 4.2 Parameters used during our image filtering processes for the selected 575-nm fluorescent image

	1st Image Filtering Process		2nd Image Filtering Process	
Parameters	Lower Value	Upper Value	Lower Value	Upper Value
Area (pixel^2)	251.00	294.00	251.00	279.00
Perimeter (pixels)	73.00	78.90	74.10	77.50
Ratio of Ellipse Axes	2.87	3.37	2.88	3.22
Elongation Factor	3.27	4.10	3.54	4.10

Another important issue is the tolerance of our identification method to the change in each parameter used during our blob filtering processes. By simultaneously adjusting the lower and upper levels of each parameter within ±0.10 steps, we find that an additional FAR of 5.7-37.1% is obtained while the change in FRR can be up to 60% for all three sets of arrangement. This low system tolerance can be improved by adjusting the imaging system in such a way that each milled rice grain can be seen clearer. Increasing the intensity of UVC light sources and making the UVC illumination more uniform across the object plane will also help increase the signal to noise ratio and reduce the intensity fluctuation across the area.

This material is reserved for educational use only, not allowed for commercial use.
Forbidden to modify the content, and cite the document when use.

4.3 Improvement of Single-Wavelength based Thai Jasmine Rice Identification with Elliptic Fourier Descriptor and Neural Network Analysis

Another optical approach that promises non-destructive analysis is the spectral imaging as it has recently been employed for several applications. These include data-non intrusive credit card verification [16-17], 2-D banana ripeness estimation [18], and blood stain detection [19]. By using higher energy light sources, a combination of two-wavelength (545 nm and 575 nm) fluorescent spectral imaging-based Thai rice breed identification was proposed and experimentally demonstrated [10]. Because the selected 20×45-pixel spectral image at 575 nm contains little detail of milled rice grain from low image magnification and fluorescent signal of the system, the system repeatability and reliability in identifying KDML105 milled rice grains were below the requirement. We also proposed and demonstrated that only a single wavelength spectral image when combined with simple image processing operations were sufficient for the identification of Thai jasmine milled rice from unwanted CNT1 HPSL2, and PTT1 milled rice varieties with measured false acceptance rates (FAR) of <26.7% and <40.0% and false rejection rates (FRR) of 0% for spectral images at 545 and 575 nm wavelengths, respectively [20].

To improve the performance of our single-wavelength based KDML105 identification system, specific information of rice grains in the spectral image needs to be deliberately taken into consideration. One interesting approach for extracting this specific information of the rice grain from the image is to apply the elliptic Fourier descriptor (EFD) [21]. The EFD can be applied to very complex curves [22] and have been effectively employed for the evaluations of various biological shapes, animal organs [23-25], and plants [26-29]. The EFD describes shape mathematically through transforming coordinates information concerning its contours into Fourier coefficients. Hence, we show here how the EFD can be applied to our spectral image and when analyzed by a trained artificial neural network [30-31] leads to an improved FAR in identifying Thai jasmine rice grains.

4.3.1 Single-Wavelength Based Thai Jasmine Milled Rice Variety Identifier

The arrangement of our single-wavelength spectral imaging-based KDML105 milled rice breed identification system is shown in Fig. 4.18. The main components are still the same previous topic. However, the LCTF was substituted by a narrow band-pass optical filter centered at the selected 546 nm fluorescent wavelength spectrum and a reflector plate was used.

This material is reserved for educational use only, not allowed for commercial use.
Forbidden to modify the content, and cite the document when use.

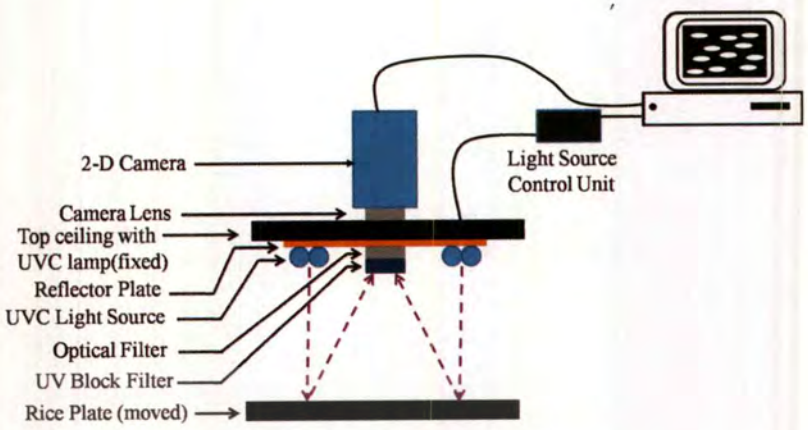

Figure 4.18 Structure of single-wavelength spectral-imaging based KDML105 milled rice breed identification.

4.3.2 Image Analysis

Once we have the desired spectral image. The spectral image is normalized by its background. Realizing that each rice breed spatially emits a different amount of fluorescent radiation due to the amount of amylose, amylopectin, and glutin [12–14], the normalized spectral image goes through an image thresholding process in order to filter out unwanted image areas. Our image thresholding can be simply expressed as Eqn. (2.8). After that, the shape of the milled rice grain is modeled using the normalized EFD of a closed-contour of the grain boundary. The closed-contour is defined with Freeman chain codes [32], represented by a sequence of unit vectors and directional coding as shown in Fig. 2.7. Individual grain boundary pixels are used to describe the chain code, starting with the upper left pixel of the contour and tracing the boundary clockwise. The chain code enumeration is completed when the original starting point is reached. From Fig. 2.7(a), a chain code of 00000000707766554544444444343432210101 is obtained by following code directions in Fig. 2.7(b). It can be assumed that a point at the starting position is travelling along the image boundary with a constant speed. The time used to travel between links depending on the code of the chain which is mathematically written as in Eqn. (2.13).

Eqn. (2.13) is equal to 1 if a code is an even and $\sqrt{2}$ if a code is an odd. For a close contour pattern, the roundtrip time (tp) can be written as Eqn. (2.14). Once the Δt_i is known, its corresponding travelling distances along the x and y axes can be found as Eqns. (2.15-2.17). Similarly, close-loop travelling distances along x and y axes can be written as Eqns. (2.18-2.19). As the chain code is a function of time and line segments along the boundary, we can consider it as a discrete periodic pattern whereby it can be mathematically analyzed by Fourier series. In this case, the Fourier series expansion of the closed-contour

This material is reserved for educational use only, not allowed for commercial use.
Forbidden to modify the content, and cite the document when use.

which is a projection of the contour on the x and y axes can be obtained as Eqns. (2.20-2.21). And, Fourier coefficients can be found by using Eqns. (2.22-2.27). Here, as shown in Fig. 2.8, Δx_p and Δy_p are the segments between p and p + 1 of the closed-contour projected onto the x and y axes, respectively. Δt_p is the step between p and p + 1 of the closed-contour. t_p is the curvilinear coordinate of the point p and K is the number of sampling points on the closed-contour. The shape descriptor determined using Eqns. (2.22-2.27) clearly depends upon the size of grains, the orientation of grains, and the starting point of the chain-code. As a result, they cannot directly be used to indicate the variability for comparison of the grain kernels. To alleviate these problems, the normalized Fourier coefficients are considered based upon the ellipse of the first harmonic as Eqns. (2.28-2.31). The number of sets of elliptic Fourier coefficients increases as the number of harmonics increases. For each harmonic set, four coefficients are always generated. The Fourier amplitude is related to the number of harmonics by the following expression of Eqn. (2.32).

From Eqn. (2.32), the maximum number of the harmonics in our analysis is set to N = 17 as its shape is almost matched to the original shape of the rice grain. Increasing the maximum number of harmonics under our analysis does not tremendously improve the shape similarity but does require more analytical time. Using these normalized harmonic coefficients, each harmonic can be graphically represented as an ellipse and can be analyzed in terms of semi-major axis, semi-minor axis, area, and perimeter by using Eqns. (2.34-2.37). These four parameters in each harmonic are fed into our feed-forward back-propagation neural-network (FFNN) structure. During training the FFNN, its weighting and biasing values are automatically adjusted. Performance of the developed FFNN model in identifying KDML105 milled rice grains are described in terms of the mean square error (MSE), FAR, and FRR.

4.3.3 Demonstration

4.3.3.1 Prototype Setup

Our spectral imaging system for the identification of KDML105 milled rice gain is shown in Fig. 4.19. Compared to sections 4.2, we increase the number of UVC lamps from 2 to 4 with an end-to-end connected arrangement. Each UVC light source is a 5W mercury lamp in a TUV style package from Philips. We also place a reflector plate above UVC lamps. In addition, we move the object plane closer from 195 mm in our previous work to 70 mm. In this scenario, the whole milled rice grains under investigation are uniformly illuminated by stronger UVC light in an area of 50 mm in diameter (see Fig. 4.20 (a)), inducing stronger fluorescent signals which relates to gray scale values as shown in Fig. 4.20 (b). Our 2-D image device

This material is reserved for educational use only, not allowed for commercial use.
Forbidden to modify the content, and cite the document when use.

is an 8-bit complementary metal-oxide-semiconductor- based digital camera. Its resolution is 480(V) × 752(H) pixels with specified pixel dimensions of 6.0 μm × 6.0 μm. It can capture a sequence image at a specified highest speed of 60 frames/s. A narrow bandpass optical filter centered at the selected 546 nm wavelength is used to allow only the 546-nm fluorescent wavelength spectral image pass through the camera. We also place a UV block filter in front of the narrow bandpass optical filter in order to prevent narrow band-pass optical filter and the 2-D image sensor from damaging by the UVC light.

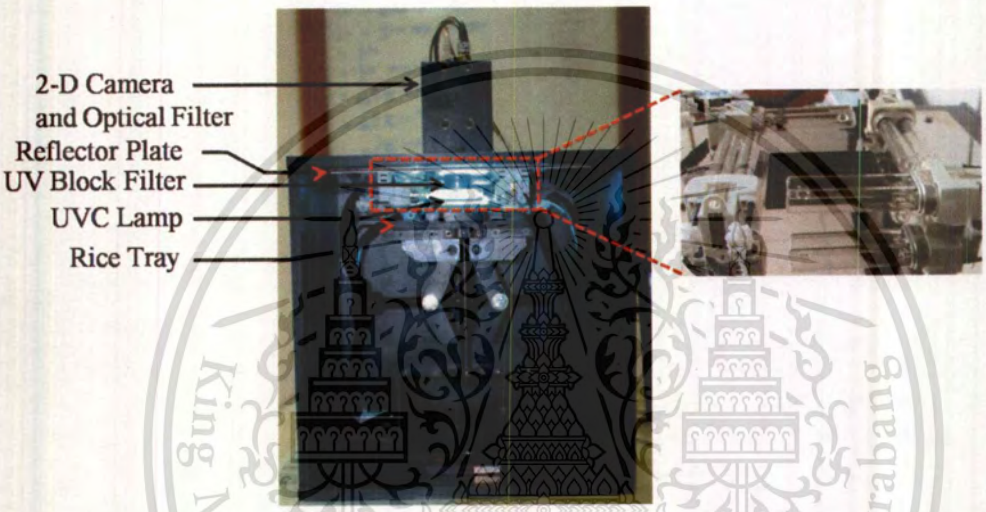

Figure 4.19 Prototype of our spectral imaging system for KDML105 milled rice breed identification.

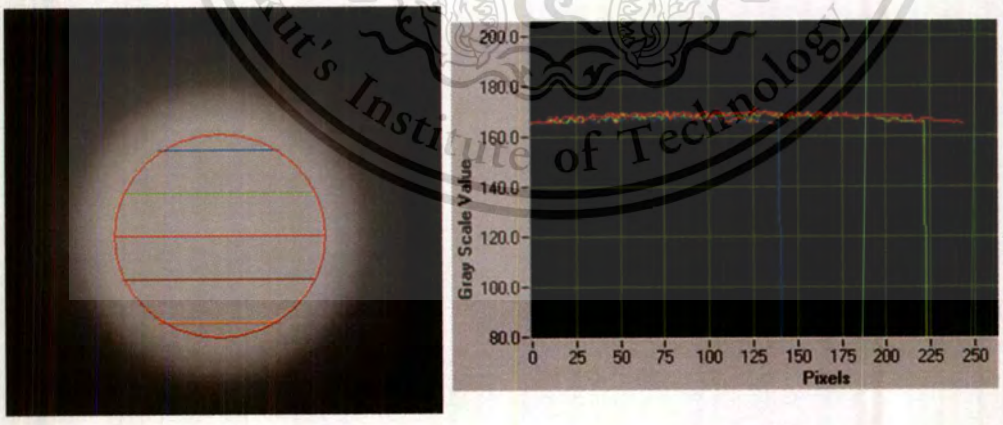

(a) (b)

Figure 4.20 Light uniformity measurement (a) 50 mm-diameter of active area with line intensity measured on white balance material and (b) gray scale value of each line on white balance material which related to light intensity measured by LabVIEW programming.

This material is reserved for educational use only, not allowed for commercial use.
Forbidden to modify the content, and cite the document when use.

4.3.3.2 Materials

Milled rice grains from CNT1, HPSL2, KDML105, and PTT1 varieties are used in our study as shown in Fig.4.21. These milled rice grains have measured average elliptic axes ratios of 0.27 ± 0.01, 0.25 ± 0.01, 0.28 ± 0.01, and 0.27 ± 0.01, respectively. These milled rice grains are positioned on a black rice tray and they are aligned in the same direction as shown in Fig. 4.22(a). A total of 800 milled rice grains, 200 for each milled rice variety, are investigated. Fig. 4.22(b) shows a 235 × 305-pixel spectral image of three CNT1 milled rice varieties captured at 546-nm wavelength. This spectral image is automatically cropped to 90 × 192 pixels in which it contains only one rice grain having an image size of 3730 pixels. This new image size of the rice grain is 1400% compared to the image of the rice grain obtained from our previous system.

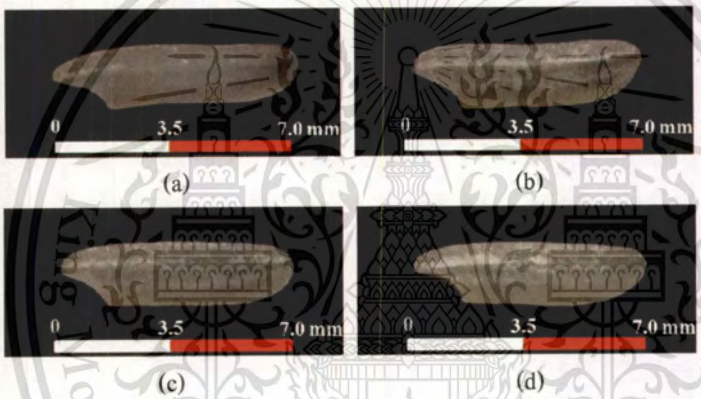

Figure 4.21 Close-up view of Thai milled rice grains (a) CNT1, (b) HPSL2, (c) KDML105, and (d) PTT1 used in our demonstration.

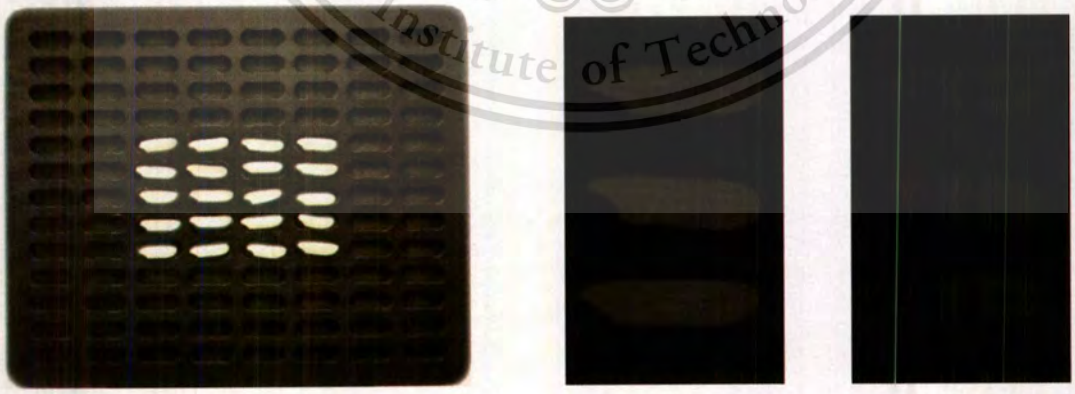

Figure 4.22 (a) Arrangement of milled rice grains on a black rice tray, (b) a spectral image of milled rice grains, and (c) a normalized spectral image of milled rice grains.

This material is reserved for educational use only, not allowed for commercial use.
Forbidden to modify the content, and cite the document when use.

4.3.4 Results and Discussion

The normalized spectral image shown in Fig. 4.22(c) goes through our image thresholding process. The lower threshold value is varied from 30 to 40. The upper threshold is fixed at 70. As a result, we obtain 11 normalized spectral images as shown in Fig. 4.23. After that, normalized elliptic Fourier coefficients are computed for each normalized spectral image. In our analysis, only the first 17 harmonics shown in Fig. 4.24 are taken into consideration.

Figure 4.23 Eleven threshold images under different levels of the lower threshold.

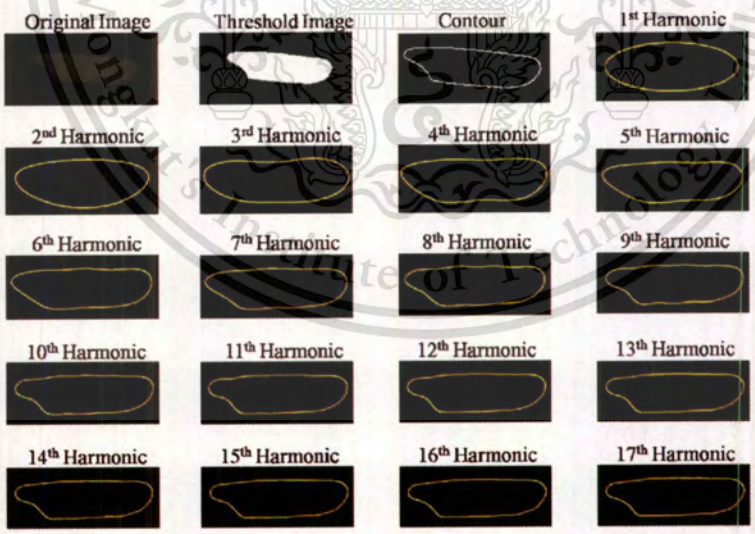

Figure 4.24 Seventeen normalized EFD harmonics of the "threshold 30" in Fig. 4.22.

For each harmonic shown in Fig. 4.24, its normalized Fourier coefficients are calculated which in turn lead to corresponding area, perimeter, semi-major, and semi-minor of that harmonic image. This indicates that there

This material is reserved for educational use only, not allowed for commercial use.
Forbidden to modify the content, and cite the document when use.

are 68 data obtained from just one threshold image. Fig.4.25 shows the principle component analysis (PCA) of elliptic parameters. The PCA results point out that a highly-accurate identification of the KMDL105 milled rice variety cannot be accomplished by just directly analyzing all elliptic parameters.

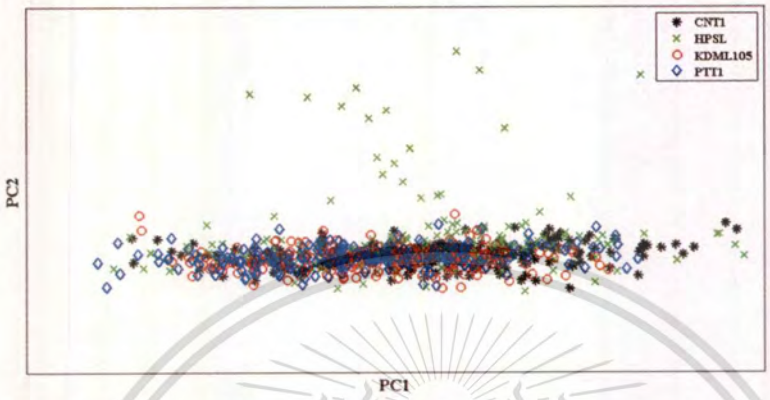

Figure 4.25 PCA of milled rice grain geometry.

With the use of the FFNN, we divide the elliptic parameters into three pairs: KDML105-CNT1, KDML105-HPSL2, and KDML105-PTT1. In each pair of the data set, randomly selected data sets from 100 milled rice grains are used for training the FFNN and the remaining data sets are used for testing the FFNN. Our FFNN configuration contains one input layer with sixty eight (i.e., 17 harmonic images × 4 elliptic parameters = 68 for one threshold image) input ports, four hidden layers, and one output layer. Our four hidden layers have seven, nine, seven, and one nodes with Log-sigmoid, Log-sigmoid, linear and linear transfer functions, respectively. The output layer is assigned to be 1 for the KMDL105 rice variety and 0 for others. During the FFNN training session for 100,000 training epochs via Levenberg–Marquardt function (see Eqn. (2.44)), we adjust all weight and bias values in all layers through the gradient descent weight and bias function with the MSE at the output layer as our learning indicator. Our training results for KDML105-CNT1, KDML105-HPSL2, and KDML105-PTT1 take 1:15 h, 2:13 h, and 1:15 h to finish with determined very low MSEs of 5.48×10^{-14}, 8.37×10^{-14}, and 3.91×10^{-15}, respectively.

This material is reserved for educational use only, not allowed for commercial use.
Forbidden to modify the content, and cite the document when use.

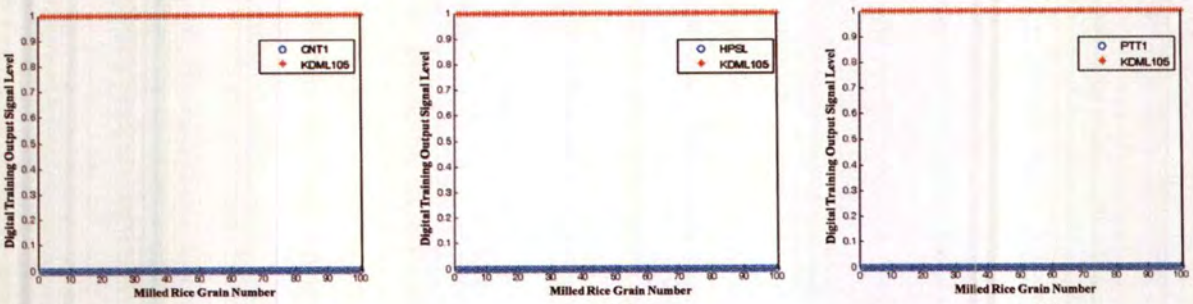

(a) (b) (c)

Figure 4.26 Training results of each data pair (a) CNT1-KDML105, (b) HPSL2-KDML105, and (c) PTT1-KDML105.

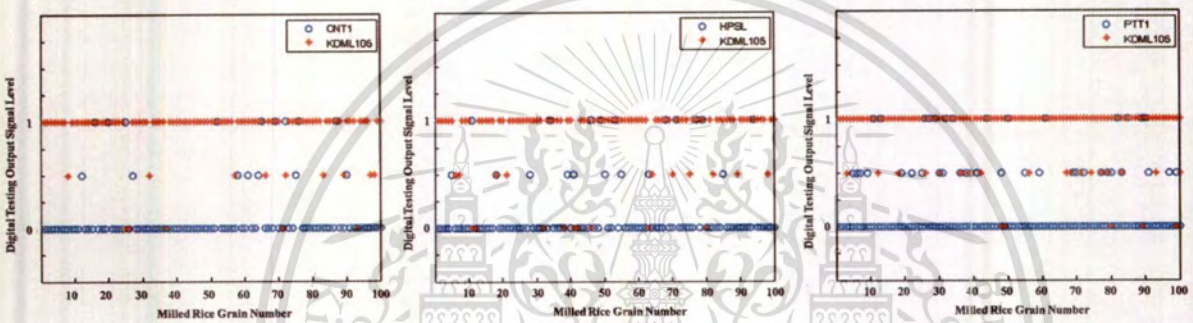

(a) (b) (c)

Figure 4.27 Testing results of each data pair (a) CNT1-KDML105, (b) HPSL2-KDML105, and (c) PTT1-KDML105.

As described earlier that one spectral image is expanded to 11 threshold images, we obtain 11 output values from the FFNN. These 11 output values are average into one output value. If the average output value is > 0.6, it will be round up to 1, indicating that the spectral image of the milled rice grain under investigation is the KDML105. Identification results of the KMDL105 milled rice grain during the training and testing session are shown in Figs. 4.26 and 4.27, respectively. It can be observed that FFNN can efficiently accomplish the goal during its training period. With unknown data sets, our FFNN can identify KDML105 milled rice variety from CNT1, HPSL2, and PTT1 with measured FARs of $100 \times (9/100) = 9.0\%$, $100 \times (10/100) = 10.0\%$, and $100 \times (14/100) = 14.0\%$, respectively. Their associated FARs of 14.0%, 19.0%, and 24.0% are also determined.

This material is reserved for educational use only, not allowed for commercial use.
Forbidden to modify the content, and cite the document when use.

4.4 Single-Wavelength based Thai Jasmine Rice Identification with Polynomial Fitting Function and Neural Network Analysis

4.4.1. Introduction

There is still a big room in lowering the FAR of our system, we have recently applied elliptic Fourier descriptors (EFDs) to find specific information from the spectral image and then employed a neural network analysis (NNA) to help identify the KDML105 from the three unwanted rice varieties, featuring lower FAR and higher FRR values of 11.0% and 19.0%, respectively [34]. Another limitation in this approach is very long computation time of > 1.1 hrs during the analysis of the specific information via EFDs, implying impracticality. To suppress the computation time and still achieve very low FAR and FRR values, a less complicated mathematical expression with high degrees of freedom is preferred. One simple mathematical expression is the polynomial as it was previously used for approximating the shape of the image and extracting some important image feature [35-38]. Here, we show that a polynomial function can be used to describe the rice shape from the spectral image and when analyzed by a trained NNA leads to the improvement of FAR, FRR, and processing time in identifying Thai jasmine rice grains.

4.4.2 Image analysis

With the chain coding image, the polynomial function is applied in order to fit line segments that travel along x and y axes with respect to the traversal time. After that, the fitting curves on x and y axes are recombined to reconstruct a new smoothing boundary. The polynomial function of n orders can be defined as Eqn. (2.33). Using the chain coding and the fitted boundary, a geometry feature can be analyzed in terms of perimeter [39], area, and eccentricity [40] by the Eqns. (2.38-2.42).

4.4.3 Materials

Milled rice grains of CNT1, HPSL2, KDML105, and PTT1 varieties (Fig.4.28) are tested. These milled rice grains have measured average eccentricity values of 0.27±0.01, 0.25±0.01, 0.28±0.01, and 0.27±0.01, respectively. These milled rice grains are positioned on a black rice tray and they are aligned in the same direction. A total of 1000 milled rice grains, 250 for each milled rice variety, are investigated.

This material is reserved for educational use only, not allowed for commercial use.
Forbidden to modify the content, and cite the document when use.

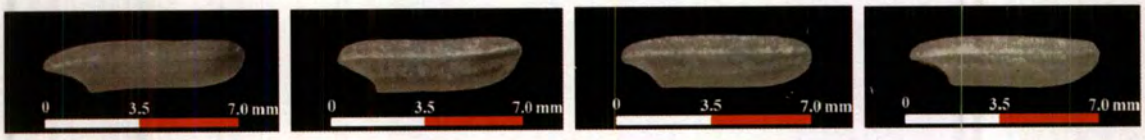

(a) (b) (c) (d)

Figure 4.28 Zoomed image of Thai milled rice grains (a) CNT1, (b) HPSL, (c) KDML105, and (d) PTT1 used in our demonstration.

Fig. 4.29(a) shows a 235×305-pixel spectral image of three CNT1 milled rice varieties captured at 546-nm wavelength. This spectral image is automatically cropped to 90×192 pixels in which it contains only one rice grain having an image size of 3730 pixels.

(a) (b)

Figure 4.29 (a) 235×305 image size of a spectral image of milled rice grains and (b) a threshold image of milled rice grains.

4.4.4. Results and Discussion

The spectral image in Fig. 4.29(a) is normalized by the background and goes through our image thresholding process whose lower and upper threshold values are fixed at 30 and 70, respectively. The threshold image is shown in Fig. 4.29(b). After that, the boundaries of the threshold images are determined by the chain coding process as shown in Fig. 4.30(a). As mentioned earlier, the image boundary can be plotted along the travelling distance on x and y axes with respect to the travelling time as shown in Fig. 4.30(b-c), respectively.

This material is reserved for educational use only, not allowed for commercial use.
Forbidden to modify the content, and cite the document when use.

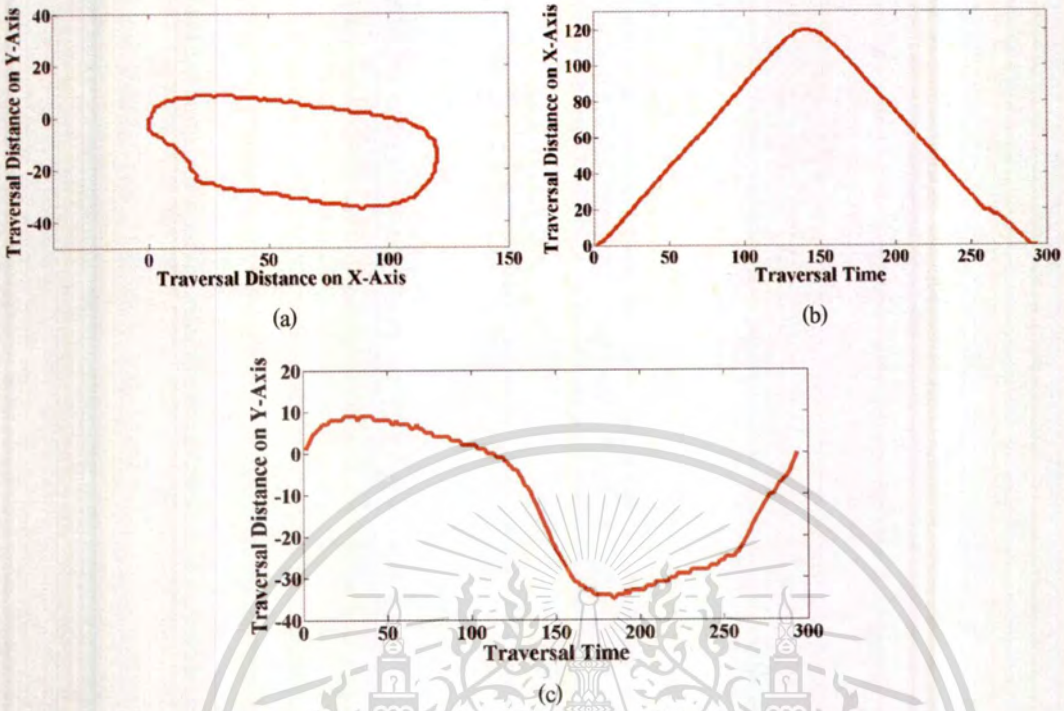

Figure 4.30 (a) Boundary of the threshold image computed from the chain coding process. (b-c) Line segments of the image boundary projected on the x and y axes, respectively.

Line segments in Fig.4.30 (b-c) are then fitted by using a polynomial function in Eqn(4.30). Fitted polynomial lines associated with the boundary segments travelling along x and y axes are manifested in Fig.4.31(a) and Fig.4.31(b), respectively. The orders of the polynomial fitting functions are 15 and 12 for the traversal distances on x and y axes with corresponding linear regression of 0.99984 and 0.99843, respectively. Finally, both fitted polynomial curves are reconstructed to form a new boundary image of a milled rice image as shown in Fig. 4.31(c).

This material is reserved for educational use only, not allowed for commercial use.
Forbidden to modify the content, and cite the document when use.

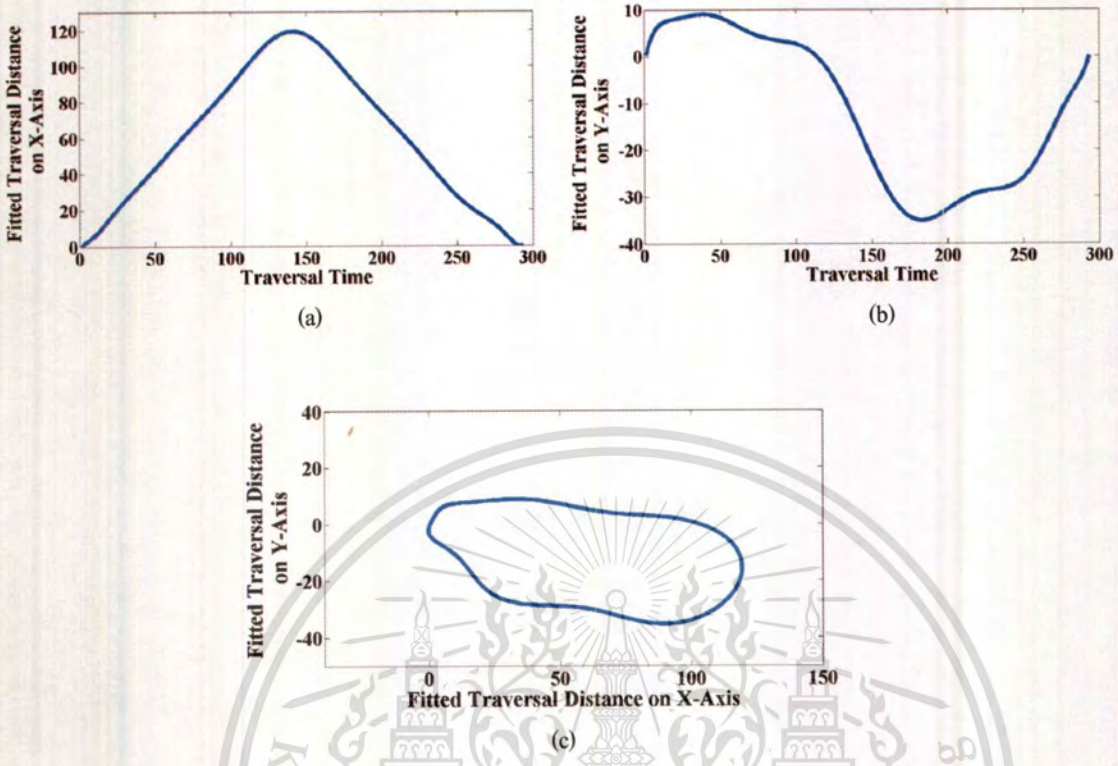

Figure 4.31 Fitted line segments of the travelling distances along the (a) x axis and (b) y axis. (c) Reconstructed image contour from the fitted line segments in (a) and (b).

With the use of the feed forward back propagation neural network (FFNN), we divide the shape parameters into three pairs: CNT1-KDML105, HPSL2-KDML105, and PTT1-KDML105. In each pair of the data set, randomly selected data sets from 150 milled rice grains are used for training the FFNN and the remaining data sets are used for testing the FFNN. Our FFNN configuration contains one input layer with three (i.e., area, perimeter and eccentricity for one threshold image) input ports, four hidden layers, and one output layer. Our four hidden layers have eleven, fifteen, eleven, and one nodes with Log-sigmoid, Log-sigmoid, Log-sigmoid and linear transfer functions, respectively. The output layer is assigned to be 1 for the KMDL105 rice variety and 0 for others. With Levenberg–Marquardt function, the training results for CNT1-KDML105, HPSL2-KDML105, and PTT1-KDML105 pairs take 1:20 h, 1:18 h, and 1:18 h to finish with determined very low MSEs of 3.95×10^{-16}, 2.21×10^{-19}, and 5.13×10^{-13}, respectively.

This material is reserved for educational use only, not allowed for commercial use.
Forbidden to modify the content, and cite the document when use.

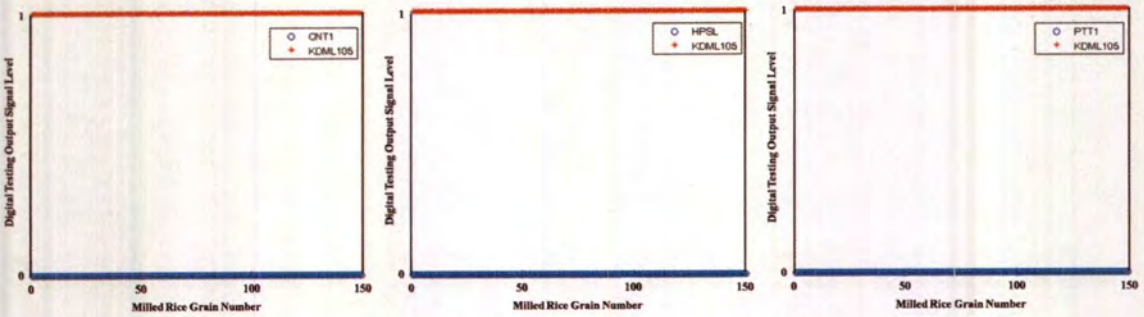

Figure 4.32 Training results of each data pair (a) CNT1-KDML105, (b) HPSL-KDML105, and (c) PTT1-KDML105.

Identification results of the KMDL105 milled rice grain during the training and testing sessions are shown in Figs. 4.32 and 4.33, respectively. It can be observed that our FFNN can efficiently accomplish the goal during its training period. With unknown data sets, our FFNN can identify KDML105 milled rice variety from CNT1, HPSL2, and PTT1 with measured FARs of 0.0%, 0.0%, and 3.0%, respectively. Their associated FRRs of 0.0%, 0.0%, and 1.0% are also determined.

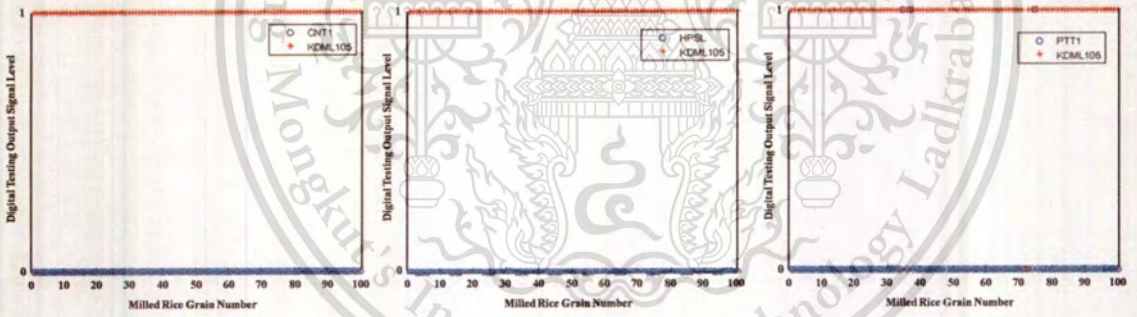

Figure 4.33 Testing results of each data pair (a) CNT1-KDML105, (b) HPSL2-KDML105, and (c) PTT1-KDML105.

4.4.5 Experimental Demonstration

In this section, we demonstrated experimentation in our laboratory to prove of concept that a combination of polynomial functions and NNA applied on the spectral image of the rice grain can identify the KDML105 milled rice variety with a much faster response time and still achieve low FAR and FRR values [41]. In particular, we perform field operation tests for 55 extra sample sets and find that a more optimized NNA revamps FAR and FRR values to 6.2% and 7.1%, respectively. This is unlike our unoptimized NNA in [41] that worsens the FAR and FRR values down to 69.7% and 22.8%, respectively. Other key features include chemical-free analysis, robustness, and adaptive learning.

This material is reserved for educational use only, not allowed for commercial use.
Forbidden to modify the content, and cite the document when use.

4.4.5.1 Materials

Milled rice grains of CNT1, HPSL2, HSPR60, KDML105, PTT1, RD15, and RD23 varieties (Fig. 4.34) are prepared by the Rice Research Institute in. Their corresponding width and length ratios average 0.27 ± 0.01, 0.25 ±0.01, 0.28±0.01, 0.28 ± 0.01, 0.27 ± 0.01, 0.27 ± 0.01, and 0.28±0.01, respectively. These milled rice grains are positioned on our black rice tray, and they are aligned in the same direction. A total of 1750 milled rice grains, 250 for each milled rice variety, are investigated. Note that, as there are variations in the image texture of milled rice grains due to the polishing and milling processes, the image texture of the milled rice grain cannot be used to distinguish these rice varieties. Since the morphological characters of grains are heritable in nature [42], this work focuses on the shape analysis for the identification ofKDML105.

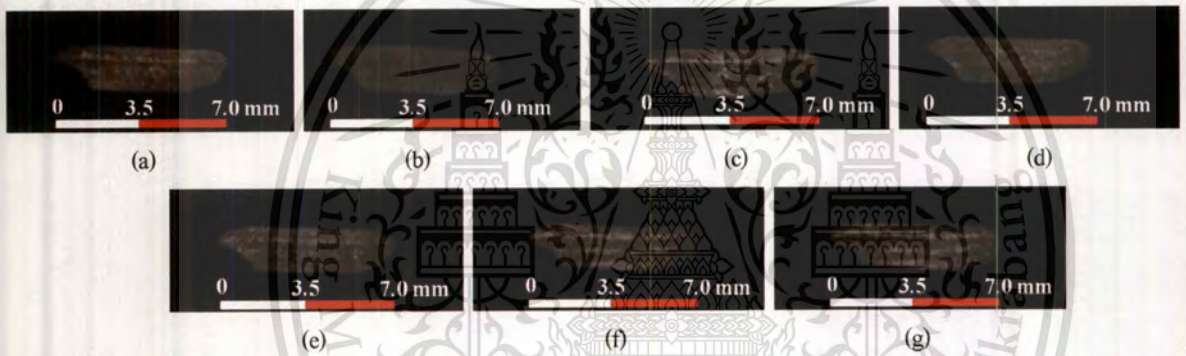

Figure 4.34 Zoomed images of Thai milled rice grains from six varieties: (a) CNT1, (b) HPSL2, (c) HSPR60, (d) KDML105, (e) PTT1, (f) RD15, and (g) RD23.

4.4.5.2 Experimental Results

With the chain coding and the polynomial fitting, three shape parameters in terms of perimeter, area, and eccentricity are extracted as shown in Fig. 4.35 with their averaging values highlighted in Table 4.3. It seems that the perimeter and area of KDML105 were strongly overlapped with RD15 and RD23, slightly mixed with CNT1 and PTT1, and clearly separated from the remaining milled rice varieties as shown in Figs. 4.35(a) and 4.35(b). On the contrary, the eccentricity of all milled rice variety seems hard to distinguish one from another as shown in Fig. 4.35(c). However, with these slight differences of the KDML105 from the unwanted milled rice varieties, a principal component analysis obviously shows high potential in separating the desired KDML105 milled rice variety from the remaining ones, as shown in Fig. 4.36.

This material is reserved for educational use only, not allowed for commercial use.
Forbidden to modify the content, and cite the document when use.

Table 4.3 Average values of three shape parameters

Rice variety	Perimeter	Area	Eccentricity
CNT1	319.33	3716.30	0.1466
HPSL2	332.83	3772.87	0.1309
HSPR60	317.79	3829.02	0.1562
KDML105	304.88	3111.57	0.1725
PTT1	319.48	3585.41	0.1457
RD15	316.44	3539.50	0.1443
RD23	299.67	2819.38	0.1518

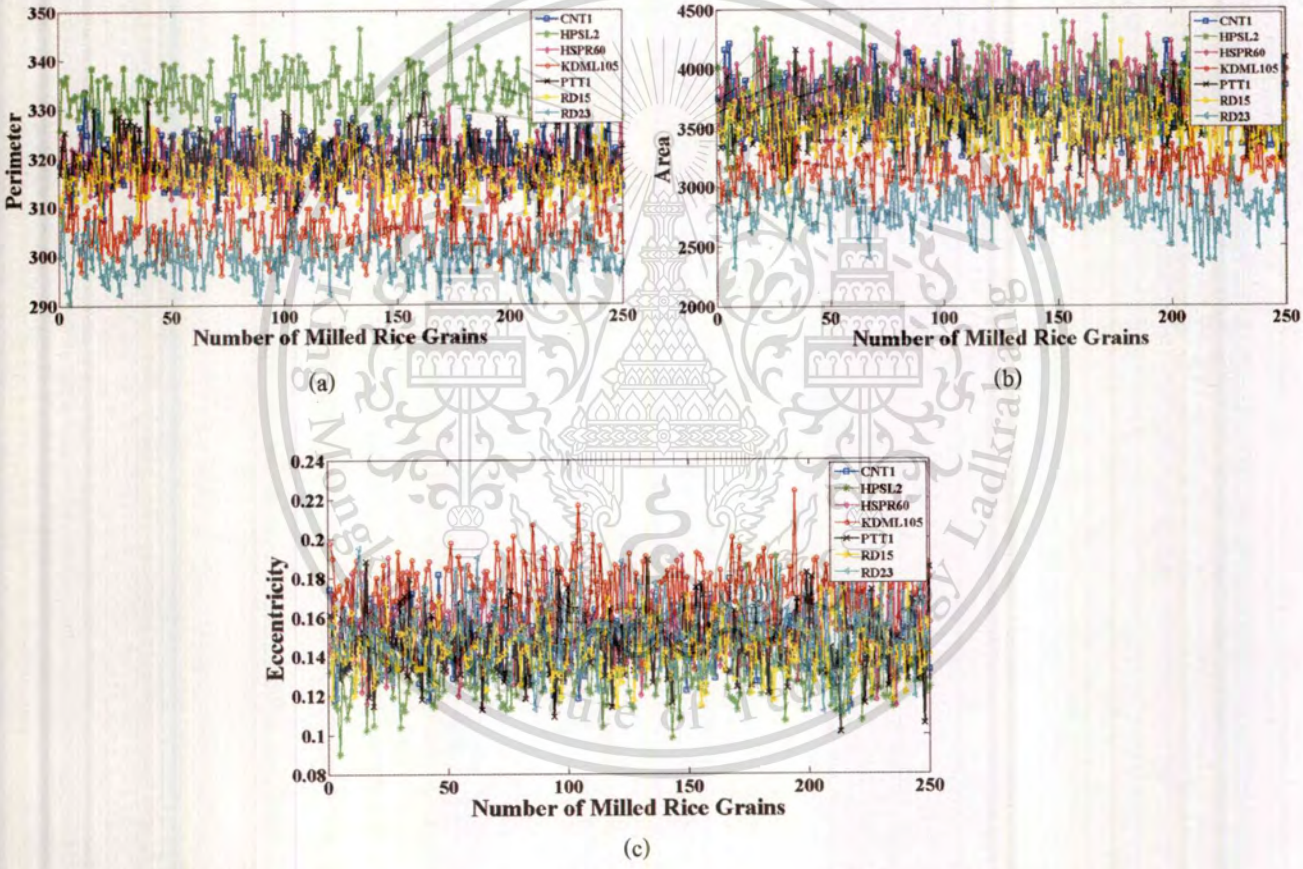

Figure 4.35 Plotted graphs of the extracted (a) perimeter, (b) area, and (c) eccentricity parameter.

This material is reserved for educational use only, not allowed for commercial use.
Forbidden to modify the content, and cite the document when use.

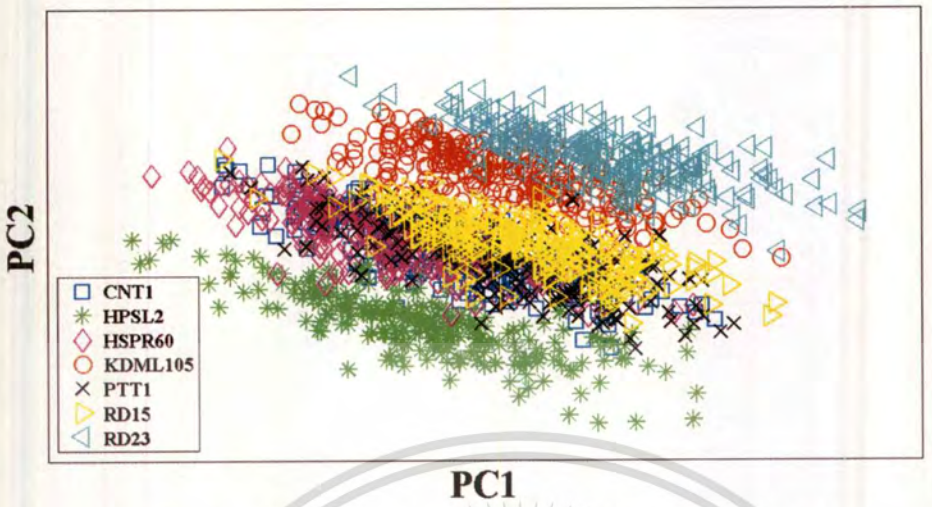

Figure 4.36 Principal component analysis of three shape parameters.

With the similar procedure but different layer nodes, all milled rice varieties are analyzed together. In the data set, randomly selected data sets from 150 milled rice grains are used for training the FFNN, and the remaining data sets are used for testing the FFNN. Our FFNN configuration contains one input layer with three input ports for receiving area, perimeter, and eccentricity parameters, four hidden layers, and one output layer. Our four hidden layers have 15, 21, 17, and 1 nodes with Log-sigmoid, Log-sigmoid, Log-sigmoid, and linear transfer functions, respectively. The output layer is assigned to be 1 for the KMDL105 milled rice variety and 0 for the others. Our training results take 8:25 h to finish with determined low MSEs of 7.40×10^{-8}. Identification results of the KMDL105 milled rice grain during the training and testing sessions are shown in Figs. 4.37(a) and 4.37(b), respectively. It can be observed that our FFNN can efficiently accomplish the goal during its training period. With unknown data sets prepared at the same time, our FFNN can identify KDML105 milled rice variety mixed with CNT1, HPSL2, HSPR60, PTT1, RD15, and RD23 with measured FARs of 1.7%. Their associated FRRs of 7.0% are also determined. In this scenario, a very fast identification time of 30.5 s is obtained, limited by a 30 s warming time for UV lamps. This indicates a much improvement in speed of 1.20 h/30.5 s = 157.4 times.

This material is reserved for educational use only, not allowed for commercial use.
Forbidden to modify the content, and cite the document when use.

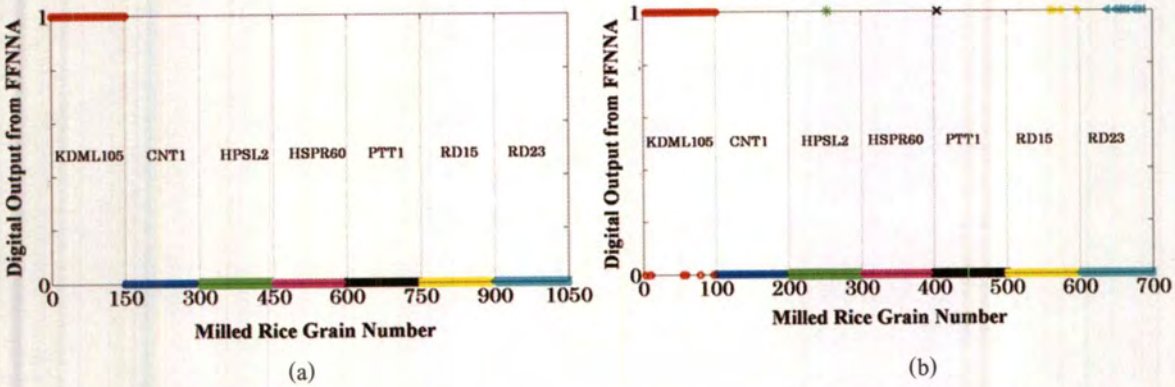

Figure 4.37 FFNN results during (a) the training period and (b) test with the unknown data set.

Figure 4.38 Examples of two spectral images used during field operation tests.

To demonstrate the robustness of our single-wavelength spectral-imaging-based Thai jasmine rice identification system, we perform field operation tests for 55 extra sample sets (i.e., 165 milled rice grains) with random arrangement of rice varieties.In this scenario, a number of KDML105 milled rice grain is 81. Fig. 4.38 shows two randomly selected spectral images used in the demonstration. We obtain five and six identification mistakes as shown in Fig. 3.39. This indicates that low FAR and FRR are (5/81) × 100 = 6.2% and (6/84) × 100 = 7.1% in identifying the KDML105 mixed with other milled rice varieties, respectively.

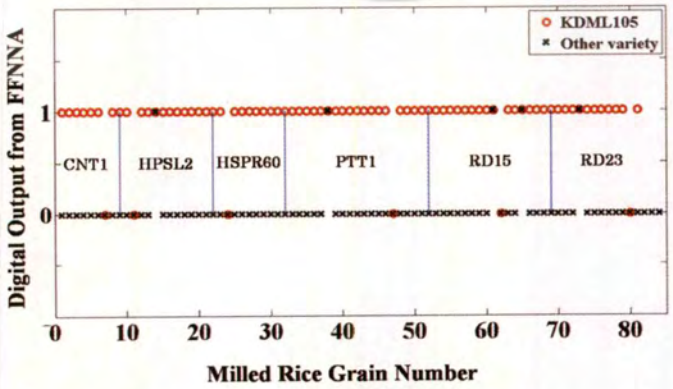

Figure 4.39 Testing results of KDML105 identification in practice.

This material is reserved for educational use only, not allowed for commercial use.
Forbidden to modify the content, and cite the document when use.

4.5 References

[1] K. Suwansukho, S. Sumriddetchkajorn, and P. Buranasiri, "Combination of simple chemical and spectroscopic methods for the identification of Thai Hom Mali rice," Proc. SPIE 7315, 73150W (2009).

[2] S. Sumriddetchkajorn, K. Suwansukho, and P. Buranasiri, "Identification of Thai Hom Mali rice using a refractometer," Proc. SPIE 7315, 73150F (2009).

[3] T. Katsumata, T. Suzuki, H. Aizama, E. Matashige, S. Komuro, and T. Morikawa, "Nondestructive evaluation of rice using two-dimensional imaging of photoluminescence," Rev. Sci. Instru:76 , pp. 073702 (2005).

[4] T. Katsumata, T. Suzuki, H. Aizawa, and E. Matashige, "Photoluminescence evaluation of cereals for a quality control application," J. Food Engg. 78, pp.588-590 (2007).

[5] M. S. Kim, A. M. Lefcourt, Y.- R. Chen, and Y. Tao, "Automated detection of fecal contamination of apples based on multispectral fluorescence image fusion," J. Food Engg. 71, pp. 85-91 (2005).

[6] M. S. Kim, A. M. Lefcourt, and Y.- R. Chen, "Multispectral laser-induced fluorescence imaging system for large biological samples," Appl. Opt. 42, pp. 3927-3934 (2003).

[7] M. S. Kim, J. E. McMurtrey, C. L. Mulchi, C. S. T. Daughtry, E. W. Chappelle, and Y.- R. Chen, "Steady-state multispectral fluorescence imaging system for plant leaves," Appl. Opt. 40, pp. 157-166 (2001).

[8] Y. Intaravanne, S. Sumriddetchkajorn, and J. Nukaew, "Development of an imaging spectrometer for R&D in Thailand," Proc. NCOA, pp. 71-76 (2010).

[9] S. Sumriddetchkajorn, "Methods and apparatus for nondestructively identifying rice breeds," Thailand Patent Application, 1001000068, Jan. 15, (2010).

[10] S. Sumriddetchkajorn, K. Suwansukho, and P. Buranasiri, "Two-wavelength spectral image-based Thai rice breed identification," Proc. SPIE 7715, 77150I (2010).

[11] T. Koutchma, "Advances in ultraviolet light technology for non-thermal processing of liquid foods," Food Bioprocess. Technol. 2, 138-155 (2009).

[12] H. Wondraczek, A. Kotiaho, P. Fardim and T. Heinze, "Photoactive polysaccharides," Carb. Pol. 83, 1048-1061 (2011).

This material is reserved for educational use only, not allowed for commercial use.
Forbidden to modify the content, and cite the document when use.

[13] H. Karatani, M. Kojima, H. Minakuchi, N. Soga and T. Shizuki, "Development and characterization of anodically initiated luminescent detection for alcohols and carbohydrates," Anal. Chim. Acta. 337, 207–215 (1997).

[14] P. J. Jenkins and A. M. Donald, "The influence of amylose on starch granule structure," Int. J. Macromol. 17, 315–321 (1995).

[15] L. F. Costa and R. M. Cesar, "Shape classification and analysis: theory and practice," in Image Processing Series, P. A. Laplants, ed. pp. 411-414 (2009).

[16] S. Sumriddetchkajorn and Y. Intaravanne, "Hyperspectral imaging-based credit card verifier structure with adaptive learning," Appl. Opt. 47, 6594-6600 (2008).

[17] S. Sumriddetchkajorn and Y. Intaravanne, "Data-nonintrusive photonics-based credit card verifier with a low false rejection rate," Appl. Opt. 49, 764-770 (2010).

[18] Y. Intaravanne, S. Sumriddetchkajorn, J. Nukeaw, "Cell phone-based two-dimensional spectral analysis for banana ripeness estimation," Sens. Act. B 168, 390-394 (2012).

[19] S. Janchaysang, S. Sumriddetchkajorn, and P. Buranasiri, "Tunable filter-based multispectral imaging for detection of blood stains on construction material substrates. part 1. developing blood stain discrimination criteria," Appl. Opt. 51, 6984-6996 (2012).

[20] K. Suwansukho, S. Sumriddetchkajorn, and P. Buranasiri "Demonstration of a single wavelength spectral- imaging-based Thai jasmine rice identification," Appl. Opt. 50, 4024-4030 (2011).

[21] F. P. Kuhl, and C. R. Giardina, "Elliptic Fourier features of a closed contour," Compo. Graph. Ima. Proc. 18, 236-258 (1982).

[22] J. S. Crampton, "Elliptic Fourier shape analysis of fossil bivalves: some practical considerations," Lethaia. 28, 179-186 (1995).

[23] J. M. Le Minor, and M. Schmittbuhl, "Importance of elliptic Fourier methods for morphometry of complex outlines: application to the distal human femur," Surg. Radiol. Anat. 21, 387-391 (1999).

[24] A. Tort, "Elliptical Fourier functions as a morphological descriptor of the genus Stenosarina Brachiopoda, Terebratulida, new caledonia," Mathematical Geology. 35, 873-885 (2003).

[25] C. Costa, P. Menesatti, J. Aguzzi, S. D'Andrea, F. Antonucci, V. Rimatori, F. Pallottino, and M. Mattoccia, "External shape differences between sympatric populations of commercial clams tapes decussates and T. philippinarum," Food Bioprocess Technol. 3, 43-48 (2010).

This material is reserved for educational use only, not allowed for commercial use.
Forbidden to modify the content, and cite the document when use.

[26] S. Ninomiya, R. Ohsawa, and M. Yoshida, "Evaluation of buckwheat and tartary buckwheat kernel shape by elliptic Fourier method," Curr. Adv. Buck. Res. 389-396 (1995).

[27] H. Iwata, S. Niikura, S. Matsuura, Y. Takano, and Y. Ukai, "Evaluation of variation of root shape of Japanese radish (Raphanus sativus L.) based on image analysis using elliptic Fourier descriptors," Euphytica 102, 143-149 (1998).

[28] J. C.Neto, G. E. Meyer, D. D. Jones, and A. K. Samal, "Plant species identification using elliptic Fourier leaf shape analysis," Comp. Elect. Argric. 50, 121-134 (2006).

[29] S. Costa, P. Menesattia, G. Paglia, F. Pallottino, J. Aguzzic, V. Rimatori, G. Russo, S. Recupero, and G. R. Recupero, "Quantitative evaluation of Tarocco sweet orange fruit shape using optoelectronic elliptic Fourier based analysis," Post. Bio. Tech. 54, 38-47 (2009).

[30] S. Sumriddetchkajorn and Y. Intaravanne, "A credit card verifier structure using diffraction and spectroscopy Concepts," Proc. SPIE 7003, 700318 (2008).

[31] S. Sumriddetchkajorn and Y. Intaravanne, "Evolution of optically nondestructive and data-non-intrusive credit card verifiers," Proc. SPIE 7726, 77261B (2010).

[32] H. Freeman, "On the encoding of arbitrary geometric configuration," IRE Trans. Elec. Comp. 260-268 (1961).

[33] R. Nafe, and W. Schlote, "Methods for shape analysis of two-dimensional closed contours – a biologically importance, but widely neglected field in histopathology," Elec. J. Pathol. Histol. 8.2, 022-02 (2002).

[34] K. Suwansukho, S. Sumriddetchkajorn, and P. Buranasiri, "Improvement of single-wavelength based Thai jasmine rice identification with elliptic Fourier descriptor and neural network analysis," *Proc. SPIE* 8558, 85580C (2012).

[35] I. Sadeh, "Polynomial Approximation of image," *Comp. Math. Appl.* 32, 99-115 (1996).

[36] L. M. Kocic, and G. V. Milovanovic, "Shape preserving approximations by polynomial and splines," *Comp. Math. Appl.* 33, 59-97 (1997).

[37] P. M. Baggenstoss, "Image distortion analysis using polynomial series expansion," *IEEE Trans. Patt. Anal. Mach. Intel.* 26, 1438-1451 (2004).

[38] A. Kaveti, K. K. Teoh, and H. Wang, "Second order implicit polynomials for segmentation of range images," *Patt. Reg.* 29, 937-949 (1996).

[39] W. Burger, and M. J. Burge, [Digital image processing: an algorithmic introduction using Java],

This material is reserved for educational use only, not allowed for commercial use.
Forbidden to modify the content, and cite the document when use.

Springer Publisher, New York, 223 (2008).

[40] Y. Mingqiang, K. Kidiyo, and R. Joseph, "A survey of shape feature extraction techniques," http://www.intechopen.com/books/pattern_recognition_techniques_technology_and_applications/a_survey_of_shape_feature_extraction_techniques (2008).

[41] K. Suwansukho, S. Sumriddetchkajorn, and P. Buranasiri, "Single-wavelength based Thai jasmine rice identification with polynomial fitting function and neural network analysis," Proc. SPIE 8883, 888318 (2013).

[42] J. L. Harper, P. H. Lovell, and K. G. Moore, "The shapes and sizes of seeds," Annu. Rev. Ecol. Syst. 1, 327–356 (1970).

King Mongkut's Institute of Technology Ladkrabang

This material is reserved for educational use only, not allowed for commercial use.
Forbidden to modify the content, and cite the document when use.

CHAPTER 5

SUMMARY

This dissertation studied the destructive and nondestructive optical investigation to identify Thai jasmine or Kaw Dawk Mali 105 milled rice variety from several milled rice varieties such as CNT1, HPSL2, HSPR60, PTT1, RD6, RD15, and RD23.

In destructive methods, the combination of chemical and spectroscopic methods is studied. The optical transmission spectrum of rice powder dissolved in our KOH solution in the 500-800 nm wavelengths is investigated. The slope value of the optical transmissivity of the milled rice solution depends on the dissolution time and the ability of the milled rice powder to be dissolved in KOH solution. In the study, the results shown that the use of a 0.1-g milled rice powder dissolved in our 10% KOH solution shows a lowest false rejection rate of 15%. Another approach, the combination of chemical and refractrometry methods is studied. Only 0.1 grams of the milled rice powder was dissolved in 10 ml of 10% KOH solution. During refractive index measurement, merely 0.5 ml of the dissolved milled rice solution is dropped onto the sensing area of the refractometer and the measurement time is less than 20 seconds. By appropriately assigning upper and lower refractive indices as the threshold interval, the results showed that a total false error rate of 6.7%.

In nondestructive methods, we studied several techniques combine with a spectral image and image processing analysis. First, a nondestructive of two-wavelength spectral-imaging based rice variety identification was studied. A high energy UVC light source was induced unknown milled rice grains to radiate fluorescent radiation in a 500-580 nm wavelength spectrum. Only two fluorescent wavelengths at 540 nm and 575 nm and simple image processing techniques are applied. The spectral image at 540 nm wavelength goes through two-level image thresholding and blob filtering twice. For the spectral image at 575 nm wavelength, it goes through these processes six times. By subtracting two selected binary images and then filtering out unwanted pixels, all eight rice varieties are effectively identified. Second, a nondestructive of single-wavelength spectral-imaging based rice variety identification was studied. A spectral image at either 545 nm or 575 nm wavelength and simple image processing processes in order to separate KDML105 milled rice grains from the remaining are investigated. These spectral images were assigned threshold value range at 57 – 91 and 90 – 144, respectively. And, the thresholded image passes one at a time through two sets of blob filtering processes. At the end, by subtracting two selected binary image, KDML105 milled rice grains can be

This material is reserved for educational use only, not allowed for commercial use.
Forbidden to modify the content, and cite the document when use.

identified with the best FAR of 8.6% with a fast identification time of 25 ms. Third, a single-wavelength at 546 nm based Thai jasmine rice identification system can be improved by analyzing the spectral image with the use of both EFD and FFNN. The chain code method and the EFD are applied in order to define the appropriate elliptic geometry. The trained FFNN is used for identifying our desired KDML105 milled rice grain via analyzing key elliptical parameters. Experimental results show the average FAR and FRR of 11.0% and 19.0% in identifying the KDML105 milled rice grain from unwanted CNT1, HPSL2, and PTT1 milled rice varieties, respectively. Fourth, the single-wavelength based Thai jasmine rice identification system can be improved by using a polynomial function and a well trained FFNN. All threshold images are applied by the chain coding and the polynomial function in order to define the appropriate geometry feature. At the end, the trained FFNN is used for identifying our desired KDML105 milled rice grain via analyzing key shape parameters (area, perimeter and eccentricity). Experimental results show much improved average FAR and FRR of < 3.0% and 0.3% in identifying the KDML105 milled rice grain from unwanted CNT1, HPSL2, and PTT1 milled rice varieties, respectively. Finally, with similar procedure but different layer node of FFNN, this leads to a fast analysis time of 30.5 s, implying a 157.4 times improvement. Experimental results show low FAR and FRR values of 1.7% and 7.0%. Taking into consideration the robustness of our system, 55 additional sample sets are tested in our system, showing FAR and FRR values of 6.2% and 7.1% in the identification of the KDML105 milled rice variety mixed with unwanted CNT1, HPSL2, HSPR60, PTT1, RD15, and RD23 milled rice varieties.

Recommendations

1. Rice grain of each variety has to use more than in the research.
2. More testing has to do in the laboratory for checking reliability.
3. Another side of rice grain should to record for accuracy shape analysis.

This material is reserved for educational use only, not allowed for commercial use.
Forbidden to modify the content, and cite the document when use.

APPENDIX A

This material is reserved for educational use only, not allowed for commercial use.
Forbidden to modify the content, and cite the document when use.

C language code write on ET-OPTO AC Dimmer controller board

```
unsigned char i;
void main() {
TRISA = 0;
PORTA = 0x02;
TRISB = 1;
PORTB = 0x00;
Usart_Init(9600);
 while(1){
       while(PORTB.F0==1)
       {
         i = Usart_Read();
         if(i=='a')
         {
          PORTA.F1 = 0;
          //PORTA.F1 = 1;          }
         else
         {
          PORTA.F1= 1;
         }
   }
 }
}                                  /* end program*/
```

This material is reserved for educational use only, not allowed for commercial use.
Forbidden to modify the content, and cite the document when use.

APPENDIX B

This material is reserved for educational use only, not allowed for commercial use.
Forbidden to modify the content, and cite the document when use.

LabVIEW source code for control UVC light bulbs

1. Lamp Warm Up Code

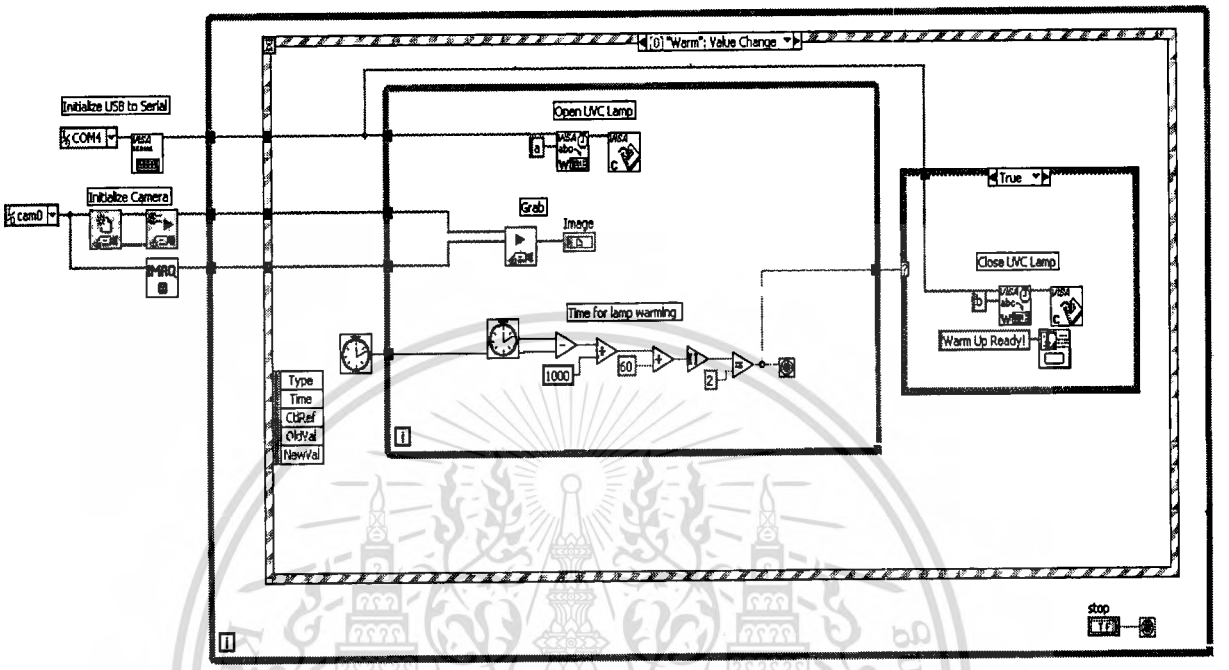

This material is reserved for educational use only, not allowed for commercial use.
Forbidden to modify the content, and cite the document when use.

2. Save Image Code

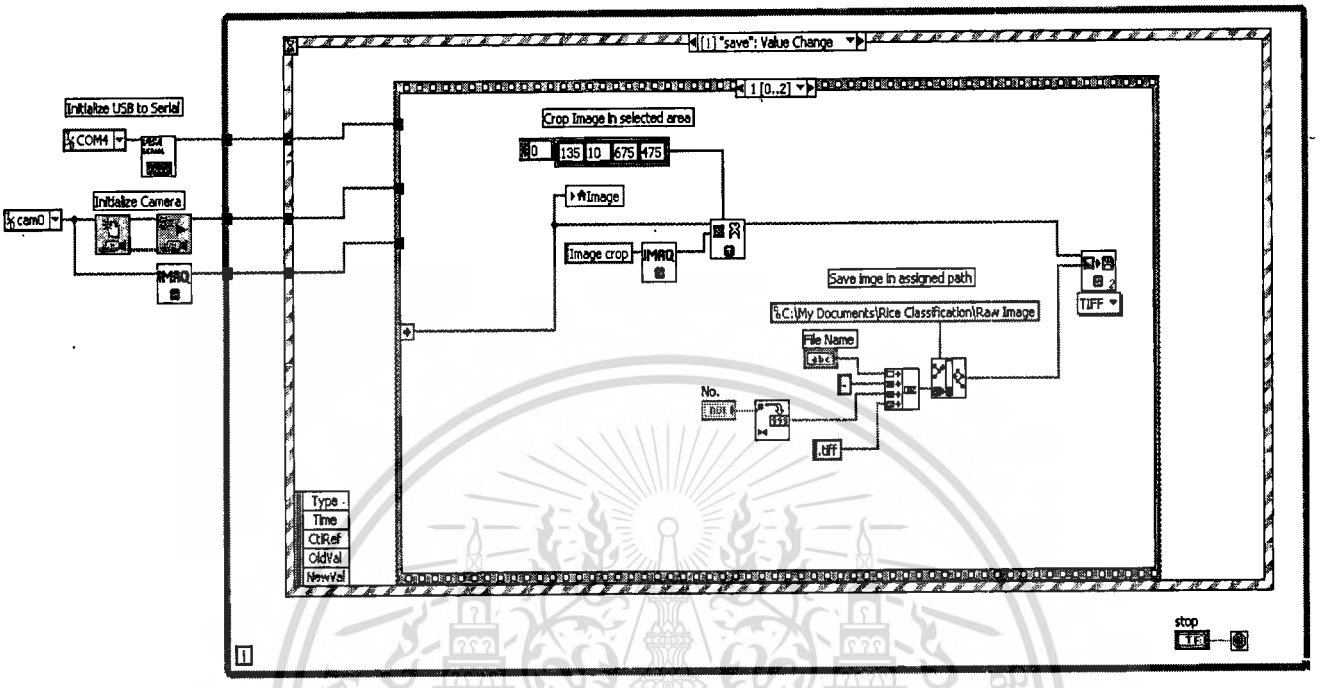

This material is reserved for educational use only, not allowed for commercial use.
Forbidden to modify the content, and cite the document when use.

APPENDIX C

This material is reserved for educational use only, not allowed for commercial use.
Forbidden to modify the content, and cite the document when use.

1. Initialized code of LabVIEW to call Matlab for use and path location.

MATLAB script

```
addpath('c:\dip\common\dipimage');
dip_initialise;
dipsetpref('imagefilepath','C:\My Documents\Rice Classification\Threshold Image')
```

2. Array size assigning for store image data.

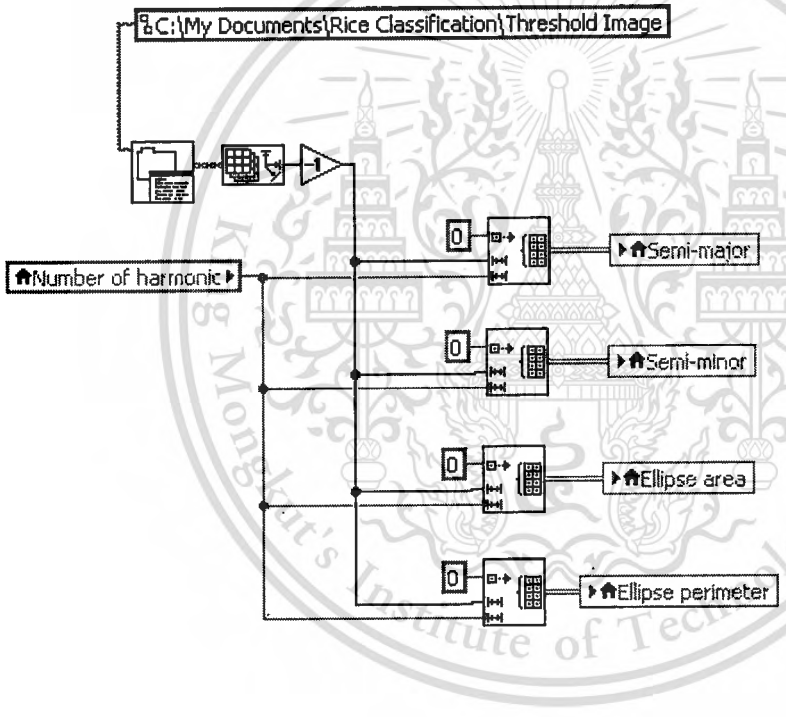

This material is reserved for educational use only, not allowed for commercial use.
Forbidden to modify the content, and cite the document when use.

3. Crop and Save image.

Image 1

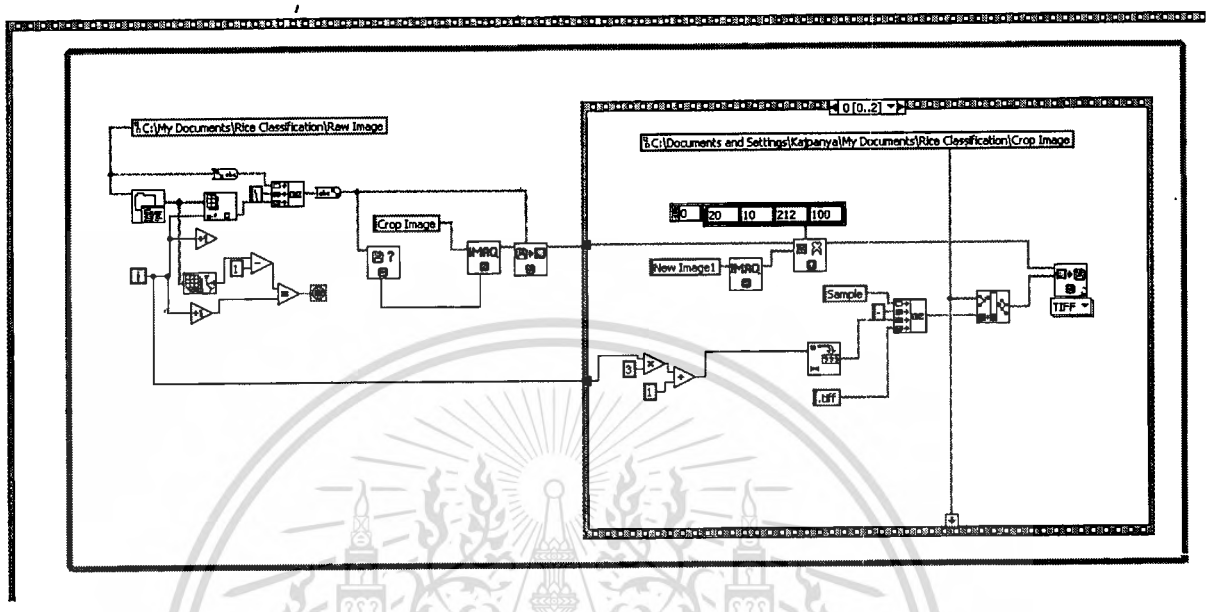

Image 2

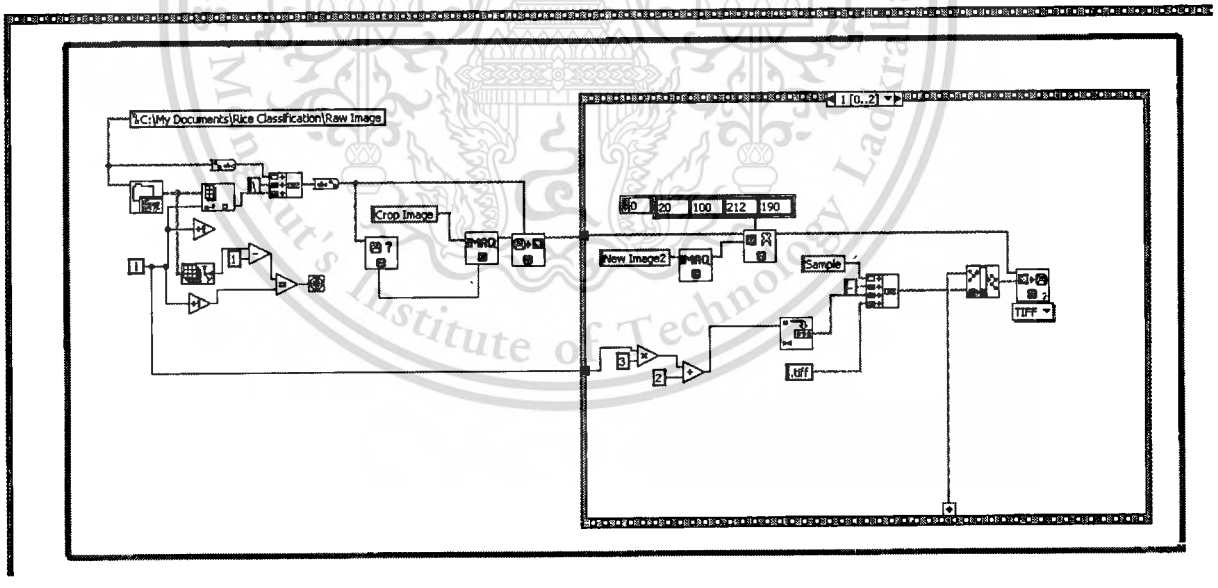

This material is reserved for educational use only, not allowed for commercial use.
Forbidden to modify the content, and cite the document when use.

Image 3

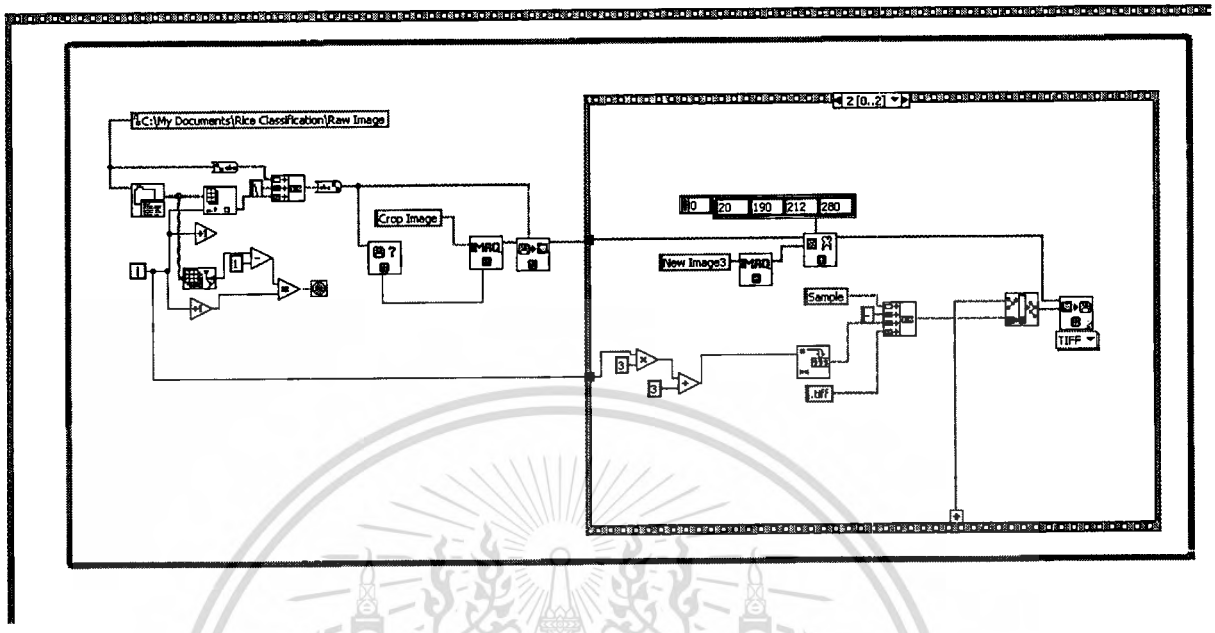

4. Load cropped image and vary threshold in each image and save threshold image in the folder.

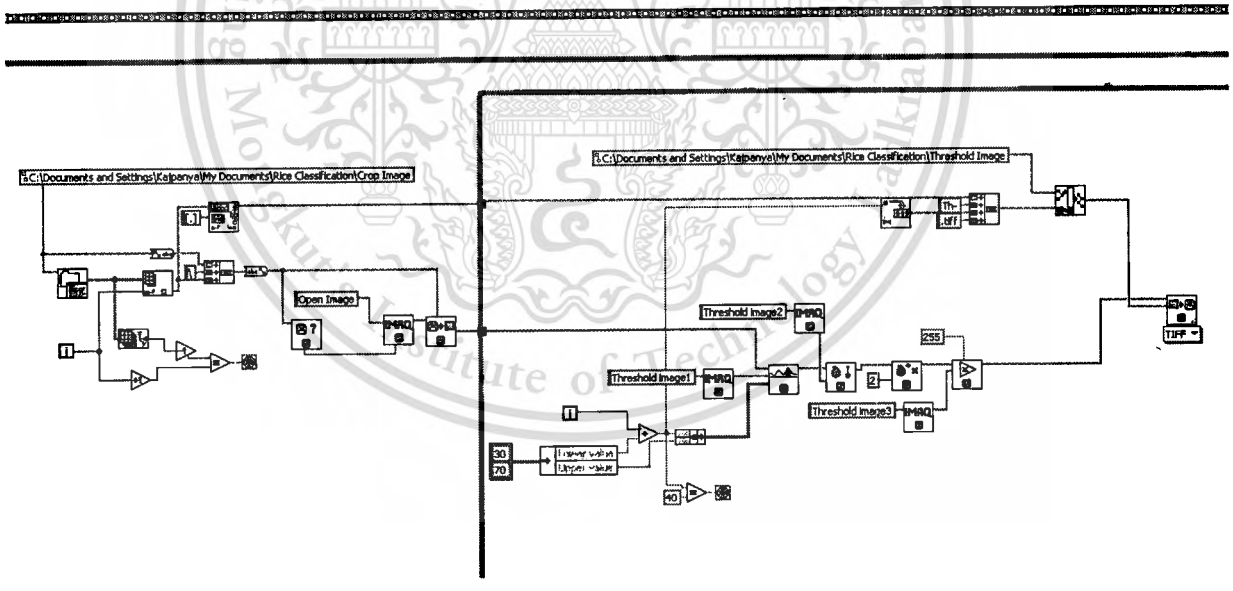

This material is reserved for educational use only, not allowed for commercial use.
Forbidden to modify the content, and cite the document when use.

5. Elliptic fourier descriptor by Matlab in LabVIEW.

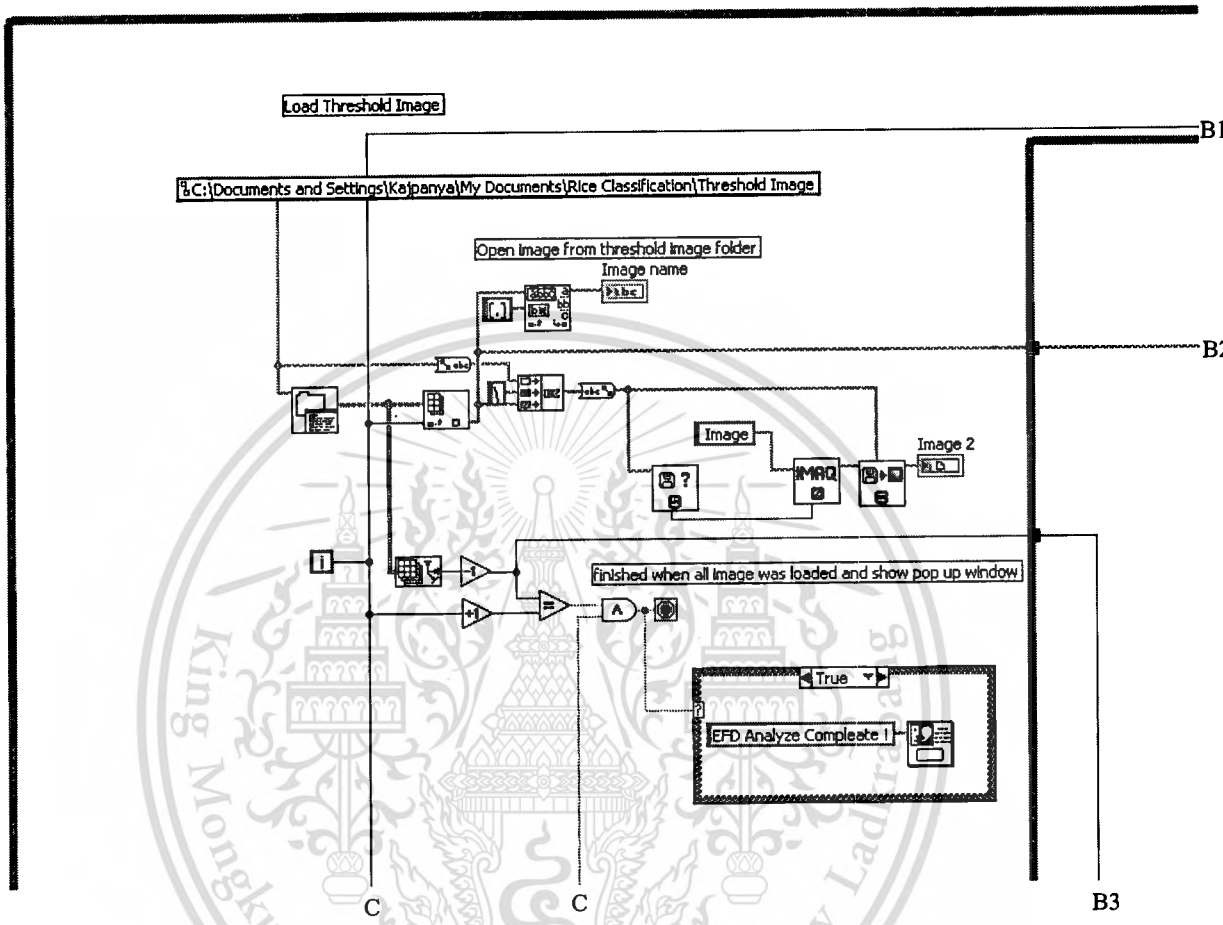

This material is reserved for educational use only, not allowed for commercial use.
Forbidden to modify the content, and cite the document when use.

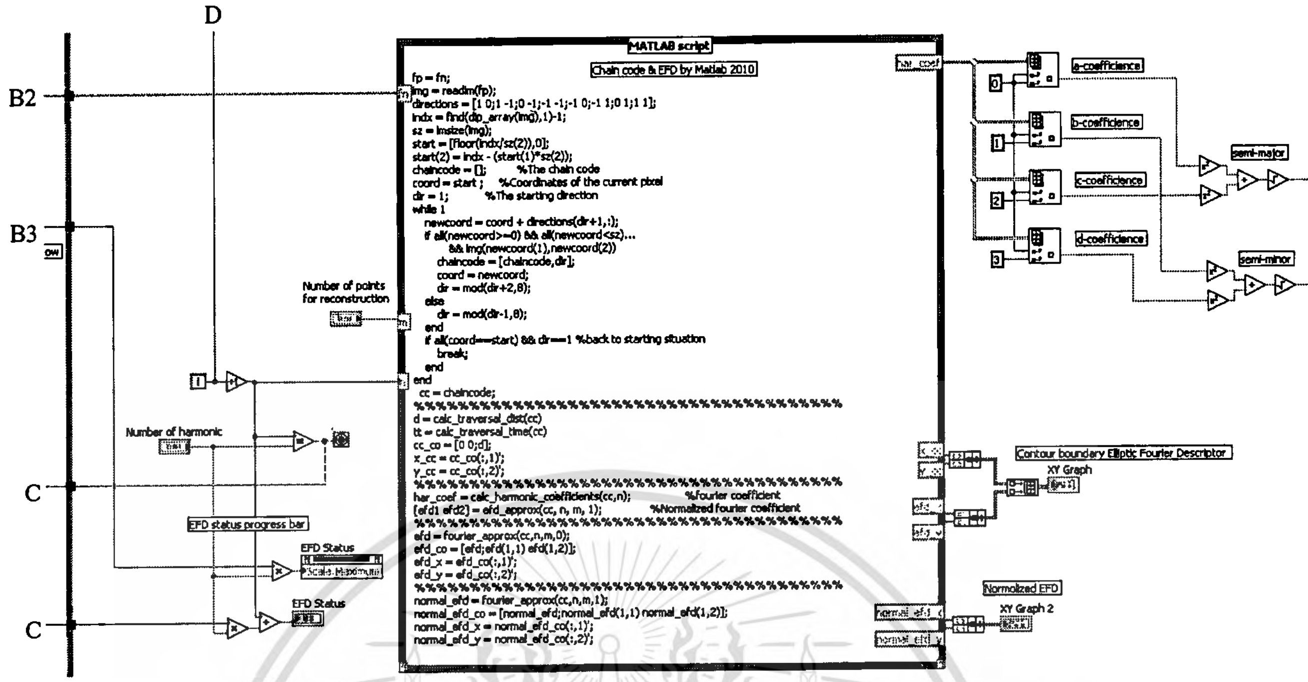

6. Storing Area, Perimeter, semi-Major axis and semi-Minor axis in Array

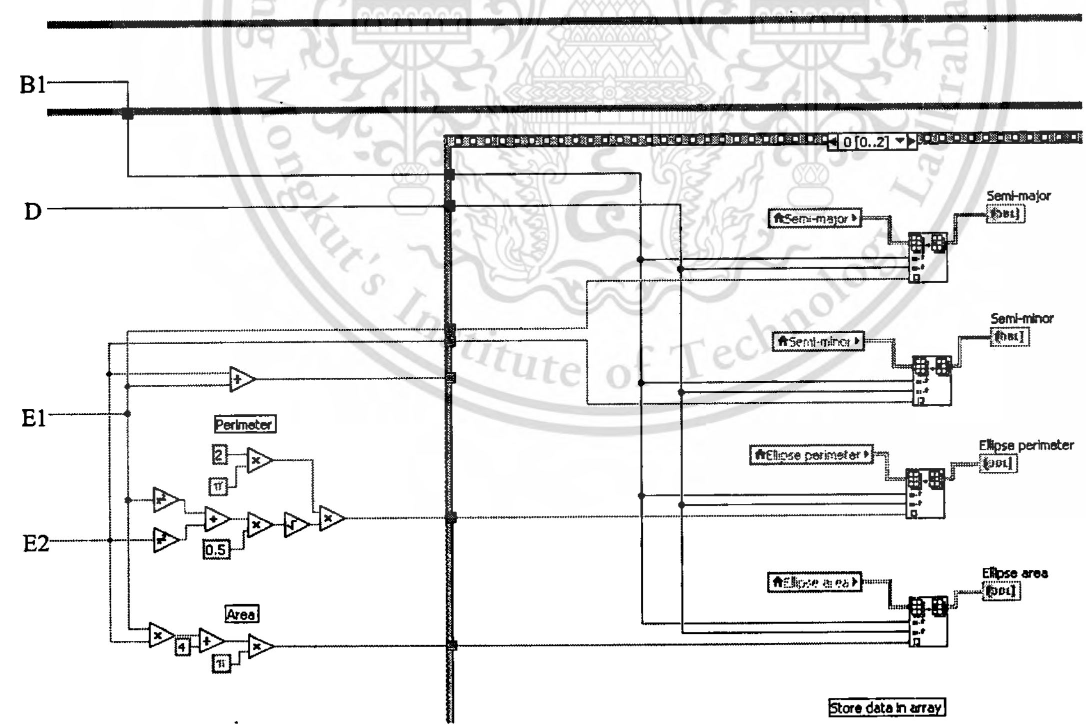

This material is reserved for educational use only, not allowed for commercial use.
Forbidden to modify the content, and cite the document when use.

7. Area, Perimeter, semi-Major axis and semi-Minor axis saving in Folder and Path that assigned

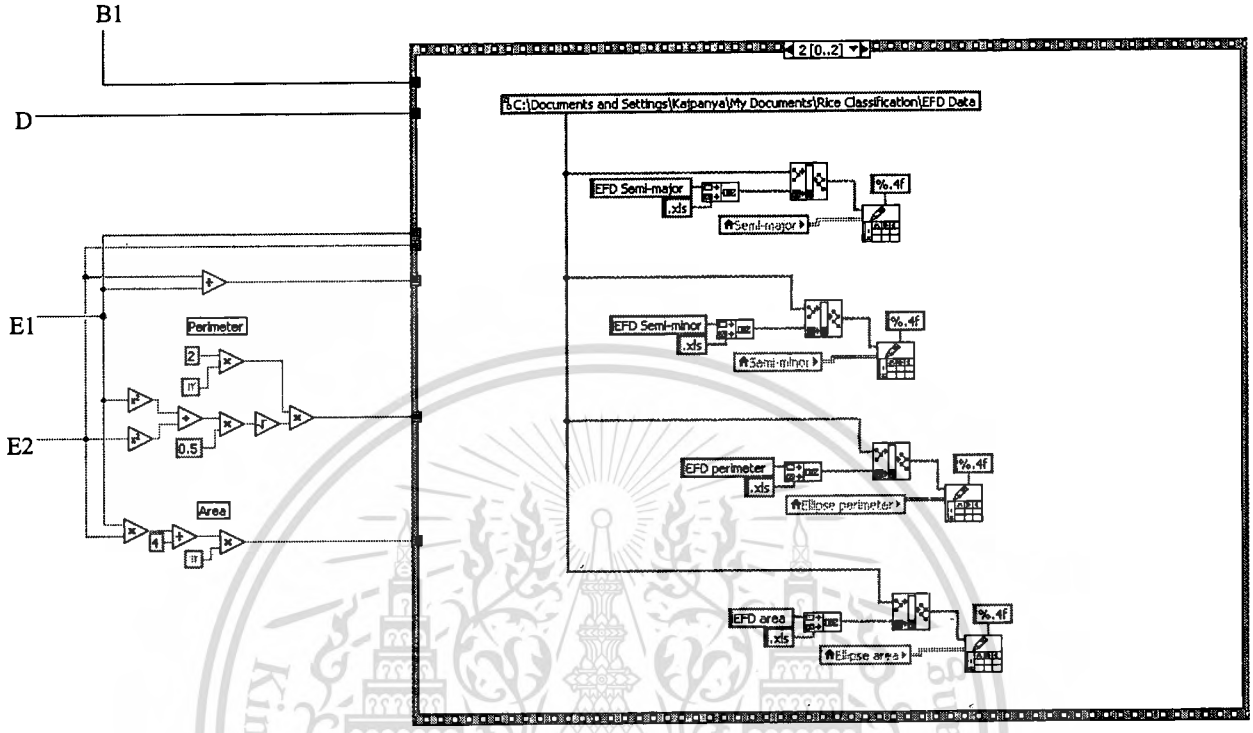

This material is reserved for educational use only, not allowed for commercial use.
Forbidden to modify the content, and cite the document when use.

APPENDIX D

This material is reserved for educational use only, not allowed for commercial use.
Forbidden to modify the content, and cite the document when use.

MATLAB source code of neural network analysis

```
% Neural Network to classify Thai jasmin rice
clear;
clc
%input data
%%%%%%%%%%CNT1%%%%%%%%%%%%%%%%%%%%%%%%%%%%%%%%%%%%
cnt_area = xlsread('Ellipse area CNT1.xls');
cnt_peri = xlsread('Ellipse perimeter CNT1.xls');
cnt_majo = xlsread('Semi-major CNT1.xls');
cnt_mino = xlsread('Semi-minor CNT1.xls');
%%%%%%%%%%HPSL2%%%%%%%%%%%%%%%%%%%%%%%%%%%%%%%%%%%%
hpsl_area = xlsread('Ellipse area HPSL2.xls');
hpsl_peri = xlsread('Ellipse perimeter HPSL2.xls');
hpsl_majo = xlsread('Semi-major HPSL2.xls');
hpsl_mino = xlsread('Semi-minor HPSL2.xls');
%%%%%%%%%%KDML105%%%%%%%%%%%%%%%%%%%%%%%%%%%%%%%%%%
kdml_area = xlsread('Ellipse area KDML105.xls');
kdml_peri = xlsread('Ellipse perimeter KDML105.xls');
kdml_majo = xlsread('Semi-major KDML105.xls');
kdml_mino = xlsread('Semi-minor KDML105.xls');
%%%%%%%%%%PTT1%%%%%%%%%%%%%%%%%%%%%%%%%%%%%%%%%%%%%
ptt_area = xlsread('Ellipse area PTT1.xls');
ptt_peri = xlsread('Ellipse perimeter PTT1.xls');
ptt_majo = xlsread('Semi-major PTT1.xls');
ptt_mino = xlsread('Semi-minor PTT1.xls');
%%%%%%%%%%%%%%%%%%%%%%%%%%%%%%%%%%%%%%%%%%%%%%%%%%%%
data1 = [cnt_area cnt_peri cnt_majo cnt_mino];
data2 = [hpsl_area hpsl_peri hpsl_majo hpsl_mino];
data3 = [kdml_area kdml_peri kdml_majo kdml_mino];
data4 = [ptt_area ptt_peri ptt_majo ptt_mino];

row1 = 1:1100;
row2 = 1101:2200;

P1 = data1(row1,:);%CNT1
P2 = data2(row1,:);%HPSL2
P3 = data3(row1,:);%KDML105
P4 = data4(row1,:);%PTT1

P = [P1;P3]';

data6 = xlsread('Testing.xls');
T1 = [data6(1:220);data6(1:220);data6(1:220);data6(1:220);data6(1:220)]';
T2 =
[data6(501:720);data6(501:720);data6(501:720);data6(501:720);data6(501:720)]'
;
T = [T1 T2];

U1 = data1(row2,:);%CNT1
U2 = data2(row2,:);%HPSL2
U3 = data3(row2,:);%KDML105
U4 = data4(row2,:);%PTT1
```

This material is reserved for educational use only, not allowed for commercial use.
Forbidden to modify the content, and cite the document when use.

```
U = [U1;U3]';

PR=minmax(P);

S1=11;
S2=13;
S3=11;
S4=1;

TF1='logsig';
TF2='logsig';
TF3='purelin';
TF4='purelin';
BTF='trainlm';
BLF='learngd';
PF='mse';

net=newff(PR,[S1 S2 S3 S4],{TF1 TF2 TF3 TF4},BTF,BLF,PF);
net.trainParam.epochs=100000;
net.trainParam.goal=1e-21;

[net,tr,Y,E,Pf,Af]=train(net,P,T);
nout=sim(net,P);
nTest=sim(net,U);
netout=round(nout);
netTest=round(nTest);
figure(1)
hold on
plot(netout(1,1:100),'o');
plot(netout(1,101:200),'r*');      %Figure for training & Testing
legend('PTT1','KDML105')
hold off
title('Traning & Testing')
%%%%%%%%%%%%%%%%%%%%%%%%%%%%%%%%%%%%%%%%%%%%%%%%%%%%%%%%%%%%%%%%%%%%%%%%%%%%%%%
d = netTest';
for i = 0:99
    m = (i*11)+1;
    n = (i*11)+11;                 %Sum the NN output
    o = 1100+m;
    p = 1100+n;
    a(i+1) = round(sum(d(m:n,1))/11);
    b(i+1) = round(sum(d(o:p,1))/11);
end
x = [1:100]';
y =  [a;b]';
%%%%%%%%%%%%%%%%%%%%%%%%%%%%%%%%%%%%%%%%%%%%%%%%%%%%%%%%%%%%%%%%%%%%%%%%%%%%%%%
figure(2)
hold on
plot(x,y(:,1),'o')
plot(x,y(:,2),'r*')            %Figure for Testing
legend('HPSL2','KDML105')
axis([0 100 0 5])
title('Testing')
hold off
```

This material is reserved for educational use only, not allowed for commercial use.
Forbidden to modify the content, and cite the document when use.

APPENDIX E

This material is reserved for educational use only, not allowed for commercial use.
Forbidden to modify the content, and cite the document when use.

MATLAB source code for chain cod

```
img = readim(fp);                % fp = file path of the binary image
directions = [1 0;1 -1;0 -1;-1 -1;-1 0;-1 1;0 1;1 1];
indx = find(dip_array(img),1)-1;
sz = imsize(img);
start = [floor(indx/sz(2)),0];
start(2) = indx - (start(1)*sz(2));
chaincode = [];          %The chain code
coord = start ;     %Coordinates of the current pixel
dir = 1;            %The starting direction
while 1
   newcoord = coord + directions(dir+1,:);
   if all(newcoord>=0) && all(newcoord<sz)...
         && img(newcoord(1),newcoord(2))
      chaincode = [chaincode,dir];
      coord = newcoord;
      dir = mod(dir+2,8);
   else
      dir = mod(dir-1,8);
   end
   if all(coord==start) && dir==1 %back to starting situation
      break;
   end
end
 cc = chaincode;                % chain code number of the boundary image
```

This material is reserved for educational use only, not allowed for commercial use.
Forbidden to modify the content, and cite the document when use.

APPENDIX F

This material is reserved for educational use only, not allowed for commercial use.
Forbidden to modify the content, and cite the document when use.

MATLAB source for Elliptic foureir descriptor

```
function output = calc_traversal_dist(ai)
% This function will generate position coordinates of chain code (ai). Number of
% harmonic elements (n), and number of points for reconstruction (m) must be
% specified.
   x_ = 0;
   y_ = 0;
   for i = 1 : size(ai, 2)
      x_ = x_ + sign(6 - ai(i)) * sign(2 - ai(i));
      y_ = y_ + sign(4 - ai(i)) * sign(ai(i));
      p(i, 1) = x_;
      p(i, 2) = y_;
   end
   output = p;
end
%%%%%%%%%%%%%%%%%%%%%%%%%%%%%%%%%%%%%%%%%%%%%%%%%%%%%%%%%%%%%%%%%%%%%%%%%%%%%%%
function output = calc_traversal_time(ai)
% Traversal time is defined as accumulated time consumed by every
% component of the chain code.
   t_ = 0;
   for i = 1 : size(ai, 2)
      t_ = t_ + 1 + ((sqrt(2)-1)/2).*(1-(-1).^ai(i));
      t(i) = t_;
   end
   output = t';
end
%%%%%%%%%%%%%%%%%%%%%%%%%%%%%%%%%%%%%%%%%%%%%%%%%%%%%%%%%%%%%%%%%%%%%%%%%%%%%%%
function [A0, C0] = calc_dc_components(ai)
% Calculate DC components.
```

This material is reserved for educational use only, not allowed for commercial use.
Forbidden to modify the content, and cite the document when use.

```
% A0 and C0 are bias coefficeis, corresponding to a frequency of zero.
  %% Maximum length of chain code
  k = size(ai, 2);
  %% Traversal time and distance
  t = calc_traversal_time(ai);
  s = calc_traversal_dist(ai);
  %% Basic period of the chain code
  T = t(k);
  %% DC Components: A0, C0
  sum_a0 = 0;
  sum_c0 = 0;
  for p = 1 : k
    delta_d = calc_traversal_dist(ai(p));
    delta_x = delta_d(:,1);
    delta_y = delta_d(:,2);
    delta_t = calc_traversal_time(ai(p));
    if (p > 2)
        zeta = s(p - 1, 1) - delta_x / delta_t * t(p - 1);
        delta = s(p - 1, 2) - delta_y / delta_t * t(p - 1);
    else
        zeta = 0;
        delta = 0;
    end
    if (p > 2)
      sum_a0 = sum_a0 + delta_x / (2 * delta_t) * ((t(p))^2 - (t(p - 1))^2) + zeta * (t(p) - t(p-1));
      sum_c0 = sum_c0 + delta_y / (2 * delta_t) * ((t(p))^2 - (t(p - 1))^2) + delta * (t(p) - t(p-1));
    else
      sum_a0 = sum_a0 + delta_x / (2 * delta_t) * (t(p))^2 + zeta * t(p);
      sum_c0 = sum_c0 + delta_x / (2 * delta_t) * (t(p))^2 + delta * t(p);
```

This material is reserved for educational use only, not allowed for commercial use.
Forbidden to modify the content, and cite the document when use.

```
    end
  end
  %% Assign  to output
  A0 = sum_a0 / T;
  C0 = sum_c0 / T;
end
%%%%%%%%%%%%%%%%%%%%%%%%%%%%%%%%%%%%%%%%%%%%%%%%%%%%%%%%%%%%%%%%%%%%%%%%%%%%%%%
function output = calc_harmonic_coefficients(ai, n)
% This function will calculate the n-th set of four harmonic coefficients.
% The output is [an bn cn dn]
  %% Maximum length of chain code
  k = size(ai, 2);
  %% Traversal time
  t = calc_traversal_time(ai);
  %% Basic period of the chain code
  T = t(k);
  %% Store this value to make computation faster
  two_n_pi = 2 * n * pi;
  %% Compute Harmonic cofficients: an, bn, cn, dn
  sigma_a = 0;
  sigma_b = 0;
  sigma_c = 0;
  sigma_d = 0;
  for p = 1 : k
    if (p > 2)
      tp_prev = t(p - 1);
    else
      tp_prev = 0;
    end
```

This material is reserved for educational use only, not allowed for commercial use.
Forbidden to modify the content, and cite the document when use.

```
    delta_d = calc_traversal_dist(ai(p));
    delta_x = delta_d(:,1);
    delta_y = delta_d(:,2);
    delta_t = calc_traversal_time(ai(p));
    q_x = delta_x / delta_t;
    q_y = delta_y / delta_t;
    sigma_a = sigma_a + q_x * (cos(two_n_pi * t(p) / T) - cos(two_n_pi * tp_prev / T));
    sigma_b = sigma_b + q_x * (sin(two_n_pi * t(p) / T) - sin(two_n_pi * tp_prev / T));
    sigma_c = sigma_c + q_y * (cos(two_n_pi * t(p) / T) - cos(two_n_pi * tp_prev / T));
    sigma_d = sigma_d + q_y * (sin(two_n_pi * t(p) / T) - sin(two_n_pi * tp_prev / T));
  end
  r = T/(2*n^2*pi^2);
  a = r * sigma_a;
  b = r * sigma_b;
  c = r * sigma_c;
  d = r * sigma_d;
  %% Assign  to output
  output = [a b c d];
end
%%%%%%%%%%%%%%%%%%%%%%%%%%%%%%%%%%%%%%%%%%%%%%%%%%%%%%%%%%%%%%%%%%%%%%%%%%%%%%%
function output = fourier_approx(ai, n, m, normalized)
% This function will generate position coordinates of fourier approximation of
% chain code (ai).Number of harmonic elements (n), and number of points for
% reconstruction (m) must be specified.
  for i = 1 : n
    harmonic_coeff = calc_harmonic_coefficients(ai, i);
    a(i) = harmonic_coeff(1, 1);
    b(i) = harmonic_coeff(1, 2);
    c(i) = harmonic_coeff(1, 3);
```

This material is reserved for educational use only, not allowed for commercial use.
Forbidden to modify the content, and cite the document when use.

```
    d(i) = harmonic_coeff(1, 4);
end
[A0, C0] = calc_dc_components(ai);
% Normalization procedure
if (normalized == 1)
    % Remove DC components
    A0 = 0;
    C0 = 0;
    % Compute theta1
    theta1 = 0.5 * atan(2 * (a(1) * b(1) + c(1) * d(1)) / ...
            (a(1)^2 + c(1)^2 - b(1)^2 - d(1)^2));
    costh1 = cos(theta1);
    sinth1 = sin(theta1);
    a_star_1 = costh1 * a(1) + sinth1 * b(1);
    b_star_1 = -sinth1 * a(1) + costh1 * b(1);
    c_star_1 = costh1 * c(1) + sinth1 * d(1);
    d_star_1 = -sinth1 * c(1) + costh1 * d(1);
    % Compute psi1
    psi1 = atan(c_star_1 / a_star_1) ;
    % Compute E
    E = sqrt(a_star_1^2 + c_star_1^2);
    cospsi1 = cos(psi1);
    sinpsi1 = sin(psi1);
    for (i = 1 : n)
      normalized = [cospsi1 sinpsi1; -sinpsi1 cospsi1] * [a(i) b(i); c(i) d(i)] * ...
              [cos(theta1 * i) -sin(theta1 * i); sin(theta1 * i) cos(theta1 * i)];

      a(i) = normalized(1,1) / E;
      b(i) = normalized(1,2) / E;
```

This material is reserved for educational use only, not allowed for commercial use.
Forbidden to modify the content, and cite the document when use.

```
        c(i) = normalized(2,1) / E;
        d(i) = normalized(2,2) / E;
      end
    end  % end if normalized
    for t = 1 : m
      x_ = 0.0;
      y_ = 0.0;
      for i = 1 : n
        x_ = x_ + (a(i) * cos(2 * i * pi * t / m) + b(i) * sin(2 * i * pi * t / m));
        y_ = y_ + (c(i) * cos(2 * i * pi * t / m) + d(i) * sin(2 * i * pi * t / m));
      end
      output(t,1) = A0 + x_;
      output(t,2) = C0 + y_;
    end
end
%%%%%%%%%%%%%%%%%%%%%%%%%%%%%%%%%%%%%%%%%%%%%%%%%%%%%%%%%%%%%%%%%%%%%%%%%%%%%%%
function plot_fourier_approx(ai, n, m, normalized, color, line_width)
% This function will plot the fourier approximation, given a chain code (ai),
% number of harmonic elements (n), and number of points for reconstruction (m).
% Normalization can be applied by setting "normalized = 1".
    if (nargin < 5)
      color = 'b';
      line_width = 2;
    end
    if (nargin < 6)
      line_width = 2;
    end
```

This material is reserved for educational use only, not allowed for commercial use.
Forbidden to modify the content, and cite the document when use.

```
    % Do Fourier approximatoin
    k = size(ai, 2);
    x_ = fourier_approx(ai, n, m, normalized)
    % Make it closed contour
    x = [x_; x_(1,1) x_(1,2)];
    plot(x(:,1), x(:,2), color, 'linewidth', line_width);
end
```

This material is reserved for educational use only, not allowed for commercial use.
Forbidden to modify the content, and cite the document when use.

APPENDIX H

This material is reserved for educational use only, not allowed for commercial use.
Forbidden to modify the content, and cite the document when use.

Combination of Simple Chemical and Spectroscopic Methods for the Identification of Thai Hom Mali Rice

Kajpanya Suwansukho[a], Sarun Sumriddetchkajorn*[b], and Prathan Buranasiri[a]
[a]Applied Physics Department, Faculty of Science, King Mongkut's Institute of Technology Ladkrabang, Bangkok, Thailand
[b]Photonics Technology Laboratory, National Electronics and Computer Technology Center, 112 Thailand Science Park, Phahonyothin Rd, Klong 1, Klong Luang Pathumthani, 12120, Thailand

ABSTRACT

As the Thai Dawk Mali (KDML105) rice variety is popular due to its high sensory after cook, there is an increase in mixing the KDML105 rice with other rice varieties that leads to unqualified KDML105 milled rice products for export and unqualified unmilled rice seeds for next plants. Instead of using traditional time consuming methods based on the disintegration of the rice kernel in an alkali solution and the inspection of rice cooked in boiling water, this paper proposes to analyze the milled rice powder dissolved in our alkali solution via a spectroscopic method. In our study, 0.1 g, 0.2 g, and 0.3 of milled rice powder from four Thai rice varieties, i.e., KDML105, Pathumthani1, Chainat1, and RD6, are selected. Then each milled rice sample is ground and then dissolved in a 10% potassium hydroxide (KOH) solution. At the specified minutes of dissolution, the relative optical transmission spectrum of the milled rice solution in a 500-800 nm wavelength is measured and only its first derivative is used for the identification of the KDML105 milled rice. We find that the use of 0.10 g of the milled rice powder dissolved in our KOH solution for 10 minutes provides the lowest false rejection rate of 15%, indicating that we have a faster approach with less amount of waste produced. With the 0.2-g milled rice powder, 5 minutes of dissolution is needed but with a slightly higher false rejection rate of 18.3%.

Keywords: Rice, Spectroscopy, Optical sensors, Biophotonics, Agriphotonics

1. INTRODUCTION

At present, the most well-known rice in Thailand is Khao Dawk Mali, also known as KDML105, due to its good texture and impressive fragrance. Because it is in the top list of Thailand export products, there is an increase in the mixture of unwanted rice varieties such as Pathumthani1 (PTT1) and Chainat1 (CNT1) in the KDML105 rice products. Although these three rice varieties have similar physical characteristics, they are different in cooking qualities and nutrient contents, leading to unqualified KDML105 milled rice grain products for export and unwanted unmilled rice seeds for next plants. This also implies that a simple machine vision technique [1] cannot be used to separate these rice varieties from each other.

Spectroscopy is one of the interesting techniques that can be used to study rice characteristics. Previously, transmission spectra in a near infrared 850-1050 nm wavelength band of milled rice grains were performed to discriminate Basmati rice grains from undesired rice grains with a 20% error rate [2]. Reflectance spectrum of one zone in visible region and two zones in the infrared region was also studied to classify 139 Korean domestic rice grains from 141 unwanted rice grains [3]. A simpler and possibly cheaper approach via the use of only a visible spectrum in 400-1000 nm wavelength was investigated, showing a classification rate of 89% in identifying two different rice varieties [4]. A more simpler approach based on refractometry has been proposed and experimentally demonstrated to identify the KDML105 milled rice with a low 6.7% false rejection rate [5]. However, a high sensitive optical refractometry with a precise temperature controller is needed.

In Thailand, several chemical and biological methods have been used for the inspection of the KDML105 milled rice. For example, DNA technology is a well known accurate method to identify rice varieties [6]. Apart from the DNA analysis, simple techniques based on iodine-binding [7] and the alkali spreading value [8] have been widely used and

*Correspondence E-mail: sarun.sumriddetchkajorn@nectec.or.th

Sensing for Agriculture and Food Quality and Safety, edited by Moon S. Kim, Shu-I Tu, Kaunglin Chao,
Proc. of SPIE Vol. 7315, 73150W · © 2009 SPIE · CCC code: 0277-786X/09/$18 · doi: 10.1117/12.819994

This material is reserved for personal study, not allowed for commercial use.
Forbidden to modify the content and cite the document when use.
Downloaded from SPIE Digital Library on 02 Dec 2011 to 203.185.129.241. Terms of Use: http://spiedl.org/terms

accepted to identify the KDML105 milled rice from other Thai rice varieties. In addition, because amylose can directly absorb water, the inspection of rice cooked in boiling water for 17 minutes can be used to determine the KDML105 milled rice [9]. The two last chemical methods are also recommended for KDML105 rice standards inspection [10].

With these concepts in mind, it would be desirable to follow standards inspection but with a faster analytical technique. This paper studies the combination of chemical and spectroscopic methods to identify the milled KDML105 rice. In our approach, we dissolve powder of the milled rice in an alkali solution and its transmission spectrum only in a 500-800 nm wavelength region is investigated.

2. MATERIALS AND METHODS

2.1 Materials

Four varieties of Thai rice, KDML105, CNT1, PTT1 and the Thai sticky rice (RD6), were obtained from the Rice Research Institute, at the Department of Rice, Ministry of Agriculture and Cooperatives of Thailand. All of them were harvested in 2007 with ≈ 12%-14% moisture content. The KDML105 has amylose content in the range of 13%-18%. The PTT1 rice has equivalent amount of amylose content to that of the KDML105 rice but its weight per seed is 80.5% less (i.e., 0.0174 grams). These two rice varieties are classified as low amylose content rice. The CNT1 rice has its amylose content in 27%-30% and it is classified as one of the high-amylose content rice varieties. Its weight is 98.6% (i.e., 0.0213 grams) compared to the KDML105 rice. For the RD6, it is classified as very low amylose content rice (0%-2%) and its weight is 88.3% (i.e., 0.0191 grams) than the KDML105 milled rice. Fig.1 shows images of four Thai rice varieties taken under white light illumination.

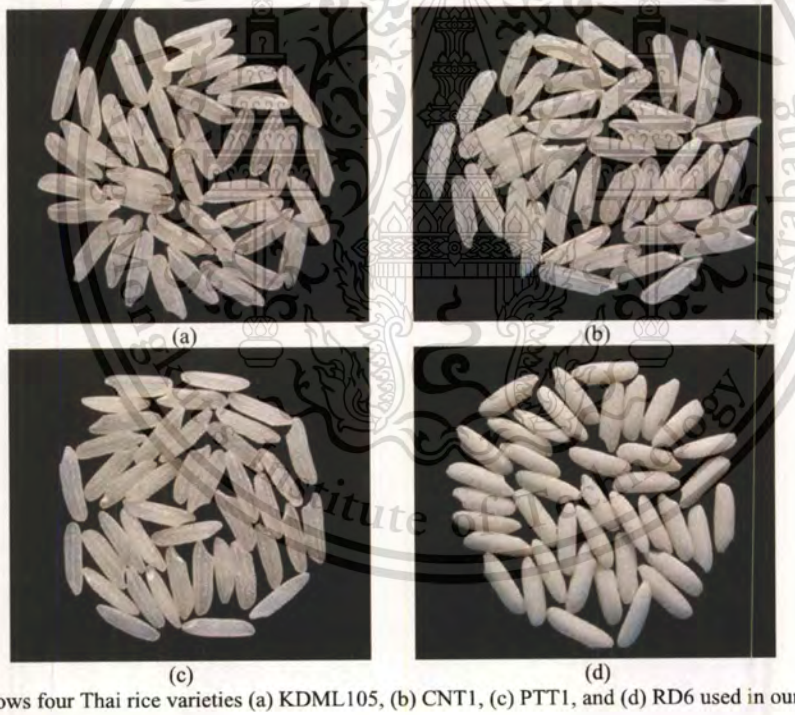

Fig.1. shows four Thai rice varieties (a) KDML105, (b) CNT1, (c) PTT1, and (d) RD6 used in our study.

2.2 Procedures for Sample Preparation

Because these four rice varieties have different weight per grain and they can be dissolved in an alkali solution, we prepare our alkali solution as follows. Our 10% solution of potassium hydroxide (KOH) was prepared by dissolving 10.0 g of KOH pallets in 100 ml of deionized water. Note that we choose a higher concentration of the KOH solution compared to a 1.7% concentration previously used in the alkali spreading method because we would like to speed up the dissolution process. Each rice variety was separately ground by using a laboratory grinder and kept in a zip pack. They were stored in a room where the temperature and the relative humidity varied between 24°C-28 °C and 50%-70%,

This material is reserved for personal use only, not allowed for commercial use.
Forbidden to modify the content and cite the document when use.
Downloaded from SPIE Digital Library on 02 Dec 2011 to 203.185.129.241. Terms of Use: http://spiedl.org/terms

respectively. In our study, we divide rice powder into different weights of 0.10 g, 0.20 g, and 0.30 g. The prepared milled rice powder was dissolved in 10 ml of our KOH solution under a magnetic stirrer for 5 minutes without heating. Then, a 2-ml milled rice solution was poured into a 10-mm wide quartz cuvette. The remaining milled rice solution was left to allow the milled rice powder dissolve more for 10, 15, and 20 minutes prior to the next measurements. In each measurement (i.e., 4 measurements for 5th, 10th, 15th, and 20th minutes), there are 15 samples per rice variety.

2.3 Spectrum Measurement

A commercial UV/VIS spectrometer model Heλios α from Thermo Electron Corporation was used to measure the transmission spectrum of our milled rice solution. Only a spectral range in 500-800 nm was analyzed. Scanning speed was set at 4 nm/s with the wavelength interval of 1 nm, indicating a complete 75 second per measurement cycle with 301 data points. Our experiment was performed in an air conditioned room having 24°C-26°C and 50%-60% relative humidity.

2.4 Data analysis

To reduce the data fluctuation during our transmission measurement, we investigated the transmission spectrum of the milled rice solution with respect to the transmission spectrum of our 10% KOH solution. After that, the first derivative of the measured relative optical transmission spectrum was analyzed. By appropriately assigning the slope interval for our classification, the KDML105 milled rice can be distinguishable.

3. RESULTS AND DISCUSSION

3.1 Visual Inspection

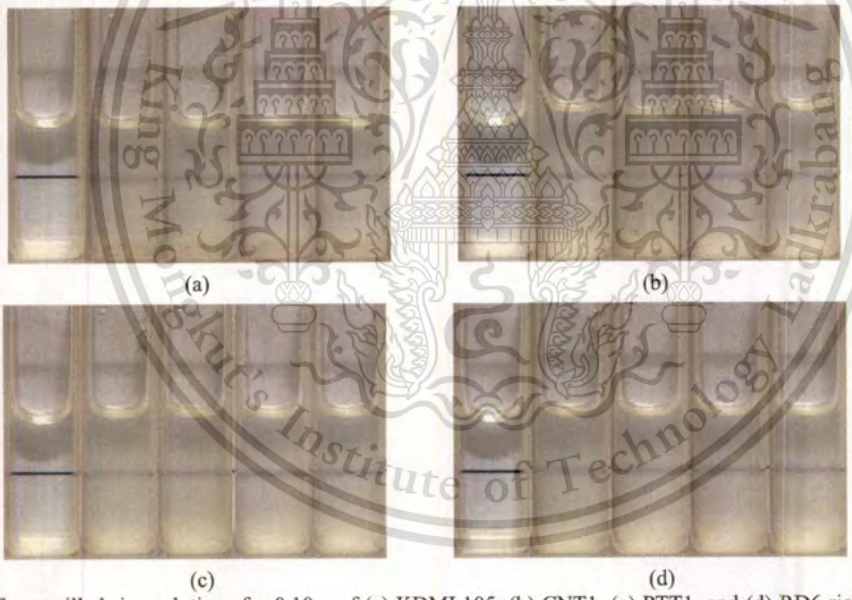

Fig.2 shows 2 ml of our milled rice solutions for 0.10 g of (a) KDML105, (b) CNT1, (c) PTT1, and (d) RD6 rice varieties. Images from left to right are for our 10% KOH solution followed by the 5th, 10th, 15th, and 20th minutes of observation, respectively. A black solid line is used to show turbidity of the solution.

Fig.2 shows our 10% KOH solution having 0.10 g of the milled rice powder dissolved in it for 5, 10, 15, and 20 minutes. Visually, these milled rice solutions have similar turbidity. At the 5th minute of dissolution, the KDML105 milled rice powder seems to show higher capability to dissolve in our 10% KOH solution than the remaining three rice varieties. In this case, a measured relative optical transmissivity at a 635-nm wavelength for the KDML105 milled solution is ~4% higher than the others. When these milled rice powders spend more time in our 10% KOH solution up to 20 minutes, there is an increase in the measured relative optical transmissivity of 2%-7%. By adding the milled rice powder more in our 10% KOH solution, the turbidity gets increased as shown in Figs.3-4 with a maximum drop of measured relative

This material is reserved for personal use; not allowed for commercial use.
Forbidden to modify the content and cite the document when use.
Downloaded from SPIE Digital Library on 02 Dec 2011 to 203.185.129.241. Terms of Use: http://spiedl.org/terms

optical transmissivity of 9%. These variations in measured relative optical transmissivities also confirm that the optical density measurement cannot be used to identify our desired KDML105 milled rice.

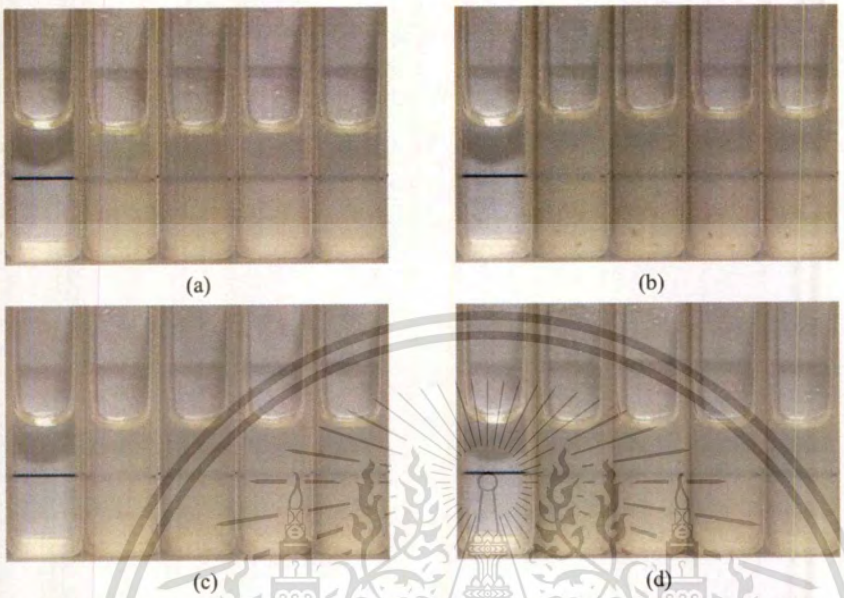

Fig.3 shows 2 ml of our milled rice solutions for 0.20 g of (a) KDML105, (b) CNT1, (c) PTT1 and (d) RD6 rice varieties. Images from left to right are for our 10% KOH solution followed by the 5th, 10th, 15th, and 20th minutes of observation, respectively. A black solid line is used to show turbidity of the solution.

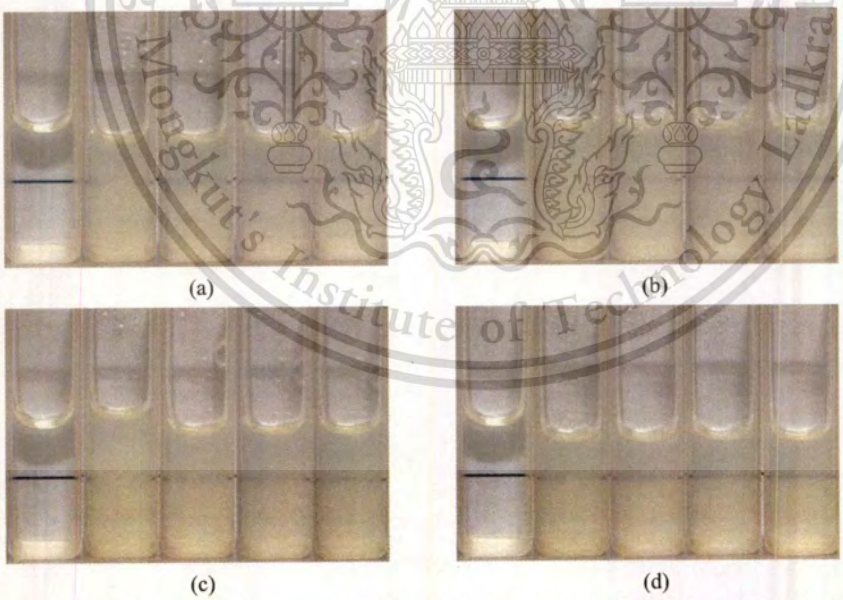

Fig.4 shows 2 ml of our milled rice solutions for 0.30 g of (a) KDML105, (b) CNT1, (c) PTT1 and (d) RD6 rice varieties. Images from left to right are for our 10% KOH solution followed by the 5th, 10th, 15th, and 20th minutes of observation, respectively. A black solid line is used to show turbidity of the solution.

This material is reserved for personal use only, not allowed for commercial use.
Forbidden to modify the content and cite the document when use.
Downloaded from SPIE Digital Library on 02 Dec 2011 to 203.185.129.241. Terms of Use: http://spiedl.org/terms

3.2 Spectral Measurement

Instead of measuring the optical density of the milled rice solution, we investigate the optical transmittance of the milled rice solution with respect to the optical transmittance of our 10% KOH solution in the visible wavelength. Fig.5 shows

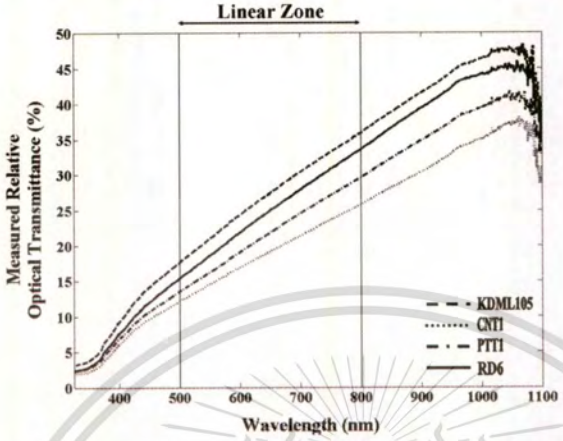

Fig.5 Example of measured relative transmission spectra for 0.10 g of the milled rice powder dissolved in our 10% KOH solution for 5 minutes.

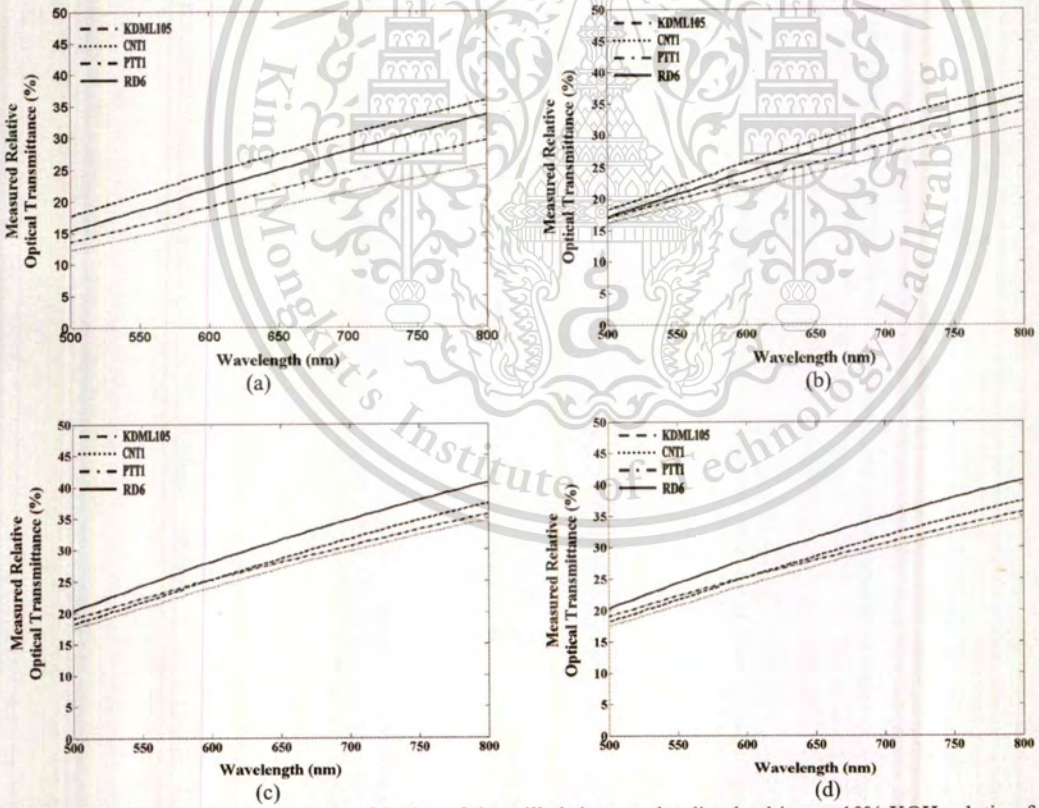

Fig.6 Measured relative optical transmittance of 0.10 g of the milled rice powder dissolved in our 10% KOH solution for four rice varieties at the (a) 5th, (b) 10th, (c) 15th, and (d) 20th minutes of our measurements.

This material is reserved for educational use only, not allowed for commercial use.
Downloaded from SPIE Digital Library on 02 Dec 2011 to 203.185.129.241. Terms of Use: http://spiedl.org/terms

measured relative optical transmittance of four milled rice solutions in a 325-1100 nm wavelength. Specifically, we analyze these spectra only in a 500-800 nm wavelength as it gives the most linear behavior. In this case, a slope of the spectrum in this zone is simply used for the identification of our KDML105 milled rice.

For the 0.10 g of the milled rice powder, measured relative optical transmittance spectra of the four rice varieties are shown in Fig.6. At the beginning of our analysis (e.g., at the 5th minute), the KDML105 milled rice solution shows a higher optical transmittance than the remaining three rice varieties over a 300-nm wavelength (see Fig.6(a)). As these milled rice powders spend more time in our 10% KOH solution for 10, 15, and 20 minutes as shown in Figs.6(b)-(d), the KDML105, CNT1, and PTT1 seem to have an equal capability to be dissolved in our 10% KOH solution. Only the RD6 rice variety has a higher efficiency in dissolving in our 10% KOH solution due to its low amylose content.

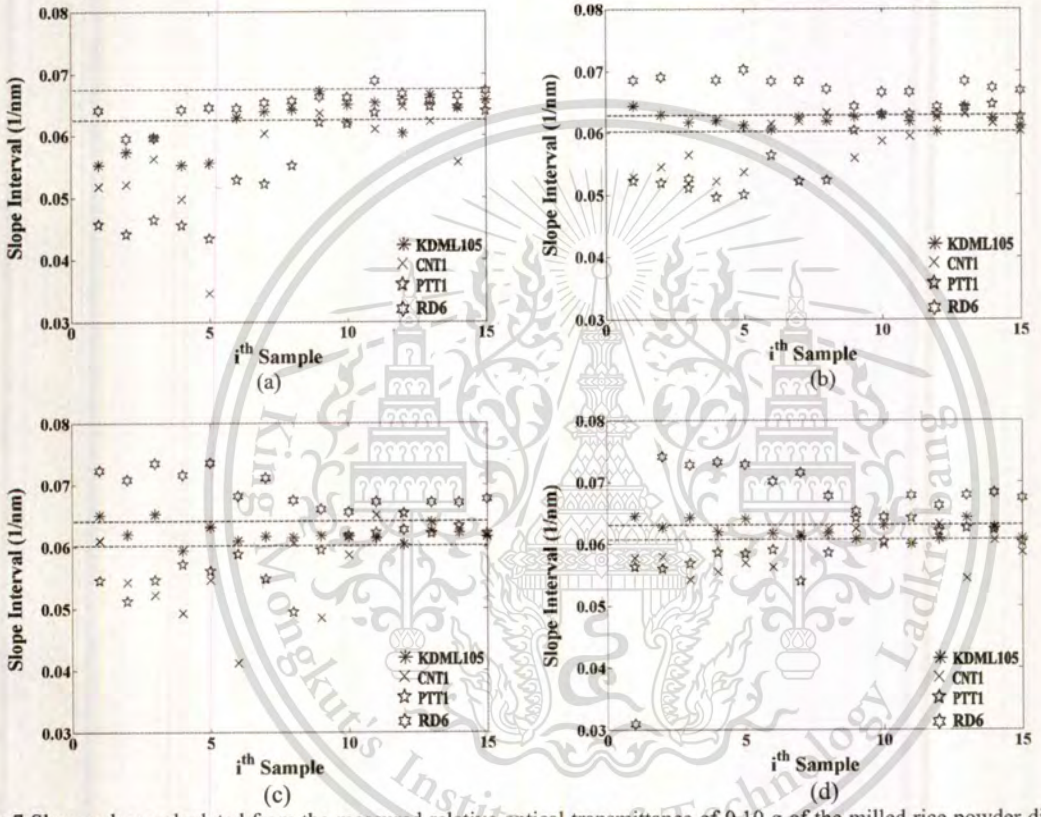

Fig.7 Slope values calculated from the measured relative optical transmittance of 0.10 g of the milled rice powder dissolved in our 10% KOH solution for (a) 5 minutes, (b) 10 minutes, (c) 15 minutes, and (d) 20 minutes.

From the linear zone shown in Fig.6, calculated slope values for all rice samples are shown in Fig.7. By appropriately assigning the slope interval, a false error rate for identifying the desired KDML105 milled rice can be simply determined. In this case, we choose slope intervals of 0.06250-0.06750 nm^{-1}, 0.06017-0.06280 nm^{-1}, 0.06015-0.06400 nm^{-1}, and 0.06065-0.06300 nm^{-1} for our 5th, 10th, 15th, and 20th minutes of measurements, respectively. As a result, we obtain corresponding false error rates of 46.7%, 15.0%, 26.7%, and 18.3%. If only 15 samples of the KDML105 milled rice are taken into account, calculated false error rates for the identification of this rice variety are 40.0%, 13.3%, 20.0%, and 33.3% at the 5th, 10th, 15th, and 20th minutes of our measurements, respectively. A narrower slope interval also gives a lower false error rate.

This material is reserved for educational use only, not allowed for commercial use.
Downloaded from SPIE Digital Library on 02 Dec 2011 to 203.185.129.241. Terms of Use: http://spiedl.org/terms

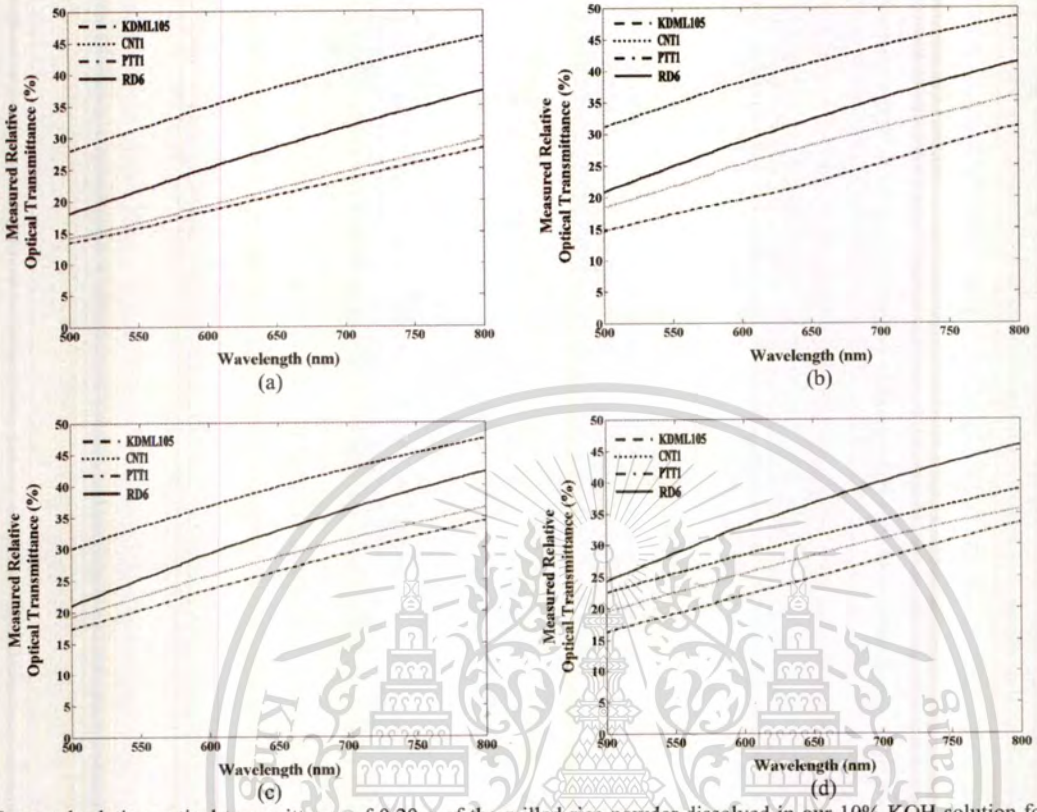

Fig.8 Measured relative optical transmittance of 0.20 g of the milled rice powder dissolved in our 10% KOH solution for four rice varieties at the (a) 5th, (b) 10th, (c) 15th, and (d) 20th minutes of our measurements.

When the 0.20 g of the milled rice powder is used, the measured relative optical transmission spectrum of the KDML105 milled rice powder slightly increases as the time passes from 5 minutes to 15 minutes and then drops below those of the CNT1, PTT1, and RD6 at the 20th minute of our measurement as shown in Fig.8(a). On the other hand, there is 5% increase in the measured relative optical transmission spectra for the remaining three rice varieties as the time goes by from 5 minutes to 20 minute (see Figs.8(b)-(c)). Calculated slope values for 4 different dissolution times are shown in Fig.9. By choosing slope intervals of 0.0550-0.0607 nm^{-1}, 0.0540-0.0633 nm^{-1}, 0.0578-0.0630 nm^{-1}, and 0.0579-0.0630 nm^{-1}, we obtain false error rates of 18.3%, 46.7%, 21.7%, and 23.3% at the 5th, 10th, 15th, and 20th minutes of our measurements, respectively. In the case, if only 15 samples of the KDML105 milled rice are taken into account, calculated false error rates for the identification of this rice variety are 26.7%, 20.0%, 33.3%, and 46.7%, respectively. As expected, slope values for the 0.20 g case are also less than those from the previous case.

This material is reserved for educational use only, not allowed for commercial use.
Forbidden to modify this material without permission when use.
Downloaded from SPIE Digital Library on 02 Dec 2011 to 203.185.129.241. Terms of Use: http://spiedl.org/terms

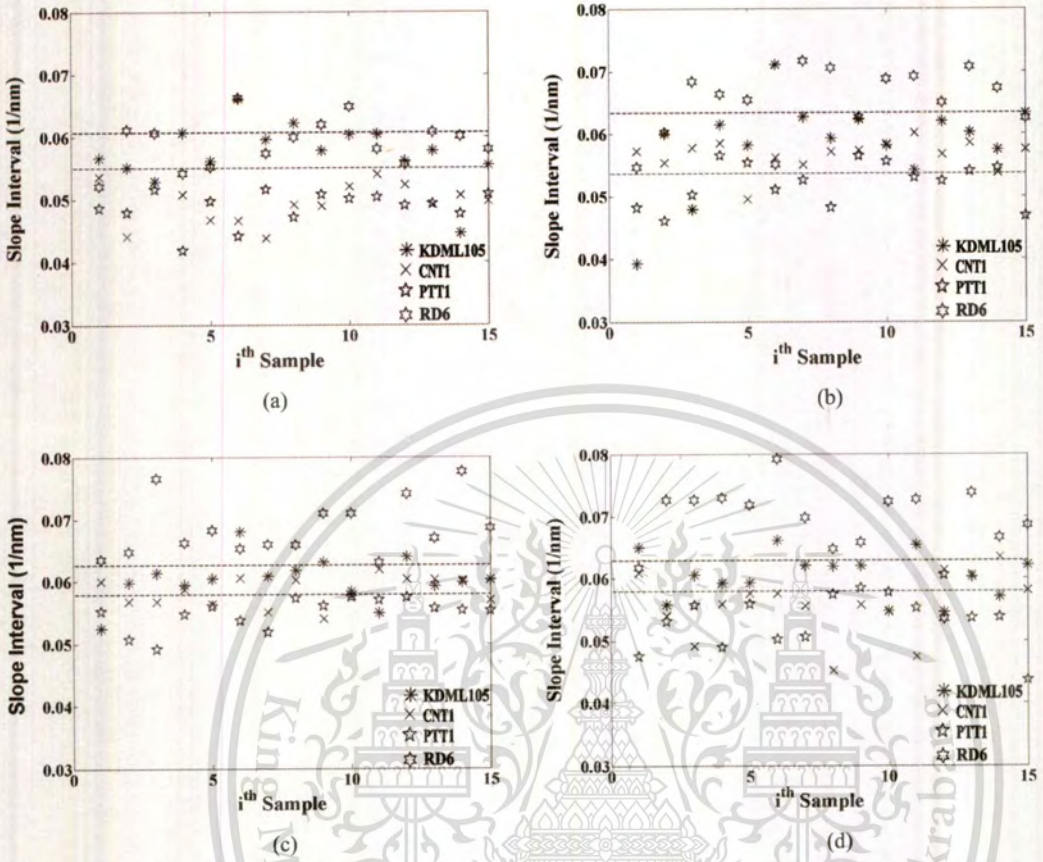

Fig.9 Slope values calculated from the measured relative optical transmittance of 0.20 g of the milled rice powder dissolved in our 10% KOH solution for (a) 5 minutes, (b) 10 minutes, (c) 15 minutes, and (d) 20 minutes.

With the use of a 0.30-g milled rice powder, the RD6 milled rice shows highest capability in dissolving in our 10% KOH solution. Measured relative optical transmission values for all rice varieties are also less than those in the two previous cases (see Fig.10). In addition, as expected, calculated slope values shown in Fig.11 are smaller. By assigning slope intervals of 0.041400-0.051500 nm^{-1}, 0.049300-0.059700 nm^{-1}, 0.049870-0.058600 nm^{-1}, and 0.050010-0.060240 nm^{-1}, high false error rates of 23.3%, 36.7%, 23.3%, and 30.0% are achieved in identifying the KDML105 milled rice at the 5^{th}, 10^{th}, 15^{th}, and 20^{th} minutes of our measurements, respectively. With only the KDML105 milled rice, higher false rejection rates of 60.0%, 53.3%, 33.3%, and 40.0% are determined.

This material is reserved for personal use only, not allowed for commercial use.
Forbidden to modify the content and cite the document when use.
Downloaded from SPIE Digital Library on 02 Dec 2011 to 203.185.129.241. Terms of Use: http://spiedl.org/terms

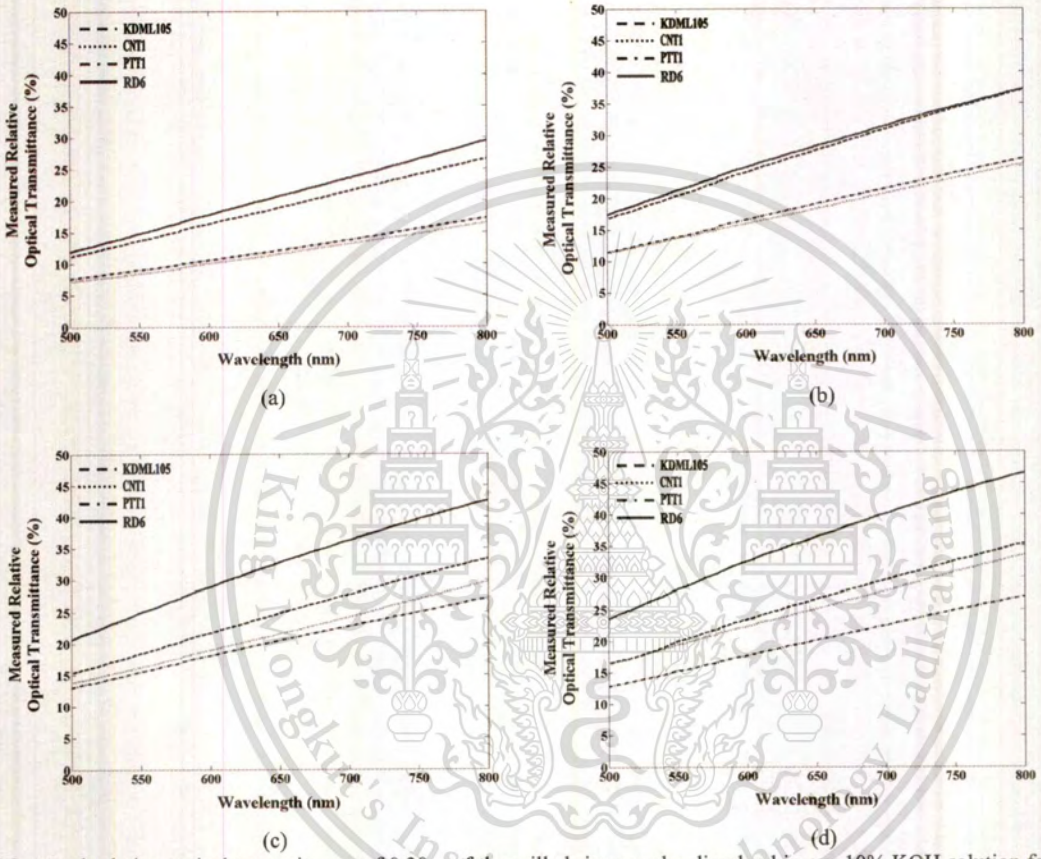

Fig.10 Measured relative optical transmittance of 0.30 g of the milled rice powder dissolved in our 10% KOH solution for four rice varieties at the (a) 5th, (b) 10th, (c) 15th, and (d) 20th minutes of our measurements.

This material is reserved for personal study, not allowed for commercial use.
Forbidden to modify the content and to the document when use.
Downloaded from SPIE Digital Library on 02 Dec 2011 to 203.185.129.241. Terms of Use: http://spiedl.org/terms

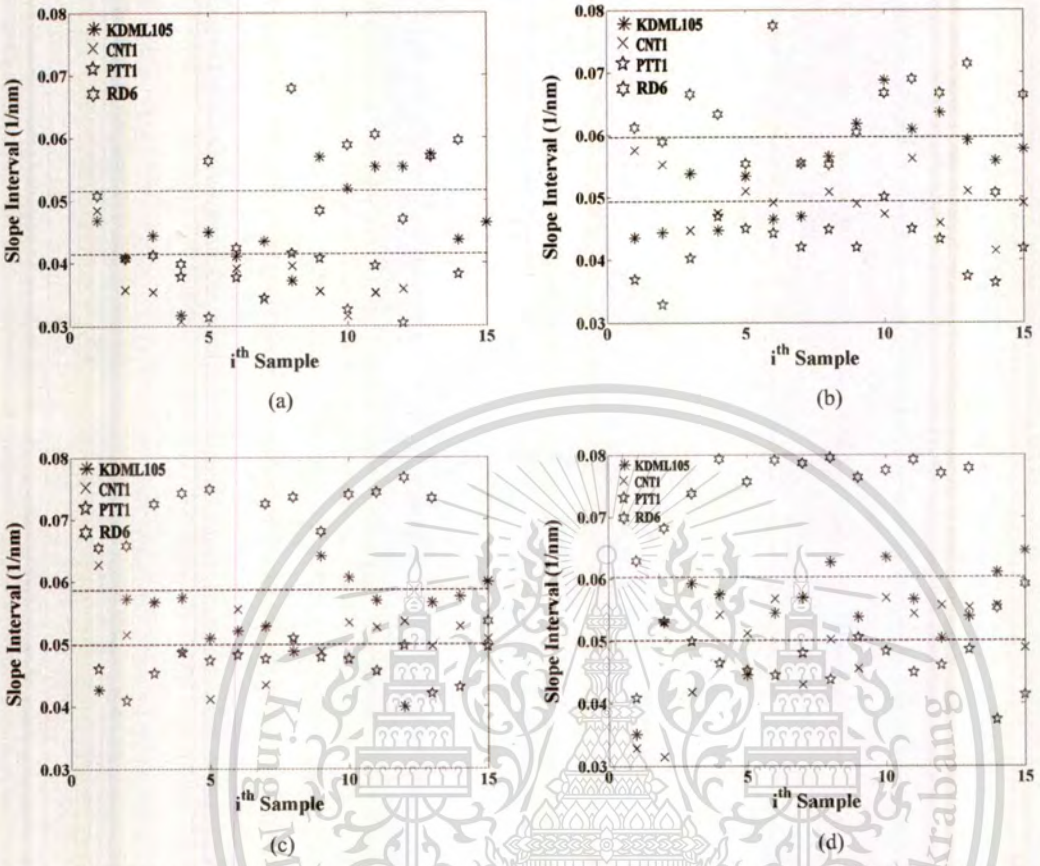

Fig.11 Slope values calculated from the measured relative optical transmittance of 0.30 g of the milled rice powder dissolved in our 10%KOH solution for (a) 5 minutes, (b) 10 minutes, (c) 15 minutes, and (d) 20 minutes.

Table 1: KDML105 identification performance

Dissolution Time (minutes)	Measured false rejection rate for three different weights of the milled rice powder (%)					
	0.10 g		0.20 g		0.30 g	
	All rice varieties (60 samples)	Only KDML105 (15 samples)	All rice varieties (60 samples)	Only KDML105 (15 samples)	All rice varieties (60 samples)	Only KDML105 (15 samples)
5	46.7	40.0	18.3	26.7	23.3	60.0
10	15.0	13.3	46.7	20.0	36.7	53.3
15	26.7	20.0	21.7	33.3	23.3	33.3
20	18.3	33.3	23.3	46.7	30.0	40.0

Table 1 summarizes our study in distinguishing the KDML105 milled rice from the remaining three rice varieties. It can be seen that the measured false rejection rate depends on the weight of the milled rice powder, its ability to be dissolved in our 10% KOH solution, and the dissolution time. Based on our study, the best procedure is to use 0.10 g of the milled rice powder and dissolve it in our 10% KOH solution for 10 minutes, offering a fast analysis with less amount of waste and a low 15% overall false rejection rate. In addition, a faster identification time with a slightly higher 18.3% false rejection rate can be obtained by using a 0.2-g milled rice powder and dissolving it in our 10% KOH solution for 5

This material is reserved for personal use only, not allowed for commercial use.
Forbidden to modify the content and cite the document when use.
Downloaded from SPIE Digital Library on 02 Dec 2011 to 203.185.129.241. Terms of Use: http://spiedl.org/terms

minutes. Optimizing the weight of the milled rice powder, the dissolution time, and the concentration of our KOH solution can help improve the efficiency in identifying the KDML105 milled rice.

4. CONCLUSION

This paper studies the efficiency in identifying the KDML105 milled rice via a combination of chemical and spectroscopic methods. In our approach, the simple chemical method is used for dissolving the milled rice powder and its optical transmission spectrum in the 500-800 nm wavelength is investigated. With four milled rice varieties having different amylose contents and measured weight per seed, their optical transmissivities increase linearly with respect to the measuring wavelength. The slope value of the optical transmissivity of the milled rice solution depends on the dissolution time and the ability of the milled rice powder to be dissolved in our KOH solution. In our study, we find that the use of a 0.1-g milled rice powder dissolved in our 10% KOH solution shows a lowest false rejection rate of 15%. Future work relates to our optimization in our KOH solution, the weight of the milled rice powder, and the dissolution time.

ACKNOWLEDGEMENTS

Our study was financially supported by the Thailand Graduate Institute of Science and Technology of Thailand (Grant No. TGIST 01-51-071) and the Photonics Technology Laboratory, at the National Electronics and Computer Technology Center. We also gratefully thank the Rice Research Institute at the Department of Rice, Ministry of Agriculture and Cooperatives of Thailand for providing rice samples used in this work.

REFERENCE

[1] Y. Liu, A. Ouyang, J. Wu, Y. Ying , "An automatic method for identifying different variety of rice seeds using machine vision technology", *Proc. of SPIE* 5996, pp.59961H-1 (2005).

[2] B. G. Osborne, B. Mertens, M. Thompson, and T. Fearn, "Authentication of Basmati rice using near infrared spectroscopy," *J. of Near Infrared Spectro.* 1, pp.77-83 (1993).

[3] S. S. Kim, M. R. Rhyu, J. M. Kim, and S. H. Lee, "Authentication of rice using near-infrared reflectance spectroscopy", *Cereal Chem.* 80, pp. 346-349 (2003).

[4] Y. Shao, Y. He, and F. Cao, "Identification of rough rice species and years by visible/near-infrared reflectance spectroscopy," *Comp. Intel. and Security* 2, 3-6 Nov. 988-991 (2006)

[5] S. Sumriddetchkajorn, K. Suwansukho, and P. Buranasiri, "Identification of Thai Hom Mali rice using a refractometer," *Proc. SPIE* 7315, Orlando, Florida, USA (2009).

[6] A. Vanavichit, S. Tragoonrung, and T. Toojinda, "Biotechnology and rice varieties improvement," Chap. 4 in Science and Technology with Thai Rice, Thailand's National Science and Technology Development Agency, June 2003.

[7] V. R. William, W. T. Wu, H. Y. Tsai, and H. G. Bates, "Varietal differences in amylose content of rice starch," *J. of Agri. Food* 6, pp. 47-48 (1958).

[8] R. R. Little, G. B. Hilder and E. H. Dawson, "Differential effect of dilute alkali on 25 varieties of milled white rice", *Cereal Chem.* 35 pp. 111-126 (1958).

[9] B. O. Juliano, "A simplified assay for milled-rice amylose," *Cereal Sci. Today* 16, pp. 334-340 (1971).

[10] "The ministry of commerce notification on rules and methodologies of commodities and Thai Hom Mali rice standards inspection B.E. 2545 (2002)", *Government Gazette* 119, Special Section 21D, March 7, 2002.

This material is reserved for personal use; not allowed for commercial use.
Forbidden to modify the content and cite the document when use.
Downloaded from SPIE Digital Library on 02 Dec 2011 to 203.185.129.241. Terms of Use: http://spiedl.org/terms

Identification of Thai Hom Mali Rice using a Refractometer

Sarun Sumriddetchkajorn*[a], Kajpanya Suwansukho[b], and Prathan Buranasiri[b]
[a]Photonics Technology Laboratory
National Electronics and Computer Technology Center
National Science and Technology Development Agency
Ministry of Science and Technology
112 Thailand Science Park, Phahonyothin Rd, Klong 1, Klong Luang
Pathumthani 12120, Thailand, Tel: +662-564-6900 ext. 2102, Fax: +66-25674-6774
E-mail: sarun.sumriddetchkajorn@nectec.or.th

[b]Department of Applied Physics, Faculty of Science
King Mongkut's Institute of Technology Lakrabang, Bangkok, Thailand

ABSTRACT

Because Thai Hom Mali, also known as Thai Dawk Mali (KDML105), rice is very popular and its price is high compared to other Thai rice varieties, there is an increase in mixing KDML105 milled and unmilled rice grains with other rice varieties, leading to unqualified KDML105 milled rice products for export and unqualified KDML105 unmilled rice seeds for next plants. Instead of using traditional time- and energy- consuming procedures such as alkaline spreading value and pasting property tests, this paper proposes a fast refractometry-based method to analyze ground milled rice grains dissolved in an alkaline solution. Our idea comes from the fact that due to differences in the amount of amylose content in each rice variety, the refractive index of the milled rice powder dissolved in an alkaline solution can be used to distinguish the desired KDML105 rice from others. In our approach, only 0.1 grams of milled rice powder is ground, it is then dissolved in a 10% potassium hydroxide, and its refractive index is investigated. Our experiment using a temperature-controlled optical refractometer and four Thai rice varieties (KDML105, Pathumthani1, Chainat1, and a Thai sticky rice) shows that the milled KDML105 rice can be distinguished from the remaining three rice varieties with a total false error rate of 6.7% and the required measurement time of < 20 seconds. Key advantages include simplicity, moderate accuracy, and less waste produced.

Keywords: Rice, Refractive index, Refractometers, Biophotonics, Agriphotonics

1. INTRODUCTION

Due to its good aroma, taste, and physical properties after cook, Thai Dawk Mali 105 (KDML105) rice is one of the most popular rice varieties. Last year, it was exported with a value of 60.68 billion baths (USD1.73 billions) and it was in the 7th export products of Thailand behind electronic components, automobiles, and jewelry [1]. As a result, there is an increase in mixing milled and unmilled KDML105 rice with other Thai rice varieties such as Pathumthani1 (PTT1) and Chainat1 (CNT1), leading to unqualified KDML105 milled rice grain products for export and unwanted unmilled rice seeds for next plants. These two added rice varieties have similar shape and color to the KMDL105 rice. This implies that a simple machine vision technique [2] cannot be used to separate these rice varieties from each other.

Today, widely used procedures for separating rice varieties are based on chemical and biological methods. For example, the DNA analysis is the most accurate method for identifying rice varieties [3]. Apart from the DNA analysis, near infrared spectroscopy was also proposed and experimentally demonstrated for this task [4-8]. Recently, we have proposed and experimentally studied a combination of chemical and spectroscopic (in the 500-800 nm wavelength region) approaches to identify the KDML105 milled rice solution with a measured 15% total false error rate [9]. Fiber-

*Correspondence E-mail: sarun.sumriddetchkajorn@nectec.or.th

Sensing for Agriculture and Food Quality and Safety, edited by Moon S. Kim, Shu-I Tu, Kaunglin Chao,
Proc. of SPIE Vol. 7315, 73150F · © 2009 SPIE · CCC code: 0277-786X/09/$18 · doi: 10.1117/12.820148

This material is reserved for educational use only, not allowed for commercial use.
Forbidden to modify the content and cite the document when use.
Downloaded from SPIE Digital Library on 02 Dec 2011 to 203.185.129.241. Terms of Use: http://spiedl.org/terms

connectorized interferometers can also be employed for characterizing the optical properties of the milled rice solution [10-11]. However, these approaches require expensive equipment and their procedures are time consuming. In addition, they cannot be easily and cost effectively modified to operate in the field.

The iodine-binding procedure designed for analyzing amylose content [12] is one of the simplest methods that is widely used and accepted to identify the KDML105 milled rice from other Thai rice varieties. Because iodine can also bind with amylopectin, it causes overestimation of the amylose content. Since the expansion of the rice starch in an alkali solution for the study of gelatinization temperature of rice was known [13], seven alkali-spreading values observed within 23 hours have been used to distinguish the KDML105 milled rice from other Thai rice varieties. In addition, because amylose content causes rice to absorb more water and consequently expand more during cooking [14], inspection of rice cooked in boiling water for 17 minutes via a pasting property test can be used to determine the KDML105 milled rice. These two last simple methods are also recommended for KDML105 rice standards inspection [15]. With these procedures in mind, a faster approach that generates less amount of waste and provides a moderate accuracy is needed for farmers and exporters.

Another promising technique is based on optical refractometry. Previously, it was used for process control [16] and the study of rice starch characteristics [17]. This paper proposes to analyze milled rice grains dissolved in an alkaline solution via an optical refractometer. Our idea comes from the fact that due to differences in the amount of amylose content in the two rice varieties typically mixed with the KDML105 rice, the refractive index of the milled rice grain dissolved in an alkaline solution can be used to identify the desired KDML105 rice.

2. OUR PROPOSED METHOD

As mentioned earlier, it is impossible to visually separate the two rice varieties PTT1 ad CNT1 from the desired KDML105 rice. This is the reason that people have to investigate them chemically and biologically. For the KDML105 rice, its amylose content is in the range of 13%-18%. The PTT1 rice has equivalent amount of amylose content to that of the KDML105 rice but its weight per seed is 80.5% less (i.e., 0.0174 grams). These two rice varieties are classified as low amylose content rices. The CNT1 rice has its amylose content in 27%-30% and it is classified as one of the high-amylose content varieties. Its weight is 98.6% (i.e., 0.0213 grams) compared to the KDML105 rice. Because these three rice varieties have different weight per grain and they can be dissolved in an alkali solution, we propose to optically analyze the milled rice solution. Our simpler proposed procedure is to grind the desired amount of milled rice, dissolve it in the potassium hydroxide (KOH) solution, and then measured its refractive index by using an optical refractometer as shown in Fig.1.

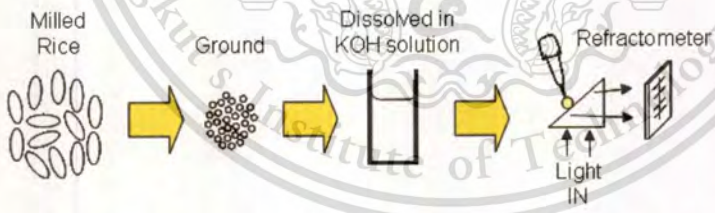

Fig.1 Our proposed method where we combine chemical and optical techniques for identifying the KDML105 milled rice.

In our proposed method, we prepare a 10% KOH solution by first dissolving 10 grams of KOH pallets in 80 ml deionized water. Note that we choose a higher concentration of the KOH solution compared to a 1.7% concentration previously used in the 7-level alkali spreading method because we would like to speed up the dissolution process. Then the volume of the solution is readjusted by adding the desired amount of deionized water until the overall volume reaches 100 ml. Our KOH solution can be prepared in advance if we plan to verify the KDML105 rice in the field. After that, the desired amount of ground milled rice grains is gradually poured into a 10-ml KOH solution under a magnetic bar stirrer at about 2400 rpm without heating. This process is finished within 2 minutes. At the 4.5th minute, the stirrer speed is adjusted to zero but the magnetic bar is still moving with the remaining inertia force. At the specified minute of measurement (e.g., 5th and 10th minutes), a dropper is used to suck a 0.5-ml milled rice solution and drop it in a

This material is reserved for personal study, not allowed for commercial use.
Forbidden to modify the content and cite the document when use.
Downloaded from SPIE Digital Library on 02 Dec 2011 to 203.185.129.241. Terms of Use: http://spiedl.org/terms

light emitting diode (LED)-based optical refractometer where a refractive index is measured with a $> \pm 0.0003$ accuracy at 25°C. The optical refractometer can be an off-the-shelf portable digital version which is suitable for field operation.

3. OUR EXPERIMENTAL PROOF OF CONCEPT

Apart from KDML105, CNT1, and PTT1 rice varieties, we bring in to our study another Thai rice variety with very low amylose content of 0%-2%. It is Thai sticky rice (RD6). The measured weight ratio of the RD6 rice with respect to the KDML105 rice is 88.3% (i.e., 0.0191 grams). All milled rice grains used in our experiment are provided by the Rice Research Institute at the Department of Rice, Ministry of Agriculture and Cooperatives of Thailand. They were harvested in 2007 with moisture content of 12%-14%.

3.1 Visual Inspection

Fig.2 shows color and shape of four Thai rice varieties used in our experiment. It can be observed that it is not effectively to separate the KMDL105 rice from PTT1 and CNT1 rice varieties by our naked eyes or using simple machine vision techniques. This is the reason why the PTT1 and CNT1 are the most popular rice varieties that are mixed with the KDML105 rice. In each rice variety, we randomly select the amount of milled rice grains for three different weights of 0.1 grams, 0.2 grams, and 0.3 grams, and then grind them by using a bench-top grinder. After that, the milled rice powder is dissolved in our 10% KOH solution prepared in section 2.

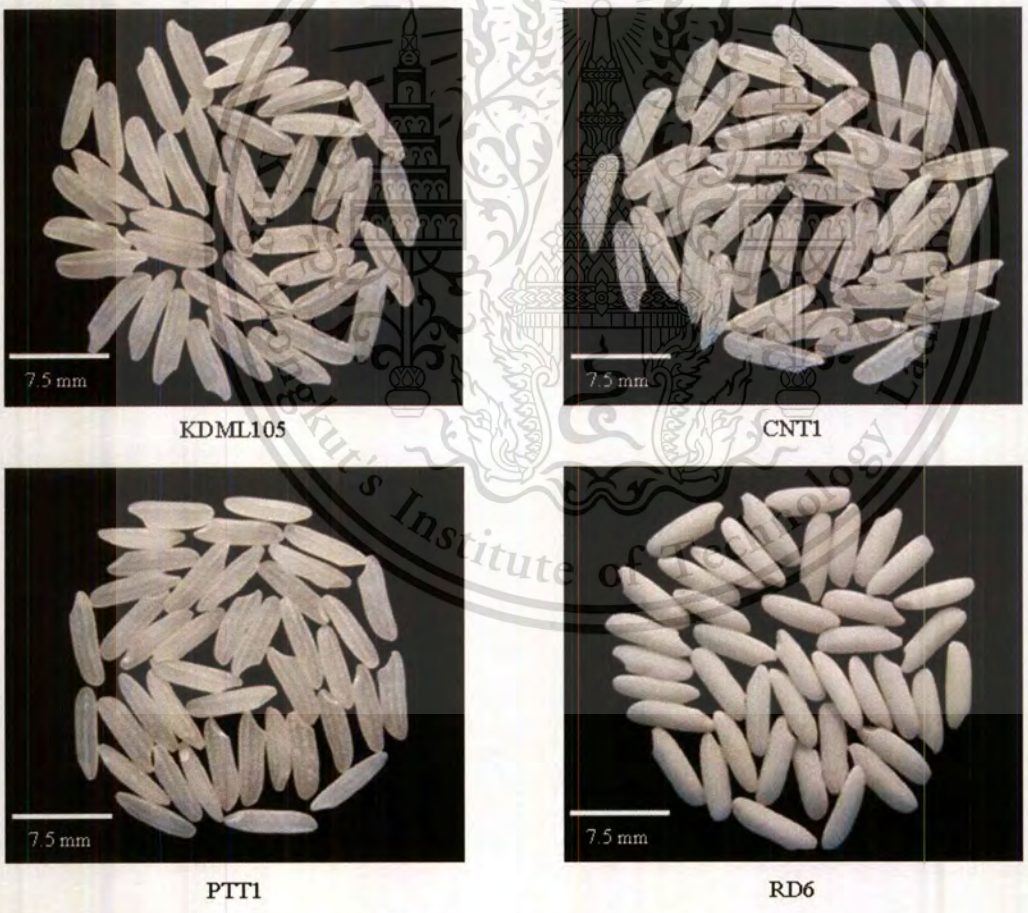

Fig.2 Snapshot of four Thai rice varieties used in our experimental study.

This material is reserved for educational use only, not allowed for commercial use.
Downloaded from SPIE Digital Library on 02 Dec 2011 to 203.185.129.241. Terms of Use: http://spiedl.org/terms

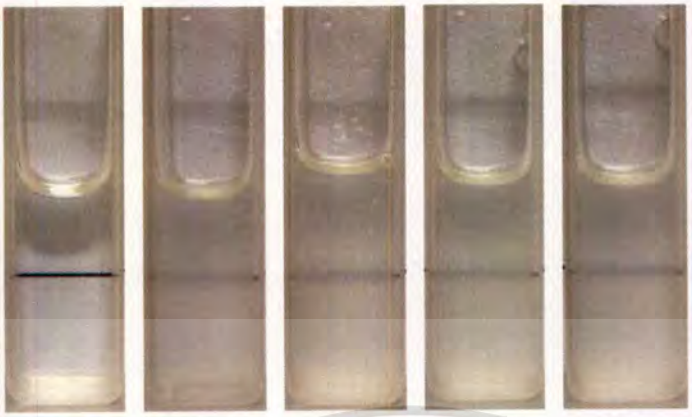

Fig.3 shows 0.1 grams of four Thai milled rice varieties dissolved in 10 ml of our 10% KOH solution for 5 minutes. A black solid line is used to show turbidity of the solution.

Fig.3 shows our 10% KOH solution having 0.1 grams of milled rice powder dissolved in it for 5 minutes. We can see that KDML105, CNT1, PTT1, and RD6 milled rice solutions have similar turbidity. Measured normalized optical transmissivity of these four milled rice solutions (15 samples per rice variety) at a 635-nm wavelength is varied between 26%-33%. Adjusting the weight of the milled rice powder to 0.2 grams and 0.3 grams increases the turbidity of the milled rice solution with a slight drop of 5%-10% in the normalized optical transmissivity. At the 10^{th} minute dissolution time, these four milled rice varieties dissolve much better and their normalized optical transmissivities increase about 5%-60%. These results confirm that merely the optical density measurement cannot be used to effectively identify the KDML105 milled rice from the remaining three rice varieties.

3.2 Refractive Index Measurement

At the 5^{th} and 10^{th} minutes of our measurements, we use a plastic dropper to suck and then drop a 0.5-ml milled rice solution on the LED-based optical refractometer from Atago model RX-7000-α. The measurement temperature is fixed at 25°C and the measurement time at this state is less than 20 seconds. Note that the sensing element of the LED-based optical refractometer is a Sapphire prism and it can determine the refractive index from 1.3250 to 1.7000 with the measurement accuracy and repeatability of $\pm$0.0001 and $\pm$0.00005, respectively.

Refractive index values of the solutions from three Thai milled rice varieties compared with one from the KDML105 milled rice measured at the 5^{th} and 10^{th} minute measurements for three different weights of milled rice powder are first studied as shown in Fig.4. As expected, the refractive index of the CNT1 milled rice solution is lower than that of the KDML105 milled rice solution while the refractive index of the PTT1 milled rice solution is higher than that of the KDML105 milled rice solution. By increasing the amount of the milled rice powder dissolved in our 10% KOH solution from 0.1 grams to 0.2 grams and 0.3 grams, the difference in refractive index between CNT1 and KDML105 milled rice solutions is larger. For the PTT1 milled rice solution, its difference with the KDML105 milled rice solution gets increased with the 0.2 grams and it is drop for the 0.3 grams. For the RD6 milled rice solution, increasing the amount of milled rice grains in our 10% KOH solution makes the refractive index difference drop. In addition, spending more time for 0.1 grams and 0.2 grams of milled rice powder to be dissolved more in our 10% KOH solution cannot enhance the refractive index differences. In this approach, using the 0.3 grams of the milled rice powder shows some enhancement only for the CNT1 and PTT1.

3.3 KDML105 Identification

Based on the comparison of the refractive indices of four milled rice solutions in Fig.4 and with requirements to use less amount of sample and reduce operating time, we select 0.1 grams of the milled rice powder dissolved in our 10% KOH solution for 5 minutes for our study in identifying the KDML105 rice. Fig.5 shows measured refractive index of 0.1 grams of KDML105, CNT1, PTT1, and RD6 milled rice powders dissolved in our 10% KOH solution. The number of samples is 15 for each rice variety. Fluctuation of measured refractive indices is due to the way we dissolve the milled

This material is reserved for personal study, not allowed for commercial use.
Forbidden to modify the content and cite the document when use.
Downloaded from SPIE Digital Library on 02 Dec 2011 to 203.185.129.241. Terms of Use: http://spiedl.org/terms

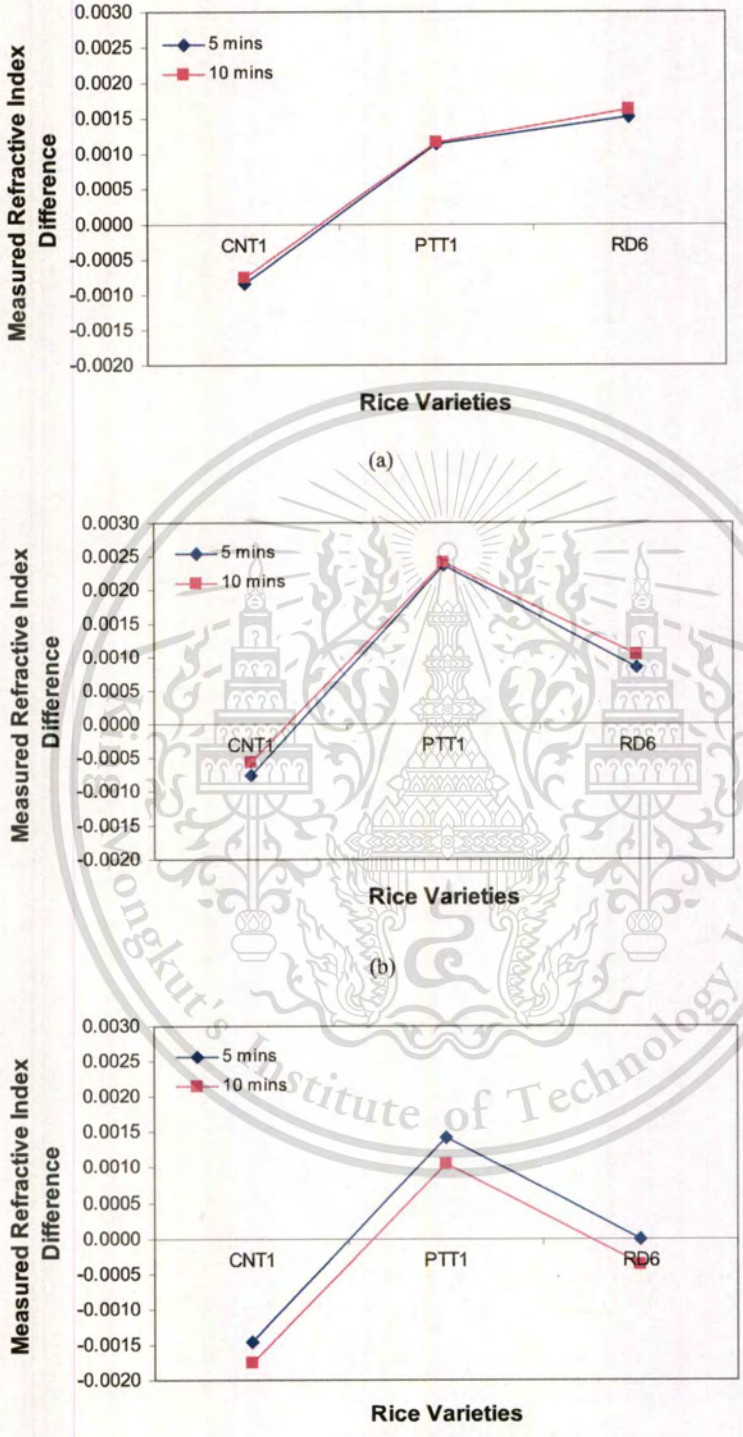

Fig.4 Measured refractive index differences of CNT1, PTT1 and RD6 milled rice solutions compared to the KDML105 milled rice solution for (a) 0.1 grams, (b) 0.2 grams, and (c) 0.3 grams of the milled rice powder.

This material is reserved for personal use only, not allowed for commercial use.
Forbidden to modify the content and cite the document when use.
Downloaded from SPIE Digital Library on 02 Dec 2011 to 203.185.129.241. Terms of Use: http://spiedl.org/terms

rice powder. By appropriately choosing the upper and lower refractive indices of 1.3494 and 1.3474 as our threshold interval, we find that we can 100% identify all milled rice grains that are not KDML105, i.e., their refractive index values stay inside our threshold interval. For the identification of the KDML105 milled rice, we achieve a false error rate of 100×4/15 = 26.7%. These results imply that we can identify 15 KDML105 milled rice samples from 60 milled rice samples with a false error rate of 100×4/60 = 6.7%. With better sample preparation processes, false error rates can significantly be reduced.

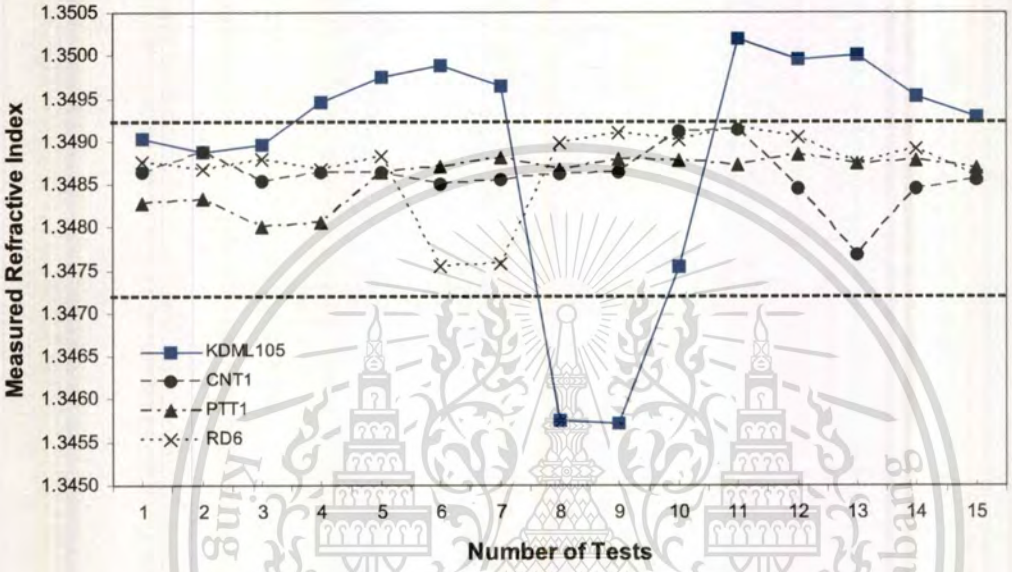

Fig.5 Measured refractive index values of 0.1 grams of KDML105, CNT1, PTT1 and RD6 milled rice powders each dissolved in 10 ml of our 10% KOH solution for 5 minutes.

4. CONCLUSION

This paper proposes a fast and low-cost procedure for the identification of the Thai Hom Mali rice from other three rice varieties. Our proposed procedure combines a chemical method for dissolving the milled rice powder with an optical refractometry for measuring the refractive index. In our experimental study, we use only 0.1 grams of the milled rice powder and dissolve it in 10 ml of our 10% KOH solution. During our refractive index measurement, merely 0.5 ml of the dissolved milled rice solution is dropped onto the sensing area of the temperature-controlled LED-based optical refractometer and the measurement time is less than 20 seconds. By appropriately assigning upper and lower refractive indices as our threshold interval, we can obtain a total false error rate of 6.7%. Improvement in sample preparation processes can help increase identification efficiency. Future work also relates to the study of repeatability.

ACKNOWLEDGEMENTS

Authors gratefully thank the Rice Research Institute at the Department of Rice, Ministry of Agriculture and Cooperatives of Thailand for supplying rice samples. K. Suwansukho would also like to thank Thailand Graduate Institute of Science and Technology for scholarship support (Grant No. TGIST 01–51-071).

This material is reserved for personal study, not allowed for commercial use.
Forbidden to modify the contents and cite the document when use.
Downloaded from SPIE Digital Library on 02 Dec 2011 to 203.185.129.241. Terms of Use: http://spiedl.org/terms

REFERENCES

[1] Department of Foreign Trade, Ministry of Commerce, Thai Government, http://www.dft.moc.go.th/, accessed on Feb. 2, 2009.

[2] Y. Liu, A. Ouyang, J. Wu, and Y. Ying, "An automatic method for identifying different variety of rice seeds using machine vision technology," *Proc. SPIE* 5996, p. 59961H (2005).

[3] A. Vanavichit, S. Tragoonrung, and T. Toojinda, "Biotechnology and rice varieties improvement," Chap. 4 in *Science and Technology with Thai Rice*, Thailand's National Science and Technology Development Agency, June 2003.

[4] S. R. Delwiche, M. M. Bean, R. E. Miller, B. D. Webb, and P. C. Williams, "Apparent amylose content of milled rice by near-infrared reflectance spectrophotometry," *Cereal Chem.* 72, pp. 182-187 (1995).

[5] S. R. Delwiche, K. S. McKenzie, and B. D. Webb, "Quality characteristics in rice by near-infrared reflectance analysis of whole-grain milled samples," *Cereal Chem.* 73, pp. 257-263 (1996).

[6] F. E. Barton, II, D. S. Himmelsbach, A. M. McClung, and E. T. Champagne, "Rice quality by spectroscopic analysis: precision of three spectral regions," *Cereal Chem.* 77, pp. 669-672 (2000).

[7] E. T. Champagne, K. L. Bett-Garber, C. C. Grimm, A. M. McClung, K. A. Moldenhauer, S. Linscombe, K. S. McKenzie, and F. E. Barton, II, "Near-infrared reflectance analysis for prediction of cooked rice texture," *Cereal Chem.* 78, pp. 358-362 (2001).

[8] S. R. Delwiche and R. A. Graybosch, "Identification of waxy wheat by near-infrared reflectance spectroscopy," *J. of Cereal Sci.* 35, pp. 29-38 (2002).

[9] K. Suwansukho, S. Sumriddetchkajorn, and P. Buranasiri, "Combination of simple chemical and spectroscopic methods for the identification of Thai Hom Mali rice," *Proc. SPIE* 7315, Orlando, Florida, USA (2009).

[10] S. Sumriddetchkajorn, "Polarization-insensitive tunable-contrast fiber-optic polarization interferometers with a polarization controller," *Optics Commun.* Vol. 217, pp. 197-203 (2003).

[11] S. Sumriddetchkajorn, K. Katanyukunanon, and T. Srikhirin, "Fiber loop mirror-based optical transmissivity and optical phase retardation measurement architecture," *Appl. Opt.* 46, pp. 8461-8465 (2007).

[12] V. R. William, W. T. Wu, H. Y. Tsai, and H. G. Bates, "Varietal differences in amylose content of rice starch," *J. of Agri. Food* 6, pp. 47-48 (1958).

[13] R. R. Little, G. B. Hilder, and E. H. Dawson, "Differential effect of dilute alkali on 25 varieties of milled white rice," *Cereal Chem.* 35, pp. 111-126 (1958).

[14] B. O. Juliano, "A simplified assay for milled-rice amylose," *Cereal Science Today* 16, pp. 334-340 (1971).

[15] "The ministry of commerce notification on rules and methodologies of commodities and Thai Hom Mali rice standards inspection B.E. 2545 (2002)", *Government Gazette* 119, Special Section 21D, March 7, 2002.

[16] A. Cusano, A. Cutolo, M. Giordano, and L. Nicolais, "Optoelectronic refractive index measurements: application to smart processing," *IEEE Sensors J.* 3, pp. 781-787 (2003).

[17] M.- H. Chen and C. J. Bergman, "Method for determining the amylose content, molecular weights, and weight- and molar-based distributions of degree of polymerization of amylose and fine-structure of amylopectin," *Carbohydrate Pol.* 69, pp. 562-578 (2007).

This material is reserved for personal use only, not allowed for commercial use.
Forbidden to modify the content and cite the document when use.
Downloaded from SPIE Digital Library on 02 Dec 2011 to 203.185.129.241. Terms of Use: http://spiedl.org/terms

Demonstration of a single-wavelength spectral-imaging-based Thai jasmine rice identification

Kajpanya Suwansukho,[1] Sarun Sumriddetchkajorn,[2,*] and Prathan Buranasiri[1]

[1]Physics Department, Faculty of Science, King Mongkut's Institute of Technology Ladkrabang, Bangkok, Thailand

[2]Intelligent Devices and Systems Research Unit, National Electronics and Computer Technology Center, National Science and Technology Development Agency, Ministry of Science and Technology, 112 Thailand Science Park, Phahonyothin Road, Klong 1, Klong Luang, Pathumthani 12120, Thailand

*Corresponding author: sarun.sumriddetchkajorn@nectec.or.th

Received 15 February 2011; accepted 3 June 2011;
posted 8 June 2011 (Doc. ID 142716); published 14 July 2011

A single-wavelength spectral-imaging-based Thai jasmine rice breed identification is demonstrated. Our nondestructive identification approach relies on a combination of fluorescent imaging and simple image processing techniques. Especially, we apply simple image thresholding, blob filtering, and image subtracting processes to either a 545 or a 575 nm image in order to identify our desired Thai jasmine rice breed from others. Other key advantages include no waste product and fast identification time. In our demonstration, UVC light is used as our exciting light, a liquid crystal tunable optical filter is used as our wavelength seclector, and a digital camera with 640 active pixels × 480 active pixels is used to capture the desired spectral image. Eight Thai rice breeds having similar size and shape are tested. Our experimental proof of concept shows that by suitably applying image thresholding, blob filtering, and image subtracting processes to the selected fluorescent image, the Thai jasmine rice breed can be identified with measured false acceptance rates of <22.9% and <25.7% for spectral images at 545 and 575 nm wavelengths, respectively. A measured fast identification time is 25 ms, showing high potential for real-time applications. © 2011 Optical Society of America

OCIS codes: 120.4630, 260.2510, 300.6280, 120.0120, 100.0100.

1. Introduction

It is known that Thai jasmine rice, also called Kaw Dawk Mali 105 (KDML105), is one of the best rice varieties in the world. In 2009, it had economic values up to $2.20 billion US [1]. As a result, there have increasingly been intentional impurities of KDML105 milled rice products with other lower price foreign rice varieties as well as other lower price Thai rice varieties, such as Chainat 1 (CNT1), Hom Pitsanulok (HPSL), Hom Supanburi (HSPR), Pathumthani 1 (PTT1), Ko Kor 15 (RD15), and Ko Kor 23 (RD23). Since those varieties have similar shape, weight per seed, and color to the KDML105 milled rice, a simple machine vision technique operating in the visible spectrum [2–7] cannot be used to distinguish our desired KDML105 milled rice from other rice varieties. Currently, several other approaches have been proposed and implemented for rice breed identification, but they rely on destructive and time-consuming chemical [8,9], physical [10,11], or DNA [12,13] analysis. One-dimensional optical spectrum analysis in the visible and near-infrared wavelength regions [14,15] and optical refractometry [16] have also been demonstrated.

One of the promising nondestructive approaches is fluorescent imaging. Several wavelength bands of fluorescent radiation under UVA illumination were previously studied for contamination detection in fruits, meats, and plant leaves [17–19]. It was also

0003-6935/11/214024-07$15.00/0
© 2011 Optical Society of America

This material is reserved for educational use only, not allowed for commercial use.

Forbidden to modify the content, and cite the document when use.

shown that fluorescent images induced by UVA light (e.g., 315 nm wavelength) could be used to diagnose the plant stress [20] and the ripening levels of the banana [21]. For identification of milled rice breeds, milled rice grains were illuminated with a 365 nm wavelength light and the induced fluorescent radiation near the 460 nm wavelength was investigated through histogram analysis [22,23]. However, this technique is suitable only for distinguishing rice breeds that contain largely different amounts of amylose content. By using higher energy light sources in the UVC spectrum, simultaneous analysis of two-wavelength spectral images near 545 and 575 nm wavelengths was preliminarily demonstrated by us for identifying a variety of Thai rice breeds [24]. The use of high-energy UVC light also provides an inherent advantage by reducing contamination levels without generating waste effluents [25]. Based on our previous work [24], we show here how efficient a single-wavelength spectral image under high-energy UVC light can be used to distinguish our high-quality KDML105 milled rice grains from other rice varieties. In particular, the selected spectral image just goes through a set of blob filtering processes twice, leading to fast identification.

2. Our Single-Wavelength Spectral-Imaging-Based KDML105 Milled Rice Breed Identifier

A. Architecture of the System

The arrangement of our single-wavelength spectral-imaging-based KDML105 milled rice breed identification system is shown in Fig. 1. The main components are a two-dimensional (2-D) digital camera, a camera lens, a narrow bandpass optical filter centered at the 545 or 575 nm wavelength, a UV block filter, high-energy light sources (e.g., UVC at 253.7 nm wavelength), and an electronic controlling and processing unit. There is a region in which we can scatter unknown breeds of milled rice grains for analysis. This region is also in the field of view of the imaging lens system. Under the UVC illumination, all milled rice grains are induced to give up their fluorescent radiation. A series of UV block filter and a narrow bandpass optical filter are mounted in front of the 2-D digital camera. The desired fluorescent spectral image is then obtained from the camera.

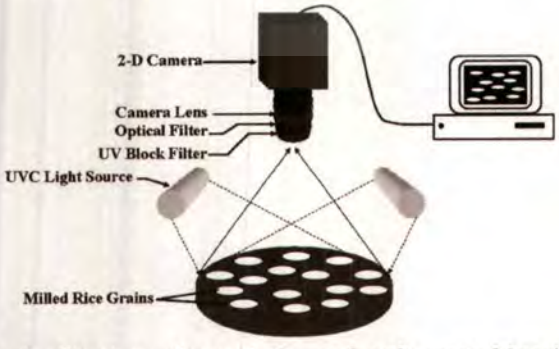

Fig. 1. Structure of our single-wavelength spectral-imaging-based KDML105 milled rice breed identification system.

B. Analytical Procedures

Once we have the desired spectral image associated with the 545 or 575 nm fluorescent wavelength emerging from the milled rice grains, we follow the procedures shown in Fig. 2. Each spectral image is normalized by a reference white image. Realizing that each rice breed spatially emits a different amount of fluorescent radiation due to the amount of amylose, amylopectin, and glutin [26–28], the normalized spectral image goes through an image thresholding process in order to filter out unwanted image areas. Our image thresholding can be simply expressed as

$$I'(x,y) = \begin{cases} 255, & \mathrm{Th}_{\min} \le I(x,y) \le \mathrm{Th}_{\min} \\ 0, & \text{Otherwise} \end{cases}. \quad (1)$$

From Eq. (1), if the gray scale value $I(x,y)$ of each image pixel remains within the desired $\mathrm{Th}_{\min}$ and $\mathrm{Th}_{\max}$, its new gray scale value $I'(x,y)$ will be changed to a maximum gray scale value (e.g., 255 for an 8 bit image). On the other hand, the new gray scale value $I'(x,y)$ of 0 will be assigned if the gray scale value $I(x,y)$ is out of the desired range.

After that, two blob filtering processes via area and perimeter analysis are applied in order to roughly eliminate unwanted pixels. Because milled rice grains have an elliptical shape, the area and perimeter of each milled rice grain can be computed as

$$\text{Area} = \pi ab, \quad (2)$$

and

$$\text{Perimeter} = \pi\sqrt{2(a^2+b^2)}, \quad (3)$$

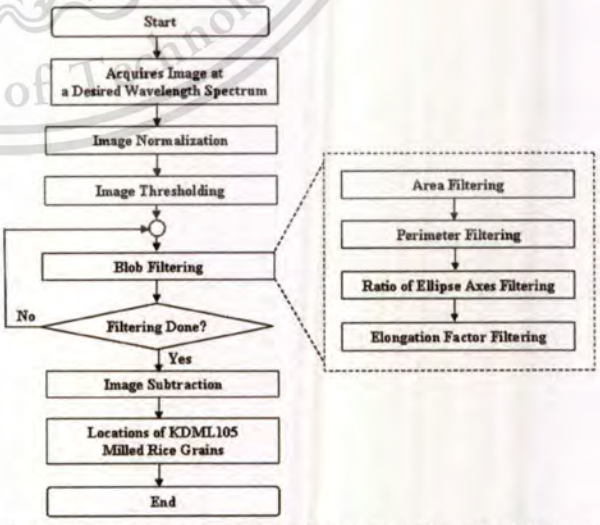

Fig. 2. Flowchart for analysis of the selected spectral image in order to identify KDML105 milled rice grains.

This material is reserved for educational use only, not allowed for commercial use.
Forbidden to modify the content, and cite the document when use.

respectively. Here, a and b are a semimajor and a semiminor axis of the ellipse, respectively. In this case, the interesting areas, whose shape falls within the desired range, will be kept. Similarly, we focus our interest in the image area inside the normalized image whose perimeter stays within the appropriate range.

Then, the other blob filtering processes via analysis of the ratio of equivalent ellipse axes (RA) and the elongation factor (EF) are applied in order to delicately eliminate the remaining unwanted pixels. RA can be simply written as

$$\mathrm{RA} = \frac{a}{b}. \tag{4}$$

The EF of each milled rice grain can be calculated as follows [29].

$$\mathrm{EF} = \frac{\mathrm{FD}_{\max}}{\overline{\mathrm{PI}}}, \tag{5}$$

where $\mathrm{FD}_{\max}$, the maximum Feret diameter, is the maximum distance between two tangents on opposite side of the interesting image area and $\overline{\mathrm{PI}}$ is the mean perpendicular intercept to the $\mathrm{FD}_{\max}$. For each milled rice grain inside the normalized spectral image, it will be kept in the image if its RA and EF values are in the desired ranges.

To identify the location of KDML105 milled rice grains, the thresholded spectral image is fed through the above set of blob filtering processes twice. Under the first set of our image filtering process, all KDML105 milled rice grains are kept in the image, while as many milled rice grains from the remaining rice breeds are filtered out as possible. On the contrary, our second image filtering process considers the thresholded spectral image and tries to eliminate all KDML105 milled rice grains without affecting milled rice grains from other rice breeds. After that, one filtered image is subtracted by another and the remaining image areas correspond to the locations of KDML105 milled rice grains.

3. Our Experimental Demonstration

A. Experimental Setup

Our fluorescent imaging spectrometer is shown in Fig. 3. Instead of mechanically changing the optical filter from the 545 to 575 nm wavelength during our demonstration, our wavelength selection scheme is based on the use of a liquid crystal tunable filter (LCTF) (VariSpec Model VIS-7-HC-20). It is electrically controlled to let one desired wavelength in the 400 to 720 nm wavelength range pass through with a full width at half-maximum (FWHM) transmission band of 7 nm at a speed of 6 nm/s. The optical transmission of the LCTF depends on the wavelength for which the lowest transmission is on the left side of the spectrum and the highest transmission is on the right edge of the spectrum. The

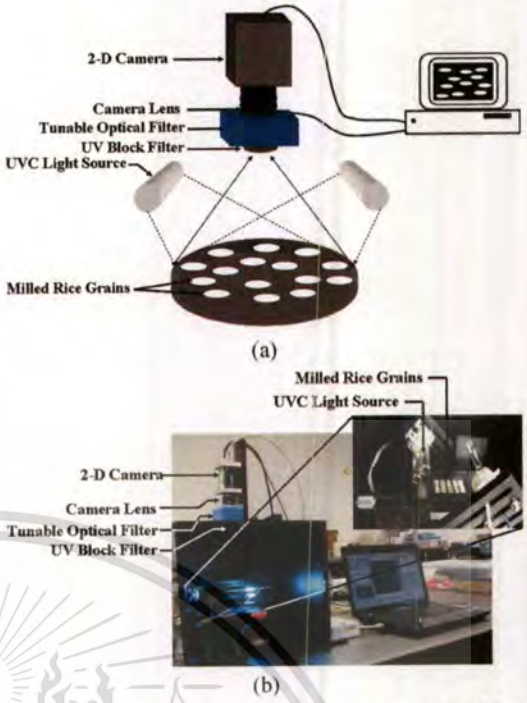

Fig. 3. (Color online) Our experimental setup for KDML105 milled rice breed identification: (a) diagram and (b) perspective view.

LCTF active area is 20 mm in diameter. It is interfaced to the computer via a universal serial bus. We also place a UV block filter in front of the LCTF in order to prevent the UVC reflection from damaging the LCTF and the 2-D digital camera. The measured distance between the object plane and the UV block filter is 195 mm. Our imaging device is an 8 bit complementary metal-oxide-semiconductor-based digital camera (Basler Model SCA750-60GC). Its resolution is 752(H) pixels × 480(V) pixels with pixel dimensions of 6.0 μm × 6.0 μm, and its specified image capturing speed is 60 frames/s.

Our UVC light source is a 5 W mercury lamp in a tubular style package in which the ozone-forming radiation at the 185 nm wavelength is filtered out. On each side of the whole milled rice grains, two UVC lamps are positioned in such a way that UVC light shines uniformly in an area 50 mm in diameter. With the use of a 50 mm × 50 mm white target from Labsphere, measured variation coefficients of the fluorescent intensity at the 545 and 575 nm wavelengths are 7.3% and 6.9%, respectively.

B. Rice Varieties under Test

Our milled rice grains are from eight different Thai rice breeds as shown in Fig. 4. The PTT1 milled rice has an equivalent amount of amylose content to that of the KDML105 milled rice. These two rice varieties are classified as having a low amylose content. The CNT1 milled rice has 27%–30% amylose content, so it is classified as a high amylose content variety. An additional low amylose content breed RD15 and high

This material is reserved for educational use only, not allowed for commercial use.
Forbidden to modify the content, and cite the document when use.

Fig. 4. (Color online) Close-up view of Thai milled rice grains (a) CNT1, (b) HPSL, (c) HSPR, (d) KDML105, (e) PTT1, (f) RD6, (g) RD15, and (h) RD23.

amylose content rice varieties such as HPSR, HPSL, and RD23 are included. Thai sticky rice (RD6), for which its amylose content is very low (0%–2%), is also included in our study.

4. Results and Discussions

A. Fluorescent Signals

For each milled rice breed, we randomly select five milled rice grains. Forty milled rice grains are placed on a specific location in a black sticky plate to prevent grains from touching one another. We prepare three black sticky plates. The first two plates (i.e., Set A and Set B) contain 40 milled rice grains arranged according to Fig. 5(a), while milled rice grains on the last plate (i.e., Set C) are positioned corresponding to their breeds as shown in Fig. 5(b). Each set is loaded and unloaded to our experimental setup shown in Fig. 3 one at a time. Each milled rice grain extends approximately 10 pixels × 32 pixels in the spectral image. Under the UVC illumination, we observe three main fluorescent spectral bands, including the 430–448 nm, 540–555 nm, and 570–585 nm wavelengths [see Fig. 6(a)]. As the last two fluorescent wavelength bands have the strongest spectral signals, we focus on these two fluorescent bands and show how effective a strong fluorescent signal at the 545 and 575 nm wavelengths can be used for distinguishing our desired KDML105 milled rice grains from ones from the other remaining seven rice breeds. It can also be seen from Figs. 6(a) and 6(b) that RD6 provides the strongest fluorescent signal as it has the lowest amylose content level. In addition, measured variation coefficients in optical intensity of the normalized spectral image at the center of each rice grain vary between 4.9% and 8.7% and between 3.1% and 7.1% for the 545 and 575 nm fluorescent radiations, respectively. RD6 also has the lowest intensity fluctuation levels of 4.9% and 3.1% at 545 and 575 nm fluorescent radiations, respectively. As a result, locations of all RD6 milled rice grains can be immediately distinguished from the remaining milled rice varieties.

CNT1	HPSL	HSPR	KDML105	PTT1
HPSL	HSPR	KDML105	PTT1	RD6
HSPR	KDML105	PTT1	RD6	RD15
KDML105	PTT1	RD6	RD15	RD23
PTT1	RD6	RD15	RD23	CNT1
RD6	RD15	RD23	CNT1	HPSL
RD15	RD23	CNT1	HPSL	HSPR
RD23	CNT1	HPSL	HSPR	KDML105

(a)

KDML105	PTT1	RD6	RD15	RD23
PTT1	RD6	RD15	RD23	CNT1
RD6	RD15	RD23	CNT1	HPSL
RD15	RD23	CNT1	HPSL	HSPR
RD23	CNT1	HPSL	HSPR	KDML105
CNT1	HPSL	HSPR	KDML105	PTT1
HPSL	HSPR	KDML105	PTT1	RD6
HSPR	KDML105	PTT1	RD6	RD15

(b)

Fig. 5. Arrangement of milled rice grains for (a) Sets A and B and (b) Set C.

B. Analysis

In this section, the selected normalized fluorescent image goes through our image thresholding process. The range of image thresholding is set to 57–91 for the normalized spectral images at the 545 nm wavelength. At this step, image pixels whose gray scale values stay within the desired ranges are highlighted as white while the remaining pixels are set to black [see Fig. 7(a)]. As a result, 57.1%, 28.6%, and 40.0% of the unwanted milled rice grains in Sets A, B, and C are eliminated, respectively. After that, the normalized spectral image passes through our first blob filtering process with all needed parameters set according to Table 1 in order to let all KDML105 milled rice grains stay in the image while simultaneously eliminating as many other milled rice breeds as possible. In this way, numbers of unwanted milled rice grains in Set A remain at 31.4%, 25.7%, 17.1%, and 11.4% inside the image, respectively, as shown in Figs. 7(b)–7(e) on the left hand side. Similarly, unwanted milled rice grains in Sets B and C are 14.3% and 37.1% , respectively, left at the end of our first blob filtering process.

The same binary image shown in Fig. 7(a) also passes through our second blob filtering process tabulated in the last column of Table 1 in order to eliminate all KDML105 milled rice grains while keeping as many other rice breeds as possible. In this case, ranges of perimeter, RA, and EF parameters are 14%, 71%, and 79% lower, respectively, compared to those used in our first blob filtering process. All KDML105 milled rice grains are gradually removed from the image when the selected binary image enters into the area filtering process and emerges at the EF filtering process. At this last step of our blob filtering process, one, two, and four grains of unwanted milled rice breeds remain in the images of Sets A [see Fig. 7(e) in the middle), B, and C, respectively. To identify locations of all KDML105 milled rice grains, we subtract Fig. 7(e) on the left hand side with Fig. 7(e) in the middle and the resulting image is

This material is reserved for educational use only, not allowed for commercial use.
Forbidden to modify the content, and cite the document when use.

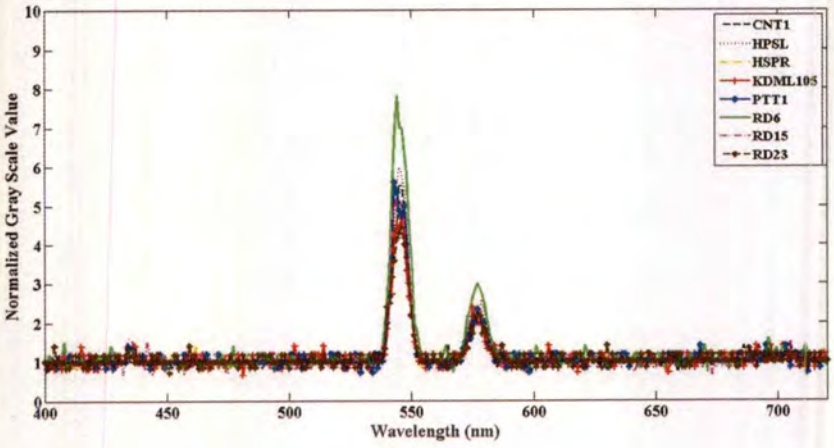

(a)

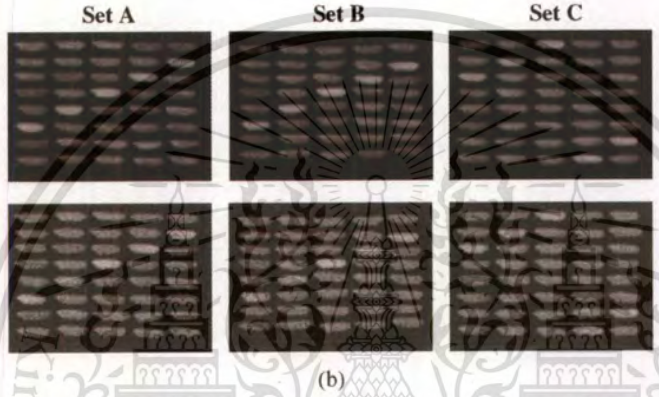

(b)

Fig. 6. (Color online) (a) Normalized fluorescent signal measured at the center of each milled rice grain under UVC illumination. (b) Normalized fluorescent images at 545 (top) and 575 nm (bottom) wavelengths for three arrangements of milled rice grains.

shown in Fig. 7(e) on the right hand side. It can be observed that all KDML105 milled rice grains still appear in the image, implying that we obtain a false rejection rate (FRR) of 0%. In addition, some of the unwanted milled rice grains remain inside the image, indicating a false acceptance rate (FAR) of $100 \times 3/35 = 8.6\%$. For Sets B and C, we achieve 0% FRR for both cases while FARs of $100 \times 3/35 = 8.6\%$ and $100 \times 8/35 = 22.9\%$ are accomplished, respectively. These results indicate an average FAR of 13.4%. Our analytical process takes only 25 ms.

Similarly, for the 575 nm spectral image, because its normalized spectral values are higher compared to those of the 545 nm spectral image [see also Fig. 6(b)], we assign a higher expected range of image thresholding to 90–144, which in turn leads to a binary image shown in Fig. 8(a). In this case, 8.6%, 8.6%, and 5.7% of the unwanted milled rice grains for Sets A, B, and C are eliminated, respectively. After that, the normalized spectral image passes through our first blob filtering process with all needed parameters set according to Table 2 in order to let all KDML105 milled rice grains stay in the image while eliminating as many other milled rice breeds as possible. In this way, numbers of unwanted milled rice grains for Set A are much reduced to 34.3%,

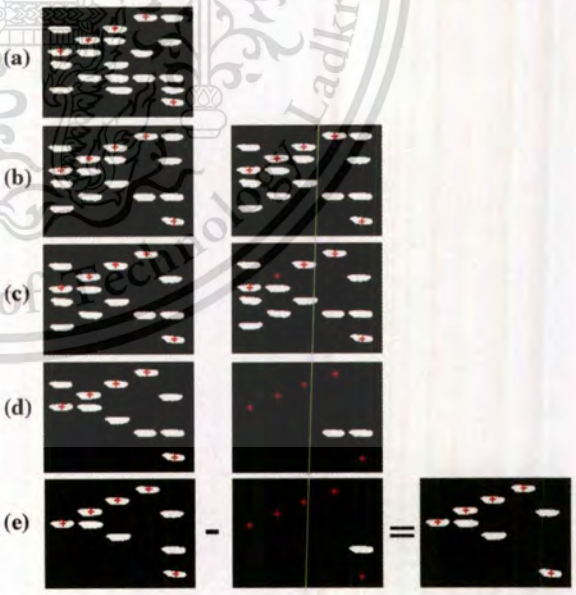

Fig. 7. (Color online) Example of the normalized spectral image at the 545 nm wavelength after it goes through (a) image thresholding, (b) area filtering, (c) perimeter filtering, (d) RA filtering, and (e) EF filtering. Our first and second image filtering processes are applied to images on the left hand side and in the middle, respectively. Grains with red marks correspond to locations of KDML milled rice grains.

This material is reserved for educational use only, not allowed for commercial use.
Forbidden to modify the content, and cite the document when use.

Table 1. Parameters Used During Our Image Filtering Processes for the Selected 545 nm Fluorescent Image

Parameters	First Image Filtering Process		Second Image Filtering Process	
	Lower Value	Upper Value	Lower Value	Upper Value
Area (pixel^2)	240.00	284.00	240.00	284.00
Perimeter (pixels)	69.30	75.90	69.60	75.30
Ratio of Ellipse Axes	2.62	2.99	2.65	2.76
Elongation Factor	3.64	4.11	3.72	3.82

Table 2. Parameters Used During Our Image Filtering Processes for the Selected 575 nm Fluorescent Image

Parameters	First Image Filtering Process		Second Image Filtering Process	
	Lower Value	Upper Value	Lower Value	Upper Value
Area (pixel^2)	251.00	294.00	251.00	279.00
Perimeter (pixels)	73.00	78.90	74.10	77.50
Ratio of Ellipse Axes	2.87	3.37	2.88	3.22

57.1%, 65.7%, and 68.6%, respectively, as shown in Figs. 8(b)–8(e) on the left hand side. Similarly, unwanted milled rice grains in Sets B and C remain at 65.7% and 65.7%, respectively, at the end of our first blob filtering process.

The same binary image shown in Fig. 8(a) also passes through our second blob filtering process tabulated in the last column of Table 2 in order to eliminate all KDML105 milled rice grains and simultaneously keep as many milled rice grains of the remaining rice breeds as possible. In this case, ranges of area, perimeter, RA, and EF parameters are 35%, 43%, 32%, and 33% lower, respectively, compared to those used in our first blob filtering process. All KDML105 milled rice grains are gradually removed from the image when it is entered into the area filtering process and emerges at the EF filtering process. At this last step of our blob filtering process, eight, three, and eight grains of unwanted milled rice breeds remain in the images of Sets A [see Fig. 8(e) in the middle), B, and C, respectively. To identify locations of all KDML105 milled rice grains, we subtract the image on the left hand side of Fig. 8(e) by the image in the middle and the resulting image is shown on the right hand side. It can be observed that all KDML105 milled rice grains still appear in the image, pointing out an FRR of 0%. Nevertheless, some of unwanted milled rice grains remain inside the image, indicating an FAR of $100 \times 3/35 = 8.6\%$. For Sets B and C, we also achieve 0% FRR for both cases, while FARs of $100 \times 9/35 = 25.7\%$ and $100 \times 4/35 = 11.4\%$ are accomplished, respectively. This result indicates an average FAR of 15.2%.

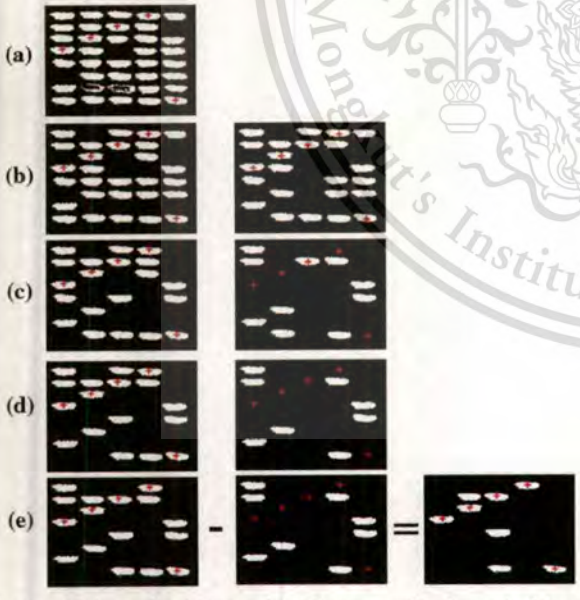

Fig. 8. (Color online) Example of the normalized spectral image at the 575 nm wavelength after it goes through (a) image thresholding, (b) area filtering, (c) perimeter filtering, (d) RA filtering, and (e) EF filtering. Our first and second image filtering processes are applied to images on the left hand side and in the middle, respectively. Grains with red marks correspond to locations of KDML milled rice grains.

Another important issue is the tolerance of our identification method to the change in each parameter used during our blob filtering processes. By simultaneously adjusting the lower and upper levels of each parameter within ±0.10 steps, we find that an additional FAR of 5.7–37.1% is obtained, while the change in FRR can be up to 60% for all three sets of arrangement. This low system tolerance can be improved by adjusting the imaging system in such a way that each milled rice grain can be seen clearer. Increasing the intensity of UVC light sources and making the UVC illumination more uniform across the object plane will also help increase the signal-to-noise ratio and reduce the intensity fluctuation across the area.

5. Conclusion

A nondestructive single-wavelength spectral-imaging-based Thai jasmine rice breed identification is demonstrated. Our key idea is based on the use of high energy UVC light to optically induce unknown milled rice grains to radiate fluorescent radiation in the 540–555 and 570–585 nm wavelength bands. In particular, we exploit a fluorescent image at either the 545 or 575 nm wavelength and then apply simple image processing processes in order to separate KDML105 milled rice grains from the remaining Thai rice breeds. In our analysis, the selected fluorescent image goes through a desired thresholding once. The thresholded image then passes one at a time through two sets of blob filtering processes. At the end, by subtracting two selected binary images, KDML105 milled rice grains can be identified with the best FAR of 8.6%. A measured identification time is 25 ms, indicating that real-time

This material is reserved for educational use only, not allowed for commercial use.
Forbidden to modify the content, and cite the document when use.

KDML105 milled rice breed identification can be realized. As our current demonstration is very sensitive to the change in image processing parameters, several issues such as the uniformity of the exciting light, imaging system, and image processing processes need to be improved in the future.

Authors gratefully thank the Rice Research Institute at the Department of Rice, Ministry of Agriculture and Cooperatives of Thailand for supplying rice samples. K. Suwansukho would also like to thank the Thailand Graduate Institute of Science and Technology for scholarship support (grant TGIST 01–51-071)

References

1. Office of Agriculture Economics, Ministry of Agriculture and Cooperatives, Thai Government, http://www.oae.go.th/oae_report/export_import/export_result.php.
2. A. J. Cullen, R. C. Hoseney, and J. M. Faubion, "Identification of wheat cultivars by visual imaging," US patent 5321764 (14 June 1994).
3. Y.-N. Wan, "Grain sorting method and a device thereof," US patent 5973286 (26 October 1999).
4. E. G. Kokko and B. D. Hill, "Method and apparatus for identifying and quantifying characteristics of seeds and other small objects," US patent 7218775 (15 May 2007).
5. Y. Liu, A. Ouyang, J. Wu, and Y. Ying, "An automatic method for identifying different variety of rice seeds using machine vision technology," Proc. SPIE **5996**, pp. 59961H (2005).
6. N. Sakai, S. Yonekawa, and A. Matsuzaki, "Two-dimensional image analysis of the shape of rice and its application to separating varieties," J. Food Eng. **27**, 397–407 (1996).
7. S. P. Shouche, R. Rastogi, S. G. Bhagwat, and J. K. Sainis, "Shape analysis of grains of Indian wheat varieties," Comput. Electron. Agric. **33**, 55–76 (2001).
8. R. R. Little, G. B. Hilder, and E. H. Dawson, "Differential effect of dilute alkali on 25 varieties of milled white rice," Cereal Chem. **35**, 111–126 (1958).
9. V. R. William, W. T. Wu, H. Y. Tsai, and H. G. Bates, "Varietal differences in amylose content of rice starch," J. Agric. Food Chem. **6**, 47–48 (1958).
10. B. O. Juliano, "A simplified assay for milled-rice amylose," Cereal Sci. Today **16**, 334–340 (1971).
11. "The Ministry of Commerce notification on rules and methodologies of commodities and Thai Hom Mali rice standards inspection B.E. 2545 (2002)," Government Gazette 119, Special Section 21D (7 March 2002).
12. A. Vanavichit, S. Tragoonrung, and T. Toojinda, "Biotechnology and rice varieties improvement," in *Science and Technology with Thai Rice*, Thailand's National Science and Technology Development Agency (Academic, 2003), pp. 79–121.
13. K. Ohtsubo, S. Nakamura, T. Miyamura, S. Kumo, and I. Kato, "Method of detecting the presence of absence of mixed varieties in grains, and identifying the mixed varieties," US patent application US2006/0183138 (17 August 2006).
14. K. Suwansukho, S. Sumriddetchkajorn, and P. Buranasiri, "Combination of simple chemical and spectroscopic methods for the identification of Thai Hom Mali rice," Proc. SPIE **7315**, 73150W (2009).
15. B. Borne, B. Mertens, M. Thomson, and T. Fearn, "Authentication of Basmati rice using near infrared spectroscopy," J. Near Infrared Spectrosc. **1**, 77–83 (1993).
16. S. Sumriddetchkajorn, K. Suwansukho, and P. Buranasiri, "Identification of Thai Hom Mali rice using a refractometer," Proc. SPIE **7315**, 73150F (2009).
17. M. S. Kim, A. M. Lefcourt, Y.-R. Chen, and Y. Tao, "Automated detection of fecal contamination of apples based on multispectral fluorescence image fusion," J. Food Eng. **71**, 85–91 (2005).
18. M. S. Kim, A. M. Lefcourt, and Y.-R. Chen, "Multispectral laser-induced fluorescence imaging system for large biological samples," Appl. Opt. **42**, 3927–3934 (2003).
19. M. S. Kim, J. E. McMurtrey, C. L. Mulchi, C. S. T. Daughtry, E. W. Chappelle, and Y.-R. Chen, "Steady-state multispectral fluorescence imaging system for plant leaves," Appl. Opt. **40**, 157–166 (2001).
20. H. K. Lichtenthaler and J. A. Mieché, "Fluorescence image as a diagnostic tool for plant stress," Trends Plant Sci. **2**, 316–320 (1997).
21. S. Moser, T. Müller, M. O. Ebert, S. Jockusch, N. J. Turro, and B. Kräutler, "Blue luminescence of ripening bananas," Angew. Chem., Int. Ed. **47**, 8954–8957 (2008).
22. T. Katsumata, T. Suzuki, H. Aizama, E. Matashige, S. Komuro, and T. Morikawa, "Nondestructive evaluation of rice using two-dimensional imaging of photoluminescence," Rev. Sci. Instrum. **76**, 073702 (2005).
23. T. Katsumata, T. Suzuki, H. Aizawa, and E. Matashige, "Photoluminescence evaluation of cereals for a quality control application," J. Food Eng. **78**, 588–590 (2007).
24. S. Sumriddetchkajorn, K. Suwansukho, and P. Buranasiri, "Two-wavelength spectral image-based Thai rice breed identification," Proc. SPIE **7715**, 77150I (2010).
25. T. Koutchma, "Advances in ultraviolet light technology for non-thermal processing of liquid foods," Food Bioprocess Technol. **2**, 138–155 (2009).
26. H. Wondraczek, A. Kotiaho, P. Fardim, and T. Heinze, "Photoactive polysaccharides," Carbohydr. Polym. **83**, 1048–1061 (2011).
27. H. Karatani, M. Kojima, H. Minakuchi, N. Soga, and T. Shizuki, "Development and characterization of anodically initiated luminescent detection for alcohols and carbohydrates," Anal. Chim. Acta **337**, 207–215 (1997).
28. P. J. Jenkins and A. M. Donald, "The influence of amylose on starch granule structure," Int. J. Biol. Macromol. **17**, 315–321 (1995).
29. L. F. Costa and R. M. Cesar, "Shape classification and analysis: theory and practice," in *Image Processing Series*, P. A. Laplants, ed. (Academic, 2009), pp. 411–414.

This material is reserved for educational use only, not allowed for commercial use.

Forbidden to modify the content, and cite the document when use.

Two-Wavelength Spectral Imaging-based Thai Rice Breed Identification

Sarun Sumriddetchkajorn[1*], Kajpanya Suwansukho[2], and Prathan Buranasiri[2]
[1]Photonics Technology Laboratory
National Electronics and Computer Technology Center
National Science and Technology Development Agency
Ministry of Science and Technology
112 Thailand Science Park, Phahonyothin Rd, Klong 1, Klong Luang
Pathumthani 12120, Thailand, Tel: +66-2564-6900 ext. 2102, Fax: +66-2564-6774
E-mail: sarun.sumriddetchkajorn@nectec.or.th

[2]Applied Physics Department, Faculty of Science
King Mongkut's Institute of Technology Ladkrabang, Bangkok, Thailand

ABSTRACT

This paper combines multispectral imaging and simple image processing techniques for the non-destructive identification of Thai rice breeds. Especially, we exploit only two fluorescent wavelengths in a 500-580 nm wavelength band and utilize simple image thresholding, blob filtering, and blob analysis techniques in order to identify 8 different Thai rice breeds. Other key features include no waste produced and fast identification time. In our experimental study, UVC light is used as our exciting light, a liquid crystal tunable optical filter is used for our wavelength selection, and a camera with 644×488 active pixels is used to capture desired wavelength images. Milled rice grains from 8 different Thai rice breeds having similar size and shape are tested. There is also one glutinous rice breed in our experiment. Our experimental result shows that by suitably applying image thresholding, blob filtering, and blob analysis to fluorescent images, all Thai rice breeds can be effectively identified.

Keywords: Rice, Multispectral imaging, Hyperspectral imaging, Fluorescent imaging, Image processing, Nondestructive testing, Agri-photonics.

1. INTRODUCTION

It is known that Thai jasmine rice, also called Khao Dawk Mali 105 (KDML105), is one of the best rice varieties in the world. It was listed at the 7th export of Thailand in 2007 with its value of 1.73 billion US dollars [1]. As a result, there is an increase in mixing KDML105 milled rice with other Thai rice varieties especially Pathumthani1 (PTT1) and Chainat1 (CNT1) rice varieties as they have similar shape, weight/seed, and color to the KDML105 milled rice. This implies that a simple machine vision technique operating in the visible spectrum [2-5] cannot be used to separate these rice varieties from each other. Today widely used rice breed identification processes rely on destructive methods through slow chemical analysis, physical analysis, and DNA analysis [6-11]. Optical spectroscopy in the visible [12] and near infrared spectra [13] also showed an identification rate of 80% with a faster analytical time of 15 minutes. Faster 7 second identification can be obtained by using a refractometer [14].

One of the promisingly nondestructive approaches is the fluorescent imaging. Previously, all milled rice grains were illuminated with 365 nm wavelength (i.e., UVA) light and its fluorescent radiation at 460 nm was investigated through histogram analysis [15-16]. However, this single wavelength concept is suitable only for the identification of rice breeds that have different amount of amylose content. Instead of investigating at only one wavelength, several wavelength bands of fluorescent radiation under the UVA light have been studied for contamination detection in fruits, meats, and plant leaves [17-19]. With this concept, this paper proposes a non-destructive multispectral-imaging based method for identifying rice breeds. Especially, we utilize only two wavelengths of the fluorescent radiation under a higher energy UVC light source that can induce more fluorescent wavelength bands.

Biophotonics: Photonic Solutions for Better Health Care II, edited by Jürgen Popp, Wolfgang Drexler, Valery V. Tuchin, Dennis L. Matthews, Proc. of SPIE Vol. 7715, 77150I
© 2010 SPIE · CCC code: 1605-7422/10/$18 · doi: 10.1117/12.853507

This material is reserved for personal use only, not allowed for commercial use.
Forbidden to modify the contents and distribute. Cite when use.
Downloaded from SPIE Digital Library on 02 Dec 2011 to 203.185.129.241. Terms of Use: http://spiedl.org/terms

2. OUR PROPOSED TWO-WAVELENGTH SPECTRAL IMAGING-BASED RICE BREED IDENTIFIER

2.1 Architecture of the system

Our proposed two-wavelength spectral imaging-based rice breed identification system is shown in Fig.1. The main components are an exciting high energy light source (e.g., UVC at 265 nm wavelength), a tunable optical filter, an imaging lens system, a two-dimensional (2-D) digital camera, and an electronic controlling and processing unit. There is a region in which we can scatter unknown breeds of milled rice grains for analysis. This region is also in the field of view of the imaging lens system. The tunable optical filter is working in the visible spectrum and it can be based on several off-the-shelf technologies with and without moving part such as optical interference filters, acousto-optic tunable filters, a combination of two prisms and a grating, tunable Bragg grating, and liquid crystal retarders [20].

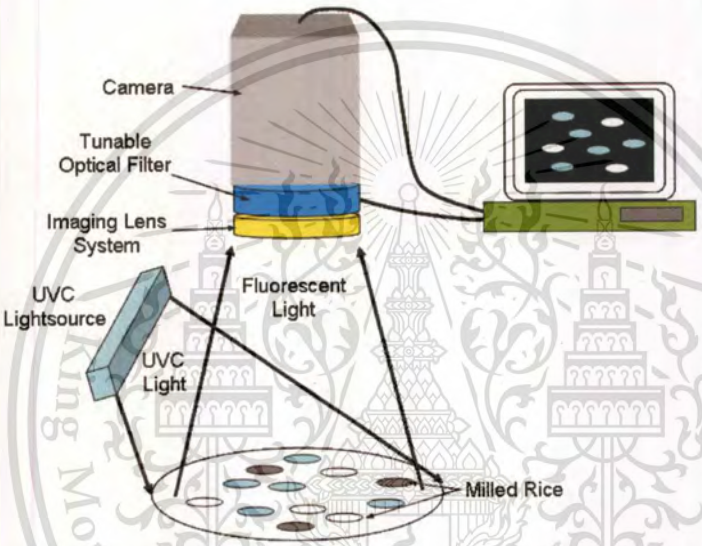

Fig. 1 Structure of our proposed multispectral imaging-based rice breed identification system.

When the UVC light is shining on all milled rice grains, the corresponding fluorescent radiation is emitted from all milled rice grains and passes through the imaging lens system. The tunable optical filter is electrically controlled in such a way that only the desired wavelength spectrum bands can get through to the 2-D digital camera. Based on our current study [21], we find two very strong fluorescent spectra in 539-553 nm and 570-585 nm bands. Especially, we choose to study fluorescent spectral signals at 540 nm and 575 nm in which their associated fluorescent signals start to appear. In addition, each rice breed gives out different amount of fluorescent radiation. This is probably due to the difference in the amount of amylose content and the level of glutinousness. Therefore, we focus on these two fluorescent wavelengths and their corresponding spectral images are transmitted to our processing unit. Note that unlike the single wavelength analysis used in refs. [15-16], our analysis of two-wavelength spectral offers more information that is needed for identifying rice breeds having the same amount of amylose content. In addition, because UVC light is known as the germicidal light, the use of UVC light during our rice breed identification provides one more advantage in that it can kill unwanted germs attached to milled rice grains.

2.2 Procedures of analysis

Once we have two spectral images associated with 540 nm and 575 nm fluorescent spectral from the milled rice grains, we follow the procedures shown in Fig.2. In this case, the maximum number of wavelengths (N) is equal to 2. Because each rice breed emits different amount of fluorescent radiation, each spectral image goes through two-level image

This material is reserved for educational use only, not allowed for commercial use.
Forbidden to modify this material without permission. Please cite when use.
Downloaded from SPIE Digital Library on 02 Dec 2011 to 203.185.129.241. Terms of Use: http://spiedl.org/terms

thresholding several times. In each time, the blob filtering is also applied in order to eliminate unwanted image areas. The total number of the resulting images is equal to M and these M images are binary.

After we have M binary images, we do image subtraction from two selected binary images. In this way, the remaining image areas correspond to the rice breeds that we are looking for. The coordinate of the remaining image areas also tells us their locations. In addition, these image areas can be used for the estimation of the number of milled rice grains corresponding to their rice breeds.

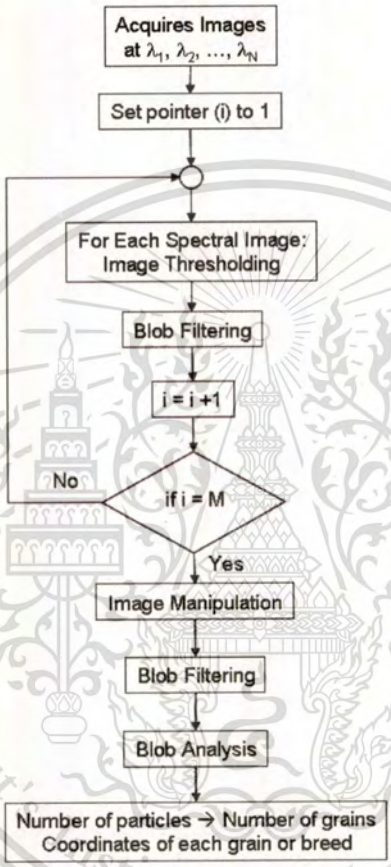

Fig. 2 Flowchart for analysis of spectral images in order to nondestructively identify breeds of all milled rice grains in real time.

3. OUR EXPERIMENTAL DEMONSTRATION

3.1 Experimental setup

Our imaging spectrometer is shown in Fig.3 and its wavelength selection scheme is based on the use of a liquid crystal tunable filter (LCTF) [20]. The LCTF is from VariSpec and its model is VIS-7-HC-20. It can be electrically controlled to let the visible light from 400 to 720 nm pass through with an FWHM of 7 nm at a speed of 6 nm/s. The optical transmission depends on the wavelength which the lowest transmission is on the left wing of the spectrum and the highest transmission is on the right edge of the spectrum. The active area is 20 mm in diameter. It is interfaced to the computer via a universal serial bus (USB). For our 2-D image device, we choose a complementary metal oxide semiconductor-based digital camera that provides an 8-bit digital image. It sensing area has 644 (H) × 488 (V) pixels with a pixel dimensions of 8.4 μm × 8.4 μm. This digital camera communicates with a computer through a USB-based frame grabber. The imaging lens system has a specified focal distance of 3.7 mm.

This material is reserved for educational use only, not allowed for commercial use.
Forbidden to modify the content and cite the document when use.
Downloaded from SPIE Digital Library on 02 Dec 2011 to 203.185.129.241. Terms of Use: http://spiedl.org/terms

Our UVC light source is an 18-W mercury lamp in a TUV style package from Philips. It emits only one peak wavelength radiation at 253.7 nm. It is settled at the left hand side of the milled rice grains at a distance of 116 mm and it is above milled rice grains at a distance of 65 mm. In this way, UVC light shines uniformly in the area of 40 mm in diameter. We also place a UV block filter in front of the LCTF to allow only the measured visible wavelength spectrum starting from 410 nm pass through the imaging lens system and fall on the 2-D digital camera.

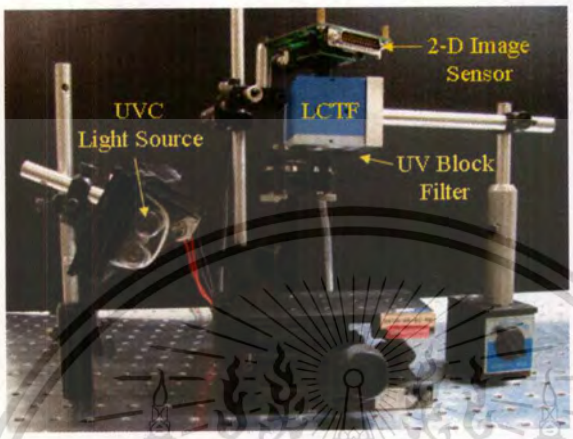

Fig. 3 Our experimental setup for milled rice breed identification.

Our milled rice grains are from 8 different Thai rice breeds as shown in Fig.4. The PTT1 rice has equivalent amount of amylose content to that of the KDML105 rice. These two rice varieties are classified as low amylose content rices. The CNT1 rice has its amylose content in 27%-30% and it is classified as one of high amylose content varieties. Other milled rice varieties with specified as low amylose content such as Ko Kor 15 (RD15) and with specified as high amylose content such as Hom Supanburi (HPSR), Hom Pitsanulok (HPSL), and Ko Kor 23 (RD23) are included. We also bring in to our study another Thai rice variety with very low amylose content of 0%-2%. It is Thai sticky rice (RD6). For each milled rice breed, we randomly select 4 milled rice grains and place them on a specific location shown in Fig.5(a). There are 3 main fluorescent spectral regions in 432-438 nm, 539-553 nm, and 570-585 nm (see Fig.5(b)). All milled rice grains emit fluorescent radiation for which the RD6 shows the strongest fluorescent signal followed with KDML105 milled rice. As the last two fluorescent wavelength bands have the strongest spectral signals for KDML105 milled rice, this paper analyzes spectral images from these two wavelengths. Especially, we choose fluorescent spectral signals at 540 nm and 575 nm (see Fig.6). In this case, a measured LCTF switching time between these two selected wavelengths is 45.1 ms. Because the fluorescent signal at 575 nm wavelength is also stronger than fluorescent signals at 540 nm wavelength, the spectral image at 575 nm wavelength is brighter than the spectral image at 540 nm wavelength.

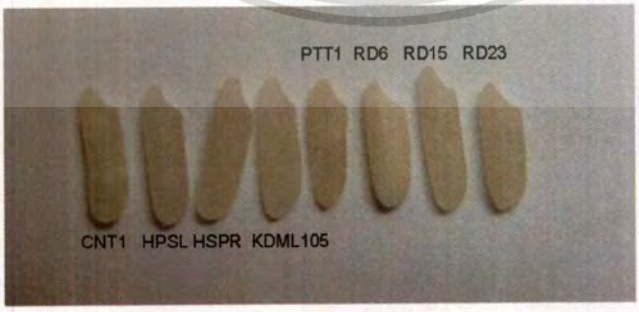

Fig. 4 Eight breeds of Thai milled rice grains.

This material is reserved for educational use only, not allowed for commercial use.
Forbidden to modify the content and to remove this notice when use.
Downloaded from SPIE Digital Library on 02 Dec 2011 to 203.185.129.241. Terms of Use: http://spiedl.org/terms

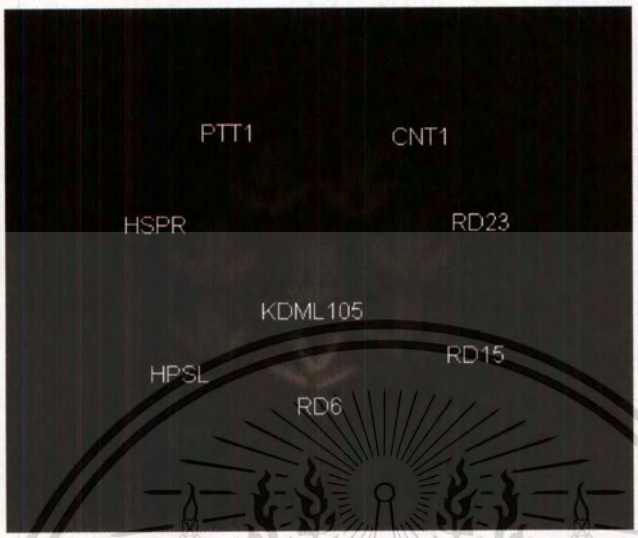

(a)

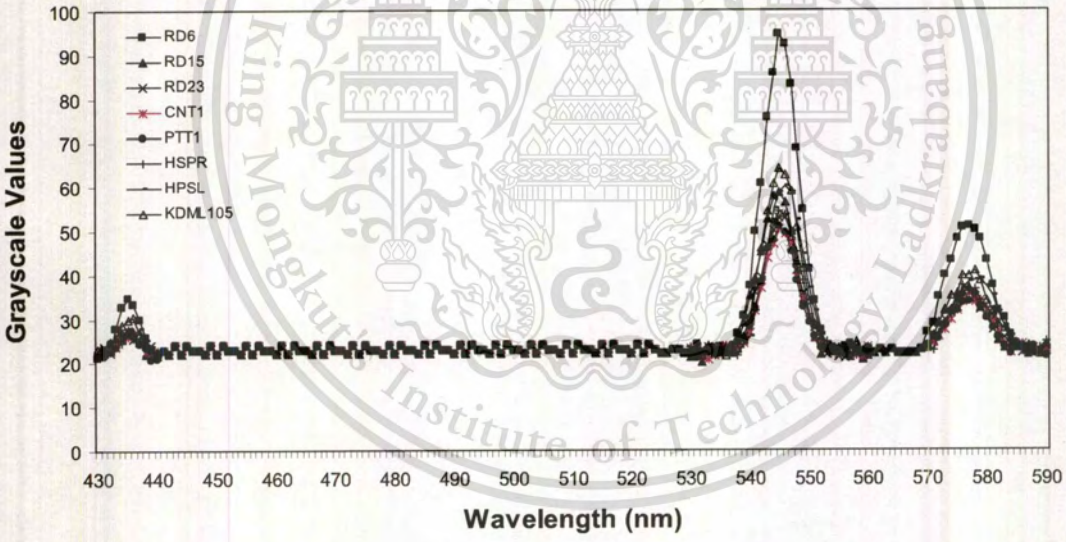

(b)

Fig. 5 (a) Fluorescent image emitted from all milled rice grains under UVC illumination and (b) fluorescent signals.

This material is reserved for educational use only, not allowed for commercial use.
Forbidden to modify the content and cite the document when use.
Downloaded from SPIE Digital Library on 02 Dec 2011 to 203.185.129.241. Terms of Use: http://spiedl.org/terms

540 nm 575 nm

Fig. 6 Fluorescent images of milled rice grains from 8 different rice breeds at 540 nm and 575 nm wavelengths.

3.2 Analysis

For the fluorescent image at 540 nm wavelength, we first set the image threshold interval at 30-150. In this way, pixels that have their grayscale values less than 30 or more than 150 are highlighted as black while the remaining pixels are set to red. By selecting image areas that contain the number of pixels in the range of 660 and 4000 pixels, we obtain the image areas where milled rice grains for RD6 and RD15 appear as shown in Fig.7(a). Lowering the lower limits of the image thresholding interval to 29 and of the blob filtering to 400 makes the two image areas associated with KDML105 and RD23 milled rice grains appear as shown in Fig.7(b).

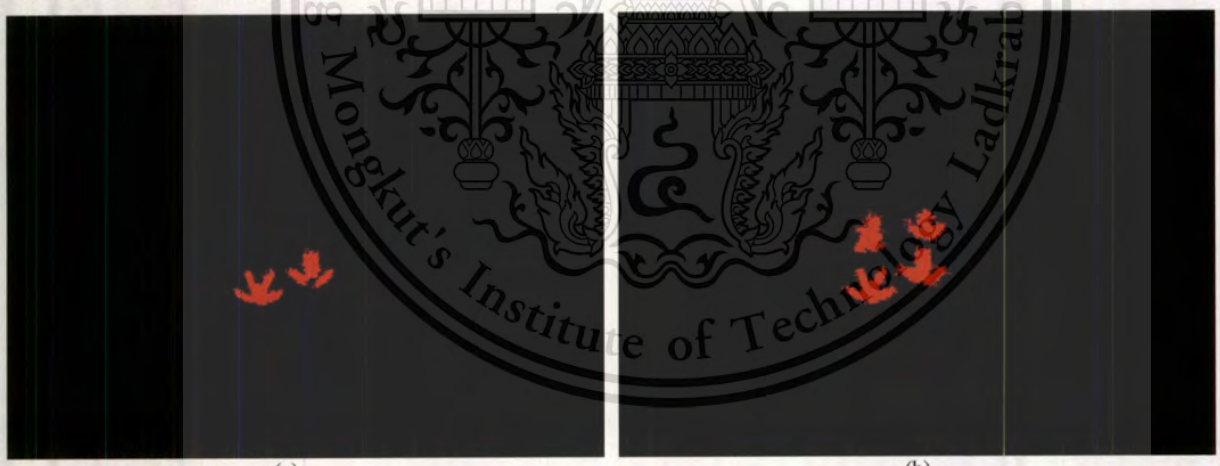

(a) (b)

Fig. 7 Results of image manipulation through image thresholding and blob filtering processes for the fluorescent image at 540 nm. (a) Thresholding interval (T) of 30-150 and blob filtering (B) between 660 and 4000 pixels. (b) T = 29-150, B = 400-4000 pixels.

Similarly, for the fluorescent image at 575 nm wavelength, we first set the image threshold interval at 39-150. In addition, by keeping image areas that contain 30-4000 pixels, we can immediately locate the areas that have only the RD6 milled rice grains as shown in Fig.8(a). Lowering the lower limit of the image threshold level to 33 and increasing the lower limit of the blob filtering to 455 pixels let the KDML105 milled rice grains appear along side with the RD6 milled rice grains as shown in Fig.8(b). Three additional image areas that contain RD23, RD15, and HSPR milled rice grains are highlighted by setting the image threshold level at 30-150 and the blob filtering between 900 and 4000 pixels as shown in Fig.8(c).

This material is reserved for personal study, not allowed for commercial use.
Forbidden to modify the content and cite the document when use.
Downloaded from SPIE Digital Library on 02 Dec 2011 to 203.185.129.241. Terms of Use: http://spiedl.org/terms

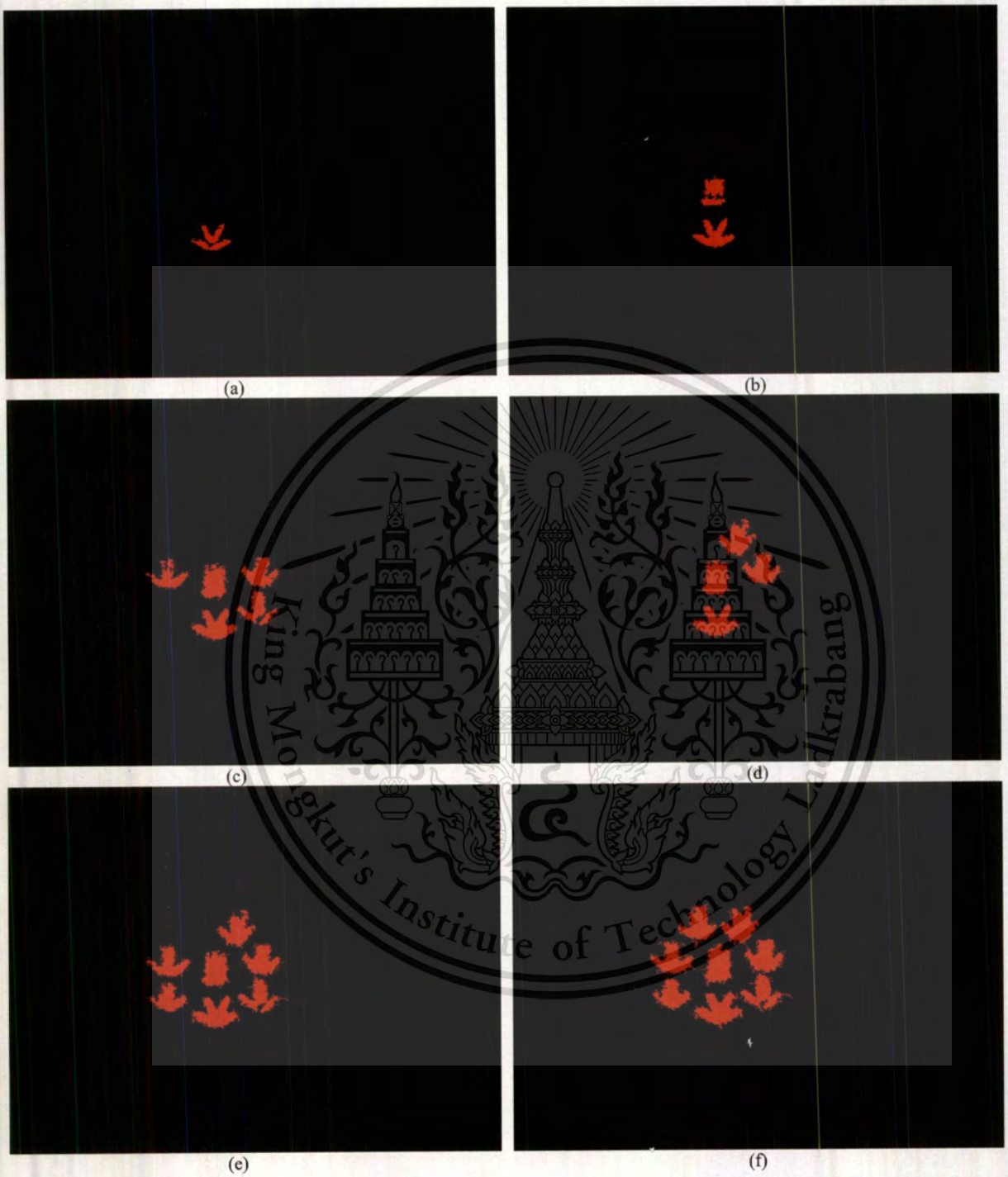

Fig. 8 Results of image manipulation through image thresholding and blob filtering processes for the fluorescent image at 575 nm with different thresholding (T) and blob filtering (B) levels. (a) T = 39-150, B = 30-4000 pixels, (b) T = 33-150, B = 455-4000 pixels, (c) T = 30-150, B = 900-4000 pixels, (d) T = 29-150, B = 1200-4000 pixels, (e) T = 28-150, B = 550-4000 pixels, and (f) T = 27-150, B = 400-4000 pixels.

This material is reserved for personal use only, not allowed for commercial use.
Forbidden to modify the content and cite the document when use.
Downloaded from SPIE Digital Library on 02 Dec 2011 to 203.185.129.241. Terms of Use: http://spiedl.org/terms

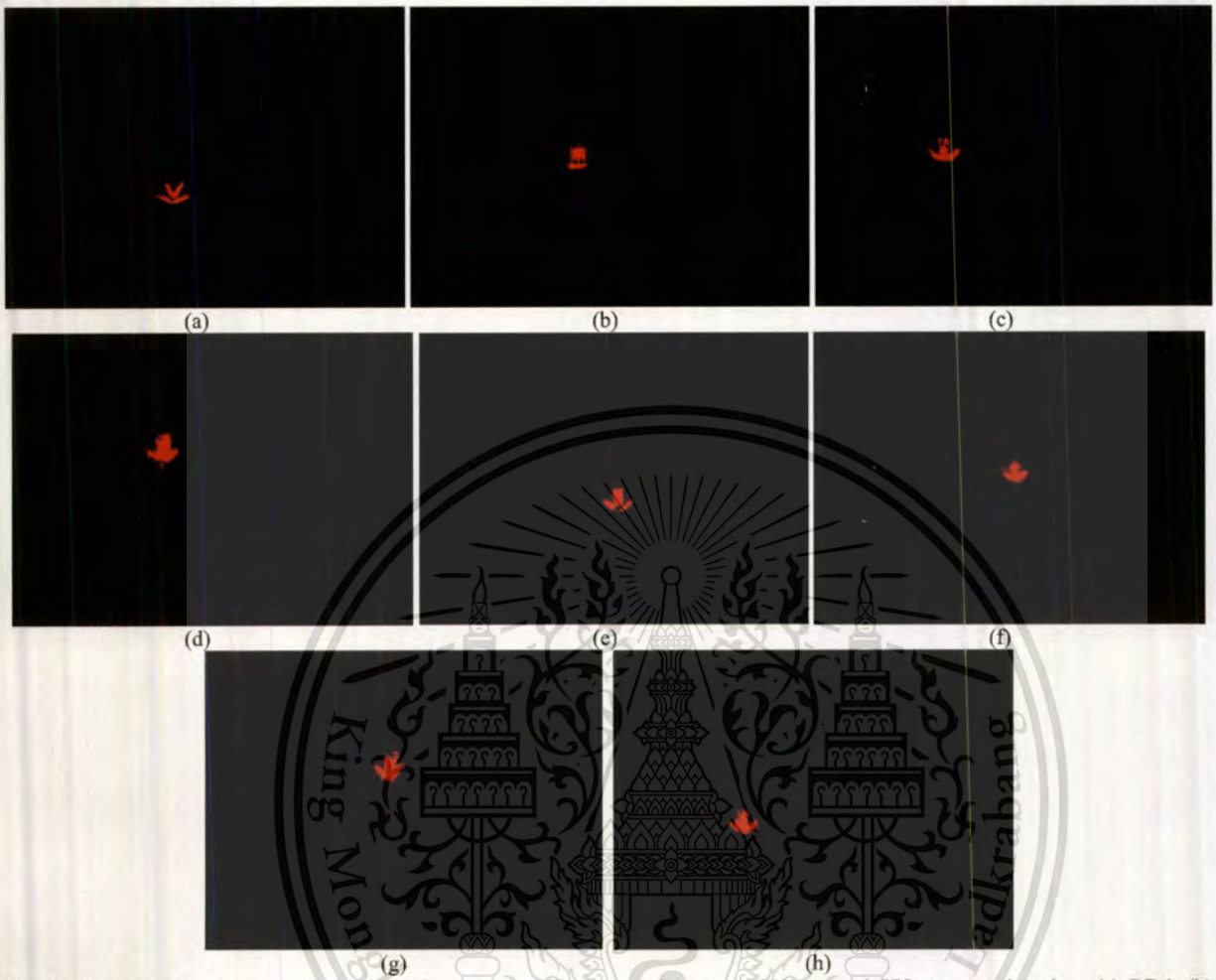

Fig. 9 All milled rice breeds are identified from the two fluorescent images at 540 nm and 575 nm wavelengths. (a) RD6, (b) KDML105, (c) HSPR, (d) PTT1, (e) RD15, (f) RD23, (g) CNT1, and (h) HPSL.

With the image threshold level of 29-150 and the blob filtering set at 1200-4000 pixels, HSPR and RD15 milled rice grains disappear while CNT1 milled rice grains show up (see Fig.8(d)). Now, all except PTT1 milled rice grains are shown up when we set the image threshold level to 28-150 and the blob filtering to 550-4000 pixels. In addition, all images of 8 different rice breeds appear when the image thresholding level and the blob filtering are set to 27-150 and 400-4000 pixels, respectively.

To identify locations of all 8 different rice breeds, simple image subtraction and blob filtering are employed as follows. Note that from Fig.8(a), RD6 milled rice grains are already identified. By subtracting Fig.8(b) with Fig.8(a) and keeping images that contain pixels between 50 and 4000 pixels, the location of the KDML105 milled rice can be determined as shown in Fig.9(b). Similarly, subtracting images in Fig.8(c) with Fig.7(b) and applying 150-4000 pixels of blob filtering indicates the location of the HSPR milled rice grains (see Fig.9(c)). The position of PTT1 milled rice grains (Fig.9(d)) can be found from Figs.8(e)-(f) with blob filtering set at 50-4000 pixels. Image manipulation of Fig.7(a) and Fig.8(a) under blob filtering set at 50-4000 pixels highlights the position of RD15 milled rice grains as manifested in Fig.9(e). With the two images shown in Fig.7 and the image of KDML105 milled rice grains in Fig.9(b), RD23 milled rice grains can be identified under the same level of blob filtering. Subtraction of two images in Fig.8(d) and Fig.7(b) together will highlight two positions corresponding to CNT1 and RD15 milled rice grains, respectively. Because RD15 milled rice grains are already determined in Fig.9(e), it can immediately identify the CNT1 milled rice grains. In this case, blob

This material is reserved for educational use only, not allowed for commercial use.
Forbidden to modify the contents and to the document when use.
Downloaded from SPIE Digital Library on 02 Dec 2011 to 203.185.129.241. Terms of Use: http://spiedl.org/terms

filtering between 200-4000 pixels is also needed. Knowing the location of the CNT1 milled rice grains, the HPSL milled rice grains can be identified by subtracting the image in Fig.8(e) with Fig.8(c) and applying blob filtering of 50-4000 pixels. At this stage, all eight breeds of milled rice are identified. As images capturing from these two wavelength spectral can be achieved at a fast 45 ms and the image processing above can be done within 100 ms, real time rice breed identification can easily be accomplished.

4. CONCLUSION

We propose a nondestructive two-wavelength spectral-imaging based rice breed identification system. Our key idea is based on the use of a high energy UVC light source to optically induce unknown milled rice grains to radiate fluorescent radiation in a 500-580 nm wavelength band. In particular, we exploit only two fluorescent wavelengths at 540 nm and 575 nm and apply simple image processing techniques to classify milled rice breeds. In our experiment, milled rice grains from 8 different Thai rice breeds are tested. The spectral image at 540 nm wavelength goes through two-level image thresholding and blob filtering twice. For the spectral image at 575 nm wavelength, it goes through these processes six times. As a result, we obtain 8 binary images. By subtracting two selected binary images and then filtering out unwanted pixels, all eight rice breeds are effectively identified. With a fast tunable optical filter, real time rice breed identification can be realized. Future work relates to repeatability and reliability tests.

ACKNOWLEDGMENTS

Authors gratefully thank the Rice Research Institute at the Department of Rice, Ministry of Agriculture and Cooperatives of Thailand for supplying rice samples. K. Suwansukho would also like to thank Thailand Graduate Institute of Science and Technology for scholarship support (Grant No. TGIST 01-51-071).

REFERENCES

[1] Department of Foreign Trade, Ministry of Commerce, Thai Government, http://www.dft.moc.go.th/, accessed on Feb. 2, (2009).

[2] A. J. Cullen, R. C. Hoseney, and J. M. Faubion, "Identification of wheat cultivars by visual imaging," *US Patent*, 5321764, Jun. 14, 1994.

[3] Y.- N. Wan, "Grain sorting method and a device thereof," *US Patent*, 5973286, Oct. 26, 1999.

[4] E. G. Kokko and B. D. Hill, "Method and apparatus for identifying and quantifying characteristics of seeds and other small objects," *US Patent*, 7218775, May 15, 2007.

[5] Y. Liu, A. Ouyang, J. Wu, and Y. Ying, "An automatic method for identifying different variety of rice seeds using machine vision technology," *Proc. SPIE* **5996**, pp. 59961H (2005).

[6] A. Vanavichit, S. Tragoonrung, and T. Toojinda, "Biotechnology and rice varieties improvement," in *Science and Technology with Thai Rice*, Thailand's National Science and Technology Development Agency, pp. 79-121 (2003).

[7] K. Ohtsubo, S. Nakamura, T. Miyamura, S. Kumo, and I. Kato, "Method of detecting the presence of absence of mixed varieties in grains, and identifying the mixed varieties," *US Pat. Appl*,. US2006/0183138, Aug. 17 (2006).

[8] V. R. William, W. T. Wu, H. Y. Tsai, and H. G. Bates, "Varietal differences in amylose content of rice starch," *J. of Agri. Food* **6**, pp. 47-48 (1958).

[9] R. R. Little, G. B. Hilder, and E. H. Dawson, "Differential effect of dilute alkali on 25 varieties of milled white rice," *Cereal Chem.* **35**, pp. 111-126 (1958).

[10] B. O. Juliano, "A simplified assay for milled-rice amylose," *Cereal Sci. Today* **16**, pp. 334-340 (1971).

[11] "The ministry of commerce notification on rules and methodologies of commodities and Thai Hom Mali rice standards inspection B.E. 2545 (2002)," *Government Gazette* **119**, Special Section 21D, March 7 (2002).

[12] K. Suwansukho, S. Sumriddetchkajorn, and P. Buranasiri, "Combination of simple chemical and spectroscopic methods for the identification of Thai Hom Mali rice," *Proc. SPIE* **7315**, p. 73150W (2009).

[13] B. borne, B. Mertens, M. Thomson, and T. Fearn, "Authentication of Basmati rice using near infrared spectroscopy," *J. Near Infrared Spectro* **1**, pp. 77-83 (1993).

This material is reserved for personal study, not allowed for commercial use.
Forbidden to modify the content, and cite the document when use.
Downloaded from SPIE Digital Library on 02 Dec 2011 to 203.185.129.241. Terms of Use: http://spiedl.org/terms

[14] S. Sumriddetchkajorn, K. Suwansukho, and P. Buranasiri, "Identification of Thai Hom Mali rice using a refractometer," *Proc. SPIE* **7315**, pp. 73150F (2009).
[15] T. Katsumata, T. Suzuki, H. Aizama, E. Matashige, S. Komuro, and T. Morikawa, "Nondestructive evaluation of rice using two-dimensional imaging of photoluminescence," *Rev. Sci. Instru.***76** , pp.073702 (2005).
[16] T. Katsumata, T. Suzuki, H. Aizawa, and E. Matashige, "Photoluminescence evaluation of cereals for a quality control application," *J. Food Engg.* **78**, pp.588-590 (2007).
[17] M. S. Kim, A. M. Lefcourt, Y.- R. Chen, and Y. Tao, "Automated detection of fecal contamination of apples based on multispectral fluorescence image fusion," *J. Food Engg.* **71**, pp. 85-91 (2005).
[18] M. S. Kim, A. M. Lefcourt, and Y.- R. Chen, "Multispectral laser-induced fluorescence imaging system for large biological samples," *Appl. Opt.* **42**, pp. 3927-3934 (2003).
[19] M. S. Kim, J. E. McMurtrey, C. L. Mulchi, C. S. T. Daughtry, E. W. Chappelle, and Y.- R. Chen, "Steady-state multispectral fluorescence imaging system for plant leaves," *Appl. Opt.* **40**, pp. 157-166 (2001).
[20] Y. Intaravanne, S. Sumriddetchkajorn, and J. Nukaew, "Development of an imaging spectrometer for R&D in Thailand," *Proc. NCOA*, pp. 71-76 (2010).
[21] S. Sumriddetchkajorn, "Methods and apparatus for nondestructively identifying rice breeds," *Thailand Patent Application*, 1001000068, Jan. 15, 2010.

King Mongkut's Institute of Technology Ladkrabang

This material is reserved for personal study, not allowed for commercial use.
Forbidden to modify the content and cite the document when use.
Downloaded from SPIE Digital Library on 02 Dec 2011 to 203.185.129.241. Terms of Use: http://spiedl.org/terms

Two-Wavelength Spectral Imaging-based Thai Rice Breed Identification

Sarun Sumriddetchkajorn[1*], Kajpanya Suwansukho[2], and Prathan Buranasiri[2]
[1]Photonics Technology Laboratory
National Electronics and Computer Technology Center
National Science and Technology Development Agency
Ministry of Science and Technology
112 Thailand Science Park, Phahonyothin Rd, Klong 1, Klong Luang
Pathumthani 12120, Thailand, Tel: +66-2564-6900 ext. 2102, Fax: +66-2564-6774
E-mail: sarun.sumriddetchkajorn@nectec.or.th

[2]Applied Physics Department, Faculty of Science
King Mongkut's Institute of Technology Ladkrabang, Bangkok, Thailand

ABSTRACT

This paper combines multispectral imaging and simple image processing techniques for the non-destructive identification of Thai rice breeds. Especially, we exploit only two fluorescent wavelengths in a 500-580 nm wavelength band and utilize simple image thresholding, blob filtering, and blob analysis techniques in order to identify 8 different Thai rice breeds. Other key features include no waste produced and fast identification time. In our experimental study, UVC light is used as our exciting light, a liquid crystal tunable optical filter is used for our wavelength selection, and a camera with 644×488 active pixels is used to capture desired wavelength images. Milled rice grains from 8 different Thai rice breeds having similar size and shape are tested. There is also one glutinous rice breed in our experiment. Our experimental result shows that by suitably applying image thresholding, blob filtering, and blob analysis to fluorescent images, all Thai rice breeds can be effectively identified.

Keywords: Rice, Multispectral imaging, Hyperspectral imaging, Fluorescent imaging, Image processing, Nondestructive testing, Agri-photonics.

1. INTRODUCTION

It is known that Thai jasmine rice, also called Khao Dawk Mali 105 (KDML105), is one of the best rice varieties in the world. It was listed at the 7th export of Thailand in 2007 with its value of 1.73 billion US dollars [1]. As a result, there is an increase in mixing KDML105 milled rice with other Thai rice varieties especially Pathumthani1 (PTT1) and Chainat1 (CNT1) rice varieties as they have similar shape, weight/seed, and color to the KDML105 milled rice. This implies that a simple machine vision technique operating in the visible spectrum [2-5] cannot be used to separate these rice varieties from each other. Today widely used rice breed identification processes rely on destructive methods through slow chemical analysis, physical analysis, and DNA analysis [6-11]. Optical spectroscopy in the visible [12] and near infrared spectra [13] also showed an identification rate of 80% with a faster analytical time of 15 minutes. Faster 7 second identification can be obtained by using a refractometer [14].

One of the promisingly nondestructive approaches is the fluorescent imaging. Previously, all milled rice grains were illuminated with 365 nm wavelength (i.e., UVA) light and its fluorescent radiation at 460 nm was investigated through histogram analysis [15-16]. However, this single wavelength concept is suitable only for the identification of rice breeds that have different amount of amylose content. Instead of investigating at only one wavelength, several wavelength bands of fluorescent radiation under the UVA light have been studied for contamination detection in fruits, meats, and plant leaves [17-19]. With this concept, this paper proposes a non-destructive multispectral-imaging based method for identifying rice breeds. Especially, we utilize only two wavelengths of the fluorescent radiation under a higher energy UVC light source that can induce more fluorescent wavelength bands.

Biophotonics: Photonic Solutions for Better Health Care II, edited by Jürgen Popp, Wolfgang Drexler, Valery V. Tuchin, Dennis L. Matthews, Proc. of SPIE Vol. 7715, 77150I
© 2010 SPIE · CCC code: 1605-7422/10/$18 · doi: 10.1117/12.853507

This material is reserved for personal use only, not allowed for commercial use.
Forbidden to modify the content and cite the document when use.
Downloaded from SPIE Digital Library on 02 Dec 2011 to 203.185.129.241. Terms of Use: http://spiedl.org/terms

2. OUR PROPOSED TWO-WAVELENGTH SPECTRAL IMAGING-BASED RICE BREED IDENTIFIER

2.1 Architecture of the system

Our proposed two-wavelength spectral imaging-based rice breed identification system is shown in Fig.1. The main components are an exciting high energy light source (e.g., UVC at 265 nm wavelength), a tunable optical filter, an imaging lens system, a two-dimensional (2-D) digital camera, and an electronic controlling and processing unit. There is a region in which we can scatter unknown breeds of milled rice grains for analysis. This region is also in the field of view of the imaging lens system. The tunable optical filter is working in the visible spectrum and it can be based on several off-the-shelf technologies with and without moving part such as optical interference filters, acousto-optic tunable filters, a combination of two prisms and a grating, tunable Bragg grating, and liquid crystal retarders [20].

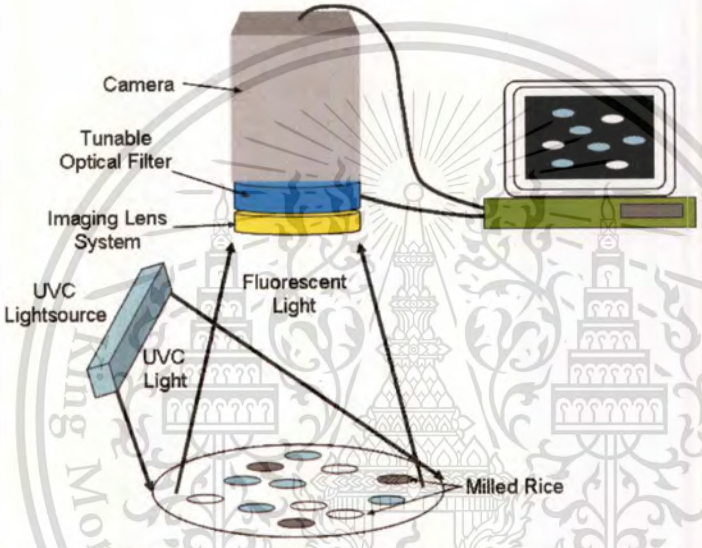

Fig. 1 Structure of our proposed multispectral imaging-based rice breed identification system.

When the UVC light is shining on all milled rice grains, the corresponding fluorescent radiation is emitted from all milled rice grains and passes through the imaging lens system. The tunable optical filter is electrically controlled in such a way that only the desired wavelength spectrum bands can get through to the 2-D digital camera. Based on our current study [21], we find two very strong fluorescent spectra in 539-553 nm and 570-585 nm bands. Especially, we choose to study fluorescent spectral signals at 540 nm and 575 nm in which their associated fluorescent signals start to appear. In addition, each rice breed gives out different amount of fluorescent radiation. This is probably due to the difference in the amount of amylose content and the level of glutinousness. Therefore, we focus on these two fluorescent wavelengths and their corresponding spectral images are transmitted to our processing unit. Note that unlike the single wavelength analysis used in refs. [15-16], our analysis of two-wavelength spectral offers more information that is needed for identifying rice breeds having the same amount of amylose content. In addition, because UVC light is known as the germicidal light, the use of UVC light during our rice breed identification provides one more advantage in that it can kill unwanted germs attached to milled rice grains.

2.2 Procedures of analysis

Once we have two spectral images associated with 540 nm and 575 nm fluorescent spectral from the milled rice grains, we follow the procedures shown in Fig.2. In this case, the maximum number of wavelengths (N) is equal to 2. Because each rice breed emits different amount of fluorescent radiation, each spectral image goes through two-level image

This material is reserved for educational use only, not allowed for commercial use.
Downloaded from SPIE Digital Library on 02 Dec 2011 to 203.185.129.241. Terms of Use: http://spiedl.org/terms

thresholding several times. In each time, the blob filtering is also applied in order to eliminate unwanted image areas. The total number of the resulting images is equal to M and these M images are binary.

After we have M binary images, we do image subtraction from two selected binary images. In this way, the remaining image areas correspond to the rice breeds that we are looking for. The coordinate of the remaining image areas also tells us their locations. In addition, these image areas can be used for the estimation of the number of milled rice grains corresponding to their rice breeds.

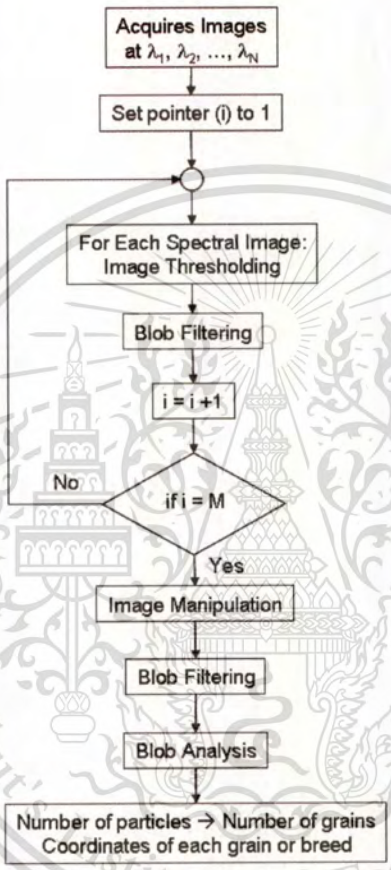

Fig. 2 Flowchart for analysis of spectral images in order to nondestructively identify breeds of all milled rice grains in real time.

3. OUR EXPERIMENTAL DEMONSTRATION

3.1 Experimental setup

Our imaging spectrometer is shown in Fig.3 and its wavelength selection scheme is based on the use of a liquid crystal tunable filter (LCTF) [20]. The LCTF is from VariSpec and its model is VIS-7-HC-20. It can be electrically controlled to let the visible light from 400 to 720 nm pass through with an FWHM of 7 nm at a speed of 6 nm/s. The optical transmission depends on the wavelength which the lowest transmission is on the left wing of the spectrum and the highest transmission is on the right edge of the spectrum. The active area is 20 mm in diameter. It is interfaced to the computer via a universal serial bus (USB). For our 2-D image device, we choose a complementary metal oxide semiconductor-based digital camera that provides an 8-bit digital image. It sensing area has 644 (H) × 488 (V) pixels with a pixel dimensions of 8.4 μm × 8.4 μm. This digital camera communicates with a computer through a USB-based frame grabber. The imaging lens system has a specified focal distance of 3.7 mm.

This material is reserved for educational use only, not allowed for commercial use.
Forbidden to modify the contents and cite the document when use.
Downloaded from SPIE Digital Library on 02 Dec 2011 to 203.185.129.241. Terms of Use: http://spiedl.org/terms

Our UVC light source is an 18-W mercury lamp in a TUV style package from Philips. It emits only one peak wavelength radiation at 253.7 nm. It is settled at the left hand side of the milled rice grains at a distance of 116 mm and it is above milled rice grains at a distance of 65 mm. In this way, UVC light shines uniformly in the area of 40 mm in diameter. We also place a UV block filter in front of the LCTF to allow only the measured visible wavelength spectrum starting from 410 nm pass through the imaging lens system and fall on the 2-D digital camera.

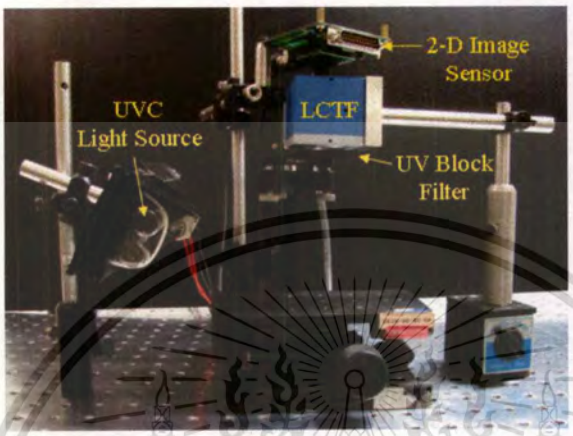

Fig. 3 Our experimental setup for milled rice breed identification.

Our milled rice grains are from 8 different Thai rice breeds as shown in Fig.4. The PTT1 rice has equivalent amount of amylose content to that of the KDML105 rice. These two rice varieties are classified as low amylose content rices. The CNT1 rice has its amylose content in 27%-30% and it is classified as one of high amylose content varieties. Other milled rice varieties with specified as low amylose content such as Ko Kor 15 (RD15) and with specified as high amylose content such as Hom Supanburi (HPSR), Hom Pitsanulok (HPSL), and Ko Kor 23 (RD23) are included. We also bring in to our study another Thai rice variety with very low amylose content of 0%-2%. It is Thai sticky rice (RD6). For each milled rice breed, we randomly select 4 milled rice grains and place them on a specific location shown in Fig.5(a). There are 3 main fluorescent spectral regions in 432-438 nm, 539-553 nm, and 570-585 nm (see Fig.5(b)). All milled rice grains emit fluorescent radiation for which the RD6 shows the strongest fluorescent signal followed with KDML105 milled rice. As the last two fluorescent wavelength bands have the strongest spectral signals for KDML105 milled rice, this paper analyzes spectral images from these two wavelengths. Especially, we choose fluorescent spectral signals at 540 nm and 575 nm (see Fig.6). In this case, a measured LCTF switching time between these two selected wavelengths is 45.1 ms. Because the fluorescent signal at 575 nm wavelength is also stronger than fluorescent signals at 540 nm wavelength, the spectral image at 575 nm wavelength is brighter than the spectral image at 540 nm wavelength.

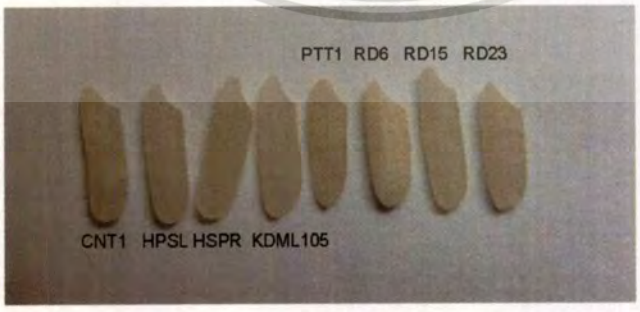

Fig. 4 Eight breeds of Thai milled rice grains.

This material is reserved for educational use only, not allowed for commercial use.
Forbidden to modify the content. Click the terms when use.
Downloaded from SPIE Digital Library on 02 Dec 2011 to 203.185.129.241. Terms of Use: http://spiedl.org/terms

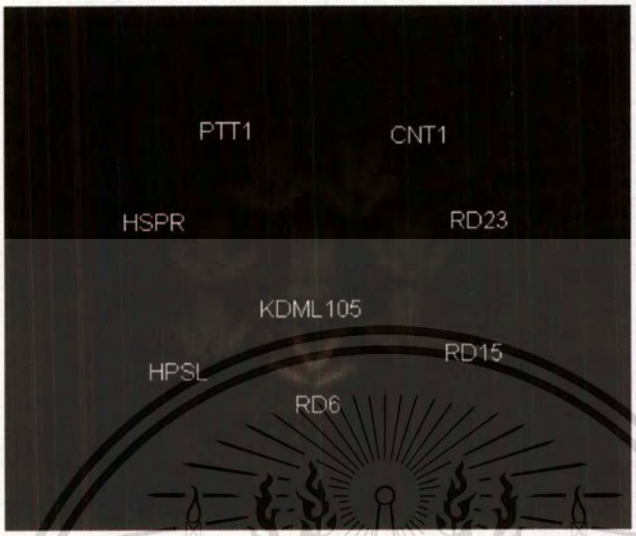

(a)

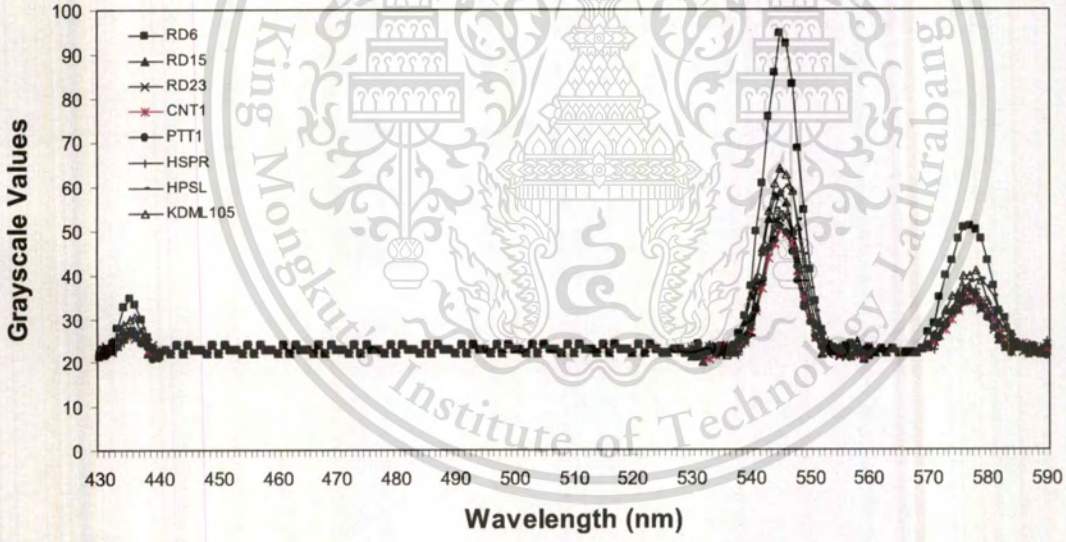

(b)

Fig. 5 (a) Fluorescent image emitted from all milled rice grains under UVC illumination and (b) fluorescent signals.

This material is reserved for personal use only, not allowed for commercial use.
Forbidden to modify the content and cite the document when use.
Downloaded from SPIE Digital Library on 02 Dec 2011 to 203.185.129.241. Terms of Use: http://spiedl.org/terms

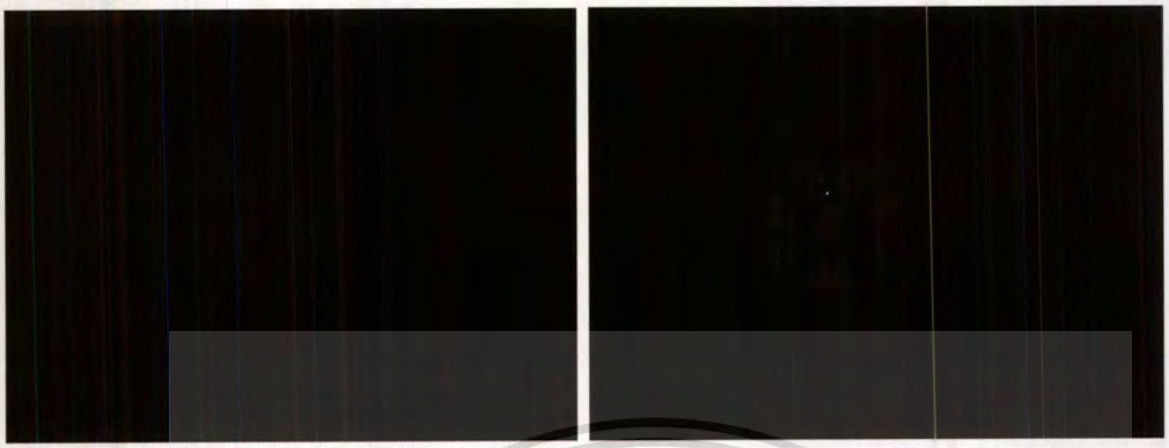

540 nm 575 nm

Fig. 6 Fluorescent images of milled rice grains from 8 different rice breeds at 540 nm and 575 nm wavelengths.

3.2 Analysis

For the fluorescent image at 540 nm wavelength, we first set the image threshold interval at 30-150. In this way, pixels that have their grayscale values less than 30 or more than 150 are highlighted as black while the remaining pixels are set to red. By selecting image areas that contain the number of pixels in the range of 660 and 4000 pixels, we obtain the image areas where milled rice grains for RD6 and RD15 appear as shown in Fig.7(a). Lowering the lower limits of the image thresholding interval to 29 and of the blob filtering to 400 makes the two image areas associated with KDML105 and RD23 milled rice grains appear as shown in Fig.7(b).

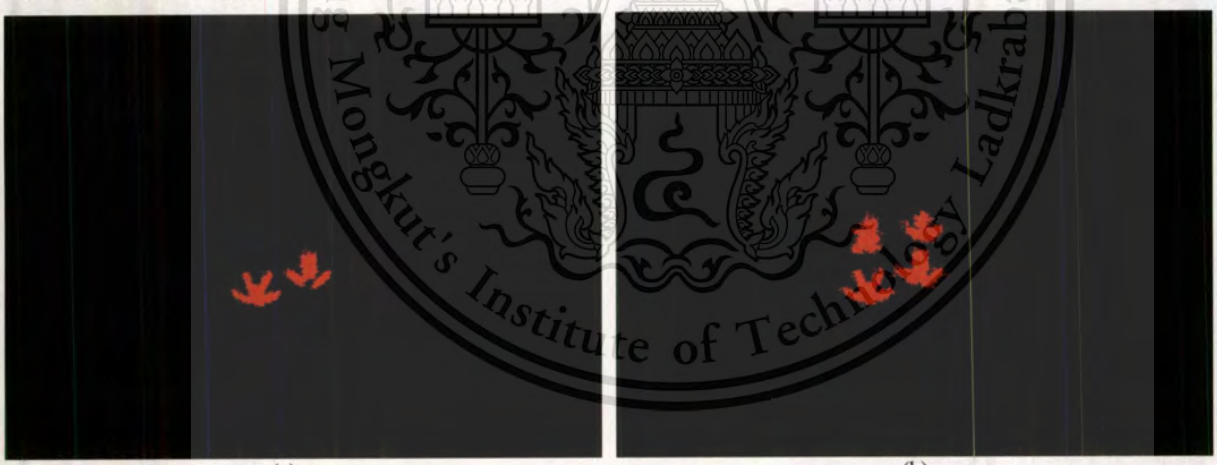

(a) (b)

Fig. 7 Results of image manipulation through image thresholding and blob filtering processes for the fluorescent image at 540 nm. (a) Thresholding interval (T) of 30-150 and blob filtering (B) between 660 and 4000 pixels. (b) T = 29-150, B = 400-4000 pixels.

Similarly, for the fluorescent image at 575 nm wavelength, we first set the image threshold interval at 39-150. In addition, by keeping image areas that contain 30-4000 pixels, we can immediately locate the areas that have only the RD6 milled rice grains as shown in Fig.8(a). Lowering the lower limit of the image threshold level to 33 and increasing the lower limit of the blob filtering to 455 pixels let the KDML105 milled rice grains appear along side with the RD6 milled rice grains as shown in Fig.8(b). Three additional image areas that contain RD23, RD15, and HSPR milled rice grains are highlighted by setting the image threshold level at 30-150 and the blob filtering between 900 and 4000 pixels as shown in Fig.8(c).

This material is reserved for educational use only, not allowed for commercial use.
Downloaded from SPIE Digital Library on 02 Dec 2011 to 203.185.129.241. Terms of Use: http://spiedl.org/terms

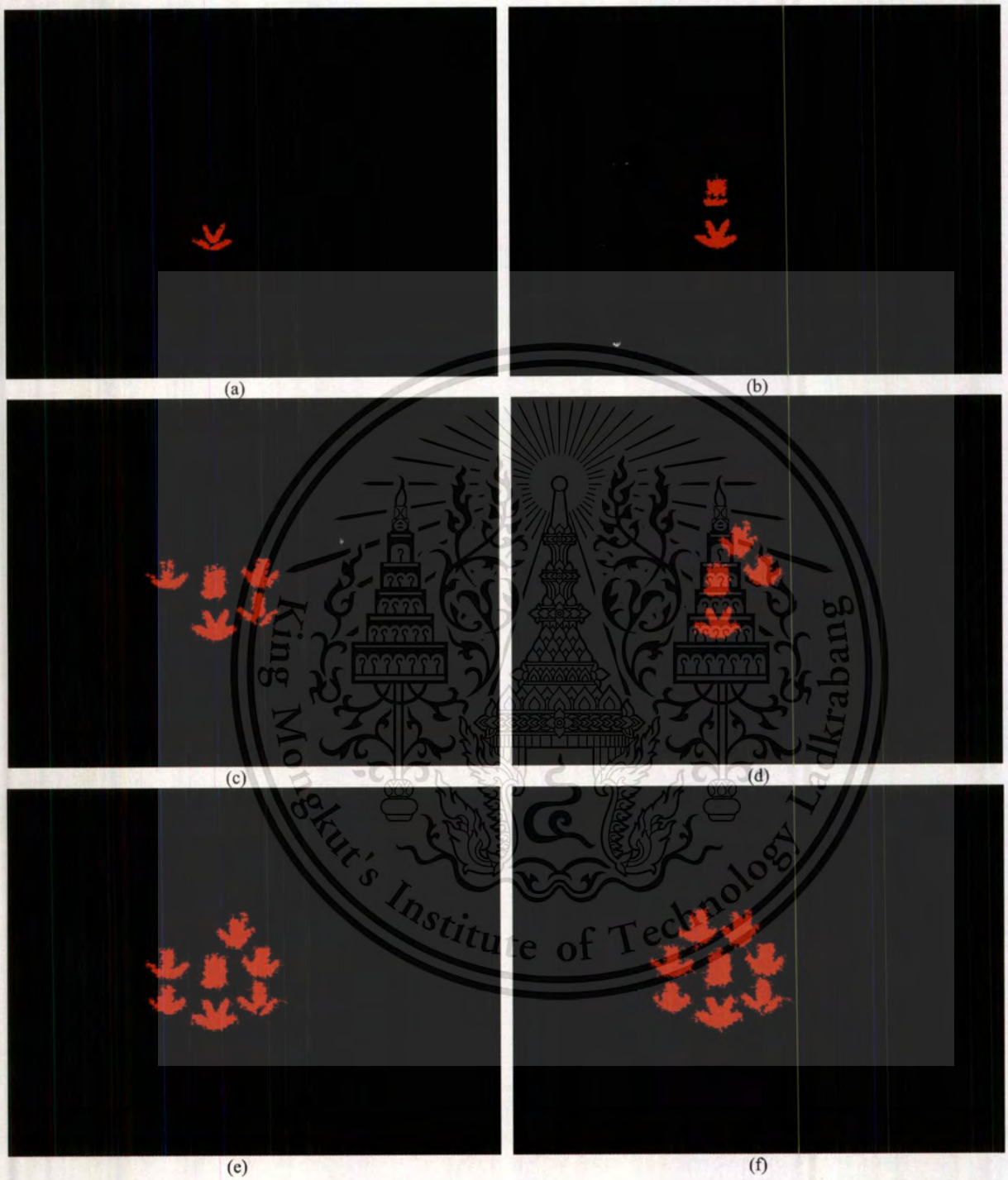

Fig. 8 Results of image manipulation through image thresholding and blob filtering processes for the fluorescent image at 575 nm with different thresholding (T) and blob filtering (B) levels. (a) T = 39-150, B = 30-4000 pixels, (b) T = 33-150, B = 455-4000 pixels, (c) T = 30-150, B = 900-4000 pixels, (d) T = 29-150, B = 1200-4000 pixels, (e) T = 28-150, B = 550-4000 pixels, and (f) T = 27-150, B = 400-4000 pixels.

This material is reserved for personal study, not allowed for commercial use.
Forbidden to modify the content and cite the document when use.
Downloaded from SPIE Digital Library on 02 Dec 2011 to 203.185.129.241. Terms of Use: http://spiedl.org/terms

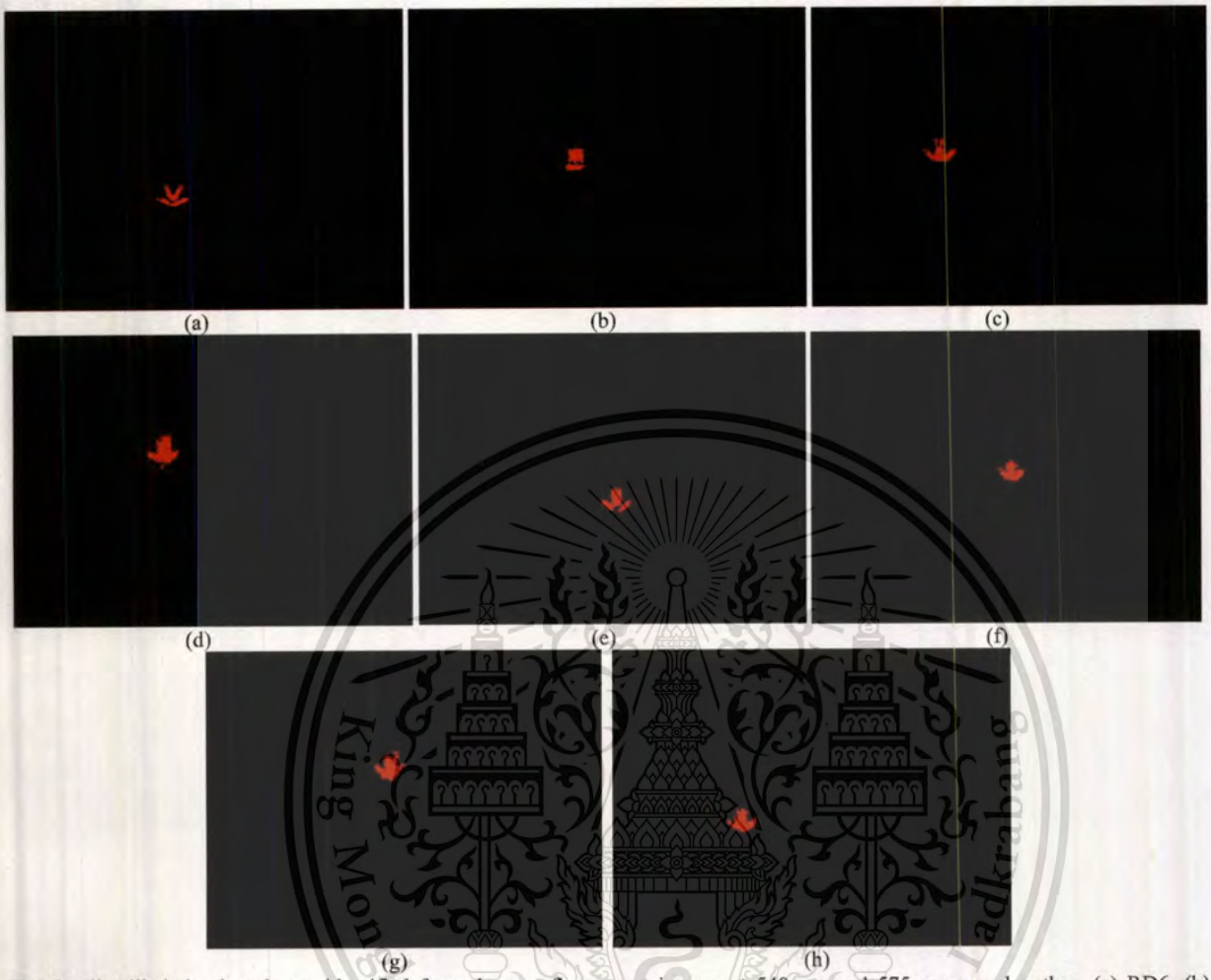

Fig. 9 All milled rice breeds are identified from the two fluorescent images at 540 nm and 575 nm wavelengths. (a) RD6, (b) KDML105, (c) HSPR, (d) PTT1, (e) RD15, (f) RD23, (g) CNT1, and (h) HPSL.

With the image threshold level of 29-150 and the blob filtering set at 1200-4000 pixels, HSPR and RD15 milled rice grains disappear while CNT1 milled rice grains show up (see Fig.8(d)). Now, all except PTT1 milled rice grains are shown up when we set the image threshold level to 28-150 and the blob filtering to 550-4000 pixels. In addition, all images of 8 different rice breeds appear when the image thresholding level and the blob filtering are set to 27-150 and 400-4000 pixels, respectively.

To identify locations of all 8 different rice breeds, simple image subtraction and blob filtering are employed as follows. Note that from Fig.8(a), RD6 milled rice grains are already identified. By subtracting Fig.8(b) with Fig.8(a) and keeping images that contain pixels between 50 and 4000 pixels, the location of the KDML105 milled rice can be determined as shown in Fig.9(b). Similarly, subtracting images in Fig.8(c) with Fig.7(b) and applying 150-4000 pixels of blob filtering indicates the location of the HSPR milled rice grains (see Fig.9(c)). The position of PTT1 milled rice grains (Fig.9(d)) can be found from Figs.8(e)-(f) with blob filtering set at 50-4000 pixels. Image manipulation of Fig.7(a) and Fig.8(a) under blob filtering set at 50-4000 pixels highlights the position of RD15 milled rice grains as manifested in Fig.9(e). With the two images shown in Fig.7 and the image of KDML105 milled rice grains in Fig.9(b), RD23 milled rice grains can be identified under the same level of blob filtering. Subtraction of two images in Fig.8(d) and Fig.7(b) together will highlight two positions corresponding to CNT1 and RD15 milled rice grains, respectively. Because RD15 milled rice grains are already determined in Fig.9(e), it can immediately identify the CNT1 milled rice grains. In this case, blob

This material is reserved for personal use only, not allowed for commercial use.
Forbidden to modify the content and cite the document when use.
Downloaded from SPIE Digital Library on 02 Dec 2011 to 203.185.129.241. Terms of Use: http://spiedl.org/terms

filtering between 200-4000 pixels is also needed. Knowing the location of the CNT1 milled rice grains, the HPSL milled rice grains can be identified by subtracting the image in Fig.8(e) with Fig.8(c) and applying blob filtering of 50-4000 pixels. At this stage, all eight breeds of milled rice are identified. As images capturing from these two wavelength spectral can be achieved at a fast 45 ms and the image processing above can be done within 100 ms, real time rice breed identification can easily be accomplished.

4. CONCLUSION

We propose a nondestructive two-wavelength spectral-imaging based rice breed identification system. Our key idea is based on the use of a high energy UVC light source to optically induce unknown milled rice grains to radiate fluorescent radiation in a 500-580 nm wavelength band. In particular, we exploit only two fluorescent wavelengths at 540 nm and 575 nm and apply simple image processing techniques to classify milled rice breeds. In our experiment, milled rice grains from 8 different Thai rice breeds are tested. The spectral image at 540 nm wavelength goes through two-level image thresholding and blob filtering twice. For the spectral image at 575 nm wavelength, it goes through these processes six times. As a result, we obtain 8 binary images. By subtracting two selected binary images and then filtering out unwanted pixels, all eight rice breeds are effectively identified. With a fast tunable optical filter, real time rice breed identification can be realized. Future work relates to repeatability and reliability tests.

ACKNOWLEDGMENTS

Authors gratefully thank the Rice Research Institute at the Department of Rice, Ministry of Agriculture and Cooperatives of Thailand for supplying rice samples. K. Suwansukho would also like to thank Thailand Graduate Institute of Science and Technology for scholarship support (Grant No. TGIST 01–51-071).

REFERENCES

[1] Department of Foreign Trade, Ministry of Commerce, Thai Government, http://www.dft.moc.go.th/, accessed on Feb. 2, (2009).

[2] A. J. Cullen, R. C. Hoseney, and J. M. Faubion, "Identification of wheat cultivars by visual imaging," *US Patent*, 5321764, Jun. 14, 1994.

[3] Y.- N. Wan, "Grain sorting method and a device thereof," *US Patent*, 5973286, Oct. 26, 1999.

[4] E. G. Kokko and B. D. Hill, "Method and apparatus for identifying and quantifying characteristics of seeds and other small objects," *US Patent*, 7218775, May 15, 2007.

[5] Y. Liu, A. Ouyang, J. Wu, and Y. Ying, "An automatic method for identifying different variety of rice seeds using machine vision technology," *Proc. SPIE* **5996**, pp. 59961H (2005).

[6] A. Vanavichit, S. Tragoonrung, and T. Toojinda, "Biotechnology and rice varieties improvement," in *Science and Technology with Thai Rice*, Thailand's National Science and Technology Development Agency, pp. 79-121 (2003).

[7] K. Ohtsubo, S. Nakamura, T. Miyamura, S. Kumo, and I. Kato, "Method of detecting the presence of absence of mixed varieties in grains, and identifying the mixed varieties," *US Pat. Appl*,. US2006/0183138, Aug. 17 (2006).

[8] V. R. William, W. T. Wu, H. Y. Tsai, and H. G. Bates, "Varietal differences in amylose content of rice starch," *J. of Agri. Food* **6**, pp. 47-48 (1958).

[9] R. R. Little, G. B. Hilder, and E. H. Dawson, "Differential effect of dilute alkali on 25 varieties of milled white rice," *Cereal Chem.* **35**, pp. 111-126 (1958).

[10] B. O. Juliano, "A simplified assay for milled-rice amylose," *Cereal Sci. Today* **16**, pp. 334-340 (1971).

[11] "The ministry of commerce notification on rules and methodologies of commodities and Thai Hom Mali rice standards inspection B.E. 2545 (2002)," *Government Gazette* **119**, Special Section 21D, March 7 (2002).

[12] K. Suwansukho, S. Sumriddetchkajorn, and P. Buranasiri, "Combination of simple chemical and spectroscopic methods for the identification of Thai Hom Mali rice," *Proc. SPIE* **7315**, p. 73150W (2009).

[13] B. borne, B. Mertens, M. Thomson, and T. Fearn, "Authentication of Basmati rice using near infrared spectroscopy," *J. Near Infrared Spectro* **1**, pp. 77-83 (1993).

This material is reserved for personal use only, not allowed for commercial use.
Forbidden to modify the content and cite the document when use.
Downloaded from SPIE Digital Library on 02 Dec 2011 to 203.185.129.241. Terms of Use: http://spiedl.org/terms

[14] S. Sumriddetchkajorn, K. Suwansukho, and P. Buranasiri, "Identification of Thai Hom Mali rice using a refractometer," *Proc. SPIE* **7315**, pp. 73150F (2009).
[15] T. Katsumata, T. Suzuki, H. Aizama, E. Matashige, S. Komuro, and T. Morikawa, "Nondestructive evaluation of rice using two-dimensional imaging of photoluminescence," *Rev. Sci. Instru.***76** , pp.073702 (2005).
[16] T. Katsumata, T. Suzuki, H. Aizawa, and E. Matashige, "Photoluminescence evaluation of cereals for a quality control application," *J. Food Engg.* **78**, pp.588-590 (2007).
[17] M. S. Kim, A. M. Lefcourt, Y.- R. Chen, and Y. Tao, "Automated detection of fecal contamination of apples based on multispectral fluorescence image fusion," *J. Food Engg.* **71**, pp. 85-91 (2005).
[18] M. S. Kim, A. M. Lefcourt, and Y.- R. Chen, "Multispectral laser-induced fluorescence imaging system for large biological samples," *Appl. Opt.* **42**, pp. 3927-3934 (2003).
[19] M. S. Kim, J. E. McMurtrey, C. L. Mulchi, C. S. T. Daughtry, E. W. Chappelle, and Y.- R. Chen, "Steady-state multispectral fluorescence imaging system for plant leaves," *Appl. Opt.* **40**, pp. 157-166 (2001).
[20] Y. Intaravanne, S. Sumriddetchkajorn, and J. Nukaew, "Development of an imaging spectrometer for R&D in Thailand," *Proc. NCOA*, pp. 71-76 (2010).
[21] S. Sumriddetchkajorn, "Methods and apparatus for nondestructively identifying rice breeds," *Thailand Patent Application*, 1001000068, Jan. 15, 2010.

King Mongkut's Institute of Technology Ladkrabang

This material is reserved for personal use only, not allowed for commercial use.
Forbidden to modify the content and cite the document when use.
Downloaded from SPIE Digital Library on 02 Dec 2011 to 203.185.129.241. Terms of Use: http://spiedl.org/terms

Improvement of Single-Wavelength based Thai Jasmine Rice Identification with Elliptic Fourier Descriptor and Neural Network Analysis

Kajpanya Suwansukho[a], Sarun Sumriddetchkajorn[b,*], and Prathan Buranasiri[a]
[a]Physics Department, Faculty of Science
King Mongkut's Institute of Technology Ladkrabang, Bangkok, Thailand

[b]Intelligent Devices and Systems Research Unit
National Electronics and Computer Technology Center
National Science and Technology Development Agency
Ministry of Science and Technology
112 Thailand Science Park, Phahonyothin Rd, Klong 1, Klong Luang
Pathumthani 12120, Thailand

ABSTRACT

Instead of considering only the amount of fluorescent signal spatially distributed on the image of milled rice grains this paper shows how our single-wavelength spectral-imaging-based Thai jasmine (KDML105) rice identification system can be improved by analyzing the shape and size of the image of each milled rice variety especially during the image threshold operation. The image of each milled rice variety is expressed as chain codes and elliptic Fourier coefficients. After that, a feed-forward back-propagation neural network model is applied, resulting in an improved average FAR of 11.0% and FRR of 19.0% in identifying KDML105 milled rice from the unwanted four milled rice varieties.

Keywords: Rice, Optical Sensors, Biophotonics, Fluorescent imaging, Neural networks, Image processing, Elliptic Fourier descriptors.

1. INTRODUCTION

Thai jasmine rice or Khaw Dok Mali 105 (KDML105) is a well known rice variety due to high quality for cooking and unique fragrance. As a result, there have increasingly been intentional impurities of KDML105 milled rice products with other lower price foreign and local rice varieties such as Chainat 1 (CNT1), Hom Pitsanulok (HPSL), and Pathumthani 1 (PTT1). Previously, we demonstrated that one-dimensional (1-D) optical spectrum analysis in the visible wavelength region [1] and optical refractometry [2] were able to distinguish KDML105 from unwanted rice varieties. However, due to their destructive analysis in nature with poor repeatability, they were not practically acceptable. Another optical approach that promises non-destructive analysis is the spectral imaging as it has recently been employed for several applications. These include data-non intrusive credit card verification [3-4], 2-D banana ripeness estimation [5], and blood stain detection [6]. By using higher energy light sources, a combination of two-wavelength (545 nm and 575 nm) fluorescent spectral imaging-based Thai rice breed identification was proposed and experimentally demonstrated [7]. Because the selected 20×45-pixel spectral image at 575 nm contains little detail of milled rice grain from low image magnification and fluorescent signal of the system, the system repeatability and reliability in identifying KDML105 milled rice grains were below the requirement. We also proposed and demonstrated that only a single wavelength spectral image when combined with simple image processing operations were sufficient for the identification of Thai jasmine milled rice from unwanted CNT1 HPSL, and PTT1 milled rice varieties with measured false acceptance rates (FAR) of <26.7% and <40.0% and false rejection rates (FRR) of 0% for spectral images at 545 and 575 nm wavelengths, respectively [8].

* sarun.sumriddetchkajorn@nectec.or.th; Phone+66-2564-6900 ext. 2102, Fax: +66-2564-6771

Optoelectronic Imaging and Multimedia Technology II, edited by Tsutomu Shimura, Guangyu Xu, Linmi Tao, Jesse Zheng, Proc. of SPIE Vol. 8558, 85580C · © 2012 SPIE
CCC code: 0277-786/12/$18 · doi: 10.1117/12.999852

This material is reserved for educational use only, not allowed for commercial use.

Forbidden to modify the content and delete the document when use.
From: http://proceedings.spiedigitallibrary.org/ on 01/09/2013 Terms of Use: http://spiedl.org/terms

To improve the performance of our single-wavelength based KDML105 identification system, specific information of rice grains in the spectral image needs to be deliberately taken into consideration. One interesting approach for extracting this specific information of the rice grain from the image is to apply the elliptic Fourier descriptor (EFD) [9]. The EFD can be applied to very complex curves [10] and have been effectively employed for the evaluations of various biological shapes, animal organs [11-13], and plants [14-17]. The EFD describes shape mathematically through transforming coordinates information concerning its contours into Fourier coefficients. Hence, we show here how the EFD can be applied to our spectral image and when analyzed by a trained artificial neural network [18-19] leads to an improved FAR in identifying Thai jasmine rice grains.

2. OUR SINGLE-WAVELENGTH BASED THAI JASMINE MILLED RICE VARIETY IDENTIFIER

The arrangement of our single-wavelength spectral imaging-based KDML105 milled rice breed identification system is shown in Fig. 1. The main components are a 2-D digital camera, a camera lens, a narrow band-pass optical filter centered at the selected 546 nm fluorescent wavelength spectrum, a UV block filter, high-energy light sources (e.g., UVC at 253.7 nm wavelength), and an electronic controlling and processing unit. There is a region in which we can scatter unknown breeds of milled rice grains for analysis. This region is also in the field of view of the imaging lens system. Under the UVC illumination, all milled rice grains are induced to give up their fluorescent radiation. A series of UV block filter and a narrow band-pass optical filter are mounted in front of the 2-D digital camera. The desired fluorescent spectral image is then obtained from the camera and is fed to the electronic controlling and processing unit.

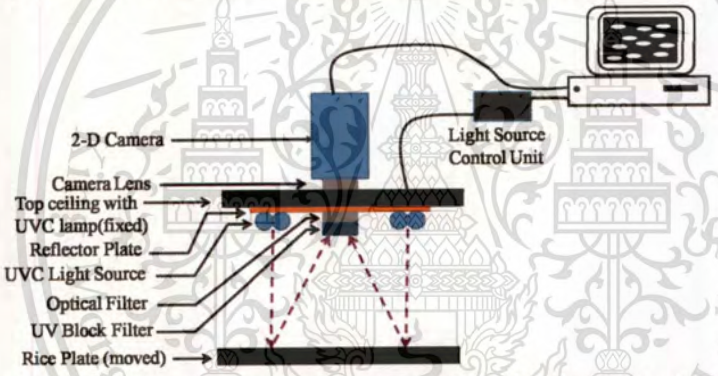

Figure 1. Structure of our single-wavelength spectral-imaging based KDML105 milled rice breed identification.

3. IMAGE ANALYSIS

Once we have the desired spectral image. The spectral image is normalized by its background. Realizing that each rice breed spatially emits a different amount of fluorescent radiation due to the amount of amylose, amylopectin, and glutin [20–22], the normalized spectral image goes through an image thresholding process in order to filter out unwanted image areas. Our image thresholding can be simply expressed as

$$I'(x,y)=\begin{cases}255, Th_{\min}\le I(x,y)\le Th_{\max}\\ 0, Otherwise\end{cases}. \quad (1)$$

From Eqn(1), if the gray scale value I(x, y) of each image pixel (x,y) remains within the desired Th_{min} and Th_{max}, its new gray scale value I′(x, y) will be changed to a maximum gray scale value (e.g., 255 for an 8-bit image). On the other hand, the new gray scale value I′(x, y) of 0 will be assigned if the gray scale value I(x, y) is out of the desired range.

This material is reserved for educational use only, not allowed for commercial use.

Downloaded From: http://proceedings.spiedigitallibrary.org/ on 01/09/2013 Terms of Use: http://spiedl.org/terms
Redistribution subject to SPIE license or copyright; see terms of use document when use.

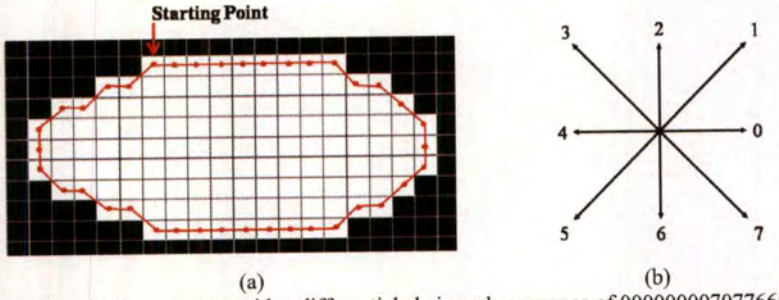

(a) (b)

Figure 2. (a) Binary pixels of a shape pattern with a differential chain code sequence of 00000000707766554544444444343432210101 starting from upper left hand corner and (b) eight connected grids [16].

After that, the shape of the milled rice grain is modeled using the normalized EFD of a closed-contour of the grain boundary. The closed-contour is defined with Freeman chain codes [23], represented by a sequence of unit vectors and directional coding as shown in Fig. 2. Individual grain boundary pixels are used to describe the chain code, starting with the upper left pixel of the contour and tracing the boundary clockwise. The chain code enumeration is completed when the original starting point is reached. From Fig. 2(a), a chain code of 00000000707766554544444444343432210101 is obtained by following code directions in Fig. 2(b). It can be assumed that a point at the starting position is travelling along the image boundary with a constant speed. The time used to travel between links depending on the code of the chain which is mathematically written as in Eqn.(2).

$$\Delta t_i = 1 + \left(\frac{\sqrt{2}-1}{2}\right)\left(1-(-1)^{a_i}\right), \tag{2}$$

where a_i is the i^{th} code of the chain code. Eqn(2) is equal to 1 if a code is an even and $\sqrt{2}$ if a code is an odd. For a close contour pattern, the roundtrip time (t_p) can be written as.

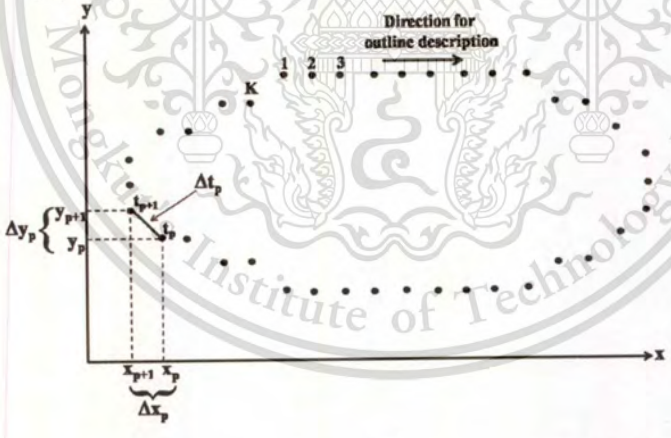

Figure 3. Illustration of the parameters used for computing the Fourier coefficients of an EFD on an outline [12].

$$t_p = \sum_{i=1}^{p} \Delta t_i \,. \tag{3}$$

Once the Δt_i is known, its corresponding travelling distances along the x and y axes can be found as follows.

$$\Delta x_i = signum(6-a_i)\,signum(2-a_i), \tag{4}$$

$$\Delta y_i = signum(4-a_i)\,signum(a_i), \tag{5}$$

This material is reserved for educational research, not allowed for commercial use.

Forbidden to modify the content and cite the document when use.

d From: http://proceedings.spiedigitallibrary.org/ on 01/09/2013 Terms of Use: http://spiedl.org/terms

where

$$signum(z)=\begin{cases} 1, & z>0 \\ 0, & z=0 \\ -1, & z<0 \end{cases}. \tag{6}$$

Similarly, close-loop travelling distances along x and y axes can be written as.

$$x_p=\sum_{i=1}^{p}\Delta x_i, \tag{7}$$

$$y_p=\sum_{i=1}^{p}\Delta y_i\,. \tag{8}$$

As the chain code is a function of time and line segments along the boundary, we can consider it as a discrete periodic pattern whereby it can be mathematically analyzed by Fourier series. In this case, the Fourier series expansion of the closed-contour which is a projection of the contour on the x and y axes can be obtained as follows.

$$x_n=A_0+\sum_{n=1}^{N}a_n\cos\frac{2n\pi t}{T}+b_n\sin\frac{2n\pi t}{T}, \tag{9}$$

$$y_n=C_0+\sum_{n=1}^{N}c_n\cos\frac{2n\pi t}{T}+d_n\sin\frac{2n\pi t}{T}, \tag{10}$$

where n is the order of the harmonic being considered and N is a maximum number of harmonics. T is the perimeter of the closed contour. From Eqns(9-10), a_n, b_n, c_n and d_n are the Fourier coefficients of the n^{th} harmonic and they can be found by using the following expressions.

$$a_n=\frac{T}{2n^2\pi^2}\sum_{p=1}^{K}\frac{\Delta x_p}{\Delta t_p}\left[\cos\frac{2n\pi t_p}{T}-\cos\frac{2n\pi t_{p-1}}{T}\right], \tag{11}$$

$$b_n=\frac{T}{2n^2\pi^2}\sum_{p=1}^{K}\frac{\Delta x_p}{\Delta t_p}\left[\sin\frac{2n\pi t_p}{T}-\sin\frac{2n\pi t_{p-1}}{T}\right], \tag{12}$$

$$c_n=\frac{T}{2n^2\pi^2}\sum_{p=1}^{K}\frac{\Delta y_p}{\Delta t_p}\left[\cos\frac{2n\pi t_p}{T}-\cos\frac{2n\pi t_{p-1}}{T}\right], \tag{13}$$

$$d_n=\frac{T}{2n^2\pi^2}\sum_{p=1}^{K}\frac{\Delta y_p}{\Delta t_p}\left[\sin\frac{2n\pi t_p}{T}-\sin\frac{2n\pi t_{p-1}}{T}\right]. \tag{14}$$

The two constant terms A_0 and C_0 are calculated as

$$A_0=\frac{1}{T}\sum_{p=1}^{K}\frac{1}{2}\frac{\Delta x_p}{\Delta t_p}\left(t_p^2-t_{p-1}^2\right)-\frac{\Delta x_p}{\Delta t_p}t_p, \tag{15}$$

$$C_0=\frac{1}{T}\sum_{p=1}^{K}\frac{1}{2}\frac{\Delta y_p}{\Delta t_p}\left(t_p^2-t_{p-1}^2\right)-\frac{\Delta y_p}{\Delta t_p}t_p. \tag{16}$$

This material is reserved for personal use; not allowed for commercial use.
From: http://proceedings.spiedigitallibrary.org/ on 01/09/2013 Terms of Use: http://spiedl.org/terms
Redistribution subject to SPIE license or copyright; see terms of use document when use.

Here, as shown in Fig. 3, Δx_p and Δy_p are the segments between p and p + 1 of the closed-contour projected onto the x and y axes, respectively. Δt_p is the step between p and p + 1 of the closed-contour. t_p is the curvilinear coordinate of the point p and K is the number of sampling points on the closed-contour. The shape descriptor determined using Eqns(11–16) clearly depends upon the size of grains, the orientation of grains, and the starting point of the chain-code. As a result, they cannot directly be used to indicate the variability for comparison of the grain kernels. To alleviate these problems, the normalized Fourier coefficients (a_n^{**},b_n^{**} ,c_n^{**} and d_n^{**}) are considered based upon the ellipse of the first harmonic as follows.

$$\begin{bmatrix} a_n^{**} & b_n^{**} \\ c_n^{**} & d_n^{**} \end{bmatrix} = \frac{1}{E^*} \begin{bmatrix} \cos\psi & \sin\psi \\ -\sin\psi & \cos\psi \end{bmatrix} \begin{bmatrix} a_n & b_n \\ c_n & d_n \end{bmatrix} \begin{bmatrix} \cos n\theta & -\sin n\theta \\ \sin n\theta & \cos n\theta \end{bmatrix}, \tag{17}$$

where

$$E^* = \left(a_1^{*2} + c_1^{*2}\right)^{1/2}, \begin{bmatrix} a_1^* \\ c_1^* \end{bmatrix} = \begin{bmatrix} a_1 & b_1 \\ c_1 & d_1 \end{bmatrix} \begin{bmatrix} \cos\theta \\ \sin\theta \end{bmatrix}, \tag{18}$$

$$\theta = \frac{1}{2}\arctan\left[\frac{2(a_1 b_1 + c_1 d_1)}{a_1^2 + c_1^2 - b_1^2 - d_1^2}\right], \; 0 \le \theta \le \pi, \tag{19}$$

$$\psi = \arctan\left[\frac{c_1^*}{a_1^*}\right], \; 0 \le \psi \le 2\pi. \tag{20}$$

The number of sets of elliptic Fourier coefficients increases as the number of harmonics increases. For each harmonic set, four coefficients are always generated. The Fourier amplitude (FA) is related to the number of harmonics by the following expression [24].

$$FA = 2n\pi\sqrt{\frac{\left(a_n^{**}\cos\psi + c_n^{**}\sin\psi\right)^2 + \left(-b_n^{**}\sin\psi + d_n^{**}\cos\psi\right)^2}{2}}. \tag{21}$$

From Eqn(21), the maximum number of the harmonics in our analysis is set to N = 17 as its shape is almost matched to the original shape of the rice grain. Increasing the maximum number of harmonics under our analysis does not tremendously improve the shape similarity but does require more analytical time. Using these normalized harmonic coefficients, each harmonic can be graphically represented as an ellipse and can be analyzed in terms of semi-major axis (SMJA), semi-minor axis (SMNA), area, and perimeter by using the following equations.

$$SMJA = abs(a_n^{**}\cos\psi + c_n^{**}\sin\psi), \tag{22}$$

$$SMNA = abs(-b_n^{**}\sin\psi + d_n^{**}\cos\psi), \tag{23}$$

$$Area = \pi \cdot SMJA \cdot SMNA, \tag{24}$$

$$Perimeter = 2\pi\sqrt{\frac{SMJA^2 + SMNA^2}{2}}. \tag{25}$$

These four parameters in each harmonic are fed into our feed-forward back-propagation neural-network (FFNN) structure. During training the FFNN, its weighting and biasing values are automatically adjusted. Performance of the developed FFNN model in identifying KDML105 milled rice grains are described in terms of the mean square error (MSE), FAR, and FRR.

This material is reserved for educational purposes. Permission is not allowed for commercial use.
Downloaded From: http://proceedings.spiedigitallibrary.org/ on 01/09/2013 Terms of Use: http://spiedl.org/terms
Please cite this document when use.

4. DEMONSTRATION

4.1 PROTOTYPE SETUP

Our spectral imaging system for the identification of KDML105 milled rice gain is shown in Fig. 5. Compared to our previous work [8], we increase the number of UVC lamps from 2 to 4 with an end-to-end connected arrangement. Each UVC light source is a 5W mercury lamp in a TUV style package from Philips. We also place a reflector plate above UVC lamps. In addition, we move the object plane closer from 195 mm in our previous work to 70 mm. In this scenario, the whole milled rice grains under investigation are uniformly illuminated by stronger UVC light in an area of 50 mm in diameter, inducing stronger fluorescent signals. Our 2-D image device is an 8-bit complementary metal-oxide-semiconductor-based digital camera (Basler Model SCA750-60GC). Its resolution is 480(V) × 752(H) pixels with specified pixel dimensions of 6.0 μm × 6.0 μm. It can capture a sequence image at a specified highest speed of 60 frames/s. A narrow bandpass optical filter centered at the selected 546 nm wavelength is used to allow only the 546-nm fluorescent wavelength spectral image pass through the camera. We also place a UV block filter in front of the narrow bandpass optical filter in order to prevent narrow bandpass optical filter and the 2-D image sensor from damaging by the UVC light.

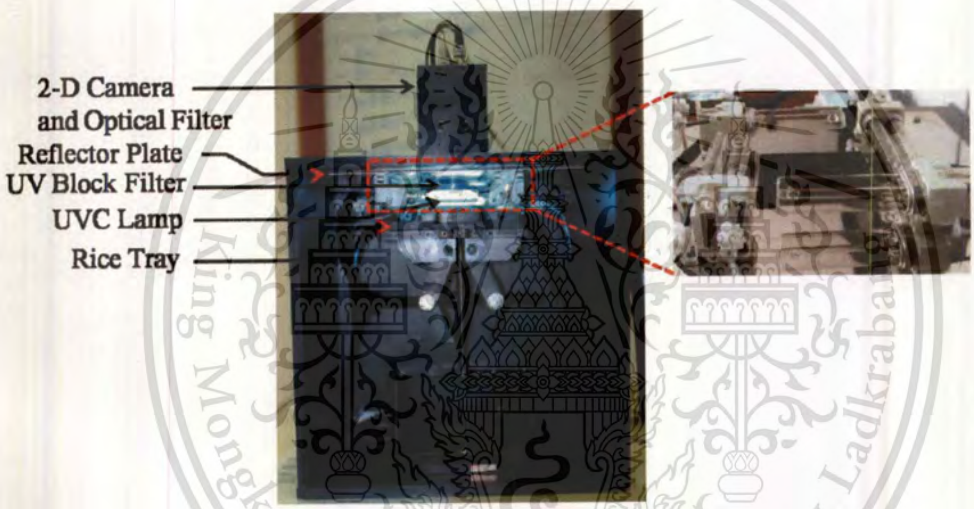

Figure 5. Prototype of our spectral imaging system for KDML105 milled rice breed identification.

4.2 MATERIALS

Milled rice grains from CNT1, HPSL, KDML105, and PTT1 varieties are used in our study as shown in Fig. 6. These milled rice grains have measured average elliptic axes ratios of 0.27 ± 0.01, 0.25 ± 0.01, 0.28 ± 0.01, and 0.27 ± 0.01, respectively. The CNT1 and HPSL have an equivalent amount of amylose content and they are categorized in to a high amylose content type. For KDML105 and PTT1, they both are classified into a low amylose content variety. These milled rice grains are positioned on a black rice tray and they are aligned in the same direction as shown in Fig. 7(a). A total of 800 milled rice grains, 200 for each milled rice variety, are investigated. Fig. 7(b) shows a 235 × 305-pixel spectral image of three CNT1 milled rice varieties captured at 546-nm wavelength. This spectral image is automatically cropped to 90 × 192 pixels in which it contains only one rice grain having an image size of 3730 pixels. This new image size of the rice grain is 1400% compared to the image of the rice grain obtained from our previous system.

This material is reserved for personal use; not allowed for commercial use.
Downloaded From: http://proceedings.spiedigitallibrary.org/ on 01/09/2013 Terms of Use: http://spiedl.org/terms
Redistribution subject to modify the content, and cite the document when use.

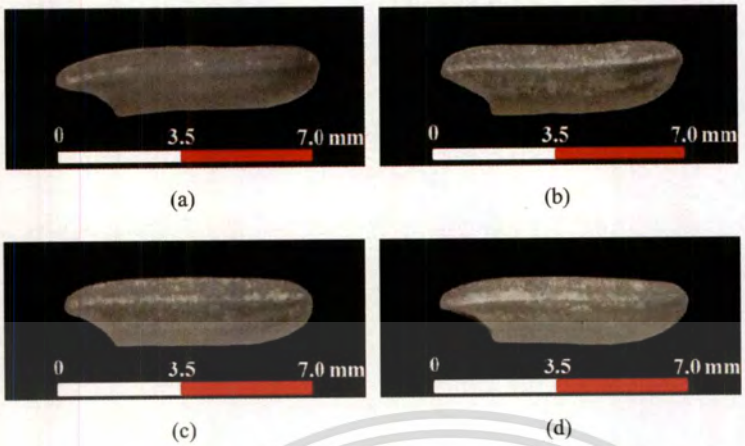

Figure 6. Close-up view of Thai milled rice grains (a) CNT1, (b) HPSL, (c) KDML105, and (d) PTT1 used in our demonstration.

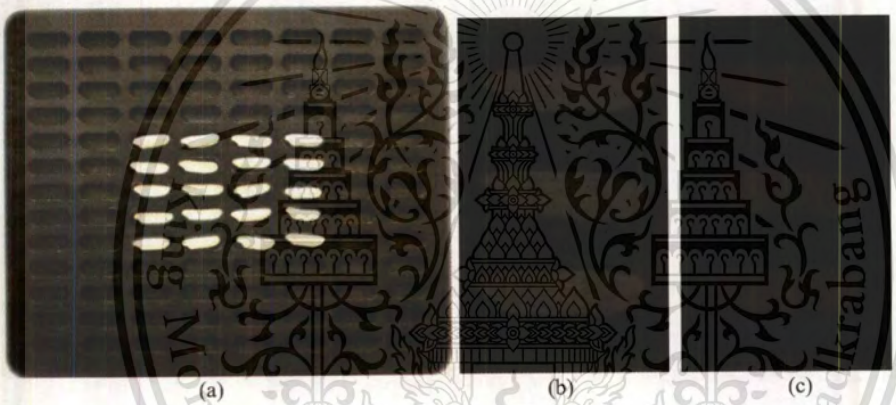

Figure 7. (a) Arrangement of milled rice grains on a black rice tray, (b) a spectral image of milled rice grains, and (c) a normalized spectral image of milled rice grains.

5 RESULTS AND DISCUSSION

The normalized spectral image shown in Fig. 7(c) goes through our image thresholding process. The lower threshold value is varied from 30 to 40. The upper threshold is fixed at 70. As a result, we obtain 11 normalized spectral images as shown in Fig. 8. After that, normalized elliptic Fourier coefficients are computed for each normalized spectral image. In our analysis, only the first 17 harmonics shown in Fig. 9 are taken into consideration.

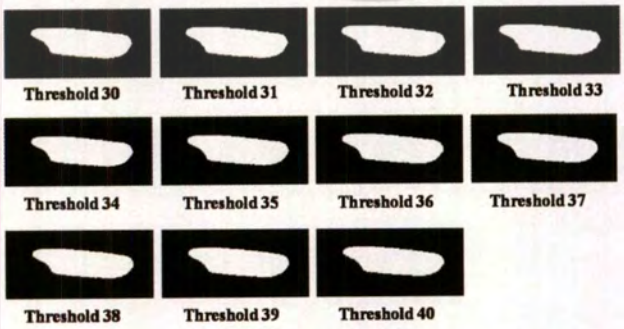

Figure 8. Eleven threshold images under different levels of the lower threshold.

This material is reserved for educational purposes, not allowed for commercial use.
Find more information about this document when use.

From: http://proceedings.spiedigitallibrary.org/ on 01/09/2013 Terms of Use: http://spiedl.org/terms

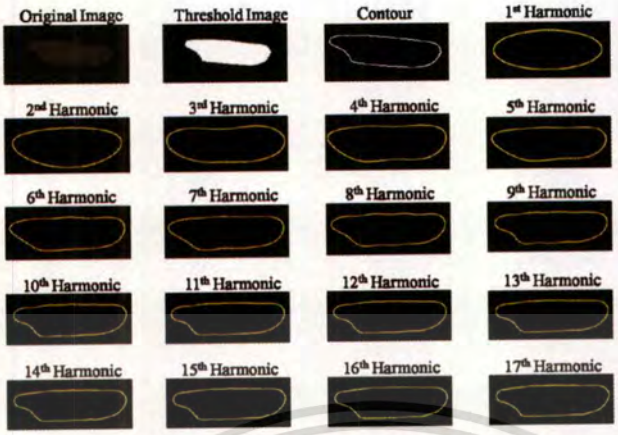

Figure 9. Seventeen normalized EFD harmonics of the "threshold 30" in Fig. 8.

For each harmonic shown in Fig. 9, its normalized Fourier coefficients are calculated which in turn lead to corresponding area, perimeter, semi-major, and semi-minor of that harmonic image. This indicates that there are 68 data obtained from just one threshold image. Fig.10 shows the principle component analysis (PCA) of elliptic parameters. The PCA results point out that a highly-accurate identification of the KMDL105 milled rice variety cannot be accomplished by just directly analyzing all elliptic parameters.

Figure 10. PCA of milled rice grain geometry.

With the use of the FFNN, we divide the elliptic parameters into three pairs: KDML105-CNT1, KDML105-HPSL, and KDML105-PTT1. In each pair of the data set, randomly selected data sets from 100 milled rice grains are used for training the FFNN and the remaining data sets are used for testing the FFNN. Our FFNN configuration contains one input layer with sixty eight (i.e., 17 harmonic images × 4 elliptic parameters = 68 for one threshold image) input ports, four hidden layers, and one output layer. Our four hidden layers have seven, nine, seven, and one nodes with Log-sigmoid, Log-sigmoid, linear and linear transfer functions, respectively. The output layer is assigned to be 1 for the KMDL105 rice variety and 0 for others. During the FFNN training session for 100,000 training epochs via Levenberg–Marquardt function, we adjust all weight and bias values in all layers through the gradient descent weight and bias function with the MSE at the output layer as our learning indicator. Our training results for KDML105-CNT1, KDML105-HPSL, and KDML105-PTT1 take 1:15 h, 2:13 h, and 1:15 h to finish with determined very low MSEs of 5.48×10^{-14}, 8.37×10^{-14}, and 3.91×10^{-15}, respectively.

As described earlier that one spectral image is expanded to 11 threshold images, we obtain 11 output values from the FFNN. These 11 output values are average into one output value. If the average output value is ≥ 0.6, it will be round up to 1, indicating that the spectral image of the milled rice grain under investigation is the KDML105. Identification results of the KMDL105 milled rice grain during the training and testing session are shown in Figs. 11 and 12, respectively. It can be observed that FFNN can efficiently accomplish the goal during its training period. With unknown data sets, our

This material is reserved for educational purposes. Not allowed for commercial use.
Downloaded From: http://proceedings.spiedigitallibrary.org/ on 01/09/2013 Terms of Use: http://spiedl.org/terms
Publication Inc. on behalf of SPIE. Terms of use of this document when use.

FFNN can identify KDML105 milled rice variety from CNT1, HPSL, and PTT1 with measured FARs of 100 × (9/100) = 9.0%, 100 × (10/100) = 10.0%, and 100 × (14/100) = 14.0%, respectively. Their associated FARs of 14.0%, 19.0%, and 24.0% are also determined.

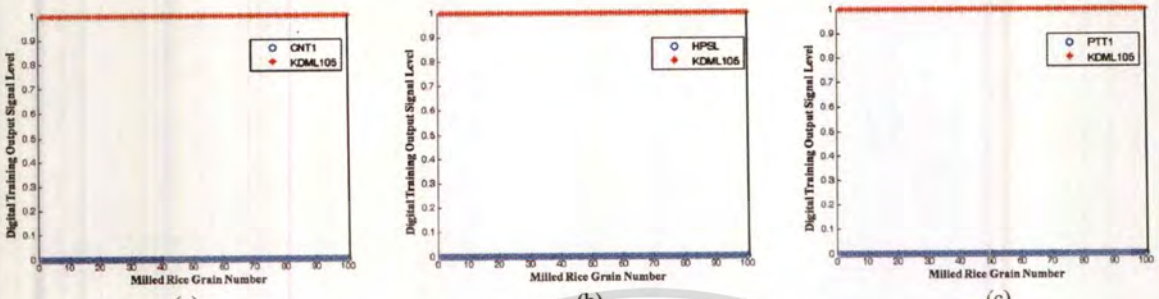

(a) (b) (c)

Figure 11. Training results of each data pair (a) CNT1-KDML105, (b) HPSL2-KDML105, and (c) PTT1-KDML105.

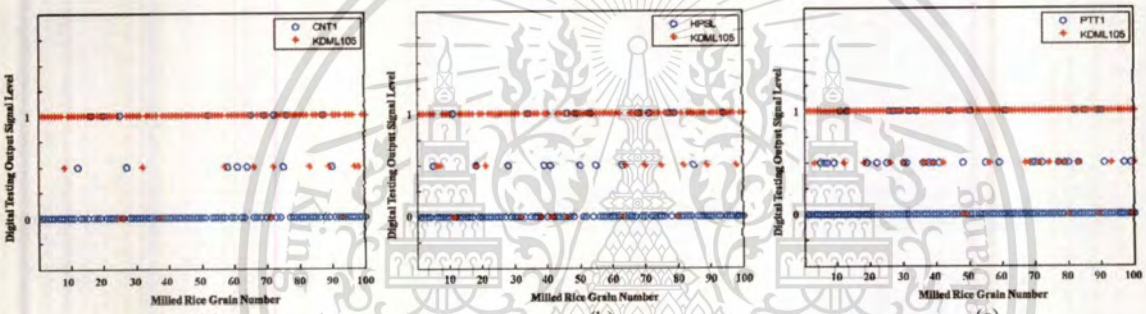

(a) (b) (c)

Figure 11. Testing results of each data pair (a) CNT1-KDML105, (b) HPSL2-KDML105, and (c) PTT1-KDML105.

6 CONCLUSION

We show here our single-wavelength based Thai jasmine rice identification system can be improved by analyzing the spectral image with the use of both EFD and FFNN. Our key approach is to expand one spectral image into 11 threshold images. Then, all threshold images are passed through the chain code method and the EFD is applied in order to define the appropriate elliptic geometry. At the end, the trained FFNN is used for identifying our desired KDML105 milled rice grain via analyzing key elliptical parameters. In our experimental demonstration, we use four UVC light sources, a reflective plate, a 2-D digital camera, a 546-nm wavelength optical filter, and a UV block filter. We also adjust the system such that the shape of the milled rice grain is clear and the fluorescent signal is stronger. For each threshold image, 17 harmonic coefficients are obtained that leads to 17×4 = 68 elliptic parameters for use in the FFNN. Experimental results show the improved average FAR and FRR of 11.0% and 19.0% in identifying the KDML105 milled rice grain from unwanted CNT1, HPSL2, and PTT1 milled rice varieties, respectively.

7 ACKNOWLEDGEMENT

Authors gratefully thank the Rice Research Institute at the Department of Rice, Ministry of Agriculture and Cooperatives of Thailand for supplying rice samples. K. Suwansukho would also like to thank Thailand Graduate Institute of Science and Technology for scholarship support (Grant No. TGIST 01–51-071) and Science Faculty, King Mongkut's Institute of Technology Ladkrabang of Thailand for financial support to attend the conference.

This material is reserved for personal use; redistribution not allowed for commercial use.
From: http://proceedings.spiedigitallibrary.org/ on 01/09/2013 Terms of Use: http://spiedl.org/terms
Explanation of any terms, and cite the document when use.

REFERENCES

[1] Suwansukho, K., Sumriddetchkajorn, S., and Buranasiri, P., "Combination of simple chemical and spectroscopic methods for the identification of Thai Hom Mali rice," Proc. SPIE 7315, 73150W (2009).
[2] Sumriddetchkajorn, S., Suwansukho, K., and Buranasiri, P., "Identification of Thai Hom Mali rice using a refractometer," Proc. SPIE 7315, 73150F (2009).
[3] Sumriddetchkajorn, S. and Intaravanne, Y., "Hyperspectral imaging-based credit card verifier structure with adaptive learning," Appl. Opt. 47, 6594-6600 (2008).
[4] Sumriddetchkajorn, S. and Intaravanne, Y., "Data-nonintrusive photonics-based credit card verifier with a low false rejection rate," Appl. Opt. 49, 764-770 (2010).
[5] Intaravanne, Y., Sumriddetchkajorn, S., Nukeaw, J., "Cell phone-based two-dimensional spectral analysis for banana ripeness estimation," Sens. Act. B 168, 390-394 (2012).
[6] Janchaysang, S., Sumriddetchkajorn, S., and Buranasiri, P., "Tunable filter-based multispectral imaging for detection of blood stains on construction material substrates. part 1. developing blood stain discrimination criteria," Appl. Opt. 51, 6984-6996 (2012).
[7] Sumriddetchkajorn, S., Suwansukho, K., and Buranasiri, P., "Two-wavelength spectral imaging-based Thai rice breed identification," Proc. SPIE 7715, 77150I (2010).
[8] Suwansukho, K., Sumriddetchkajorn, S., and Buranasiri, P., "Demonstration of a single wavelength spectral-imaging-based Thai jasmine rice identification," Appl. Opt. 50, 4024-4030 (2011).
[9] Kuhl, F. P. and Giardina, C. R., "Elliptic Fourier features of a closed contour," Compo. Graph. Ima. Proc. 18, 236-258 (1982).
[10] Crampton, J. S., "Elliptic Fourier shape analysis of fossil bivalves: some practical considerations," Lethaia. 28, 179-186 (1995).
[11] Le Minor, J. M. and Schmittbuhl, M., "Importance of elliptic Fourier methods for morphometry of complex outlines: application to the distal human femur," Surg. Radiol. Anat. 21, 387-391 (1999).
[12] Tort, A., "Elliptical Fourier functions as a morphological descriptor of the genus Stenosarina Brachiopoda, Terebratulida, new caledonia," Mathematical Geology. 35, 873-885 (2003).
[13] Costa, C., Menesatti, P., Aguzzi, J., D'Andrea, S., Antonucci, F., Rimatori, V., Pallottino, F., and Mattoccia, M., "External shape differences between sympatric populations of commercial clams tapes decussates and T. philippinarum," Food Bioprocess Technol. 3, 43-48 (2010).
[14] Ninomiya, S., Ohsawa, R. and Yoshida, M., "Evaluation of buckwheat and tartary buckwheat kernel shape by elliptic Fourier method," Curr. Adv. Buck. Res. 389-396 (1995).
[15] Iwata, H., Niikura, S., Matsuura, S., Takano, Y. and Ukai, Y., "Evaluation of variation of root shape of Japanese radish (Raphanus sativus L.) based on image analysis using elliptic Fourier descriptors," Euphytica 102, 143-149 (1998).
[16] Neto, J. C., Meyer, G. E., Jones, D. D. and Samal, A. K., "Plant species identification using elliptic Fourier leaf shape analysis," Comp. Elect. Argric. 50, 121-134 (2006).
[17] Costa, C., Menesattia, P., Paglia, G., Pallottino, F., Aguzzic, J., Rimatori, V., Russo, G., Recupero, S. and Recupero, G. R., "Quantitative evaluation of Tarocco sweet orange fruit shape using optoelectronic elliptic Fourier based analysis," Post. Bio. Tech. 54, 38-47 (2009).
[18] Sumriddetchkajorn, S. and Intaravanne, Y., "A credit card verifier structure using diffraction and spectroscopy Concepts," Proc. SPIE 7003, 700318 (2008).
[19] Sumriddetchkajorn, S. and Intaravanne, Y., "Evolution of optically nondestructive and data-non-intrusive credit card verifiers," Proc. SPIE 7726, 77261B (2010).
[20] Wondraczek, H., Kotiaho, A., Fardim, P. and Heinze, T., "Photoactive polysaccharides," Carbohydr. Polym. 83, 1048–1061 (2011).
[21] Karatani, H., Kojima, M., Minakuchi, H., Soga, N. and Shizuki, T., "Development and characterization of anodically initiated luminescent detection for alcohols and carbohydrates," Anal. Chim. Acta 337, 207–215 (1997).
[22] Jenkins, P. J. and Donald, A. M., "The influence of amylase on starch granule structure," Int. J. Biol. Macromol. 17,315–321 (1995).
[23] Freeman, H., "On the encoding of arbitrary geometric configuration," IRE Trans. Elec. Comp. 260-268 (1961).
[24] Nafe, R. and Schlote, W., "Methods for shape analysis of two-dimensional closed contours – a biologically importance, but widely neglected field in histopathology," Elec. J. Pathol. Histol. 8.2, 022-02 (2002).

This material is reserved for educational use only, not allowed for commercial use. Forbidden to modify the content and cite the document when use.

From: http://proceedings.spiedigitallibrary.org/ on 01/09/2013 Terms of Use: http://spiedl.org/terms

Single-Wavelength based Thai Jasmine Rice Identification with Polynomial Fitting Function and Neural Network Analysis

Kajpanya Suwansukho[a], Sarun Sumriddetchkajorn[b,*], and Prathan Buranasiri[a]

[a]Physics Department, Faculty of Science
King Mongkut's Institute of Technology Ladkrabang, Bangkok, Thailand

[b]Intelligent Devices and Systems Research Unit
National Electronics and Computer Technology Center (NECTEC)
National Science and Technology Development Agency
Ministry of Science and Technology
112 Thailand Science Park, Phahonyothin Rd, Klong 1, Klong Luang
Pathumthani 12120, Thailand

ABSTRACT

We previously showed that a combination of image thresholding, chain coding, elliptic Fourier descriptors, and artificial neural network analysis provided a low false acceptance rate (FAR) and a false rejection rate (FRR) of 11.0% and 19.0%, respectively, in identify Thai jasmine rice from three unwanted rice varieties. In this work, we highlight that only a polynomial function fitting on the determined chain code and the neural network analysis are highly sufficient in obtaining a very low FAR of < 3.0% and a very low 0.3% FRR for the separation of Thai jasmine rice from Chainat 1 (CNT1), Prathumtani 1 (PTT1), and Hom-Pitsanulok (HPSL) rice varieties. With this proposed approach, the analytical time is tremendously suppressed from 4,250 seconds down to 2 seconds, implying extremely high potential in practical deployment.

Keywords: Rice, Fluorescent imaging, Spectral imaging, Image processing, Chain coding, Polynomial function, Artificial neural network.

1. INTRODUCTION

A well known rice variety of Thailand is Thai jasmine rice or Khaw Dok Mali 105 (KDML105). Sometimes, it was mixed by other lower quality foreign and local rice varieties such as Chainat 1 (CNT1), Hom-Pitsanulok (HPSL), and Prathumtani 1 (PTT1). Previously, we had proposed one-dimensional (1-D) optical spectrum analysis in the visible wavelength region [1] and optical refractometry [2] for separating KDML105 from unwanted rice varieties. However, due to their destructive analysis with poor repeatability, they were not practically acceptable. Another optical approach that promises non-destructive analysis is the spectral imaging technology. This technology has been applied specifically in the research group at NECTEC for data non-intrusive credit card verification [3-5], fruit ripeness estimation [6], and chemical-free blood stain detection [7]. Analysis of the spectral images of rice grains at 545 nm and 575 nm wavelength spectra that were created under high energy ultraviolet light sources was also demonstrated [8]. Because the 575-nm spectral image obtained from available imaging system was weak and it contained little detail of the milled rice grain, the system repeatability and reliability in identifying KDML105 milled rice grains were below the requirement. To improve overall system performance, we proposed and demonstrated that only a single wavelength spectral image at 545 nm wavelength when combined with simple image processing operations was sufficient for the identification of Thai jasmine milled rice grains from the unwanted CNT1, HPSL, and PTT1 milled rice varieties with a measured false acceptance rates (FAR) of <26.7% and a measured false rejection rates (FRR) of 0% [9].

* kajpanya@kmitl.ac.th; Phone+66-2329-8000 ext. 6272

ICPS 2013: International Conference on Photonics Solutions, edited by Prathan Buranasiri, Sarun Sumriddetchkajorn,
Proc. of SPIE Vol. 8883, 888318 · © 2013 SPIE · CCC code: 0277-786X/13/$18 · doi: 10.1117/12.2021861

This material is reserved for personal use, not allowed for commercial use.

From: http://proceedings.spiedigitallibrary.org/ on 02/18/2014 Terms of Use: http://spiedl.org/terms

As there is still a big room in lowering the FAR of our system, we have recently applied elliptic Fourier descriptors (EFDs) to find specific information from the spectral image and then employed a neural network analysis (NNA) to help identify the KDML105 from the three unwanted rice varieties, featuring lower FAR and higher FRR values of 11.0% and 19.0%, respectively [10]. Another limitation in this approach is very long computation time of > 1.1 hrs during the analysis of the specific information via EFDs, implying impracticality.

To suppress the computation time and still achieve very low FAR and FRR values, a less complicated mathematical expression with high degrees of freedom is preferred. One simple mathematical expression is the polynomial as it was previously used for approximating the shape of the image and extracting some important image feature [11-14]. Here, we show that a polynomial function can be used to describe the rice shape from the spectral image and when analyzed by a trained NNA leads to the improvement of FAR, FRR, and processing time in identifying Thai jasmine rice grains.

2. SYSTEM FOR SPECTRAL IMAGE ACQUISITION

The schematic diagram of our single-wavelength spectral imaging system for the identification of KDML105 milled rice breed is illustrated in Fig.1. Main components include a 2-D digital camera, a camera lens, a narrow band-pass optical filter centered at the selected 546 nm fluorescent wavelength spectrum, a UV block filter, high-energy light sources (e.g., UVC at 253.7 nm wavelength), and an electronic controlling and processing unit. The image resolution of 480×752 pixels is assigned and stored as a widely-used TIFF format. This spectral imaging system is controlled by a notebook computer having Intel Core i5 CPU at 2.67 GHz and 1.92 GB RAM.

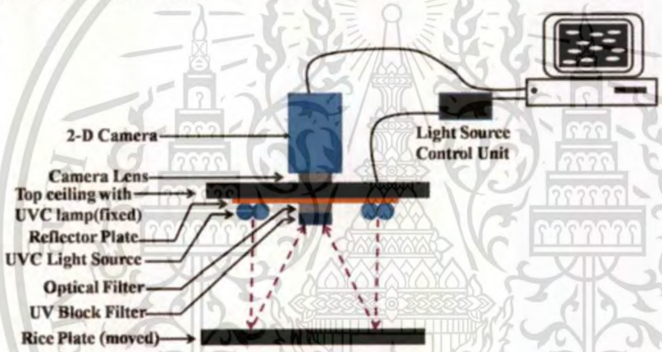

Figure 1. Structure of our single-wavelength spectral imaging system.

3. IMAGE ANALYSIS

The spectral image provide by our spectral imaging-based system in Fig.1 is normalized by its background. The normalized spectral image goes through an image thresholding process in order to filter out unwanted image areas. Our image thresholding can be simply expressed as

$$I'(x,y)=\begin{cases} 255, & Th_{min} \le I(x,y) \le Th_{max} \\ 0, & Otherwise \end{cases} . \quad (1)$$

From Eqn(1), the new gray scale value I′(x, y) will be changed between a minimum and maximum value (e.g.,0-255 for an 8-bit image) depending on our desired range.

This material is reserved for educational use only, not allowed for commercial use.

Forbidden to modify the content and cite the document when use.
From: http://proceedings.spiedigitallibrary.org/ on 02/18/2014 Terms of Use: http://spiedl.org/terms

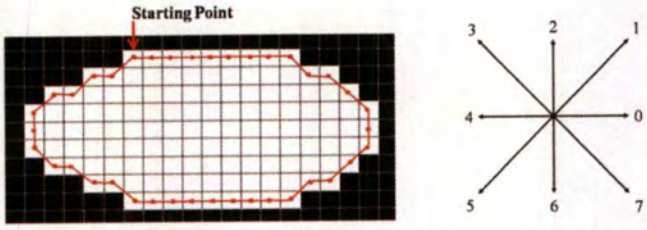

(a) (b)

Figure 2. (a) Binary edge image of a shape pattern with the specific line connection of chain code starting from upper left hand corner and (b) eight specific line direction.

After that, the boundary of a threshold image was defined with Freeman chain codes [15], represented by a sequence of unit vectors and directional coding as shown in Fig. 2. Individual grain boundary pixels are used to describe the chain code, starting with the upper left pixel of the boundary and tracing the boundary clockwise. The chain code enumeration is completed when the original starting point is reached. From Fig. 2(a), a chain code of 00000000707766554544444444343432210101 is obtained by following code directions in Fig. 2(b). It can be assumed that a point at the starting position is travelling along the image boundary with a constant speed. The time used to travel between links depending on the code of the chain which is mathematically written as in Eqn(2).

$$\Delta t_i = 1 + \left(\frac{\sqrt{2}-1}{2} \right) \left(1 - (-1)^{c_i} \right), \tag{2}$$

where c_i is the i^{th} code of the chain code. Eqn(2) is equal to 1 if a code is an even and $\sqrt{2}$ if a code is an odd. For a close contour pattern, the roundtrip time (t_p) can be written as.

$$t_p = \sum_{i=1}^{P} \Delta t_i . \tag{3}$$

Once Δt_i is known, its corresponding travelling distances along the x and y axes can be found as follows.

$$\Delta x_i = signum\ (6 - c_i)\, signum\ (2 - c_i), \tag{4}$$

$$\Delta y_i = signum\ (4 - c_i)\, signum\ (c_i), \tag{5}$$

where

$$signum\ (z) = \begin{cases} 1, & z > 0 \\ 0, & z = 0 \\ -1, & z < 0 \end{cases}. \tag{6}$$

Similarly, close-loop travelling distances along x and y axes can be written as.

$$x_p = \sum_{i=1}^{P} \Delta x_i , \tag{7}$$

$$y_p = \sum_{i=1}^{P} \Delta y_i . \tag{8}$$

To smooth the boundary of the chain coding image, the polynomial function is applied in order to fit line segments that travel along x and y axes with respect to the traversal time. After that, the fitting curves on x and y axes are recombined to reconstruct a new smoothing boundary. The polynomial function of n orders can be defined as

This material is reserved for educational use only, not allowed for commercial use.

Forbidden to modify the content and delete the document when use.

d From: http://proceedings.spiedigitallibrary.org/ on 02/18/2014 Terms of Use: http://spiedl.org/terms

$$f(x) = a_n x^n + a_{n-1} x^{n-1} + \cdots + a_2 x^2 + a_1 x + a_0 . \quad (9)$$

Using the chain coding and the fitted boundary, a geometry feature can be analyzed in terms of perimeter [16], area, and eccentricity [17] by the following equations.

$$length\ (c) = \begin{cases} 1 & for\ \ c = 0,2,4,6, \\ \sqrt{2} & for\ \ c = 1,3,5,7. \end{cases} . \quad (10)$$

$$Area\ = \frac{1}{2}\left|\sum_{i=0}^{p-1} (x_i y_{i+1} - x_{i+1} y_i)\right| . \quad (11)$$

$$Perimeter\ = 0.95 \cdot \sum_{i=0}^{p-1} length\ (c_i) . \quad (12)$$

The lengths of the two principal axes, known as major and minor axes, are equal to the eigenvalues λ_1 and λ_2 of the covariance matrix C of a closed contour, respectively. The matrix C contains a sequence of the ordered pair (x, y) of an image boundary which is projected on x and y axes. The eigenvalues λ_1, λ_2, and the eccentricity can be computed as

$$\det(C - \lambda_{1,2} I) = 0 . \quad (13)$$

$$Eccentrici\ ty = \frac{\lambda_2}{\lambda_1} . \quad (14)$$

4. MATERIALS

Milled rice grains of CNT1, HPSL, KDML105, and PTT1 varieties (Fig.3) are tested. These milled rice grains have measured average eccentricity values of 0.27±0.01, 0.25±0.01, 0.28±0.01, and 0.27±0.01, respectively. These milled rice grains are positioned on a black rice tray and they are aligned in the same direction. A total of 1000 milled rice grains, 250 for each milled rice variety, are investigated.

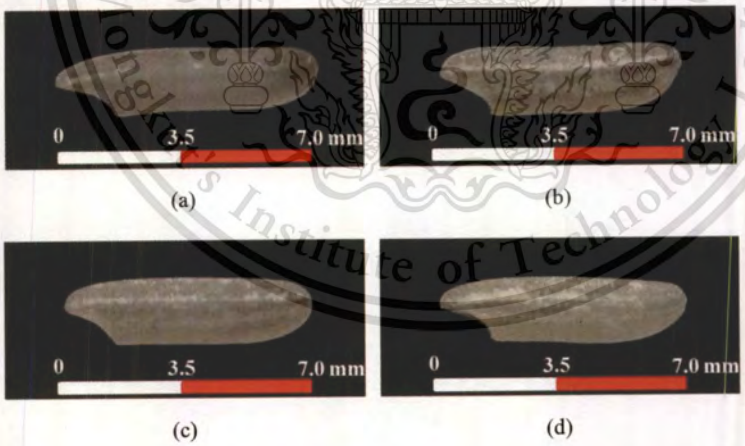

Figure 3. Zoomed image of Thai milled rice grains (a) CNT1, (b) HPSL, (c) KDML105, and (d) PTT1 used in our demonstration.

Fig. 4(a) shows a 235×305-pixel spectral image of three CNT1 milled rice varieties captured at 546-nm wavelength. This spectral image is automatically cropped to 90×192 pixels in which it contains only one rice grain having an image size of 3730 pixels.

This material is reserved for educational use. not allowed for commercial use.
Downloaded From: http://proceedings.spiedigitallibrary.org/ on 02/18/2014 Terms of Use: http://spiedl.org/terms
Terms of use: document when use.

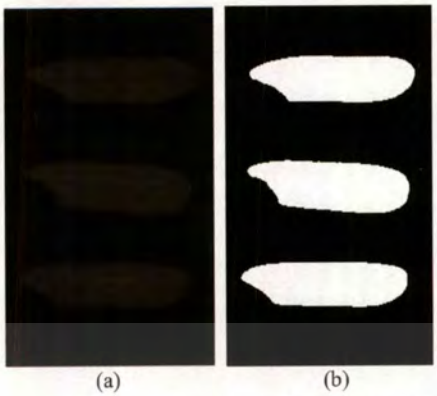

(a) (b)

Figure 4. (a) 235×305 image size of a spectral image of milled rice grains and (b) a threshold image of milled rice grains.

5. RESULTS AND DISCUSSION

The spectral image in Fig. 4(a) is normalized by the background and goes through our image thresholding process whose lower and upper threshold values are fixed at 30 and 70, respectively. The threshold image is shown in Fig. 4(b). After that, the boundaries of the threshold images are determined by the chain coding process as shown in Fig. 5(a). As mentioned earlier, the image boundary can be plotted along the travelling distance on x and y axes with respect to the travelling time as shown in Fig. 5(b-c), respectively.

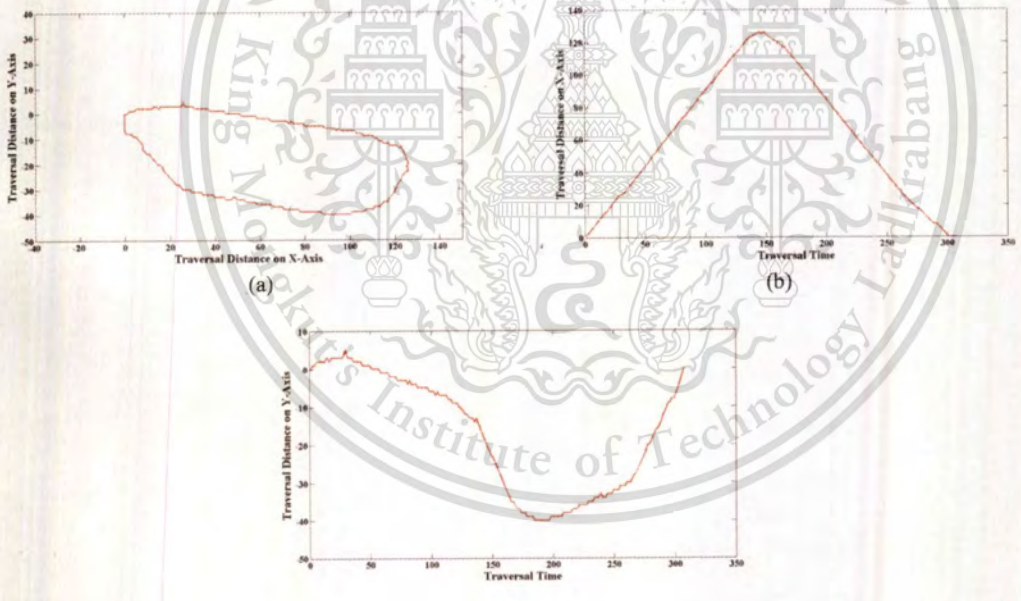

(a) (b)

(c)

Figure 5. (a) Boundary of the threshold image computed from the chain coding process. (b-c) Line segments of the image boundary projected on the x and y axes, respectively.

Line segments in Fig.5 (b-c) are then fitted by using a polynomial function in Eqn(9). Fitted polynomial lines associated with the boundary segments travelling along x and y axes are manifested in Fig.6(a) and Fig.6(b), respectively. The orders of the polynomial fitting functions are 15 and 12 for the traversal distances on x and y axes with corresponding linear regression of 0.99984 and 0.99843, respectively. Finally, both fitted polynomial curves are reconstructed to form a new boundary image of a milled rice image as shown in Fig. 6(c).

This material is reserved for educational use only, not allowed for commercial use.

Forbidden to modify the content and logo of this document when use.

From: http://proceedings.spiedigitallibrary.org/ on 02/18/2014 Terms of Use: http://spiedl.org/terms

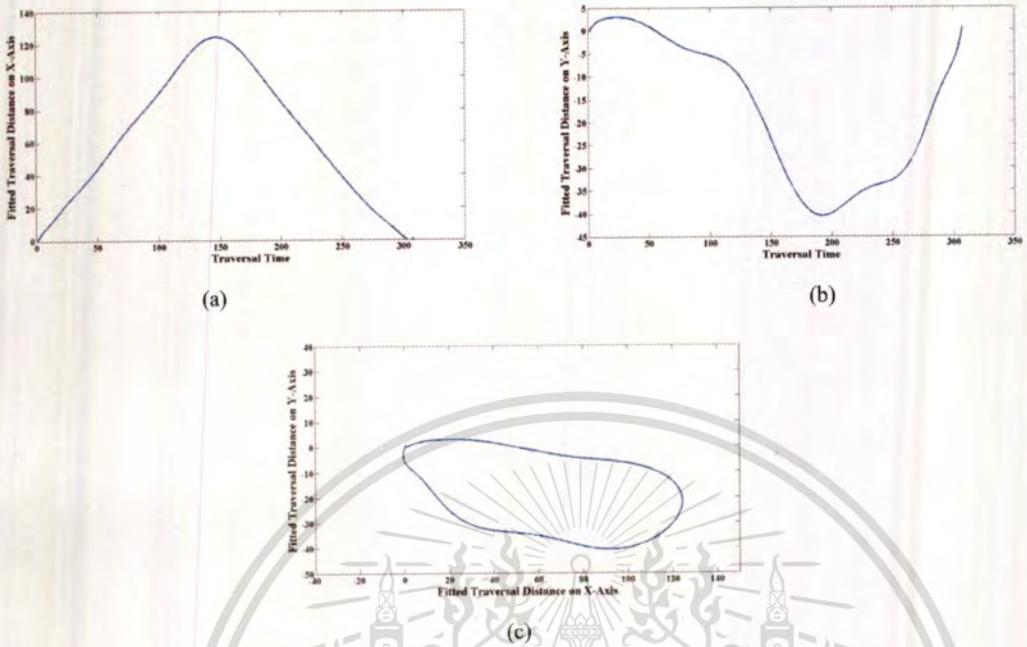

Figure 6. Fitted line segments of the travelling distances along the (a) x axis and (b) y axis. (c) Reconstructed image contour from the fitted line segments in (a) and (b).

With the use of the feed forward back propagation neural network (FFNN), we divide the shape parameters into three pairs: CNT1-KDML105, HPSL-KDML105, and PTT1-KDML105. In each pair of the data set, randomly selected data sets from 150 milled rice grains are used for training the FFNN and the remaining data sets are used for testing the FFNN. Our FFNN configuration contains one input layer with three (i.e., area, perimeter and eccentricity for one threshold image) input ports, four hidden layers, and one output layer. Our four hidden layers have eleven, fifteen, eleven, and one nodes with Log-sigmoid, Log-sigmoid, Log-sigmoid and linear transfer functions, respectively. The output layer is assigned to be 1 for the KMDL105 rice variety and 0 for others. During the FFNN training session for 100,000 training epochs via Levenberg–Marquardt function, all weight and bias values in all layers are automatically adjusted through the gradient descent weight and bias function with the mean square error (MSE) at the output layer as our learning indicator. Our training results for CNT1-KDML105, HPSL-KDML105, and PTT1-KDML105 pairs take 1:20 h, 1:18 h, and 1:18 h to finish with determined very low MSEs of 3.95×10^{-16}, 2.21×10^{-19}, and 5.13×10^{-13}, respectively.

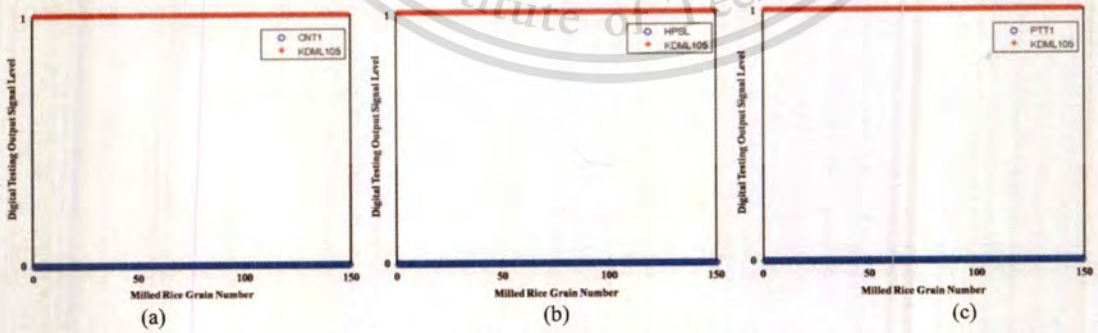

Figure 7. Training results of each data pair (a) CNT1-KDML105, (b) HPSL-KDML105, and (c) PTT1-KDML105.

Identification results of the KMDL105 milled rice grain during the training and testing sessions are shown in Figs. 7 and 8, respectively. It can be observed that our FFNN can efficiently accomplish the goal during its training period. With

This material is reserved for personal use; not allowed for commercial use.

Downloaded From: http://proceedings.spiedigitallibrary.org/ on 02/18/2014 Terms of Use: http://spiedl.org/terms
Terms of use: http://spiedl.org/terms Use of this document when use.

unknown data sets, our FFNN can identify KDML105 milled rice variety from CNT1, HPSL, and PTT1 with measured FARs of 0.0%, 0.0%, and 3.0%, respectively. Their associated FRRs of 0.0%, 0.0%, and 1.0% are also determined.

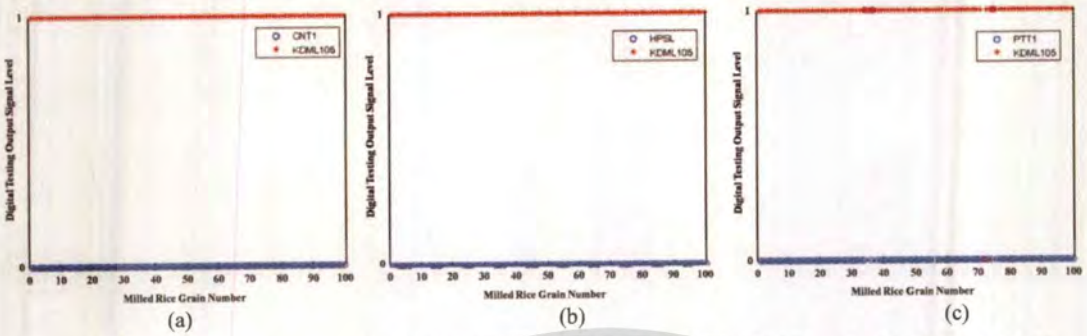

Figure 8. Testing results of each data pair (a) CNT1-KDML105, (b) HPSL-KDML105, and (c) PTT1-KDML105.

6. CONCLUSION

We show that our single-wavelength based Thai jasmine rice identification system can be improved by using a polynomial function and a well trained FFNN. All threshold images are passed through the chain code method and the polynomial function is applied in order to define the appropriate geometry feature. At the end, the trained FFNN is used for identifying our desired KDML105 milled rice grain via analyzing key shape parameters (area, perimeter and eccentricity). Experimental results show much improved average FAR and FRR of < 3.0% and 0.3% in identifying the KDML105 milled rice grain from unwanted CNT1, HPSL, and PTT1 milled rice varieties, respectively.

7. ACKNOWLEDGEMENT

Authors gratefully thank the Rice Research Institute at the Department of Rice, Ministry of Agriculture and Cooperatives of Thailand for supplying rice samples. K. Suwansukho would also like to thank Thailand Graduate Institute of Science and Technology for scholarship support (Grant No. TGIST 01–51-071) and Science Faculty, King Mongkut's Institute of Technology Ladkrabang of Thailand for financial support to attend the conference.

REFERENCES

[1] Suwansukho, K., Sumriddetchkajorn, S., and Buranasiri, P., "Combination of simple chemical and spectroscopic methods for the identification of Thai Hom Mali rice," *Proc. SPIE* 7315, 73150W (2009).

[2] Sumriddetchkajorn, S., Suwansukho, K., and Buranasiri, P., "Identification of Thai Hom Mali rice using a refractometer," *Proc. SPIE* 7315, 73150F (2009).

[3] Sumriddetchkajorn, S. and Intaravanne, Y., "Hyperspectral imaging-based credit card verifier structure with adaptive learning," *Appl. Opt.* 47, 6594-6600 (2008).

[4] Sumriddetchkajorn, S. and Intaravanne, Y., "Data-nonintrusive photonics-based credit card verifier with a low false rejection rate," *Appl. Opt.* 49, 764-770 (2010).

[5] Sumriddetchkajorn, S. and Intaravanne, Y., "Evolution of optically nondestructive and data-non-intrusive credit card verifiers," *Proc. SPIE* 7726, 77261B (2010).

[6] Intaravanne, Y., Sumriddetchkajorn, S., Nukeaw, J., "Cell phone-based two-dimensional spectral analysis for banana ripeness estimation," *Sens. Act. B* 168, 390-394 (2012).

[7] Janchaysang, S., Sumriddetchkajorn, S., and Buranasiri, P., "Tunable filter-based multispectral imaging for detection of blood stains on construction material substrates. Part 1. Developing blood stain discrimination criteria," *Appl. Opt.* 51, 6984-6996 (2012).

[8] Sumriddetchkajorn, S., Suwansukho, K., and Buranasiri, P., "Two-wavelength spectral imaging-based Thai rice breed identification," *Proc. SPIE* 7715, 77150l (2010).

[9] Suwansukho, K., Sumriddetchkajorn, S., and Buranasiri, P., "Demonstration of a single wavelength spectral-imaging-based Thai jasmine rice identification," *Appl. Opt.* 50, 4024-4030 (2011).

This material is reserved for educational use only, not allowed for commercial use.
Downloaded From: http://proceedings.spiedigitallibrary.org/ on 02/18/2014 Terms of Use: http://spiedl.org/terms
Additional terms may apply to the use of this document when use.

[10] Suwansukho, K., Sumriddetchkajorn, S., and Buranasiri, P., "Improvement of single-wavelength based Thai jasmine rice identification with elliptic Fourier descriptor and neural network analysis," *Proc. SPIE* 8558, 85580C (2012).
[11] Sadeh, I., "Polynomial Approximation of image," *Comp. Math. Appl.* 32, 99-115 (1996).
[12] Kocic, L. M., and Milovanovic, G. V., "Shape preserving approximations by polynomial and splines," *Comp. Math. Appl.* 33, 59-97 (1997).
[13] Baggenstoss, P. M., "Image distortion analysis using polynomial series expansion," *IEEE Trans. Patt. Anal. Mach. Intel.* 26, 1438-1451 (2004).
[14] Kaveti, A., Teoh, K. K., and Wang, H., "Second order implicit polynomials for segmentation of range images," *Patt. Reg.* 29, 937-949 (1996).
[15] Freeman, H., "On the encoding of arbitrary geometric configuration," *IRE Trans. Elec. Comp.* 10(2), 260-268 (1961).
[16] Burger, W., and Burge, M. J., [Digital image processing: an algorithmic introduction using Java], Springer Publisher, New York, 223 (2008).
[17] Mingqiang, Y., Kidiyo, K., and Joseph, R., "A survey of shape feature extraction techniques," *Patt. Rec.* 43-90 (2008).

King Mongkut's Institute of Technology Ladkrabang

This material is reserved for personal use; redistribution not allowed for commercial use.
Downloaded From: http://proceedings.spiedigitallibrary.org/ on 02/18/2014 Terms of Use: http://spiedl.org/terms
Additional terms may apply to the document when use.

Fast fluorescent imaging-based Thai jasmine rice identification with polynomial fitting function and neural network analysis

Kajpanya Suwansukho,[1] Sarun Sumriddetchkajorn,[2,*] and Prathan Buranasiri[1]

[1]Physics Department, Faculty of Science, King Mongkut's Institute of Technology Ladkrabang, Bangkok, Thailand

[2]Intelligent Devices and Systems Research Unit, National Electronics and Computer Technology Center (NECTEC), National Science and Technology Development Agency, Ministry of Science and Technology, 112 Thailand Science Park, Phahonyothin Rd. Klong 1, Klong Luang, Pathumthani 12120, Thailand

*Corresponding author: sarun.sumriddetchkajorn@nectec.or.th

Received 17 February 2014; accepted 24 February 2014;
posted 28 February 2014 (Doc. ID 206227); published 31 March 2014

With our single-wavelength spectral-imaging-based Thai jasmine rice identification system, we emphasize here that a combination of an appropriate polynomial fitting function on the determined chain code and a well-trained neural network configuration is highly sufficient in achieving a low false acceptance rate (FAR) and a low false rejection rate (FRR). Experimental demonstration shows promising results in identifying our desired Thai jasmine rice from six unwanted rice varieties with FAR and FRR values of 6.2% and 7.1%, respectively. Additional key performances include a much faster identification time of 30.5 s, chemical-free analysis, robustness, and adaptive learning. © 2014 Optical Society of America

OCIS codes: (260.2510) Fluorescence; (120.0120) Instrumentation, measurement, and metrology; (100.0100) Image processing; (100.5010) Pattern recognition; (120.4290) Nondestructive testing.
http://dx.doi.org/10.1364/AO.53.002206

1. Introduction

As Thai jasmine rice or Khaw Dok Mali 105 (KDML105) is one of the best rice varieties, it is sometimes blended with other cheaper rice varieties, such as Chainat 1 (CNT1), Hom-Pitsanulok 2 (HPSL2), Hom-Supanburi 60 (HSPR60), Prathumtani 1 (PTT1), RD15, and RD23. Instead of analyzing the rice starch solution via a 1D optical spectrometer [1] and an optical refractometer [2], a nondestructive approach via a 2D spectral imaging analysis is preferred. This technology has been applied in a variety of applications, including data nonintrusive credit card verification [3–5], fruit ripeness estimation [6], silkworm gender classification [7–9], and chemical-free blood-stain detection [10–12], to name a few.

For the KDML105 rice identification point of view, the analysis of the fluorescent spectral images of rice grains at 545 and 575 nm wavelength strongly created under the excitation of high-energy ultraviolet light sources were proposed and demonstrated [13,14]. Especially, our single-wavelength spectral imaging-based approach via a combination of simple image processing, elliptic Fourier descriptor (EFD), and neural network analysis (NNA) promisingly showed a moderate false acceptance rate (FAR) of 11.0% and false rejection rate (FRR) of 19.0%, respectively [15]. However, its main limitation is the long identification time of 1.20 h in the EFD process. With this concern, one interesting approach is to use a simple polynomial function instead of complicated EFDs. Previously, polynomial functions were used for approximating the shape of the image in order to help in extracting some important image features [16–19]. Hence we propose and experimentally

1559-128X/14/102206-07$15.00/0
© 2014 Optical Society of America

This material is reserved for educational use only, not allowed for commercial use.
Forbidden to modify the content, and cite the document when use.

demonstrate in this work that a combination of polynomial functions and NNA applied on the spectral image of the rice grain can identify the KDML105 milled rice variety with a much faster response time and still achieve low FAR and FRR values [20]. In particular, we perform field operation tests for 55 extra sample sets and find that a more optimized NNA revamps FAR and FRR values to 6.2% and 7.1%, respectively. This is unlike our unoptimized NNA in [20] that worsens the FAR and FRR values down to 69.7% and 22.8%, respectively. Other key features include chemical-free analysis, robustness, and adaptive learning.

2. Our Fluorescent Imaging-Based Thai Jasmine Rice Identification System

A. Setup

The schematic diagram of our single-wavelength spectral imaging system for the identification of KDML105 milled rice variety is illustrated in Fig. 1. The main components include a 2D digital camera, a camera lens, a narrow bandpass optical filter centered at the selected 546 nm fluorescent wavelength spectrum, a UV block filter, high-energy light sources (e.g., UVC lamps at 253.7 nm wavelength), and an electronic controlling and processing unit. The image resolution of 480 × 752 pixels is assigned and stored as a widely used TIFF format in 8-bit. This spectral imaging system is controlled by a notebook computer having an Intel Core i5 CPU at 2.67 GHz clock speed and 1.92 GB RAM. The black rice tray in Fig. 2 contains 104 rice slots with 75 mm × 90 mm. It is made from black anodized aluminum. Each rice slot has dimensions of 2 mm × 8 mm × 2 mm. Note that, with today's advanced electronics industry, the 2D camera in our single-wavelength spectral imaging system can be a mass-produced color camera such as a web-based camera and a camera embedded in a mobile phone or a tablet.

B. Image Analysis

In the beginning of our image analysis, the spectral image provided by our single-wavelength spectral imaging-based Thai jasmine rice identification system in Fig. 1 is normalized by its background.

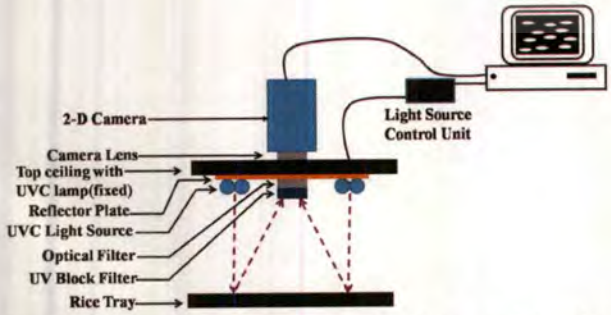

Fig. 1. Structure of our single-wavelength spectral imaging-based Thai jasmine rice identification system.

Fig. 2. Our rice tray with 20 milled rice grains on the rice slot.

The normalized spectral image goes through an image-thresholding process in order to filter out unwanted image areas. Our image thresholding can be simply expressed as

$$I'(x,y) = \begin{cases} 255, & \mathrm{Th}_{\min} \le I(x,y) \le \mathrm{Th}_{\max} \\ 0, & \text{Otherwise} \end{cases}. \quad (1)$$

From Eq. (1), the new gray-scale value $I'(x,y)$ will be changed between minimum and maximum values (e.g., 0–255 for an 8-bit image) depending on our desired range.

After that, Freeman chain codes [21] are applied in order to define the edge of the threshold image, which is represented by a sequence of unit vectors and their associated directional codes as shown in Fig. 3. Individual grain boundary pixels are used to describe the chain code, starting with the upper-left pixel of the boundary and tracing the boundary clockwise. The chain code enumeration is completed when the original starting point is reached. From Fig. 3(a), a chain code of 00000000707766554544444444343432210101 is obtained by following code directions in Fig. 3(b). It can be assumed that a point at the starting position is travelling along the image boundary with a constant speed. The time used to travel between links is dependant on the code of the chain which is mathematically written as

$$\Delta t_i = 1 + \left(\frac{\sqrt{2}-1}{2}\right)(1-(-1)^{c_i}), \quad (2)$$

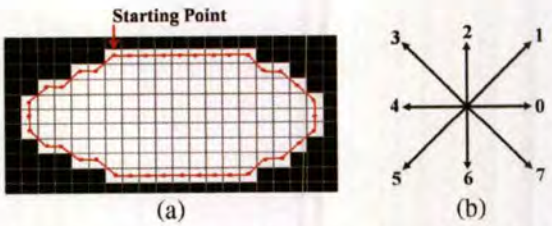

Fig. 3. (a) Binary edge image of a shape pattern with the specific line connection of chain codes starting from upper-left-hand corner and (b) eight specific line directions.

This material is reserved for educational use only, not allowed for commercial use.
Forbidden to modify the content, and cite the document when use.

where c_i is the ith code of the chain code. Equation (2) is equal to 1 if a code is an even and $\sqrt{2}$ if a code is an odd. For a close contour pattern, the roundtrip time is the sum of Eq. (2). Once Δt_i is known, its corresponding travelling distances along the x and y axes can be found as follows:

$$\Delta x_i = \text{signum}(6 - c_i)\text{signum}(2 - c_i), \tag{3}$$

$$\Delta y_i = \text{signum}(4 - c_i)\text{signum}(c_i), \tag{4}$$

where

$$\text{signum}(z) = \begin{cases} 1 & z > 0 \\ 0 & z = 0 \\ -1 & z < 0 \end{cases}. \tag{5}$$

Similarly, close-loop travelling distances along x and y axes can be written as

$$x_p = \sum_{i=1}^{p} \Delta x_i, \tag{6}$$

$$y_p = \sum_{i=1}^{p} \Delta y_i. \tag{7}$$

To smooth the edge of the chain coding image, the polynomial function is applied in order to fit line segments that travel along the x and y axes with respect to the traversal time. After that, the fitting curves on x and y axes are recombined to reconstruct a new smoothing boundary. The polynomial function of n orders can simply be defined as

$$f(x) = a_n x^n + a_{n-1}x^{n-1} + \cdots + a_2 x^2 + a_1 x + a_0. \tag{8}$$

Using the chain coding and the fitted boundary, a geometry feature can be analyzed in terms of perimeter and area [22] by the following equations:

$$\text{Perimeter} = 0.95 \cdot \sum_{i=0}^{p-1} \text{length}(c_i), \tag{9}$$

and

$$\text{Area} = \frac{1}{2}\left|\sum_{i=0}^{p-1}(x_i y_{i+1} - x_{i+1}y_i)\right|, \tag{10}$$

where,

$$\text{length}(c) = \begin{cases} 1 & \text{for } c = 0, 2, 4, 6, \\ \sqrt{2} & \text{for } c = 1, 3, 5, 7 \end{cases}. \tag{11}$$

Another important parameter is the eccentricity. Theoretically, the lengths of the two principal axes, known as major and minor axes, are equal to the eigenvalues λ_1 and λ_2 of the covariance matrix C of a closed contour, respectively. The matrix C contains a sequence of the ordered pair (x,y) of an image boundary, which is projected on the x and y axes [23]. In this scenario, the λ_1 and λ_2 can be found from $\det(C - \lambda_{1,2}I) = 0$. Once the two eigenvalues are known, the eccentricity can be computed as

$$\text{Eccentricity} = \frac{\lambda_2}{\lambda_1}. \tag{12}$$

3. Materials

Milled rice grains of CNT1, HPSL2, HSPR60, KDML105, PTT1, RD15, and RD23 varieties (Fig. 4) are prepared by the Rice Research Institute in Thailand. Their corresponding width and length ratios average 0.27 ± 0.01, 0.25 ± 0.01, 0.28 ± 0.01, 0.28 ± 0.01, 0.27 ± 0.01, 0.27 ± 0.01, and 0.28 ± 0.01, respectively. These milled rice grains are positioned on our black rice tray, and they are aligned in the same direction. A total of 1750 milled rice grains, 250 for each milled rice variety, are investigated. Note that, as there are variations in the image texture of milled rice grains due to the polishing and milling processes, the image texture of the milled rice grain cannot be used to distinguish these rice varieties. Since the morphological characters of grains are heritable in nature [24], this work focuses on the shape analysis for the identification of KDML105.

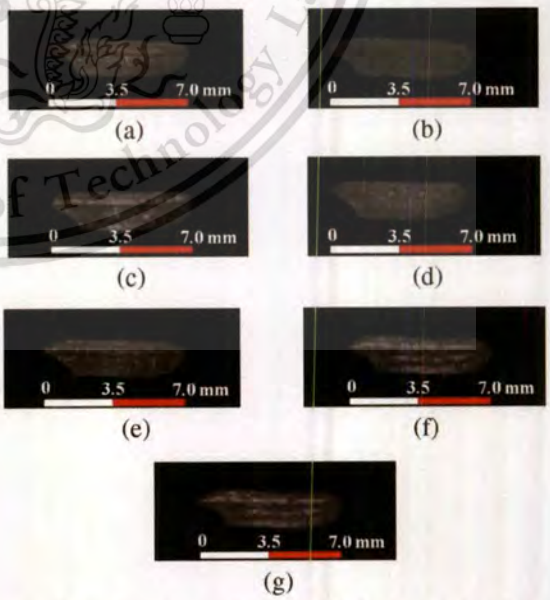

Fig. 4. Zoomed images of Thai milled rice grains from six varieties: (a) CNT1, (b) HPSL2, (c) HSPR60, (d) KDML105, (e) PTT1, (f) RD15, and (g) RD23.

This material is reserved for educational use only, not allowed for commercial use.
Forbidden to modify the content, and cite the document when use.

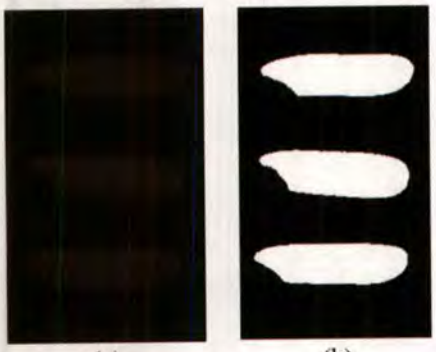

(a) (b)

Fig. 5. (a) 235 × 305 pixel image size of a spectral image of milled rice grains and (b) its threshold image.

4. Results and Discussion

The spectral image in Fig. 5(a) shows a 235 × 305 pixel spectral image of three CNT1 milled rice grains captured at 546 nm wavelength. This spectral image is normalized by the background and goes through our image-thresholding process whose lower and upper threshold values are fixed at 30 and 70, respectively, as shown in Fig. 5(b). After that, it is automatically cropped to 90 × 192 pixels in which it contains only one rice grain having an image size of 3730 pixels.

After that, the edges of the threshold images are determined by the chain coding process as shown in Fig. 6(a). As mentioned earlier, the image boundary can be manifested in terms of travelling distances along the x and y axes with respect to the travelling time as shown in Figs. 6(b) and 6(c), respectively.

Each line segment in Figs. 6(b) and 6(c) is then fitted by using a polynomial function in Eq. (8). Fitted polynomial lines associated with the boundary segments travelling along the x and y axes are manifested in Figs. 7(a) and 7(b), respectively. The orders of the fitted polynomial functions are 15 and 12 for the traversal distances on the x and y axes, with the corresponding linear regression of better than 99.9%. Finally, both fitted polynomial curves are reconstructed to form a new edge image of a milled rice image as shown in Fig. 7(c). Immediately, three shape parameters in terms of perimeter, area, and eccentricity are extracted as shown in Fig. 8 with their averaging values highlighted in Table 1.

It seems that the perimeter and area of KDML105 were strongly overlapped with RD15 and RD23, slightly mixed with CNT1 and PTT1, and clearly separated from the remaining milled rice varieties as shown in Figs. 8(a) and 8(b). On the contrary, the eccentricity of all milled rice variety seems hard to distinguish one from another as shown in Fig. 8(c). However, with these slight differences of the KDML105 from the unwanted milled rice varieties, a principal component analysis obviously shows high potential in separating the desired KDML105 milled rice variety from the remaining ones, as shown in Fig. 9.

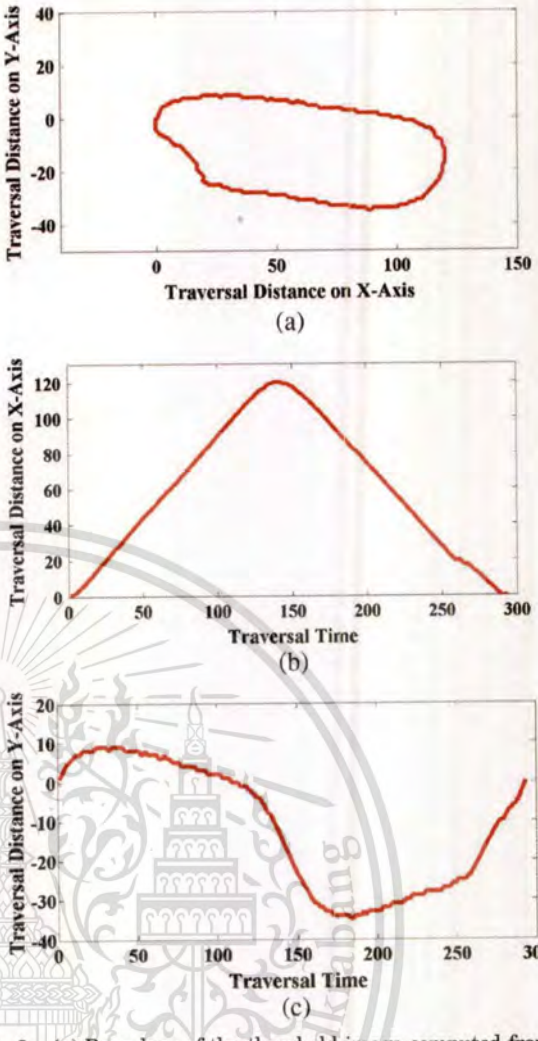

Fig. 6. (a) Boundary of the threshold image computed from the chain coding process. (b) and (c) Line segments of the image boundary projected on the x and y axes, respectively.

With the use of the FFNNA, all milled rice varieties are analyzed together. In the data set, randomly selected data sets from 150 milled rice grains are used for training the FFNNA, and the remaining data sets are used for testing the FFNNA. Our FFNNA configuration contains one input layer with three input ports for receiving area, perimeter, and eccentricity parameters, four hidden layers, and one output layer. Our four hidden layers have 15, 21, 17, and 1 nodes with Log-sigmoid, Log-sigmoid, Log-sigmoid, and linear transfer functions, respectively. The output layer is assigned to be 1 for the KMDL105 milled rice variety and 0 for the others.

During the FFNNA training session for 100,000 training epochs via Levenberg–Marquardt function, all weight and bias values in all layers are automatically adjusted through the gradient descent weight and bias function with the mean square error (MSE) at the output layer as our learning indicator. Our training results take 8:25 h to finish with determined low MSEs of 7.40×10^{-8}. Identification results

This material is reserved for educational use only, not allowed for commercial use.
Forbidden to modify the content, and cite the document when use.

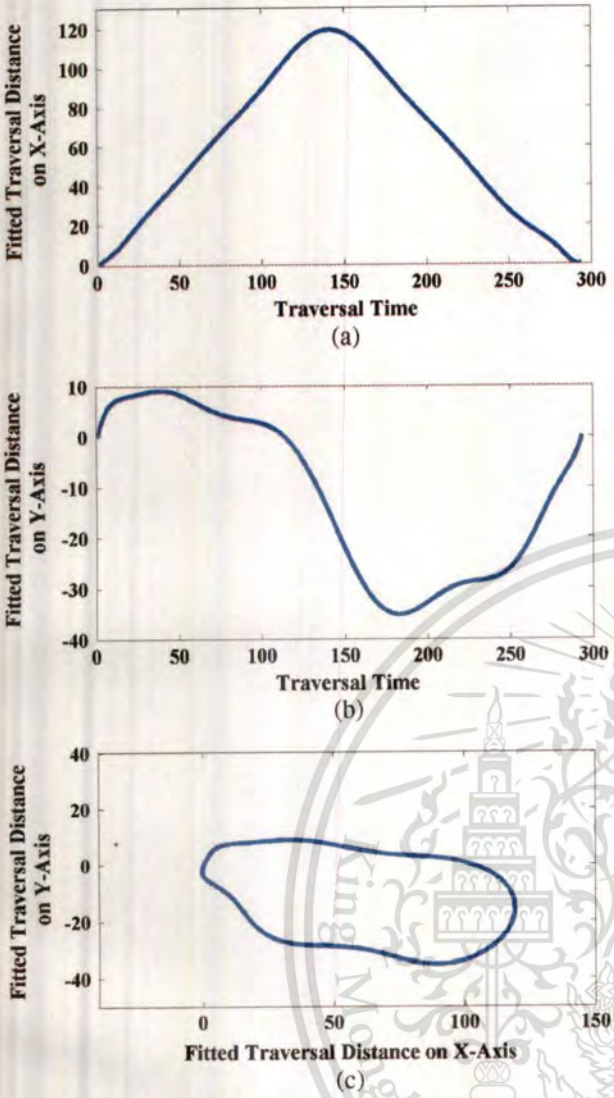

Fig. 7. Fitted line segments of the travelling distances along the (a) x axis and (b) y axis. (c) Reconstructed image contour from the fitted line segments in (a) and (b).

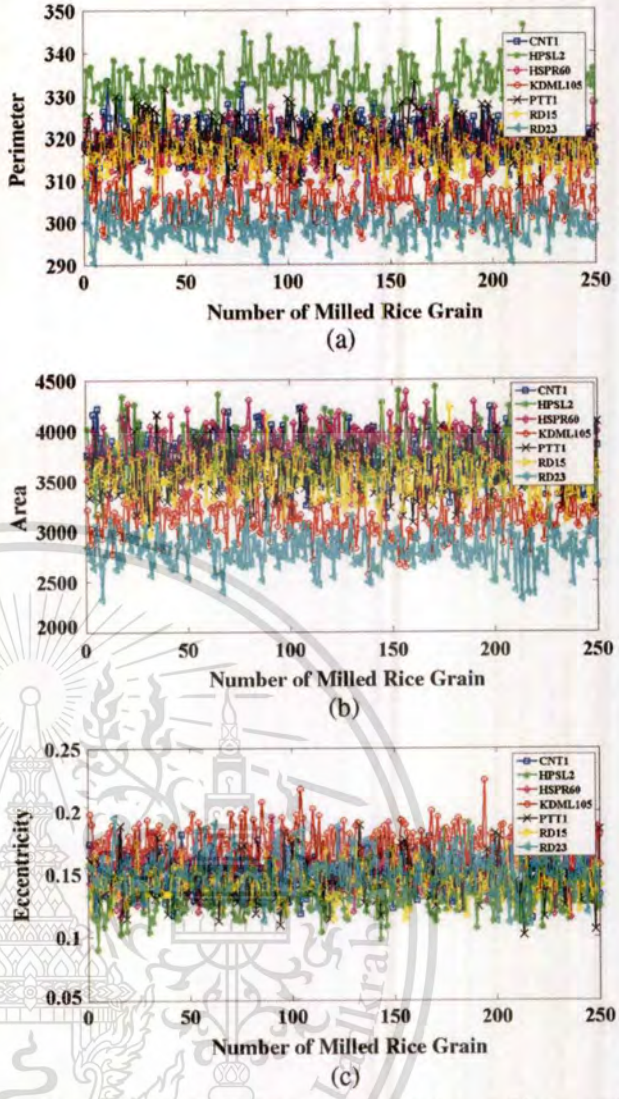

Fig. 8. Plotted graphs of the extracted (a) perimeter, (b) area, and (c) eccentricity parameter.

of the KMDL105 milled rice grain during the training and testing sessions are shown in Figs. 10(a) and 10(b), respectively. It can be observed that our FFNNA can efficiently accomplish the goal during its training period. With unknown data sets prepared at the same time, our FFNNA can identify KDML105 milled rice variety mixed with CNT1, HPSL2, HSPR60, PTT1, RD15, and RD23 with measured FARs of 1.7%. Their associated FRRs of 7.0% are also determined. In this scenario, a very fast identification time of 30.5 s is obtained, limited by a 30 s warming time for UV lamps. This indicates a much improvement in speed of 1.20 h/30.5 s = 157.4 times.

To demonstrate the robustness of our single-wavelength spectral-imaging-based Thai jasmine rice identification system, we perform field operation tests for 55 extra sample sets (i.e., 165 milled rice grains) with random arrangement of rice varieties. In this scenario, a number of KDML105 milled rice grain is 81. Figure 11 shows two randomly selected spectral images used in the demonstration. We obtain five and six identification mistakes as shown in Fig. 12. This indicates that low FAR and FRR are $(5/81) \times 100 = 6.2\%$ and $(6/84) \times 100 = 7.1\%$ in identifying the KDML105 mixed with other milled rice varieties, respectively.

Table 1. Average Values of Three Shape Parameters

Rice Variety	Perimeter	Area	Eccentricity
CNT1	319.33	3716.30	0.1466
HPSL2	332.83	3772.87	0.1309
HSPR60	317.79	3829.02	0.1562
KDML105	304.88	3111.57	0.1725
PTT1	319.48	3585.41	0.1457
RD15	316.44	3539.50	0.1443
RD23	299.67	2819.38	0.1518

This material is reserved for educational use only, not allowed for commercial use.
Forbidden to modify the content, and cite the document when use.

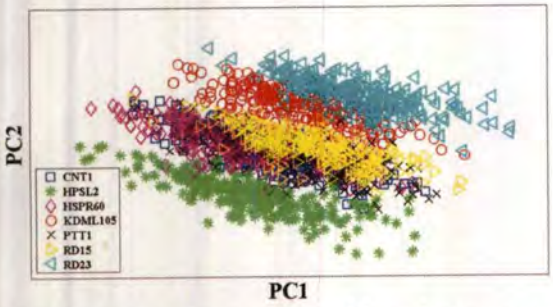

Fig. 9. Principal component analysis of three shape parameters.

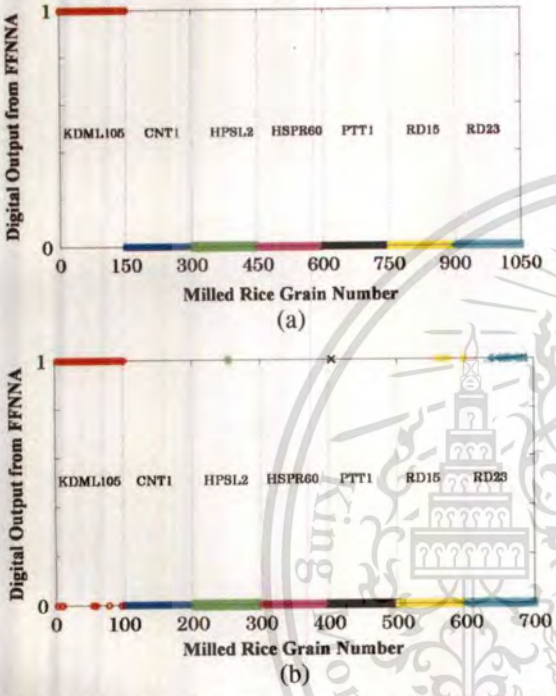

Fig. 10. FFNNA results during (a) the training period and (b) test with the unknown data set.

Fig. 11. Examples of two spectral images used during field operation tests.

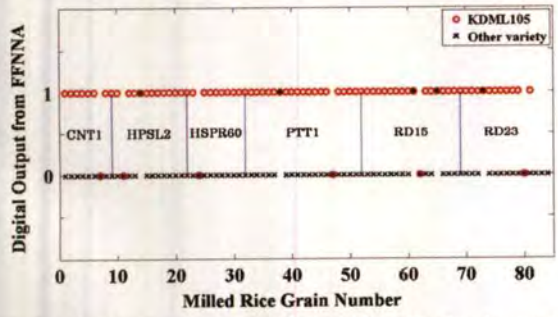

Fig. 12. Testing results of KDML105 identification in practice.

5. Conclusion

We show that the overall performance of our single-wavelength spectral-imaging-based Thai jasmine rice identification system can be improved by using a polynomial function and a well-trained FFNNA. All threshold images are passed through the chain code method, and the simple polynomial function, rather than the complicated EFD, is applied in order to define the appropriate geometry feature. This leads to a fast analysis time of 30.5 s, implying a 157.4 times improvement. At the end, the well trained FFNNA is used for identifying our desired KDML105 milled rice grain via analyzing three key shape parameters: area, perimeter, and eccentricity. With the initial preparation of rice samples, experimental results show low FAR and FRR values of 1.7% and 7.0%. Taking into consideration the robustness of our system, 55 additional sample sets are tested in our system, showing FAR and FRR values of 6.2% and 7.1% in the identification of the KDML105 milled rice variety mixed with unwanted CNT1, HPSL2, HSPR60, PTT1, RD15, and RD23 milled rice varieties. Future work relates to a long-term study on the performance of our system with a variety of rice sample conditions.

The authors gratefully thank the Rice Research Institute at the Department of Rice, Ministry of Agriculture and Cooperatives of Thailand for supplying rice samples. K. Suwansukho would also like to thank Thailand Graduate Institute of Science and Technology for scholarship support (grant no. TGIST 01–51-071) and the Science Faculty, King Mongkut's Institute of Technology Ladkrabang of Thailand for financial support to attend the conference.

References

1. K. Suwansukho, S. Sumriddetchkajorn, and P. Buranasiri, "Combination of simple chemical and spectroscopic methods for the identification of Thai Hom Mali rice," Proc. SPIE **7315**, 73150W (2009).
2. S. Sumriddetchkajorn, K. Suwansukho, and P. Buranasiri, "Identification of Thai Hom Mali rice using a refractometer," Proc. SPIE **7315**, 73150F (2009).
3. S. Sumriddetchkajorn and Y. Intaravanne, "Hyperspectral imaging-based credit card verifier structure with adaptive learning," Appl. Opt. **47**, 6594–6600 (2008).
4. S. Sumriddetchkajorn and Y. Intaravanne, "Data-nonintrusive photonics-based credit card verifier with a low false rejection rate," Appl. Opt. **49**, 764–770 (2010).
5. S. Sumriddetchkajorn and Y. Intaravanne, "Evolution of optically nondestructive and data-non-intrusive credit card verifiers," Proc. SPIE **7726**, 77261B (2010).
6. Y. Intaravanne, S. Sumriddetchkajorn, and J. Nukeaw, "Cell phone-based two-dimensional spectral analysis for banana ripeness estimation," Sens. Actuators B **168**, 390–394 (2012).
7. S. Sumriddetchkajorn and C. Kamtongdee, "Optical penetration-based silkworm pupa gender sensor structure," Appl. Opt. **51**, 408–412 (2012).
8. C. Kamtongdee, S. Sumriddetchkajorn, and C. Sa-ngiamsak, "Feasibility study of silkworm pupa sex identification with pattern matching," Comput. Eletron. Agric. **95**, 31–37 (2013).
9. S. Sumriddetchkajorn, C. Kamtongdee, and C. Sa-ngiamsak, "Spectral imaging analysis for silkworm gender classification," Proc. SPIE **8881**, 888106 (2013).

This material is reserved for educational use only, not allowed for commercial use.
Forbidden to modify the content, and cite the document when use.

S. Janchaysang, S. Sumriddetchkajorn, and P. Buranasiri, "Tunable filter-based multispectral imaging for detection of blood stains on construction material substrates. Part 1. Developing blood stain discrimination criteria," Appl. Opt. **51**, 6984–6996 (2012).
S. Janchaysang, S. Sumriddetchkajorn, and P. Buranasiri, "Improved tunable filter-based multispectral imaging system for detection of blood stains on construction material substrates," Proc. SPIE **8883**, 888316 (2013).
S. Janchaysang, S. Sumriddetchkajorn, and P. Buranasiri, "Tunable filter-based multispectral imaging for detection of blood stains on construction material substrates. Part 2," Appl. Opt. **52**, 4898–4910 (2013).
S. Sumriddetchkajorn, K. Suwansukho, and P. Buranasiri, "Two-wavelength spectral imaging-based Thai rice breed identification," Proc. SPIE **7715**, 77150I (2010).
K. Suwansukho, S. Sumriddetchkajorn, and P. Buranasiri, "Demonstration of a single wavelength spectral-imaging-based Thai jasmine rice identification," Appl. Opt. **50**, 4024–4030 (2011).
K. Suwansukho, S. Sumriddetchkajorn, and P. Buranasiri, "Improvement of single-wavelength based Thai jasmine rice identification with elliptic Fourier descriptor and neural network analysis," Proc. SPIE **8558**, 85580C (2012).
I. Sadeh, "Polynomial approximation of image," Comput. Math. Appl. **32**, 99–115 (1996).
L. M. Kocic and G. V. Milovanovic, "Shape preserving approximations by polynomial and splines," Comput. Math. Appl. **33**, 59–97 (1997).
P. M. Baggenstoss, "Image distortion analysis using polynomial series expansion," IEEE Trans. Pattern Anal. Mach. Intell. **26**, 1438–1451 (2004).
A. Kaveti, K. K. Teoh, and H. Wang, "Second order implicit polynomials for segmentation of range images," Pattern Recogn. **29**, 937–949 (1996).
K. Suwansukho, S. Sumriddetchkajorn, and P. Buranasiri, "Single-wavelength based Thai jasmine rice identification with polynomial fitting function and neural network analysis," Proc. SPIE **8883**, 888318 (2013).
H. Freeman, "On the encoding of arbitrary geometric configuration," IRE Trans Electron Comput **EC-10**, 260–268 (1961).
W. Burger and M. J. Burge, *Digital Image Processing: An Algorithmic Introduction Using Java* (Springer 2008).
Y. Mingqiang, K. Kidiyo, and R. Joseph, "A survey of shape feature extraction techniques," 2008, http://www.intechopen.com/books/pattern_recognition_techniques_technology_and_applications/a_survey_of_shape_feature_extraction_techniques.
J. L. Harper, P. H. Lovell, and K. G. Moore, "The shapes and sizes of seeds," Annu. Rev. Ecol. Syst. **1**, 327–356 (1970).

King Mongkut's Institute of Technology Ladkrabang

This material is reserved for educational use only, not allowed for commercial use.
Forbidden to modify the content, and cite the document when use.